

SUBSPACE-BASED IDENTIFICATION AND CONTROL USING WAVELETS

By

VINEET VAJPAYEE

ENGG01201304016

BHABHA ATOMIC RESEARCH CENTRE, MUMBAI

*A thesis submitted to the
Board of Studies in Engineering Sciences*

In partial fulfillment of requirements

for the Degree of

DOCTOR OF PHILOSOPHY

of

HOMI BHABHA NATIONAL INSTITUTE

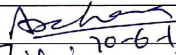
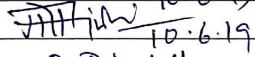
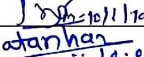
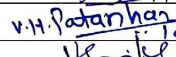
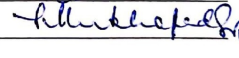


June, 2019

Homi Bhabha National Institute

Recommendations of the Viva Voce Committee

As members of the Viva Voce Committee, we certify that we have read the dissertation prepared by **Vineet Vajpayee** entitled “**Subspace-based Identification and Control Using Wavelets**” and recommend that it may be accepted as fulfilling the thesis requirement for the award of Degree of Doctor of Philosophy.

Chairman	Dr. Archana Sharma	
Guide/convenor	Dr. A. P. Tiwari	 10.6.19
Co-guide	Dr. B. Dikshit	
Examiner	Dr. B. M. Patre	 10/10/19
Member-1	Dr. V. H. Patankar	 10.06.2019
Member-2	Dr. Gopika Vinod	
Technical Advisor	Dr. S. Mukhopadhyay	 10/06/19

We hereby certify that we have read this thesis prepared under our direction and recommend that it may be accepted as fulfilling the thesis requirement.

Date: 11-6-19

Place : MUMBAI



Signature

Guide



Signature

Co-guide



Signature 10/06/19

Technical

Advisor

STATEMENT BY AUTHOR

This dissertation has been submitted in partial fulfillment of requirements for an advanced degree at Homi Bhabha National Institute (HBNI) and is deposited in the Library to be made available to borrowers under rules of the HBNI.

Brief quotations from this dissertation are allowable without special permission, provided that accurate acknowledgement of source is made. Requests for permission for extended quotation from or reproduction of this manuscript in whole or in part may be granted by the Competent Authority of HBNI when in his or her judgment the proposed use of the material is in the interests of scholarship. In all other instances, however, permission must be obtained from the author.

(VINEET VAJPAYEE)



DECLARATION

I, hereby declare that the investigation presented in the thesis has been carried out by me. The work is original and has not been submitted earlier as a whole or in part for a degree/diploma at this or any other Institution/University.

(VINEET VAJPAYEE)



List of Publications arising from the thesis

Journal

1. “Multiscale Subspace Identification of Nuclear Reactor using Wavelet Basis Function”, Vineet Vajpayee, Siddhartha Mukhopadhyay, and Akhilanand Pati Tiwari, *Annals of Nuclear Energy*, vol. 111, pp. 280–292, Jan 2018.
2. “Data-driven Subspace Predictive Control of a Nuclear Reactor”, Vineet Vajpayee, Siddhartha Mukhopadhyay, and Akhilanand Pati Tiwari, *IEEE Transactions on Nuclear Science*, vol. 65, no. 2, pp. 666–679, Feb 2018.
3. “Wavelet Operator for Multiscale Modeling of Nuclear Reactor”, Vineet Vajpayee, Siddhartha Mukhopadhyay, and Akhilanand Pati Tiwari, *Nuclear Engineering and Technology*, vol. 50, no. 5, pp. 698–708, June 2018.

Conferences

1. “A Multiresolution Wavelet based Subspace Identification”, Vineet Vajpayee, Siddhartha Mukhopadhyay, and Akhilanand Pati Tiwari, *IFAC–PapersOnLine*, vol. 49, no. 1, pp. 247–253, 2016.
2. “Subspace based Wavelet preprocessed Data-driven Predictive Control”, Vineet Vajpayee, Siddhartha Mukhopadhyay, and Akhilanand Pati Tiwari, *INCOSE International Symposium*, vol. 26, no. s1, pp. 357–371, 2016.
3. “Wavelet-based On-line Multiscale Subspace Identification of Nuclear Reactor”, Vineet Vajpayee, Siddhartha Mukhopadhyay, and Akhilanand Pati Tiwari, *IFAC–PapersOnLine*, vol. 51, no. 15, pp. 347–352, 2018.



(VINEET VAJPAYEE)

Dedicated to my family

Acknowledgment

I would like to express my sincere gratitude towards my guides **Dr. A P Tiwari** and **Dr. S Mukhopadhyay** for formulating this research topic and for their guidance and encouragement to work to the best of my abilities. Their knowledge, insightful and consistent care for the best output have been great assets without which this research would not have been possible. I would also like to thank my co-guide **Dr. B Dikshit** for constant encouragement.

I am indebted to the chairman **Dr. Archana Sharma** and other members of the doctoral committee for their valuable comments and suggestions during various occasions. I would also like to thank anonymous reviewers of the journals who reviewed my manuscripts. They helped not only in making the work presentable but also especially the negative ones which were adequate in amount, helped in giving the work a better shape. Without these reviewers this work would not have reached the conclusions it has.

My sincere thanks to **Dr. S R Shimjith**, **Mr. T U Bhatt**, **Mr. K N V Sairam**, **Mr. Ch S Subudhi**, and **Mr. Amit Mishra** for numerous discussions and for arranging necessary lab facilities. The friendly and supportive environment created by all the lab mates especially, **Mr. P V Surjagade** and **Mr. S B Patel** made the job easier and technical discussions with them improved the learning part. I would like to thank my fellow research scholars at HBNI for making my stay pleasant. I also like to thank my friends for motivating and cheering me up during tough times. My special thanks to **Mr. A Kushwaha** for proofreading the thesis.

I am also thankful to Bhabha Atomic Research Centre, Mumbai and Board of Research in Nuclear Sciences, India for my fellowship to make my PhD financially stable.

Acknowledgment

Last but not least, I want to express my heartfelt thanks to my family. I am grateful to my wife **Mrs. Divya Vajpayee** for encouraging me to pursue the doctoral studies. I express my deep gratitude and admiration towards my parents **Mrs. Radha Vajpayee** and **Mr. Rakesh Vajpayee** for the unconditional love.

(VINEET VAJPAYEE)



List of Figures

1.1	Block diagram representation of a system.	2
2.1	Flow diagram of the system identification loop.	16
2.2	Comparison of system identification with subspace identification.	19
2.3	Time-frequency tilings	30
2.4	Block diagram of analysis filter bank	31
2.5	Block diagram of synthesis filter bank	31
2.6	Block diagram representation of the MPC approach.	38
2.7	Representation of model predictive control strategy.	39
2.8	Representation of receding horizon control strategy.	40
3.1	Block diagram of analysis and synthesis filter bank	52
3.2	Block diagram of the proposed projection space modeling technique.	55
3.3	Variation of reference reactivity estimation input.	59
3.4	Outputs of estimated models with observed data for reference input.	59
3.5	Variation of reference reactivity validation input (Case A).	62
3.6	Variation of reference reactivity validation input (Case B).	62
3.7	Outputs of estimated models with observed data for Case A input.	63
3.8	Outputs of estimated models with observed data for Case B input.	63
3.9	Variation of plant reactivity estimation input.	66
3.10	Outputs of estimated models with observed data for plant input.	67
3.11	Variation of plant reactivity validation input.	67
3.12	Outputs of estimated models with observed data for plant input.	68
4.1	Block diagram representation of multiscale system identification using dyadic discretization for two levels of decomposition.	72
4.2	Block diagram representation of multiscale subspace identification for two levels of decomposition.	78
4.3	Block diagram representation of on-line ms-SID for two scale decomposition.	84
4.4	Implementation of wavelet transform in on-line ms-SID for two scale decomposition.	84
4.5	Assumed reactivity variation (Training input dataset).	87
4.6	Reactor power variation for Figure 4.5 (Training output dataset).	88

4.7	The discrete-time Fourier transform of the reactor power signal shown in Figure 4.6.	89
4.8	Scatter plots between one-step-ahead-prediction and observed values at different scales.	89
4.9	Autocorrelation function of the residuals for output power at significant scales for different lags.	90
4.10	Cross-correlation function of the residuals with the input reactivity at significant scales for different lags.	91
4.11	Triangular variation in reactivity (Validation dataset input).	93
4.12	Step variation in reactivity (Validation dataset input).	93
4.13	Outputs of estimated ms-SID, ms-ARX, classical subspace (SID), ARX, and BJ models with observed data for input shown in Figure4.11 (simulation).	94
4.14	Outputs of estimated ms-SID, ms-ARX, classical subspace (SID), ARX, and BJ models with observed data for input shown in Figure 4.12 (simulation).	94
4.15	Singular values of the covariance martix constructed from estimation data.	97
4.16	Variation of reactivity.	99
4.17	Reactor power added with white Gaussian noise.	99
4.18	Fourier transform of the input-output signal.	100
4.19	Scatter plots between one-step-ahead prediction and observed output.	100
4.20	Variation of reactivity (Case I).	101
4.21	Comparison of simulation outputs of SID, MSARX, and MSID approaches (Case I).	101
4.22	Variation of reactivity (Case II).	102
4.23	Comparison of simulation outputs of SID, MSARX, and MSID approaches (Case II).	102
5.1	Block diagram representation of the proposed scheme with application to nuclear reactor.	121
5.2	Assumed reactivity variation (estimation input data).	123
5.3	Reactor power variation corresponding to reactivity variation shown in Figure 5.2 (estimation output data).	123
5.4	The discrete-time Fourier transform of the reactor power signal shown in Figure 5.3.	126
5.5	First 40 singular values of extended Hankel matrices for measured and pre-processed data.	126
5.6	Reactor power variation for 50% load rejection transient.	127
5.7	Reactor power variation for 75% load rejection transient.	128
5.8	Comparison of the performance between SPC with feed-forward control and SPC without feed-forward control, (a) reactor power, (b) control input, and (c) rate of change of control input.	130

5.9	Comparison of the performance between SPC with integrator and SPC without integrator, (a) reactor power, (b) control input, and (c) rate of change of control input.	131
5.10	Comparison of the performance between recursive and non-recursive SPC, (a) reactor power, (b) control input, and (c) rate of change of control input.	132
5.11	Variation of (a) MSE in output, (b) TV of input, and (c) l_2 norm of input for different prediction and control horizons.	135
5.12	Variation of MSE in output, TV of input, and l_2 norm of input for different value of Q	136
5.13	Variation of MSE in output, TV of input, and l_2 norm of input for different value of R	136
5.14	Sum of squared error between output and desired set point at different SNR for white Gaussian noise sequence.	138
5.15	TV of input at different SNR for white Gaussian noise sequence.	138
5.16	l_2 -norm of input at different SNR for white Gaussian noise sequence.	138
5.17	Sum of squared error between output and desired set point at different SNR for integrating white Gaussian noise sequence.	140
5.18	TV of input at different SNR for integrating white Gaussian noise sequence.	140
5.19	l_2 -norm of input at different SNR for integrating white Gaussian noise sequence.	140

List of Tables

3.1	Estimated wavelet filter coefficients for different states.	60
3.2	RMSE for simulated reference dataset.	64
3.3	Estimated filter coefficients for different states for simulated plant dataset.	65
3.4	RMSE for simulated plant dataset.	66
4.1	RMSE in output prediction by various approaches for different validation datasets (Monte Carlo simulation)	96
4.2	RMSE of ms-SID model simulations at various decomposition depths for triangular input validation dataset (Monte Carlo simulation)	97
4.3	RMSE of ms-SID model simulations at various decomposition depths for sum of step input validation dataset (Monte Carlo simulation)	98
4.4	Comparison of the root mean squared error (10 Monte Carlo runs)	103
5.1	Neutronic and thermal-hydraulic parameters	121
5.2	Comparison of performances of denoised signal for Haar, Daubechies, Symlet and Coiflet wavelet families at $J = 7$	124
5.3	Comparison of performances of denoised signal with respect to depth of decomposition for Daubechies-4 wavelet.	125
5.4	Comparison of performances of classical SPC with wavelet pre-processed SPC.	133
C.1	Neutronic and Thermal-Hydraulic Parameters	161

Abbreviations

ANN	Artificial Neural Network
ARIMA	Auto Regressive Integrated Moving Average
ARMAX	Auto Regressive Moving Average with eXogenous input
ARX	Auto Regressive with eXogenous input
BJ	Box Jenkins
BWR	Boiling Water Reactor
CLSPC	Closed Loop Subspace Predictive Control
CR	Control Rod
CVA	Canonical Variate Analysis
CWT	Continuous Wavelet Transform
DMC	Dynamic Matrix Control
DWT	Discrete Wavelet Transform
FFT	Fast Fourier Transform
FIR	Finite Impulse Response
GPC	Generalized Predictive Control
HPF	High Pass Filter
IV	Instrumental Variable
LPF	Low Pass Filter
LPV	Linear Parameter Varying
LQG	Linear Quadratic Gaussian
LTI	Linear Time Invariant
LTV	Linear Time Varying

LZCS	L iquid Z one C ontrol S ystem
MIMO	M ulti I nput M ulti O utput
MOESP	M ulti-variable O utput E rror S tate S pace
MPC	M odel P redictive C ontrol
MRA	M ulti R esolution A pproximation
MSE	M ean S quared E rror
ms-SID	M ulti S cale S ubspace I Dentification
N4SID	N umerical algorithms for S ub S pace S tate S pace I Dentification
NI	l_2 N orm of I nput
NPP	N uclear P ower P lant
OE	O utput E rror
OLSPC	O pen L oop S ubspace P redictive C ontrol
PCA	P rincipal C omponent A nalysis
PEM	P rediction E rror M ethod
PHWR	P resurized H eavy W ater R eactor
PRMSE	P ercentage R oot M ean S quared E rror
PWR	P resurized W ater R eactor
RR	R egulating R od
RMSE	R oot M ean S quared E rror
SG	S tream G enerator
SID	S ubspace I Dentification
SISO	S ingle I nput S ingle O utput
SNR	S ignal to N oise R atio
SPC	S ubspace P redictive C ontrol
SSE	S um of S quared E rror
SVD	S ingular V alue D ecomposition
SVR	S upport V ector R egression
T-S	T akagi S ugeno
TVI	T otal V ariation of I nput

VARX	V ector A uto R egressive with eX ogenous input
VVER	V odo V odyanoi E nergetichesky R eaktor
WSPC	W avelet-preprocessed S ubspace P redictive C ontrol

Nomenclature

A	System dynamics matrix
A_j^v	System dynamics matrix in approximation space
A_j^w	System dynamics matrix in detail space
B	Input matrix
B_j^v	Input matrix in approximation space
B_j^w	Input matrix in detail space
c_j	Approximation coefficients
C	Output matrix
C_j^v	Output matrix in approximation space
C_j^w	Output matrix in detail space
C_i	Delayed neutron precursor's concentration
d_j	Detail coefficients
D	Feed through matrix
D_j^v	Feed through matrix in approximation space
D_j^w	Feed through matrix in detail space
$e[k]$	Innovation
E_f	Innovation data block Hankel matrix
f	Future horizon
f_c	Central frequency
f_s	Natural frequency of sampled signal
F	Wavelet Transform operator
\bar{F}	Inverse Wavelet Transform operator
$g[k]$	Analysis high pass filter
$\tilde{g}[k]$	Synthesis high pass filter

G_j	Analysis high pass filter matrix at j^{th} scale
\bar{G}_j	Synthesis high pass filter matrix at j^{th} scale
G_v	Givens rotation matrix
H_f^d	Deterministic lower block-triangular Toeplitz matrix
H_f^s	Stochastic lower block-triangular Toeplitz matrix
$h[k]$	Analysis low pass filter
$\tilde{h}[k]$	Synthesis low pass filter
H_j	Analysis low pass filter matrix at j^{th} scale
\bar{H}_j	Synthesis low pass filter matrix at j^{th} scale
H_C	Rate of rise of coolant
H_F	Rate of rise of fuel
I	Identity matrix
j	Scale
j_0	Initial scale or level of decomposition
J	Initial scale of decomposition
$J + 1$	Approximation at J^{th} scale
k	Time instant
K	Kalman gain
K_j^v	Kalman gain in approximation space
K_j^w	Kalman gain in detail space
l	Output order
l^2	Vector space of square summable discrete sequences
$L^2(\mathbb{R})$	Hilbert space of square integrable function
L_x	Product of observability and controllability matrices
L_T	Turbine load
m	Input order
n	System order
N_c	Control horizon
N_p	Prediction horizon
p	past horizon
P	Neutronic power
q	Forward shift operator

Q_f	Weighing matrix
R_f	Weighing matrix
s	Dilation parameter
T_{cold}	Cold leg temperature
T_{hot}	Hot leg temperature
T_C	Coolant temperature
T_F	Fuel temperature
T_{in}	Core inlet temperature
T_{out}	Core outlet temperature
T_s	Sampling period
T_{sg}	Steam generator temperature
$u(t)$	Continuous input
$u[k]$	Discrete input
$u_j^v[k]$	Projection of input on scaling function
$u_j^w[k]$	Projection of input on wavelet function
U	Input time-series
U_f	Input data block Hankel matrix
U^w	Wavelet coefficients of input
$\{V_j\}_{j \in \mathbb{Z}}$	Approximation space
V_u	Input approximation subspace
V_y	Output approximation subspace
$\{W_j\}_{j \in \mathbb{Z}}$	Difference space
W_p	Combined input-output data block Hankel matrix
W_j^X	Local diagonalizing operator
\tilde{W}_j^X	Wavelet operator
$x[k]$	State vector
$y(t)$	Continuous output
$y[k]$	Discrete output
$y_j^v[k]$	Projection of output on scaling function
$y_j^w[k]$	Projection of output on wavelet function
Y	Output time-series
Y_f	Output data block Hankel matrix

Y^w	Wavelet coefficients of output
α^i	Eigen value
α^C	Coolant temperature coefficients of reactivity
α^F	Fuel temperature coefficients of reactivity
β	Fraction of delayed neutrons
σ_i	Singular value
λ	Decay constant
ρ_F	Reactivity due to fuel
ρ_C	Reactivity due to coolant
ρ_T	Total reactivity
ρ_Z	Reactivity due to LZCS
γ_F	Inverse meantime for heat transfer from fuel to coolant
γ_F	Inverse meantime for heat transfer from core outlet to inlet
ϕ	Analysis scaling function
$\tilde{\phi}$	Synthesis scaling function
ψ	Analysis wavelet function
$\tilde{\psi}$	Synthesis wavelet function
τ	Translation parameter
τ_{hot}	Time constant for hot leg
τ_{cold}	Time constant for cold leg
τ_{sg}	Time constant for steam generator
z^{-1}	Backward shift operator
Δ	Difference operator
θ	Coefficient vector
Γ_f	Extended observability matrix
Ξ^w	Wavelet coefficients of noise vector
ζ	regression vector
ζ^w	Wavelet coefficients of regression vector
Π_U^\perp	Orthogonal projection of U
Σ	Singular value matrix
Λ	Prompt neutron life time
\mathbb{R}	Set of real numbers

\mathbb{Z}	Set of integers
\otimes	Kronecker product
\oplus	Direct sum

Chapter 1

Introduction

A system is described as an object consisting of different interacting components or variables to generate consequential observable signals [1]. Figure 1.1 shows the block diagram representation of such a typical system where the observable signal is called as output and external signal that can be manipulated by observer is called as input. External stimulus that can not be manipulated is known as disturbance and it can be divided into two categories, one that can be directly measured and one that can only be observed by their impact on the output. Interaction among variables is formalized by the model of the system which characterizes the supposed relationship among variables. There are various types of models depending on intended use such as graphical models, software models, mathematical or analytical models, *etc.* Out of various mentioned models, mathematical models are of particular interest in this work. Mathematical models illustrate the dynamic behavior of a system as a function of time. They describe the relationship among variables in term of difference or differential equations. They are widely found in all scientific disciplines for various purposes like process monitoring, prediction, forecasting, simulation, optimization, design of control system, fault detection and identification, *etc.*

Traditionally, Nuclear Power Plants (NPPs) are mathematically modeled using first principles approach. It necessitates detailed knowledge about underlying mechanisms

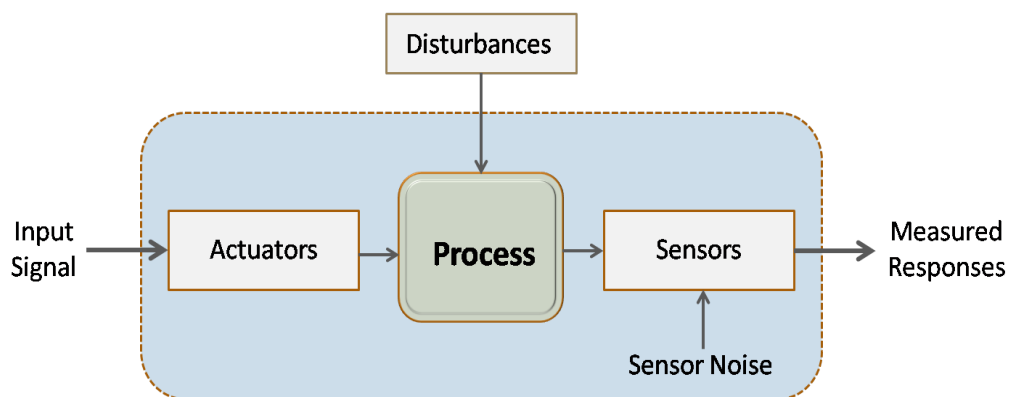


FIGURE 1.1: Block diagram representation of a system.

of the reactor system. Usually, the system is divided into subsystems whose properties are well comprehended. The mathematical models of such subsystems are derived using physics laws. The complete model of the reactor system is obtained by integrating subsystems models together. However, underlying assumptions, complexity, and high order associated with model derived from first principles often make them difficult to handle and unsuitable for control applications. Moreover, NPPs belong to the class of highly constrained complex systems with time-varying characteristics [2]. They exhibit multi-scale behavior when operated through different power regimes. The variation in system parameters due to fuel burnup, internal reactivity feedbacks, and modeling uncertainties of reactor dynamics can significantly influence system response. For instance, during load-following mode of operation, daily load cycles can considerably affect plant performance due to wide range of power variations. In addition, gradually changing operating conditions, ever stringent performance regulations, and safety concerns often necessitate re-tuning or re-designing of different systems in an NPP. Sometimes modeling of certain new subsystems are also required for retrofitting and optimal functioning of a plant. Therefore, mathematical modeling and control of an NPP represents enormous challenge.

With the recent advancement in technology for harnessing nuclear power for electricity generation, there is a tremendous increase in the percentage of nuclear generated electricity. This development is further accelerated by the need to reduce carbon emissions

and to generate clean energy. Currently, there are around 440 commercial NPPs operating in 31 countries with over 380 GW of total capacity and about 65 more reactors are under construction. They form approximately 11.5% of the world's electricity. Other than commercial NPPs, around 240 research reactors are operating in about 56 countries. Furthermore, 180 reactors power some 140 ships and submarines [3]. In India, nuclear power is the fifth-largest source of electricity after coal, gas, hydroelectricity, and wind power. As of 2016, India has 22 nuclear reactors in operation in 7 NPPs, having a total installed capacity of 6,780 MW while 3 other reactors are under construction and are expected to generate an additional 3,800 MW. This tremendous growth led to an increased interest in modeling and control strategies that would enhance plant operation. Advanced controllers that can replace conventional controllers with significantly improved performance are of particular interest in nuclear community.

In recent times, the availability of content-rich data from NPPs post strong motivation behind wide applications of empirical modeling or system identification. System identification is a systematic way of constructing simple mathematical model of a dynamical system from recorded input-output data [1]. It is preferred over first principles approach of modeling while refurbishing a control design technique in an existing NPP which has aged over time. System identification, by perturbing a plant to excite its dynamic modes is carried out for various other reasons such as modeling, designing of controllers, simulation, optimization, *etc.* Measurements being a potent source of information carry almost all useful details about plant dynamics. These informations can be utilized for the diagnostic and monitoring of a plant. In most of the model-based approaches, the achievement of design objective is largely depend on the accuracy of employed model. Thus, it is important to arrive at a plant model which is reasonably accurate and at the same time, simple enough to be relevant to the design objective.

Dynamic response of a nuclear reactor contains simultaneously interacting variables with multi-timescale characteristics. For such multivariable processes, state-space representation offers better tractability in controller synthesis and implementation [4]. It is

preferred over transfer function or impulse response descriptions. Subspace identification is an important class of modeling approaches in time-domain for the identification of state-space models [5]. It estimates Kalman filter states directly from input-output data and then system matrices are determined. This notion of first state calculation and then parameter estimation can be seen as *input–state–output* modeling and it makes subspace identification different from classical system identification based on *input–output* model *e.g.*, Prediction Error Method (PEM) where first system matrices are estimated and states are derived thereafter. Theoretically, PEM can be adapted to work with state-space models. However, in practice this may lead to very large number of unknowns during optimization and is quite cumbersome in case of modeling multivariable systems. It may also cause numerical ill-conditioning due to sensitivity to small perturbations for large system orders. On the other side, subspace methods avoid explicit model parameterization and thus can be easily extended to Multi-Input Multi-Output (MIMO) systems. Subspace techniques are numerically robust and computationally efficient as they are based on stable QR decomposition and Singular Value Decomposition (SVD) algorithms. Subspace methods being non-iterative are free from non-convergence, local minima, and initial condition problems. Their implementation is fast as compared to PEM methods, despite the fact that they are implemented using QR and SVD. They possess better numerical properties of parametrization over classical PEM methods. Subspace methods work to estimate reduced order model inherently without computing first the high order model followed by a model order reduction step. Further, they do not require any selection of model structures a priori.

In practice, measurement datasets are obtained during operation of an NPP in which various complex time varying processes exist possibly with inherent nonlinear characteristics. It is well known that modeling of multiscale systems using conventional (single scale) approaches may sometimes lead to ill-conditioning [6]. Thus, over the years, different modeling approaches exploiting the two-timescale or three-timescale properties of the system have been proposed [7, 8, 9]. However, various multiscale features may not be clearly visible in measurement domain. Therefore, it is imperative to

have the transformation of data and visualization in a multiresolution framework around a proper set of scales. This consideration has led to system identification using generalized basis function. Modeling of complex systems, *e.g.*, a nuclear reactor system with complex sine or sinc basis may pose some restrictions because of simultaneous presence of multiple dynamic modes and interaction exhibiting multiscale behavior. Furthermore, these modes may be located in widely separated clusters governing slow as well as fast timescale behavior. It demands very high frequency resolution to discriminate closely spaced poles as well as very high time resolution for modeling multiscale pole clusters. However, both resolutions can not be made arbitrarily high and thus, the solution to this identification could use any other basis functions.

Wavelet basis functions have attracted a great deal of attention in the last two decades [10, 11]. They are the new families of generalized basis functions for the better representation of signals simultaneously in time and frequency domain. The classical Fourier basis functions are perfectly localized in frequency but not in time. Small frequency changes in the Fourier domain will tend to produce changes everywhere in the time domain. On the other hand, wavelets are localized in time-frequency and provide a compact representation of broad classes of functions. Wavelet bases are generally preferred over other bases due to their excellent approximation ability. The idea central to this class of modeling methodology is the invocation of Multi Resolution Analysis (MRA) in data-driven modeling. It builds a relation among set of approximations and details at various resolutions level. It is equivalent to breaking down a complex process into a number of relatively simpler subprocesses each seen at an appropriate resolution. Thus, the estimated model usually turns out to be of low order in projection space. In addition, wavelet bases are especially suitable for modeling and analysis of non-stationery time varying systems. They have the capability to approximate any linear or nonlinear time varying process. In fact, the convergence rate of wavelet approximation is nearly equal to that of the other general nonlinear approximation approaches. This is because the correlation structure of wavelet coefficients decay faster than those in case of original signal in time. In terms of computational complexity, the wavelet transform is better

having the $O(n)$ complexity as compared to the Fast Fourier Transform (FFT) which has $O(n \log_2(n))$ [12].

Traditionally, a large class of nonlinear systems are modeled as linear systems with time varying coefficients. However, if nonlinearities are accompanied with high order and integrating type effects such as a reactor system then modeling in the classical input-output description requires significantly large number of parameters. On the other hand, modeling of such effects in wavelet domain is likely to greatly reduce number of model parameters [13]. Thus, the objective translates to building a linear description in multi-resolution of a nonlinear system using wavelets basis functions. The model defined in wavelet basis can capture complexities such as nonlinearity, integrating and multiple time scale behavior very effectively in fewer parameters. This provides a strong motivation for modeling a nuclear reactor with a derived wavelet based sub band model. In addition, wavelet basis functions naturally accommodate preprocessing of data resulting in increased Signal to Noise Ratio (SNR).

In last few decades, various research works have been attempted for system identification from measurement data projected on wavelet basis functions [14, 15, 16, 17, 18]. Some of the existing works have proposed identification of Linear Time Varying (LTV) models that attempt to linearly approximate the system output although wavelets are known to provide near-optimal nonlinear estimates of signals. Usually, a LTI model is estimated in least squares sense as there are more samples available than the number of parameters. However, a strict LTV model becomes under determined because dynamic solution requires derivation of more than one system parameters at each time instant [19]. Several approaches have been adopted to solve the LTV parameter estimation problem. Most of the aforementioned techniques have relied more on the linear function approximation approach with wavelet basis, relegating the techniques to off-line identification of the process models.

Recent studies have employed the filter bank aspects of wavelets [20, 21, 22, 23, 24, 25]. The underlying idea in all of these works is to develop separate models on relevant

scales after multiscale data representation while selecting a single model using a specified criterion. These methods demonstrate their superiority over single-scale methods but do not fully exploit the advantages of multiscale decomposition. In addition, the approaches demonstrate their suitability in terms of one-step-ahead prediction while, validation through simulation (infinite-step-ahead prediction) model is missing in most of the works.

A different approach has been taken in this thesis, whereby it does not necessitate the assumption of local time invariance. The method of parameter estimation proposed here naturally accommodates nonlinear behavior by recursively updating parameters in an efficient manner. In the proposed scheme, the system is modeled in approximation space as well as in detail space in which both input and output are projected. An important contribution of the proposed work is to develop a framework for state-space modeling at significant scales leading to parsimonious model description with less computational burden. It integrates the proficiency of wavelets for multiscale data representation with the robust parameter estimation ability of subspace methods. It estimates subspace based models at significant scales in both prediction and simulation framework. The efficacy of the proposed multiscale subspace identification technique is illustrated by modeling a nuclear reactor. The model parameters are updated efficiently as and when a new dataset is available thereby yielding an on-line state space model identification strategy in multiresolution framework. Case studies with different datasets prove superiority of the proposed multiscale subspace identification over the classical approach of measurement space modeling. Further, to draw statistically valid argument, Monte Carlo simulations are performed at different noise levels as well as at various decomposition depths. It has been found that in most of the modeling exercises, the proposed approach reduces dimensionality with improved output prediction capability. Moreover, the application of subspace methods for modeling of nuclear reactor is not common and the approach undertaken in this thesis can be considered as the first such attempt.

This thesis work further proposes a technique to efficiently isolate multiple timescales

in a LTI system, a problem that has been of interest and challenge in identification and control of nuclear reactors [9]. The notion adopted here is similar to the Multiscale Principal Component Analysis (MSPCA) approach for modeling multivariable statistical processes [26]. It extracts cross-correlation between the variables by diagonalizing the covariance matrix while wavelets approximately decorrelate the autocorrelation among the measurements. Wavelet operator has been formulated from the eigen values of the given system thus utilizing the inherent structure of the system. Application of the proposed technique for modeling a nuclear reactor from measurements is demonstrated. It diagonalizes the system matrix to decouple system modes completely for applying independent control actions along the eigen functions [27]. It proves that one can work with a diagonalized state space model in wavelet sub-spaces as well. The technique can be used for designing on-line estimation and control strategy because wavelet based modeling approaches identify a system with a set of multiscale minimum memory models that are amenable for real time applications. For on-line applications of multi-timescale processes it is useful to work with models operating at appropriate scales.

Another aspect of this thesis is the design of a data-driven predictive control utilizing the subspace matrix structure. Model Predictive Control (MPC) is an advanced predictive control design strategy. It is widely popular in industries due to its ability to incorporate design constraints, on-line optimization, and easy adaptability to new operating conditions. A broad class of the MPC design strategies solve a cost function optimization problem at each time step to determine a set of future control moves, over a finite time horizon. Conventionally, the MPC methodology requires, an explicit process model for the prediction of future behavior of the system and the design of an optimal control law by solving the cost function optimization. Some existing works have integrated subspace identification with the MPC, leading to a class of approaches called Subspace Predictive Control (SPC) [28, 29, 30, 31, 32]. The basic idea of integrating subspace algorithms with predictive control is conceived with the purpose of creating a reliable control architecture that can be rapidly deployed in plants. This fusion of two steps

into a single step offers robustness and efficiency of subspace methods with the flexibility and comprehensive nature of the MPC, making SPC an attractive candidate for the solution of data-driven control design problem. However, in practical applications of data-driven control, care has to be exercised as these methods are sensitive to noise and may sometimes lead to ill-conditioning of the predictor matrices. Recent developments of wavelet-based denoising techniques offer better solutions to these problems. Wavelet transform represents the noisy dynamics as the sum of scaled and shifted wavelets and extracts features that are associated only with process dynamics. Wavelet preprocessing of measurements improves parameter estimation task with minimum distortion of process dynamics. It also minimizes the distortion of signal bandwidth and thus improves the SNR of processed signal.

Data-driven predictive control technique utilizing the subspace matrix structure proposed in the thesis integrates wavelet pre-processing and subspace predictive control approaches. It removes the need of any physical model of the system thus reducing the error arising due to model-plant mismatch. The controller is directly obtained from wavelet preprocessed input-output data such that the overall system is less sensitive to noise. The work also discusses systematic incorporation of feed-forward control, integrating action, and constraints in the control design. The efficacy of the proposed algorithm is demonstrated in typical situations involving demand variations and load rejection transients. In order to analyze the control performances, detailed parameter sensitivity analysis has also been carried out.

Contribution of the thesis

Primary objective of this thesis is to develop a systematic approach for the identification and control of multiscale systems using wavelets. In this work, MRA with wavelet basis is utilized for subspace based modeling of a nuclear reactor. In a reactor, different dynamic modes evolve at various scales of time and use of same model at different scales would be rather limiting. The current proposition is to develop a class of models defined

in different frequency bands of the process. It estimates state space models at significant scales in both prediction and simulation framework. Systems with nonlinearity can be approximated by a set of LTI models in multiresolution environment. Thus, the estimated model shows significantly better output prediction over classical single scale modeling techniques. Moreover, for on-line applications of multi-timescale processes it is often more meaningful to work with models at appropriate scales. The proposed approach inherits the features of robust subspace identification with added advantages of wavelet based modeling enabling multiresolution state-space model development.

The thesis presents the design of wavelet operators for multiscale modeling in order to impose a specific structure in the space spanned by wavelet projections. In this regard, this work proposes designing of wavelet operator from the measurements. It advocates to employ different wavelet filter banks for the analysis of modes/states evolving at different scale of time so as to minimize modeling error. It establishes that there exists a definite relationship between the model in measurement space and that in projection space. Methodology for deriving multirate perfect reconstruction filter bank associated with wavelet operator is presented. The efficacy of the proposed technique is validated on a nuclear reactor system using reference as well as plant datasets.

The thesis further aims to investigate the application of wavelet MRA in data-driven control design approach for a nuclear reactor. It integrates wavelet pre-processing with the SPC design technique. Specifically, here we focused onto the filtering prospective of the wavelets in order to negate the effects of disturbances in the measurement. The central idea is to implement predictive control law directly from the wavelet-preprocessed input-output data without using any explicit process model. The controller is designed to include design constraints, feed-forward control, and integral control action effectively. Furthermore, time variations in the process are taken into account by recursively updating control parameters with the arrival of new data set. A parameter sensitivity analysis has been proposed to find the desired control performance. The performance of proposed controller is compared with different controllers using Monte Carlo simulations at different SNRs for the statistical validation of the technique.

Organization of thesis

In this section, we present the thesis's outline and summarize the contribution of each chapter.

Chapter 2 provides an in depth literature review of wavelet basis functions, system identification, subspace methods, model predictive control, subspace predictive control, and other data-driven control techniques. It also account their applicability in nuclear science and engineering. It further presents the fundamentals concepts required for proposed work.

Chapter 3 discusses design of wavelet operators for multiscale modeling to impose a certain structure on the system in wavelet space. The methodology employs different wavelet filters for analyzing different states of the system. The efficacy of the proposed approach is demonstrated on point kinetics nuclear reactor. The outcome of the multiscale modeling approach is compared with that in single scale to bring out the merits of the proposed method using simulated reference and plant datasets.

Chapter 4 is dedicated to the multiscale system identification technique using wavelets. To be specific, it proposes multiscale subspace identification using data collected in open-loop as well as in closed-loop settings. It demonstrates an efficient on-line implementation scheme for the proposed technique. The chapter further discusses various subtle issues while working with wavelets like selection of wavelet, decomposition depth, and significant scales. The efficacy of proposed approach is demonstrated by modeling point kinetics nuclear reactor in prediction as well as in simulation framework. The proposed technique is further compared comprehensively with other single scale and multiscale approaches proposed in literature at different SNRs.

Chapter 5 integrates wavelet filtering with the SPC to formulate the wavelet preprocessed SPC approach. It discusses open-loop and closed-loop design approaches. The chapter discusses incorporation of feed-forward control, integrating control, and constraints in the controller design. The efficacy of the proposed technique is demonstrated

for tracking various load rejection as well as load-following transients for a nuclear reactor. A detailed parameter sensitivity analysis is carried out to analyze the controller performance. It is further compared with other controllers at different SNRs.

Chapter 6 presents the outcome of the work. It also discusses future research directions in which the results presented in the thesis can be further extended.

Appendix A discusses general family of model structures. Appendix B presents the Vandermonde structure of the wavelet operator and also demonstrates an analytical example for filter designing. Appendix C describes the nuclear reactor dynamics. It presents the point kinetics reactor model of nuclear reactor, model of core thermal-hydraulics, internal reactivity feedbacks due to the effects of temperature and fission product poisons, and model of reactivity.

Chapter 2

Literature Survey

This chapter describe fundamentals of system identification, subspace identification, and wavelet basis functions. It discusses different applications of wavelets as found in the field of modeling and control. It further reviews model predictive control, subspace predictive control, and other data-driven control techniques. Their relevance and applicability in nuclear science and engineering are clearly pointed out. Significance of the proposed work is also discussed.

2.1 System Identification

Data-driven modeling or system identification has played an increasingly dominant role in a wide range of engineering applications starting from process simulation and control to identification of vibrational modes in flexible structures. The maturity in the field of system identification results from culmination of various domains such as signal processing, econometrics, and statistics. In the domain of systems and control engineering, there exists an extensive literature on system identification and its applications. Some useful texts on system identification with detailed discussions on various techniques and

algorithms are by Ljung [1], Soderstrom and Stoica [33], and Tangirala [34]. An interesting historical perspective of the developments from the purview of a control engineer is presented by Gevers [35].

The basic procedure of system identification involves four basic entities:

- **Data collection**– The objective of this step is to design experiments to record input-output data. Here, careful considerations need to be exercised so that the measurements contain maximum information about underlying process. The design of manipulated input is of prime significance as it should be able to excite the system effectively. Other important parameters such as sampling period and operating region need to be chosen carefully.
- **Selection of model structure**– This is one of the crucial and time taking step in the system identification procedure. A set of model structures are selected such that they are able to represent the process suitably. Model structures are selected by analyzing the data combined with formal properties of models. Generally, non-parametric models like impulse or frequency response can be estimated to find insights into the properties of the system. For more specific model descriptions, one can choose from a wide array of black box model structures. Parametric model structures such as ARX (Auto Regressive with eXogenous input), ARMAX (Auto Regressive Moving Average with eXogenous input), BJ (Box-Jenkins), OE (Output Error), *etc.* models can be employed to acquire specific process description.
- **Model estimation**– This step determines the ‘best model’ that describes data among different model sets according to the chosen criterion. There are various classes of system identification such as Prediction Error Method (PEM) [1], Instrumental Variable (IV) [36], and subspace methods [5]. PEM contain various computational approaches in finding model parameters like linear regression, least-squares, and maximum-likelihood methods. The IV approach belongs to the correlation family of algorithms. Subspace methods are another class of algorithms which can be used to estimate state space models from experimental data.

- **Model Validation**– It is carried out by residual analysis and by cross-validation. Residual analysis examines innovation sequence/residuals obtained after model estimation from training dataset. Residual analysis consists of *whiteness test* and *independence test*. The whiteness test checks autocorrelation of the residuals at the output. If correlation coefficients lie within the confidence interval, then it is concluded that the residuals do not contain any significant information. On the other hand, test of linear independence calculates dependency of residuals on past input signal through cross-correlation. Insignificant value of coefficients guarantees that there is nothing lying in the residual to be governed by input to the system. Cross-validation is another rigorous approach where the estimated model is validated by various test datasets which are different from the training dataset.

The flow diagram of the system identification loop is shown in Figure 2.1, which starts from collecting data followed by choosing the model set and then selecting the best model from this set. Finally, it is to be remember that a model can never be a true description of the system. Rather, it can be taken as a good enough description of certain aspects that are of particular interest to its end use.

2.2 Modeling of Nuclear Reactors

Operational transients in a nuclear reactor usually evolve at different scale of time ranging from seconds to minutes. The prompt neutrons have influence till some milliseconds whereas delayed neutrons, xenon build-up, and core composition changes are responsible for longer transients. Theoretically, dynamics of nuclear reactors can be described by the time-dependent Boltzmann transport equation [37]. However, its use coupled with delayed neutron precursors' equations is difficult for neutron kinetics problems of practical interest. Nevertheless, these problems can be solved with approximate methods such as time-dependent group diffusion equation. The simplest form derived from

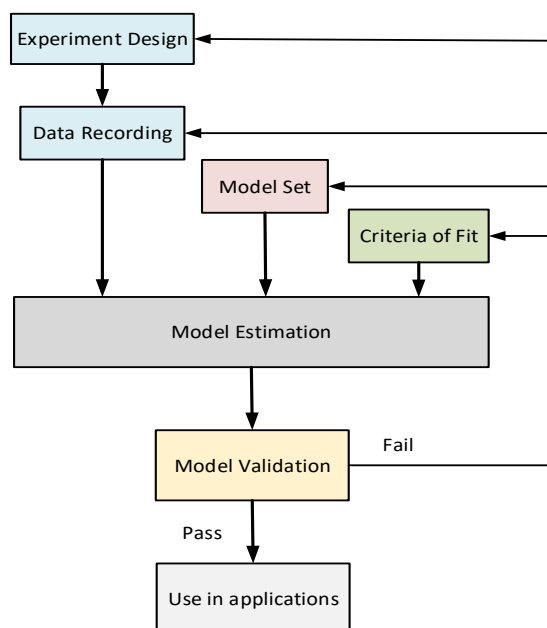


FIGURE 2.1: Flow diagram of the system identification loop.

the original Boltzmann equation is known as the point reactor kinetics model. It assumes that production, diffusion, absorption, and leakage of neutrons take place at single energy independent of space variables. The point kinetics model have been widely used for developing control strategies. In a recent work, Subudhi et al. [38] used the point kinetics equations for total power control studies of Pressurized Heavy Water Reactor (PHWR).

In large nuclear reactors where physical size is quite a lot of times the neutron migration length, point reactor kinetics model will not suffice since the flux shape undergoes variations and due to probability of occurrence of spatial oscillations. Moreover, large reactors have functionally distinct materials, *e.g.* fuel, coolant, moderator, reflector, and control mechanisms *etc.*, distributed in the core. In addition, they have various regions with different burn-ups and coolant densities. Within the core periphery, neutrons continuously either loose or gain energy, diffuse from one location to another, and undergo several interactions with matter. Thus, time dependent group diffusion equation should be supported by the methods for treating the spatial variables. Such advanced methods

can be classified as space-time methods, modal and synthesis methods, and direct methods. Core neutronics model of large PHWR based on the nodal approximation of the neutron diffusion equation has been reported in [39, 40]. Gaikwad *et al.* [41] presented a simplified core thermal hydraulics model for large PHWR for evaluating the transient performance of the pressure control loop.

Applications of system identification have been found in modeling, designing controller, and in analyzing dynamic properties of NPP. For instance, Pomerantz *et al.* [42] validated a theoretical model with experimental data for flux mapping. Lathouwers *et al.* [43] presented a linear dynamic model of a fluidized bed nuclear reactor. Linear system identification techniques have been applied to obtain mathematical models of a simulation of the pebble bed modular reactor [44]. Gabor *et al.* [4] discussed system identification of a LTI state-space model of a Vodo Vodyanoi Energetichesky Reaktor (VVER). System identification techniques have been used to model plant dynamics around various operating points during step-back transients [45]. Validation of model of primary loop of VVER-type nuclear power plants for controller design purposes has been reported in [46]. Sohn *et al.* [47] utilized system identification approach to build simplified Steam Generator (SG) model for designing the feed-water control system. Polifke [48] combined computational fluid dynamics simulation with system identification to characterize dynamic response of a sub-system to incoming flow perturbations.

In some recent works, system identification has been combined with Artificial Neural (ANN) and fuzzy logic. Kim *et al.* [49] estimated parameters of Pressurized Water-type Reactor (PWR) cores using ANN models. Recurrent neural network based algorithms have been proposed to identify reactor core models [50, 51]. Boroushaki *et al.* [52] combined a nonlinear ARX model structure with ANN for the core identification of VVER-type nuclear reactor and the identified model is used in predicting the behavior of reactor dynamics. Khalafi *et al.* [53] developed a research reactor simulator using identified ANN model. A neuro-fuzzy model based identification techniques has been applied to predict the water level in the SG of a PWR [54].

In most of the reported works, reactor is considered as a LTI process evolving at single-scale. Although, nuclear reactors are multiscale processes in which multiple modes exist at different scales of time and frequency. It manifests multi-timescale behavior when operated under different power regimes. These multiscale features may not be modeled correctly by the above discussed approaches. Thus, it is essential to conduct a process visualization and modeling exercise in a multiresolution framework.

2.3 Subspace Identification

Subspace identification is a standard technique for time-domain state-space model estimation from measured input-output data [5]. Precisely, subspace identification estimates the model by employing prediction first and then using geometrical projection for parameter estimation making it different from usual identification approaches. A comparison between classical identification and subspace identification is depicted in Figure 2.2.

The initial introduction to subspace methods is found in the works of Ho and Kalman [55], Zeiger and McEwen [56], and others. These works are based on realization theory and attempt to estimate state-space models through the Hankel matrix formulation of the impulse response or Markov parameters of the system. Since then, there are several variants of subspace methods proposed in the literature and out of them three are very popular and widely used. They are Canonical Variate Analysis (CVA) introduced by Larimore [57], Multi-variable Output Error State Space (MOESP) presented by Verhaegen and Dewilde [58, 59], and Numerical algorithms for Subspace State-Space System Identification (N4SID) proposed by Van Overschee and De Moor [60]. The CVA algorithm is based on canonical correlation analysis. The MOESP estimate the extended observability matrix to compute the state-space matrices using the joint input-output data matrices representation. The N4SID projects the future data onto past data to estimate the state sequences. The state sequences are then combined with original input-output data to find system matrices as least squares solution. Viberg [61] discussed about the

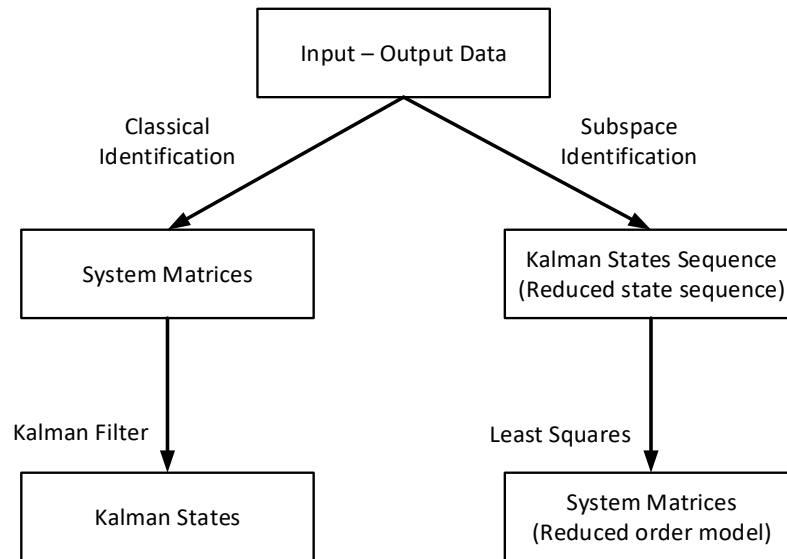


FIGURE 2.2: Comparison of system identification with subspace identification.

relationship among different algorithms. Further, a unifying framework of different algorithms is presented in [62] where it is concluded that all of the algorithms differ in the choice of weighing matrix. Detailed surveys on subspace methods providing insightful discussion are given in the works of Haverkamp [63] and Trnka [64]. Wahlberg *et al.* [65] discusses subspace methods from the perspective of process industry users.

Subspace methods have been designed to suit recursive application by Kameyama and Ohsumi [66], Lovera *et al.* [67], Mercre *et al.* [68] and Oku and Kimura [69]. Furthermore, subspace methods have been extended to the application on frequency domain data by Van Overschee and De Moor [70] and Pintelon [71].

In spite of their wide applicability, subspace-based methods have found very few applications in nuclear science [72, 73, 74, 75]. Bittani *et al.* [72, 73] applied subspace methods for the identification of the poles and zeros position of an analog amplifier for nuclear spectroscopy. Shiguo *et al.* [74] combined subspace approaches with data pre-filtering techniques to enhance the prediction accuracy in pole identification. In [75], the methodology is used for the identification of light charged particles.

2.3.1 Notation

Let us consider a discrete time Linear Time Invariant (LTI) system, expressed by state-space model in *innovation* form, *i.e.*,

$$\begin{aligned} x[k+1] &= Ax[k] + Bu[k] + Ke[k], \\ y[k] &= Cx[k] + Du[k] + e[k], \end{aligned} \quad (2.1)$$

where the state $x[k] \in \mathbb{R}^n$, the input $u[k] \in \mathbb{R}^m$, the output $y[k] \in \mathbb{R}^l$, innovation sequence $e[k] \in \mathbb{R}^l$ with $E(e[k]e^T[k]) = S$, and k is the current time instant. $A \in \mathbb{R}^{n \times n}$, $B \in \mathbb{R}^{n \times m}$, $C \in \mathbb{R}^{l \times n}$, $D \in \mathbb{R}^{l \times m}$, and $K \in \mathbb{R}^{n \times l}$ are system dynamics matrix, input matrix, output matrix, feed through matrix, and Kalman gain respectively. The problem of subspace identification deals with estimation of system matrices A, B, C, D , and K directly from the input-output data. Let us set up the input data block Hankel matrix as

$$U_f = \begin{bmatrix} u[k] & u[k+1] & \cdots & u[k+N-1] \\ u[k+1] & u[k+2] & \cdots & u[k+N] \\ \vdots & \vdots & \ddots & \vdots \\ u[k+f-1] & u[k+f] & \cdots & u[k+f+N-2] \end{bmatrix} \quad (2.2)$$

$$(2.3)$$

$$U_{fi} = \begin{bmatrix} U_{f1} \\ U_{f2} \\ \vdots \\ U_{fi} \end{bmatrix}; \text{ and } U_i = \begin{bmatrix} U_{f1} \\ U_{f2} \\ \vdots \\ U_{fi} \end{bmatrix}; i = 1, 2, \dots, f \quad (2.4)$$

where $U_{fi} = \begin{bmatrix} u[k+i-1] & u[k+i] & \cdots & u[k+N+i-2] \end{bmatrix}$ and f is the order of predictor matrix and represents the future horizon. Similarly, we can define Y_f, Y_{fi} and Y_i using output data and E_f, E_{fi} , and E_i using innovations. The state sequence is defined as,

$$X_k = \begin{bmatrix} x[k] & x[k+1] & \cdots & x[k+N-1] \end{bmatrix}. \quad (2.5)$$

Thus, we can write

$$Y_f = \Gamma_f X_k + H_f^d U_f + H_f^s E_f \quad (2.6)$$

where $\Gamma_f \in \mathbb{R}^{f l \times n}$ is the extended observability matrix given by

$$\Gamma_f = \begin{bmatrix} C^T & (CA)^T & \dots & (CA^{f-1})^T \end{bmatrix}^T; \quad (2.7)$$

$H_f^d \in \mathbb{R}^{f l \times f m}$ and $H_f^s \in \mathbb{R}^{f l \times f l}$ are deterministic and stochastic lower block-triangular Toeplitz matrices consisting of impulse response coefficients to respective inputs, given by

$$H_f^d = \begin{bmatrix} D & 0 & 0 & \dots & 0 \\ CB & D & 0 & \dots & 0 \\ CAB & CB & D & \dots & 0 \\ \vdots & \vdots & \vdots & \ddots & \vdots \\ CA^{f-2}B & CA^{f-3}B & CA^{f-4}B & \dots & D \end{bmatrix}; \quad (2.8)$$

$$\text{and } H_f^s = \begin{bmatrix} I & 0 & 0 & \dots & 0 \\ CK & I & 0 & \dots & 0 \\ CAK & CK & I & \dots & 0 \\ \vdots & \vdots & \vdots & \ddots & \vdots \\ CA^{f-2}K & CA^{f-3}K & CA^{f-4}K & \dots & I \end{bmatrix}; \quad (2.9)$$

2.3.2 Open-loop Subspace Identification

The system given by (2.1) can be represented in *predictor* form as

$$x[k+1] = A_K x[k] + \bar{B}_K z[k], \quad (2.10)$$

$$y[k] = Cx[k] + Du[k] + e[k], \quad (2.11)$$

where $A_K = A - KC$, $B_K = B - KD$, $\bar{B}_K = \begin{bmatrix} B - KD & K \end{bmatrix}$, and $z[k] = \begin{bmatrix} u^T[k] & y^T[k] \end{bmatrix}^T$. Using recursion, we can write (2.11) as

$$x[k] = L_p z_p[k] + A_K^p x[k-p] \quad (2.12)$$

where p denotes the past horizon, $z_p[k] = \begin{bmatrix} z^T[k-1] & z^T[k-2] & \cdots & z^T[k-p] \end{bmatrix}^T$ and $L_p = \begin{bmatrix} \bar{B}_K & A_K \bar{B}_K & \cdots & A_K^{p-1} \bar{B}_K \end{bmatrix}$.

From (2.5) and (2.12), we can write

$$X_k = L_p Z_p + A_K^p X_{k-p}, \quad (2.13)$$

where $X_{k-p} = \begin{bmatrix} x[k-p] & x[k-p+1] & \cdots & x[k-p+N-1] \end{bmatrix}$ and $Z_p = \begin{bmatrix} z_p[k] & z_p[k+1] & \cdots & z_p[k+N-1] \end{bmatrix}$.

Now, using (2.13) in (2.6), we get

$$\begin{aligned} Y_f &= \Gamma_f L_p Z_p + \Gamma_f A_K^p X_{k-p} + H_f^d U_f + H_f^s E_f, \\ &= L_x Z_p + \Gamma_f A_K^p X_{k-p} + H_f^d U_f + H_f^s E_f, \end{aligned} \quad (2.14)$$

where $L_x = \Gamma_f L_p$ is the product of the process observability matrix and predictor controllability matrix. The output equation is expressed as the product of observability and controllability matrix and Toeplitz matrix using the dataset. There are two primary routes for solving this open-loop subspace identification problem. The first approach estimates the state sequence and observability matrix and determines full system matrices in a single step through the least squares. The second technique estimates only the observability matrix. It is observed that most of open-loop subspace identification approaches involve primarily three basic steps: projection or regression, model reduction, and parameter estimation. We will discuss each steps in detail in Chapter 4.2.

2.3.3 Closed-loop Subspace Identification

The earlier approaches on subspace identification deal with open-loop identification problem. They suffer from biases in model estimation if the data is collected under closed-loop settings due to correlation of the input signal with the process and noise sources. Recent studies have established closed loop subspace identification to handle the bias issue effectively. Verhaegen [76] proposed combine identification of the closed-loop system with the knowledge about controller. Chou et al. proposed an IV-based identification technique for a restricted class of closed-loop systems [77]. Van Overschee et al. [78] proposed closed-loop identification method using a priori knowledge about controller. Ljung [79] proposed a high-order ARX modeling approach to deal with correlation issues. Qin et al. [80] proposed an algorithm based on the estimation of innovations. Jansson [81] developed a predictor based closed-loop state estimation. Most of these methods require explicit knowledge of the controller or are based on assumptions that limit their applicability. Recently, Chiuso et al. [82] developed a method that does not require explicit knowledge of the controller. In the survey paper by Qin [83], different variations of open-loop and closed-loop subspace identification algorithms are presented. A recent paper by Van der Veen *et al.* [84] presents an overview of closed-loop subspace identification methods.

In case of closed-loop operations, the future input is correlated with past output measurement or past noise *i.e.* the last two terms of (2.14) are correlated for closed-loop systems. This leads to biasing in open-loop identification methods. Most of the closed-loop approaches proposed in the literature try to decouple these two terms. Using the

predictor form (2.11), we can write using recursion

$$\begin{bmatrix} y[k] \\ y[k+1] \\ \vdots \\ y[k+f-1] \end{bmatrix} = \begin{bmatrix} C \\ CA_K \\ \vdots \\ CA_K^{f-1} \end{bmatrix} x[k] + \begin{bmatrix} 0 & 0 & \cdots & 0 \\ C\bar{B}_K & 0 & \cdots & 0 \\ \vdots & \vdots & \ddots & \vdots \\ CA_K^{f-2}\bar{B}_K & CA_K^{f-2}\bar{B}_K & \cdots & C\bar{B}_K \end{bmatrix} \begin{bmatrix} z[k] \\ z[k+1] \\ \vdots \\ z[k+f-2] \end{bmatrix} + \begin{bmatrix} D \\ D \\ \vdots \\ D \end{bmatrix} \begin{bmatrix} u[k] \\ u[k+1] \\ \vdots \\ u[k+f-1] \end{bmatrix} + \begin{bmatrix} e[k] \\ e[k+1] \\ \vdots \\ e[k+f-1] \end{bmatrix} \quad (2.15)$$

or simply,

$$y_f[k] = \bar{\Gamma}_f x[k] + \bar{G}_f[k] z_{f-1}[k] + D_f u_f[k] + e_f[k] \quad (2.16)$$

Using (2.12), we can further write

$$y_f[k] = \bar{\Gamma}_f L_p z_p[k] + \bar{\Gamma}_f A_K^p x[k-p] + \bar{G}_f[k] z_{f-1}[k] + D_f u_f[k] + e_f[k]. \quad (2.17)$$

Typically, $D = 0$ is considered. In case that $D \neq 0$, there must be a delay in the feedback loop, making $u_f[k]$ uncorrelated with $e_f[k]$. For large of p , $A_K^p \simeq 0$ and (2.17) can be approximated as

$$y_f[k] = \bar{\Gamma}_f L_p z_p[k] + \bar{G}_f z_{f-1}[k] + e_f[k] \quad (2.18)$$

Note that due to feedback $e_f(k)$ is correlated with $z_{f-1}[k]$. Equation (2.18) is composed of f block rows in each term. Partitioning it row-wise and defining

$$\bar{\Gamma}_{fi} = CA_K^{i-1} \quad (2.19)$$

$$\bar{G}_f = \begin{bmatrix} CA_K^{i-2} B_K & CA_K^{i-3} B_K & \cdots & CB_K \end{bmatrix} \quad (2.20)$$

$$\text{and } z_{i-1}[k] = \begin{bmatrix} z^T[k] & z^T[k+1] & \cdots & z^T[k+i-2] \end{bmatrix}^T. \quad (2.21)$$

Thus, the i^{th} row is given by

$$y[k + i - 1] = \bar{\Gamma}_{fi} L_p z_p[k] + \bar{G}_{fi} z_{i-1}[k] + e[k + i - 1], \quad i = 1, 2, \dots, f. \quad (2.22)$$

Using least squares $\bar{\Gamma}_{fi} L_p$ can be estimated, which then form $\widehat{\bar{\Gamma}_f L_p}$. One can then perform weighted SVD to estimate $\widehat{\bar{\Gamma}_f}$ which further gives model parameters.

2.4 Wavelet Basis Functions

Wavelet was first introduced by Hungarian mathematician Haar [85] back in 1909 for functional analysis and now is known as Haar wavelet. In 1946, Gabor introduced a transform to separate a wave into time-frequency packets and called it Gabor transform. In 1970s and 1980s, signal processing community have developed techniques such as sub-band coding, quadrature mirror filters, and pyramidal algorithm which have similar features to wavelets. However, the term wavelet was first used by Morlet and Grossman in 1984. Meyer realized the connection between Morlet's wavelets and earlier mathematical wavelets and formulated orthogonal wavelets. Mallat and Meyer created a framework for wavelet expansions called Multi Resolution Analysis (MRA) and established link among orthonormal wavelet bases [86], subband coding [87], and pyramid coding. The current impact of wavelet is due to integration of parallel works in the field of mathematics, signal & image processing, and computer vision. The literature of wavelets is overwhelmed with different variants of wavelet transforms and their implementations. Wavelets have inspired several researchers to develop new transforms such as ridgelet, curvelet, and contourlet transforms to name a few. Some profound development in the field of wavelets is due to the works by Mallat [86], Vetterli [87], Meyer [88], Daubechies [89], Donoho [90, 91] and others.

2.4.1 Fundamentals

The function space $L^2(\mathbb{R})$ is a Hilbert space of square integrable functions *i.e.* all real functions which have finite energy and whose L^2 -norms are finite. The L^2 -norm of a function A is given by

$$\|A\| = \left(\int_{-\infty}^{+\infty} |A(t)|^2 dt \right)^{1/2} = \sqrt{\langle A, A \rangle} \quad (2.23)$$

where \langle, \rangle represents the inner product. Assume that the input-output signals belong to L^2 space. V_u and V_y are the corresponding subspaces of L^2 containing approximation of input and output signals respectively. These subspaces are called as projection spaces and are spanned by the shift invariant basis function χ and ξ respectively. Cardinal series expansions of input and output on to generalized basis functions are given by

$$u(x) = \sum_{k \in \mathbb{Z}} C_u[k] \chi(x - kT) \quad (2.24)$$

$$y(x) = \sum_{k \in \mathbb{Z}} C_y[k] \xi(x - kT) \quad (2.25)$$

where $C_u[k]$ and $C_y[k]$ are coefficients of basis function belonging to l^2 (l^2 is vector space of square summable discrete sequences). An orthogonal projection of input/output on subspace V_u/V_y with minimum error is given by

$$\tilde{u}(x) = \sum_{k \in \mathbb{Z}} \langle u(x), \chi(x - kT) \rangle \chi(x - kT) \quad (2.26)$$

$$\tilde{y}(x) = \sum_{k \in \mathbb{Z}} \langle y(x), \xi(x - kT) \rangle \xi(x - kT) \quad (2.27)$$

$C_u[k] = \langle u(x), \chi(x - kT) \rangle$ and $C_y(k) = \langle y(x), \xi(x - kT) \rangle$ give the signal contribution along the direction of specified basis function. The inner product can be implemented in terms of filtering and sampling [92]

$$(u * \chi)(x)|_{x=kT} = \sum_{k \in \mathbb{Z}} u(x) \chi(kT - x) = \langle u(x), \bar{\chi}(x - kT) \rangle \quad (2.28)$$

$$(y * \xi)(x)|_{x=kT} = \sum_{k \in \mathbb{Z}} y(x) \xi(kT - x) = \langle y(x), \bar{\xi}(x - kT) \rangle \quad (2.29)$$

where $\bar{\chi}(x) = \chi(-x)$ and $\bar{\xi}(x) = \xi(-x)$. The inner product of measurement function with the integer shift of time reversed impulse response is equivalent to first low pass filtering and sampling thereafter. In Shannon's sampling theory orthonormal *sinc* basis function are chosen for function expansion. In general, basis functions are not necessarily need to be orthogonal. They can be biorthogonal or spline in nature.

2.4.2 Continuous Wavelet Transform

Continuous Wavelet Transform (CWT) of a finite energy signal $f(t)$ is given as the correlation between $f(t)$ and the dilated version of wavelet function. It is calculated using the inner product as

$$\left\langle f(t), \frac{1}{\sqrt{s}} \psi \left(\frac{t - \tau}{s} \right) \right\rangle = \frac{1}{\sqrt{s}} \int_{-\infty}^{\infty} f(t) \psi^* \left(\frac{t - \tau}{s} \right) dt, \quad (2.30)$$

where $s \in \mathbb{R}^+$ and $\tau \in \mathbb{R}$ are dilation and translation parameters respectively. The change in scale governs dilation parameter, it either stretches or contracts to keep the energy contained as constant. Translation parameter shifts the wavelet on to the given signal in a continuous fashion. Wavelet transformation is achieved by continued scaling and translation of the wavelet function along the length of a signal. Equation (2.30) can also be written in convolution form as

$$\left\langle f(t), \frac{1}{\sqrt{s}} \psi \left(\frac{t - \tau}{s} \right) \right\rangle = f * \frac{1}{\sqrt{s}} \psi^* \left(\frac{-\tau}{s} \right) \quad (2.31)$$

which shows that the computation of CWT is equivalent to filtering $f(t)$ by a filter with impulse response $\frac{1}{\sqrt{s}}\psi^*\left(\frac{-t}{s}\right)$. The basic property for qualifying $\psi(t)$ as a wavelet is known as admissibility condition. It is given as

$$C_\psi = \int_0^\infty \frac{|\psi(\omega)|}{\omega} d\omega < \infty \quad (2.32)$$

where $\psi(\omega)$ represents the Fourier transform. The admissibility condition ensures that $\psi(\omega)$ goes to zero as $\omega \rightarrow 0$. It is equivalent to

$$\int_{-\infty}^\infty \psi(t) dt = 0. \quad (2.33)$$

One more thing to note is the relation between dilation parameter or scale to frequency. Scale s is inversely proportional to frequency f and is related by the following relation

$$s = \frac{f_c \cdot T_s}{f} \quad (2.34)$$

where T_s is sampling period and f_c is center frequency.

2.4.3 Discrete Wavelet Transform

Discrete Wavelet Transform (DWT) is a computationally efficient wavelet transform calculated by making $s = 2^j$ and $\tau = 2^j * k$, where j and k are scale and position indices with $j, k \in \mathbb{Z}$. The DWT of a signal $f(t)$ is calculated as an inner product with dilates of wavelet $\frac{1}{\sqrt{2^j}}\psi\left(\frac{t-2^j k}{2^j}\right)$.

$$\left\langle f(t), \frac{1}{\sqrt{2^j}}\psi\left(\frac{t-2^j k}{2^j}\right) \right\rangle = \frac{1}{\sqrt{2^j}} \int_{-\infty}^\infty f(t)\psi\left(\frac{t-2^j k}{2^j}\right)^* dt, \quad (2.35)$$

The function $f(t)$ can be represented using wavelet as

$$f(t) = \sum_{x=-\infty}^{\infty} c_{J+1,x} \phi_{J+1,x}(t) + \sum_{j=j_0}^J \sum_{x=-\infty}^{\infty} d_{j,x} \psi_{j,x}(t), \quad (2.36)$$

where ϕ and ψ respectively denote the scaling function and wavelet function. The coefficients $c_{J+1,x}$ and $d_{j,x}$ are called as approximation and detail coefficients respectively and together referred as wavelet coefficients. Scale j_0 and J represent the initial and final level of decomposition while $J + 1$ represents approximation at J^{th} scale. These coefficients are calculated through the inner product of (2.36) with respective basis function. Moreover, they can be efficiently obtained using matrix multiplication via fast wavelet transform [86].

The computation of DWT requires both wavelet and scaling functions, whereas the CWT makes use of a single wavelet basis; the DWT also requires that both functions are orthonormal. DWT provides a compact representation, whereas CWT gives a highly redundant representation. This is further explained using the time-frequency tiling diagram in Figure 2.3. CWT is defined at all points in the plane and corresponds to a redundant representation while DWT is computed only for the dyadic values of s . Figure 2.3 also compares the time-frequency tiling of DWT with Fourier Transform and short-time Fourier Transform. In Fourier Transform, frequency axis is divided uniformly while, time info is completely lost. Whereas, in sort time Fourier Transform, a windowed Fourier Transform is computed which takes time and frequency resolutions into consideration. Here, the tiles are of uniform shape all across the plane. In case of DWT, the area under a tile remains fixed while the shape varies providing variability in time-frequency resolution. The dyadic discretization of scales and translations render a MRA attribute to DWT. The approximation and detail spaces are spanned by scaling and wavelet function respectively. In most of the cases, every wavelet function is characterized by a scaling function. The scaling function is called as father wavelet and wavelet function as mother wavelet. These functions are related through a two-scale relation. For a detailed discussion readers are advised to refer [12, 86, 87].

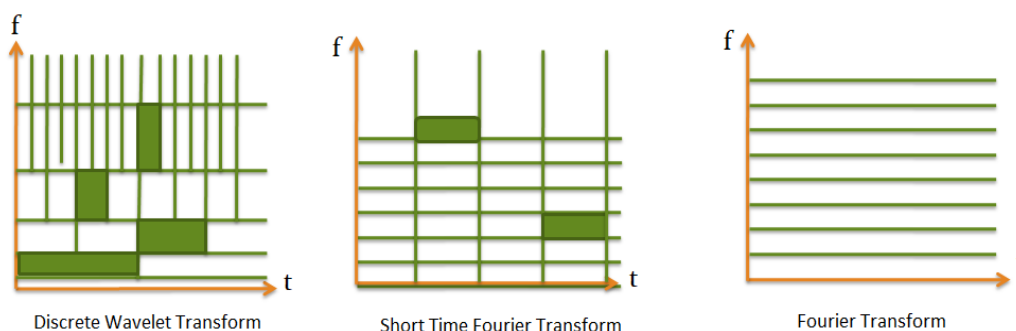


FIGURE 2.3: Time-frequency tilings

The filter bank implementation of DWT is depicted in Figures 2.4 and 2.5. The wavelet filter bank structure consists of an analysis side and a synthesis side. The analysis filter bank contains two branches one with low-pass filter (LPF) and other with high-pass filter (HPF) and are followed by downsampler. The incoming input signal is applied to the LPF and the HPF branches. The output of LPF and the HPF are called as approximation and detail coefficients respectively and together referred as wavelet coefficients. The approximation coefficients lie in the approximation space while, detail coefficients lie in detail space. Approximation is a low-frequency signal carrying trend of the signal while detail is a high-frequency information signal. These coefficients can be processed before reconstruction. The synthesis or reconstruction filter bank upsample the wavelet coefficients before feeding it to LPF and HPF branches. The output is then combined to give preprocessed reconstructed signal. The filter banks are designed to give perfect reconstruction after synthesis.

2.5 Application of Wavelets

Wavelets have been used in different forms depending on the requirement. They have been used in empirical modeling, process monitoring, control design, gross-error detection, filtering, and in deriving solutions to partial differential equations. Wavelets offered benefits such as signal compression, signal estimation, data reconciliation, and feature extraction. In engineering applications, wavelets have been used mainly in two

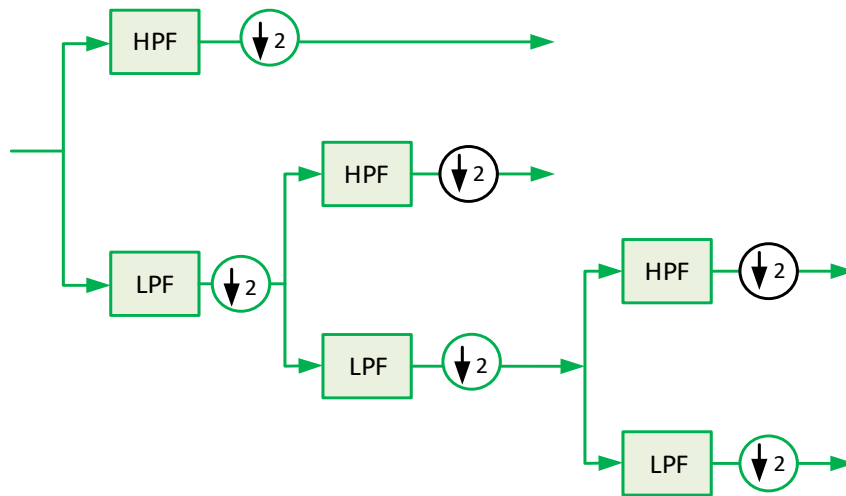


FIGURE 2.4: Block diagram of analysis filter bank

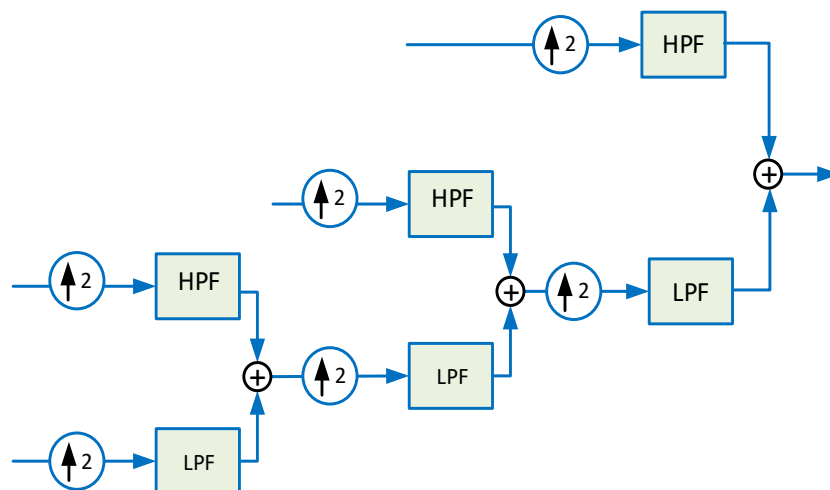


FIGURE 2.5: Block diagram of synthesis filter bank

different ways, as a preprocessing tool and in integration with other single-scale methods.

Wavelet preprocessing or thresholding followed by signal synthesis is a well established signal denoising technique that enables nonlinear approximation of a function. It preserves the relevant signal components while efficiently removing the contribution due to noise. It is proved to be near optimum in the minimax sense and gives better convergence rate as compared to other linear methods of approximation over a wide class

of function spaces. The signal to be denoised is either hard thresholded whereby the wavelet coefficients below a certain threshold are made equal to zero or soft thresholded wherein the wavelet coefficients are reduced by the given threshold. There are different wavelet-based thresholding approaches for denoising a signal corrupted with noise viz. *MiniMax*, *VisuShrink* (universal threshold) [90], and *SureShrink* (level-dependent threshold) [91]. The process of denoising starts with projecting the signal on suitable wavelet basis. The projection operation decorrelates wavelet coefficients of signal from that of the noise. The threshold is usually applied to the detail coefficients. The denoised signal in measurement domain is reconstructed by employing inverse wavelet transform to get denoised or wavelet filtered signal. The amplitude thresholding of the wavelet coefficients is justified as there is no significant loss of useful information in the denoised signal.

Wavelet transform have been integrated with some of the well known single-scale techniques such as state estimation, statistical process monitoring and control, neural networks, and system identification to design their multiscale variants. Multiscale approaches are designed to handle and take advantage of the information contained at different scales. Chou *et al.* [93] constructed Kalman filter on dyadic trees. Hong *et al.* [94] proposed Kalman filtering in a multiresolution framework implemented over data blocks and demonstrates that it outperform the classical Kalman filtering technique. Stephanopoulos *et al.* [95, 96] converted physical models in time to multiscale models on a dyadic tree and developed algorithms state estimation and model predictive control in multiresolution framework. Multiscale MPC application to a batch reactor appears in a work by Krishnan and Hoo [97]. Zhang *et al.* [98, 99] tried to improve the Hong's algorithms by developing state-space model in multiresolution to which the classical Kalman filtering technique can be directly employed. Nounou *et al.* [100] developed a multiscale Kalman filtering using stationary wavelet transform where it is shown that the model structure remains unaltered across all scales. A wavelet-based robust trans-scale state estimation algorithm is proposed by Zhao and Jia [101] for discrete-time systems.

Different works have been reported on multiscale statistical process monitoring. MSPCA [26] is one of the model-free multiscale statistical process monitoring approach. It was developed in the similar spirit of multiscale Kalman filtering by combining the variable decorrelation ability of PCA with the deterministic feature extraction quality of wavelet transform. An application of this approach to fault detection in industrial boilers can be found in Misra *et al.* [102]. Multiscale Bayesian PCA [103] and multiscale Bayesian latent variable regression [104] are proposed as model-based multiscale process monitoring approaches. A comprehensive review of multiscale statistical monitoring of both univariate and multivariate processes is given in [105].

Wavelet have been integrated with neural networks to design wavelet network structure which uses wavelets as activation functions. Bakshi and Stephanopoulos [106] introduced wavelet as noniterative and hierarchical algorithm in which dilation and translation are on dyadic scales. On the contrary, Zhang and Benveniste [107] proposed a wavelet decomposition network where the wavelet networks learn iteratively through a backpropagation algorithm. Some variations of the wavelet networks have also been proposed. For instance, Thuillard [108] proposed a fuzzy wavelet network to employ wavelet scaling function as membership functions in the Takagi-Sugeno (T-S) model for fuzzy rules. Aadaleesan *et al.* [109] combined wavelet networks with orthonormal basis functions. Lu *et al.* [110] proposed an optimal wavelet network using wavelets as kernel functions in a SVR framework.

2.6 Identification using Wavelets

In the literature of system theory, multiple perspectives exist for introducing wavelets in modeling and identification [10, 11, 111, 112], *e.g.* function approximation, filter banks, *etc.* The earliest work by Basseville *et al.* [113], framed the notion of stochastic modeling on dyadic trees for auto-regressive processes. The system is represented by different nodes of homogeneous trees. Chou *et al.* [14] constructed a class of multi-scale dynamic state-space models on dyadic trees for handling multiscale data structure.

However, these algorithms seem to model process dynamics across scales rather than along them and tend to ignore evolution of modes with time. Tsatsanis and Giannakis [114] adopted the function approximation route of modeling where the Linear Time Varying (LTV) parametric impulse response function is approximated by wavelet basis functions. Doroslovacki and Fan [115] proposed identification and adaptive filtering of LTV systems using wavelet basis. LTV impulse response is expressed as a linear combination of wavelet basis with time-varying coefficients. Nikolaou and Vuthandam [116] developed reduced-order modeling for the class of Finite Impulse Response (FIR) models. The proposition behind these approach is that the LTV coefficients can be approximated by LTI coefficients in the wavelet domain. Zhao *et al.* [117] formalizes the theory of aforementioned works using biorthogonal wavelet functions. These works assume local time invariance in the formulation which may not be valid for fast changing systems. Besides, the selection of basis function is rather difficult for such a system and one needs to know certain aspects of a process, a priori, which defeats the notion of true black-box system identification. The LTV parameter estimation of a dynamical system described by differential equation is studied in [118]. Dorfan *et al.* [119] shows that a wavelet model is suitable for adaptive identification of linear periodically time-varying systems. A related work by Satoa *et al.* [120] developed vector autoregressive models for LTV systems wavelet expansion coefficients. A general multiscale nonlinear polynomial model structure is designed by Billings *et al.* [121]. In [122], authors developed nonlinear system modeling using B-spline wavelet basis function. In a similar approach, He *et al.* [18] incorporated multiwavelets in the identification and frequency domain analysis. Nevertheless, these approaches completely ignored the effective way of inverse wavelet transform for mapping output in projection space to that in measurement space.

The filter bank aspects of wavelets are employed utilizing the computationally efficient implementation of wavelets. The basic idea in most of the cases is of multiscale input/output data representation using suitable wavelet and then selecting only the relevant sub-bands in reconstruction. The reconstructed input/output data are then used for

building models. Carrier *et al.* [13] advocated frequency domain approach where the estimation of reduced order models over a specific range of frequencies is proposed for control relevant identification. They employed the knowledge of crossover frequency to determine the relevant scales. This viewpoint is further emphasized by Vana and Preisig [123] and they discussed several theoretical aspects while working with wavelets. They proposed estimation of reduced order model in frequency domain using wavelets with a weighing matrix. Palavajhala *et al.* [124] used the criteria of maximizing SNR to select the relevant scales for identification. A wavelet-packet based approach for LTI system identification is developed by Paiva [22]. Chang and Qu [16] formulated the problem of identification of partially linear model as a l_1 -norm penalized least squares. A CWT-based time-frequency representation of input/output has been proposed for the LTV system identifying by Shan and Burl [25]. The work also proposed different scale selection measure to reduce the dimensionality of parameter vector. Mukhopadhyay and Tiwari [24] employs the notion of consistency in output estimate and developed models at all scales for the liquid zone control system. Nounou *et al.* [20, 21, 23] used the multiscale representation ability of wavelets to improve the prediction accuracy of empirical models, namely, the multiscale ARX, multiscale FIR, and multiscale T-S fuzzy models by estimating parameters only at an appropriate scale. Reis [125] proposed an algorithm to handle multiscale data structure in prediction framework. In some recent works, authors developed wavelet-based state-space model estimation technique for mechanical systems with known functional forms [126, 127]. The aforementioned methods demonstrate their superiority over single-scale methods but do not fully exploit the advantages of a multiscale decomposition. Most of the reported works identify input-output polynomial models from the data. Only a few studies focuses on state-space model estimation. However, for the purpose of control, state-space representations are usually preferred such that controllers for MIMO can be designed smoothly.

2.7 Wavelets in Nuclear Engineering

In the last two decades, wavelet-based techniques have been widely applied in NPP for noise removal [128, 129, 130, 131, 132, 133, 134], transient detection [135, 136], and for modeling and control [24, 137, 138, 139]. Estimation and monitoring of reactivity coefficients like moderator temperature coefficient using wavelet denoising technique is proposed in [128]. Heo *et al.* [129] designed a wavelet-PCA based multi-step denoising technique for the estimation of reactor power under degraded flow-meter. Park *et al.* [130] demonstrated application of wavelet denoising in water-level control of SG. DWT-based denoising technique is applied for power feedback in regulating system [131]. Hadad *et al.* [132] used wavelet transform based ANN for fault recognition and classification in a NPP. Montalvo *et al.* [133] improved the response times of in situ measurement of detectors signals using DWT. An adaptive Morlet wavelet transform based method for extracting weak impact signal and to remove interfering noise in NPP is proposed by Cao *et al.* [134]. Espinosa-Paredes *et al.* [135] studied transient instability phenomenon of neutronic power oscillation in a Boiling Water Reactor (BWR) using wavelets. Prieto-Guerrero *et al.* [136] applied wavelet ridges of the system impulse response for the estimation of decay ratio and to further evaluate stability parameters using neutronic measurements. In [137], a power spectral density based modeling strategy is formed during a transient via wavelet MRA. Integration of wavelet MRA with correlation function has been proposed for the estimation of system parameters and to determine stability of a BWR [138]. Minimum-memory ARX model with wavelet projections has been proposed for liquid zone control system [24]. Patra *et al.* [139], demonstrated the application of Haar wavelet in solving the point-kinetics model and to further study the behaviour of neutron density. It is found that most of the works are based on the prefiltering of measurements in which, the data is projected back in time followed by the usual estimation/identification exercise. In contrast, the technique developed in this thesis works with the wavelet projections of data thereby taking a different stance from that of the several existing methods.

2.8 Model Predictive Control

Predictive control is one of the industry pioneered control design technique. Dynamic Matrix Control (DMC) was its first variant reported by Cutler and Ramaker [140] in the 1970s. It employs finite impulse response and step response models in the formulation of the controller. It has been applied successfully in industrial process control field by Richalet [141]. This model structure gives a transparent description of process time delay, response time, and gain. However, they are limited to stable plants and often require large model orders. Clarke *et al.* [142, 143] introduced GPC to overcome the limitations of DMC. It uses transfer function models to design controller and is based on the receding-horizon architecture. They give a more parsimonious description of process dynamics and are applicable to both stable and unstable plants. It has the advantage of overcoming time-varying, time-delay, and nonlinearity in the processes. However, they are difficult to implement for multi variable systems. The development of model predictive control using state-space models is by Muske and Rawlings [144]. State-space formulation of a predictive controller is popular because of the simplicity of design framework and the direct link to the classical linear quadratic regulators. MPC design using state-space models have gained wide attention due to its inherent advantages and flexibility over other models representation, for *e.g.*, ease in handling constraints and natural extension to MIMO systems.

The block diagram representation of the MPC design approach applied to a plant is shown in Figure 2.6. The given set-points and constraints are applied to the MPC block which consists of a plant model, cost function, and optimization scheme. The aim of predictive controller is to compute a trajectory of future manipulated variables to optimize future behavior of the plant output. The manipulated variables are then applied to the plant to be controlled. The controlled output signal is then feed back to the MPC block to design control strategy for next instant. In the presence of measured disturbance, the scheme can be added with a feed-forward control action. The MPC strategy is shown in Figure 2.7. The measured output and past control input are assumed to

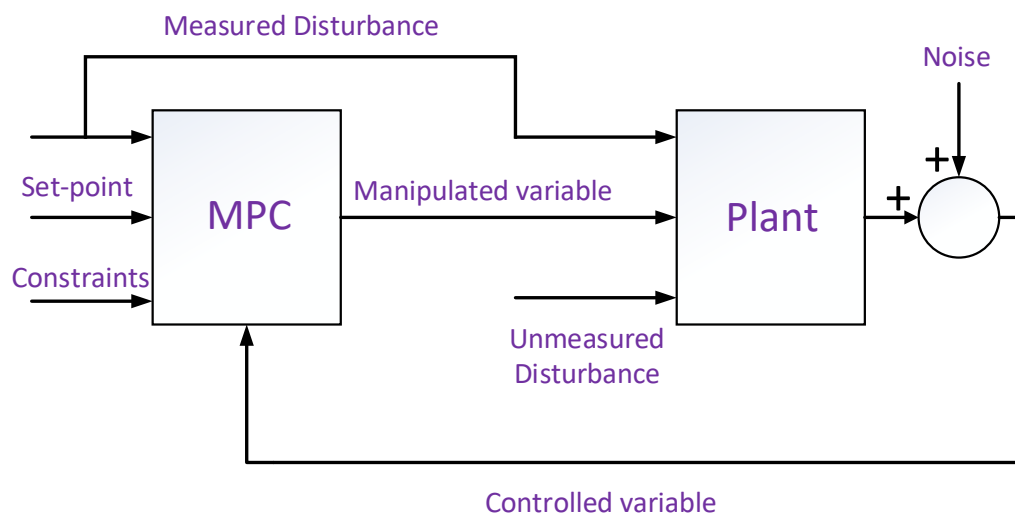


FIGURE 2.6: Block diagram representation of the MPC approach.

be available up to k instant. Now the cost function is optimized to find future control input over control horizon while output is predicted over the prediction horizon. Based on the calculation of manipulated variable, the MPC approach can be divided into two strategies. They are called as infinite horizon and receding horizon approaches. In infinite horizon control philosophy, output is predicted over prediction horizon and control strategy is calculated and implemented over the control horizon. Whereas, in the case of receding horizon control philosophy only the first control action is implemented. The receding horizon control philosophy is shown in Figure 2.8. At the next sampling instant, moving window is moved by one step and control strategy is calculated again over the control horizon while only the first control action is implemented. The same strategy is repeated for next data samples.

The application of MPC to nuclear engineering has attracted a great deal of attention in recent years. In the field of SG level control, Kothare *et al.* [145] implemented MPC by using a Linear Parameter Varying (LPV) model of the U-tube SG. Na *et al.* [146] applied the MPC technique to control the water level of nuclear SG. In [147], authors adopted multi-mode based robust MPC technique to address the nonlinearity in the water level control of SG. Eliasi *et al.* [148] used adaptive fuzzy models for predictive

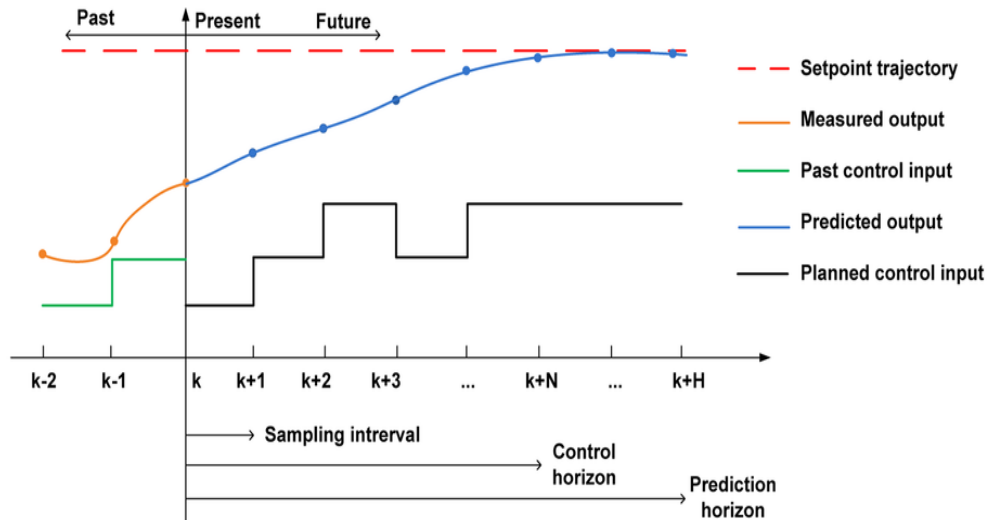


FIGURE 2.7: Representation of model predictive control strategy.

control of SG. A SVR based MPC of water level of U-tube SG is proposed by Kavaklioglu [149]. Another important application of MPC is in designing control strategy for load-following mode of operation. The load-following operation is becoming an increasingly important feature of NPPs in response to load requirements. The core power control for load-following mode of PWR is studied by various researchers. Na *et al.* [150, 151] assumed that the process is governed by ARIMA model structure similar to that of the GPC. The approach requires solution of complex Diophantine equation to obtain predictor coefficients. Na *et al.* applied MPC for the control of power level and axial power distribution. A multiple-model-based MPC technique is discussed for the load-following problem of movable plants by Yun *et al.* [152]. Robust nonlinear MPC strategies have been developed by Eliasi *et al.* for the load-following operation of PWR [153, 154]. Etchepareborda *et al.* [155] used a nonlinear receding horizon control method to regulate the power of a research reactor over a wide range in the presence of known disturbances. A recent study by Wang *et al.* [156] focused on the load tracking problem of PWR at low-load working condition using quadratic programming optimizer. A major issue with above discussed model-based control approaches is that it requires precise mathematical model of the underlying process a priori. This makes

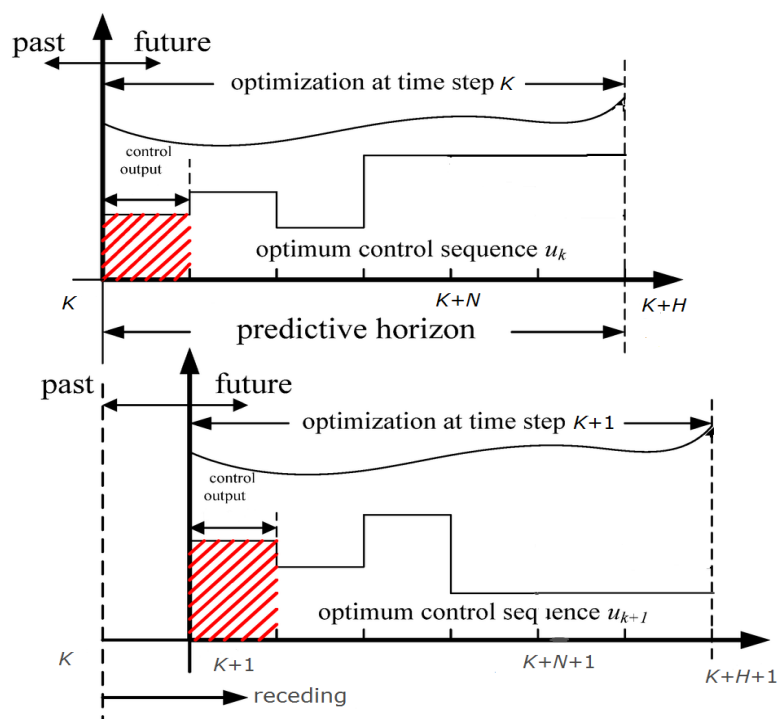


FIGURE 2.8: Representation of receding horizon control strategy.

the implementation of MPC time-consuming as the control performance is mainly dependent on the employed process model. Further, variation in reactor parameters with operating power limit model-based techniques to guarantee the desired performance.

2.9 Subspace Predictive Control

SPC has been investigated by many researchers, and different variants have been reported in the literature with applications ranging from fuel cells to networked control systems. Kadali *et al.* [29] proposed the inclusion of integral action and feed-forward action with the tradition SPC. Wang *et al.* [30] formulate SPC under incomplete output measurements. Xia *et al.* [157] applied SPC to design the networked predictive control system which consists of the control prediction generator and network delay compensator. Wu *et al.* [158] developed a multimodel based SPC for the nonlinear boiler-turbine unit. In [32], authors combined SPC with fuzzy clustering to control the nonlinear boiler-turbine unit. Favoreel *et al.* [159] have employed subspace methods

in the Linear Quadratic Gaussian (LQG) framework. Woodley *et al.* [160] combined subspace methods with H_∞ control. A number of methods have been developed in literature to deal with closed-loop data. Using the idea from closed-loop subspace identification method, Favoreel *et al.* [161] also proposed the design of closed-loop subspace-based LQG controller. Dong and Verhaegen [162] has established an equivalence between closed-loop SPC and classical LQG. An efficient closed-loop SPC based on the Vector Auto Regressive with eXogenous inputs (VARX) algorithm [82] was proposed by Dong *et al.* [163]. Hallouzi and Verhaegen [164] proposed the fault tolerant SPC based on the VARX structure. Persistency of excitation in the SPC is studied in [165]. Closed-loop SPC for LPV systems is developed in [166, 167]. A closed-loop SPC algorithm is developed for LTI systems with static nonlinearity at the plant input by Kulscar *et al.* [168]. Navalkar *et al.* [169] combined an on-line system identification with the subspace predictive repetitive control. In the presence of practical applications care has to be exercised as the data-driven control becomes sensitive to noise and may sometimes lead to ill-conditioning of the predictor matrices. A data prefiltering measure has been proposed in [31] under the assumption that the noise model is available. However, the assumption about knowledge of noise model is rather strict. Moreover, the method is less preferable for reactor where noise arises from different sources. The proposed wavelet based preprocessing shows better solution to this problem. Here, the noise is handled in the proposed approach by means of thresholding strategy, which is equivalent to a nonlinear estimation of the signal. The efficient thresholding associated with wavelets can render an identified controller insensitive to noise. Consequently, the focus is on achieving the best predictions of the deterministic component of the output in the wavelet space.

2.10 Data-driven Control Techniques

In the last two decades, different soft-computing techniques, such as ANN, Fuzzy Logic, Genetic Algorithms, and SVR have been applied to the control of U-tube SG,

reactor power, and temperature. For instance, a diagonal recurrent neural network based controller to enhance the temperature response of PWR is proposed by Ku *et al.* [170]. An ANN-based controller using the response of a self-tuning regulator has been applied for wide range power regulation in the load-following operation [171]. Arab-Alibeik *et al.* [172] developed an adaptive feed-forward neural network-based controller for power level control of PWR. Khajavi *et al.* [173] proposed a fuzzy logic-based robust optimal power level controller to improve the load-following characteristics. Khorramabadi *et al.* [174] integrated the learning ability of ANN with the decision-making capability of fuzzy logic to develop a neuro-fuzzy power controller. Na *et al.* [175] proposed a genetic algorithm optimized fuzzy model-based MPC to improve the performance of thermal power control. In the similar line of work, Lee *et al.* [176] employed a support-vector regression model in place of fuzzy model to obtain better output prediction. Na and Upadhyaya [177] applied SVR based MPC to control thermoelectric power in the SP-100 space reactor. In some recent works, nonlinear fuzzy models are employed to enhance the potential of conventional MPC techniques [178, 179].

It has been found that, most of these approaches have employed these techniques for the design of model structures. Thus their performance is dependent up on the accuracy of estimated model. Furthermore, they require more computation time for model estimation. In case of ANN based techniques, their implementation would require building up of optimal network structure. It also suffers from local minima problems. Fuzzy logic-based techniques usually require expert knowledge of the underlying system to design rule base. In contrast to fuzzy models, subspace-based approaches do not need explicit knowledge about the system. Moreover, algorithms based on subspace matrix that can directly design controller are time saving and particularly suitable for prompt installation.

Chapter 3

Wavelet Operators for Multiscale Modeling

In this chapter, methodology of wavelet operators for multiscale modeling is presented. It proposes to design wavelet operator from the given measurements such that the system matrices has a diagonal structure in the projection space. The proposed algorithm is validated on the nuclear reactor system using reference as well as plant datasets.

Wavelet operators are designed to impose certain specific structure on the system matrix in projection space. In particular, the notion is to diagonalize the system matrix to decouple system modes completely for applying independent control actions along the Eigen functions [27]. This work formulates a state-space model with wavelet states. It proves that one can work with a diagonalized state space model in wavelet sub-spaces as well. In other words, the methodology works by embedding in wavelet operator, the ability of extracting cross-correlation across variables. Wavelet operators are designed to systematically orchestrate the evolution of a system model across scales. Although, the present formulation is derived in a deterministic set-up, it can be readily adopted in a stochastic framework. Further, it suggests the use of different wavelet basis functions for different modes/states suitably selected to minimize modeling error.

3.1 Wavelet operator

3.1.1 Notations

System input $u(t)$ and output $y(t)$ are defined in Hilbert space L_2 of real-valued square integrable functions. Discrete measurements $u[k]$ and $y[k]$ respectively of input and output belong to l_2 , the vector space of square summable sequences. Measurements $u_j^w[k]/u_j^v[k]$ and $y_j^w[k]/y_j^v[k]$ are considered to be projections of $u[k]$ and $y[k]$ on wavelet basis/scaling functions at any resolution 2^{-j} . Wavelet basis functions and scaling functions span the vector space L_2 . Sequence $\{V_j\}_{j \in \mathbb{Z}}$ of closed sub-spaces of L_2 is denoted as a multiresolution approximation with difference space W_j satisfying $V_{j+1} \oplus W_{j+1} = V_j$, for all j , \oplus denoting direct sum of the subspaces.

Let us consider a discrete-time LTI SISO multivariate system of order N , given by one-step-ahead state-space model

$$x[k+1] = Ax[k] + Bu[k], \forall k, \quad (3.1)$$

where $A \in \mathbb{R}^{N \times N}$, $B \in \mathbb{R}^{N \times 1}$, and $x \in \mathbb{R}^N$ respectively denote system dynamics matrix, input matrix, and state vector. A sequence $x_j^v(x_j^w)$ belongs to $V_j(W_j)$ at any resolution 2^{-j} while $x[k]$ are considered measurable in V_0 . Operators projecting onto the respective sub-spaces $W_j(V_j)$ are also denoted by the same notation $W_j(V_j)$. Let $x_j^v[k]$ be the k^{th} sample of state vector and $x_{ij}^v[k]$ the i^{th} state variable in $x_j^v[k]$.

Let us denote the state-space model in V_j by (A_j^v, B_j^v) . The state equation in V_j at resolution 2^{-j} is written as

$$x_j^v[k+1] = A_j^v x_j^v[k] + B_j^v u_j^v[k], \quad \forall k, \quad (3.2)$$

or in expanded form

$$\begin{bmatrix} x_{1j}^v[k+1] \\ x_{2j}^v[k+1] \\ \vdots \\ x_{Nj}^v[k+1] \end{bmatrix} = A_j^v \begin{bmatrix} x_{1j}^v[k] \\ x_{2j}^v[k] \\ \vdots \\ x_{Nj}^v[k] \end{bmatrix} + B_j^v u_j^v[k], \quad \forall k. \quad (3.3)$$

In this work, we actually deal with operators with truncated support of length equal to number of states and hence, let us define the $N \times N$ regression matrix at resolution 2^{-j} as

$$X_j[k] = \begin{bmatrix} x_{1j}^v[k] & x_{1j}^v[k-1] & \cdots & x_{1j}^v[k-N+1] \\ x_{2j}^v[k] & x_{2j}^v[k-1] & \cdots & x_{2j}^v[k-N+1] \\ \vdots & \vdots & \ddots & \vdots \\ x_{Nj}^v[k] & x_{Nj}^v[k-1] & \cdots & x_{Nj}^v[k-N+1] \end{bmatrix}, \quad (3.4)$$

and $1 \times N$ input matrix at resolution 2^{-j} as

$$U_j[k] = \left[u_j^v[k] : u_j^v[k-1] : \cdots : u_j^v[k-N+1] \right], \quad (3.5)$$

such that the state-space description of a system in terms of regression matrix $X_j[k]$ can be written as,

$$X_j[k+1] = A_j^v X_j[k] + B_j^v U_j[k], \quad \forall k, \quad (3.6)$$

where A_j^v is $N \times N$ matrix and B_j^v is $N \times 1$ column vector. The elements in a row of X_j are considered to have temporal correlation, it is assumed that the elements in a column are correlated spatially. One of the objectives of the transformation is to make this spatial correlation evident by resolving the states of the system on a new set of basis. For this work, it is considered that the change of basis diagonalizes A_j^v i.e., it completely decorrelates spatially. Primary advantage of such a transformation is that the application of control input along the direction of one basis would only affect the state projected on the same basis. Returning to the formulation of the output equation,

we can simply write

$$Y_j[k] = C_j^v X_j[k], \quad (3.7)$$

where, $Y_j[k] = \begin{bmatrix} y_j^v[k] \\ y_j^v[k-1] \\ \vdots \\ y_j^v[k-N+1] \end{bmatrix}$ and C_j^v is a $1 \times N$ row vector.

3.1.2 Local Diagonalizing Transform

A local operator matrix is defined as a matrix that locally transforms system states from one resolution to another operating on the finite length regressor. To be more specific, it operates on the regression matrix at any resolution 2^{-j} to give states in the difference space W_{j+1} . Let us now define the separable local diagonalizing transform as given below

$$x_{j+1}^w[k] = \mathcal{E}(W_j^X X_j^T[k]), \quad (3.8)$$

where local operator W_j^X is also defined as an $N \times N$ matrix

$$W_j^X = \begin{bmatrix} w_{11} & w_{12} & \cdots & w_{1N} \\ w_{21} & w_{22} & \cdots & w_{2N} \\ \vdots & \vdots & \ddots & \vdots \\ w_{N1} & w_{N2} & \cdots & w_{NN} \end{bmatrix}. \quad (3.9)$$

Operator $\mathcal{E}(\cdot)$ extracts the diagonal elements of the operand matrix and arranges them in a column. Note that $x_{j+1}^w[k]$ is a column vector having diagonal elements of $W_j^X X_j^T[k]$, *i.e.*

$$x_{j+1}^w[k] = \begin{bmatrix} w_{11}x_{1j}^v[k] + w_{12}x_{1j}^v[k-1] + \cdots + w_{1N}x_{1j}^v[k-N+1] \\ w_{21}x_{2j}^v[k] + w_{22}x_{2j}^v[k-1] + \cdots + w_{2N}x_{2j}^v[k-N+1] \\ \vdots \\ w_{N1}x_{Nj}^v[k] + w_{N2}x_{Nj}^v[k-1] + \cdots + w_{NN}x_{Nj}^v[k-N+1] \end{bmatrix}. \quad (3.10)$$

The local operator transforms input and output vector as

$$U_{j+1}^w[k] = W_j^X U_j^T[k]; \quad Y_{j+1}^w[k] = (W_j^X Y_j^T[k])^T, \quad (3.11)$$

where U_{j+1}^w is $N \times 1$ column vector and Y_{j+1}^w is $1 \times N$ row vector. Rows of local operator W_j^X , defined as an $N \times N$ matrix play the role of wavelet filters. Let us also define the local inverse operator matrix $(W_j^X)^{-1}$ such that $(W_j^X)^{-1} W_j^X = I$. Computation of each state variable by application of local diagonalizing transform requires N multiplications where N is the order of the system.

It should be clearly understood at the outset that W_j^X is a local operator that operates on the approximation (indicated by superscript v) at resolution 2^{-j} to produce details (indicated by superscript w) at resolution $2^{-(j+1)}$. So, (A_j^v, B_j^v) models the system in V_j while (A_{j+1}^w, B_{j+1}^w) in W_{j+1} . The following Section 3.2 establishes a relation between (A_j^v, B_j^v) and (A_{j+1}^w, B_{j+1}^w) .

3.2 State space model in transform domain

Consider the state-space description given by (3.6),

$$X_j^T[k+1] = X_j^T[k](A_j^v)^T + U_j^T[k](B_j^v)^T. \quad (3.12)$$

Projection onto wavelet space is achieved by first pre-multiplying by W_j^X and then applying operator $\mathcal{E}(\cdot)$ on both sides of (3.12) *i.e.*,

$$\mathcal{E}(W_j^X X_j^T[k+1]) = \mathcal{E}(W_j^X X_j^T[k](A_j^v)^T) + \mathcal{E}(W_j^X U_j^T[k](B_j^v)^T). \quad (3.13)$$

The equivalent state equation in W_{j+1} space is given by

$$x_{j+1}^w[k+1] = A_{j+1}^w x_{j+1}^w[k] + B_{j+1}^w U_{j+1}^w[k], \quad (3.14)$$

with

$$A_{j+1}^w = ((W_j^X)^T)^{-1} X_j^{-1} [k] A_j^v X_j [k] (W_j^X)^T, \quad (3.15)$$

and B_{j+1}^w is defined as,

$$B_{j+1}^w W_j^X U_j^T [k] = \mathcal{E}(W_j^X U_j^T [k] (B_j^v)^T). \quad (3.16)$$

Note that A_{j+1}^w and B_{j+1}^w are defined to be diagonal matrices so that,

$$A_{j+1}^w \mathcal{E}(W_j^X X_j^T [k]) = \mathcal{E}(A_{j+1}^w W_j^X X_j^T [k]), \quad (3.17)$$

$$B_{j+1}^w = \mathcal{D}(B_j^v). \quad (3.18)$$

Operator $\mathcal{D}(\cdot)$ arranges the elements of a vector operand along the diagonal of a diagonal matrix. Observe that $\mathcal{D}(\cdot)$ would accomplish the reverse operation of $\mathcal{E}(\cdot)$ *i.e.* it would give back the original matrix only if it is diagonal to start with. By observation one can state that the sufficient condition that would satisfy (3.13) is,

$$\begin{aligned} X_j [k + 1] &= X_j [k] (W_j^X)^T A_{j+1}^w ((W_j^X)^T)^{-1} \\ &\quad + (\mathcal{D}(B_{j+1}^w W_j^X U_j^T [k]))^T ((W_j^X)^T)^{-1}, \end{aligned} \quad (3.19)$$

subject to the condition that W_j^X is invertible. System parameters in V_j and those in W_{j+1} are then related as

$$A_{j+1}^w = ((W_j^X)^T)^{-1} \overline{A_j^v} (W_j^X)^T, \quad (3.20)$$

where $\overline{A_j^v} = X_j^{-1} [k] A_j^v X_j [k]$ and $\overline{B_j^v} = B_j^v$. An important implication of (3.14)–(3.20) is that one can work with a state-space model having a specific structure in projection space, spanned by local diagonalizing basis, as well. Also, given a local diagonalizing operator, there exists a definite relationship between the model in measurement space and that in projection space. This formulation is fundamental to the design of wavelet operator for multiscale modeling. Since A_{j+1}^w is diagonal, to ensure controllability of

the transformed system column vector B_{j+1}^w should not have any zero row.

In practice, $\mathcal{E}(W_j^X X_j^T[k])$ is implemented by appropriately designing analysis multi-rate filter bank associated with a wavelet operator. The derived relationship between A_j^v and A_{j+1}^w signifies the data dependent or adaptive nature of the local diagonalizing transform. This is expected because the transform is designed to meet the objectives locally and hence the operator is data dependent. However, the basic structure of the operator matrix remains invariant. On the contrary, wavelet transform, in its basic form is non-adaptive in nature. Later in this chapter, the factorization of local diagonalizing operator matrix into a non-adaptive and an adaptive matrix is investigated. Further, the design of a non-adaptive operator matrix that qualifies as a wavelet transform operator is also derived.

The output relation in projection space is derived as follows. Taking the transpose of the output equation (3.7) gives,

$$Y_j^T[k] = X_j^T[k](C_j^v)^T. \quad (3.21)$$

Pre-multiplying both sides of (3.21) by W_j^X gives,

$$W_j^X Y_j^T[k] = W_j^X X_j^T[k](C_j^v)^T. \quad (3.22)$$

Using (3.8) and (3.11), above equation can be written as,

$$(Y_{j+1}^w[k])^T = \mathcal{D}(x_{j+1}^w[k]) R^{-1}(C_j^v)^T, \quad (3.23)$$

or simply,

$$Y_{j+1}^w[k] = C_j^v (R^{-1})^T \mathcal{D}(x_{j+1}^w[k]), \quad (3.24)$$

where $R = (W_j^X X_j^T)^{-1} \mathcal{D}(\mathcal{E}(W_j^X X_j^T))$ and $C_{j+1}^w = C_j^v (R^{-1})^T$.

Let us define $y_{j+1}^w[k] = Y_{j+1}^w[k] Z$, where $Z = \begin{bmatrix} 1 & 1 & \dots & 1 \end{bmatrix}^T$. Now (3.24) can be

written as,

$$y_{j+1}^w[k] = C_{j+1}^w x_{j+1}^w[k]. \quad (3.25)$$

3.2.1 Design of a Non-Adaptive Wavelet Operator Matrix

A careful look at (3.20) reveals that the rows of the matrix $((W_j^X)^T)^{-1}$ are left eigenvectors of \overline{A}_j^v and diagonal elements of A_{j+1}^w are the corresponding eigenvalues. Let,

$$A_{j+1}^w = \text{diag}[\alpha_1 \quad \alpha_2 \quad \cdots \quad \alpha_N], \quad (3.26)$$

where $\alpha_1, \alpha_2, \dots, \alpha_N$ are non-zero distinct eigenvalues. Any linear transformation $((W_j^X)^T)^{-1}$, satisfying

$$A_{j+1}^w = ((W_j^X)^T)^{-1} \overline{A}_j^v (W_j^X)^T, \quad (3.27)$$

can in general be given by [180],

$$((W_j^X)^T)^{-1} = \mathcal{W}_j \mathcal{V}_j \Rightarrow (W_j^X)^T = \mathcal{V}_j^{-1} \mathcal{W}_j^{-1}. \quad (3.28)$$

One possible choice is $\mathcal{V}_j^{-1} = Q_j = [\overline{B}_j^v, \overline{A}_j^v \overline{B}_j^v, \dots, \overline{A}_j^{v^{N-1}} \overline{B}_j^v]$ with $Q_j \tilde{A}_j = \overline{A}_j^v Q_j$

where,

$$\tilde{A}_j = \begin{bmatrix} 0 & 0 & \cdots & -a_N \\ 1 & 0 & \cdots & -a_{N-1} \\ 0 & 1 & \cdots & -a_{N-2} \\ \vdots & \vdots & \ddots & \vdots \\ 0 & 0 & \cdots & -a_1 \end{bmatrix}. \quad (3.29)$$

Here (a_1, \dots, a_N) are the coefficients of the characteristic polynomial A_j . Matrix Q_j depends on $\overline{A}_j^v (= X_j^{-1}[k] A_j^v X_j[k])$ and needs to be recomputed adaptively at each k . If system is controllable, then Q_j is of rank N . Moreover, this article does not deal with uncontrollable systems.

With the choice of Q_j given above it is elementary to show that the linear transformation \mathcal{W}_j satisfying $A_{j+1}^w \mathcal{W}_j = \mathcal{W}_j \tilde{A}$ is the product of a diagonal matrix (\mathcal{M}) and the Vandermonde matrix (refer Appendix B)

$$\mathcal{W}_j = \mathcal{M} \begin{bmatrix} 1 & \alpha_1 & \cdots & \alpha_1^{N-1} \\ 1 & \alpha_2 & \cdots & \alpha_2^{N-1} \\ \vdots & \vdots & \ddots & \vdots \\ 1 & \alpha_N & \cdots & \alpha_N^{N-1} \end{bmatrix}, \quad (3.30)$$

where $\mathcal{M} = \text{diag}[m_1 \ m_2 \ \cdots \ m_N]$, in which $m_1, m_2, \dots, m_N \in \mathcal{R}$. In specific, matrix \mathcal{M} can be taken as an identity matrix. Matrix \mathcal{W}_j is translation invariant because $\overline{A_j^v}$ is similar to A_j^v and have the same eigenvalues as that of A_j^v . \mathcal{W}_j is of rank N if all the eigenvalues of $\overline{A_j^v}$ are distinct. Since both \mathcal{V}_j and \mathcal{W}_j are of rank N , W_j^X is also of rank N and is invertible.

Any system (A_j^v, B_j^v) if state-controllable in measurement space can be transformed into the controllable form $(\tilde{A}_j, \tilde{B}_j)$. Hence, without any loss of generality, one can work with the system described by $(\tilde{A}_j, \tilde{B}_j)$. In such a case, local diagonalizing operator W_j^X is independent of data (translation invariant) and is denoted by \tilde{W}_j^X ,

$$((\tilde{W}_j^X)^T)^{-1} = \mathcal{W}_j \Rightarrow \tilde{W}_j^X = (\mathcal{W}_j^{-1})^T. \quad (3.31)$$

It may be observed that although translation invariant, \tilde{W}_j^X is not scale invariant as it depends on the eigenvalues at that resolution.

3.2.2 Design of Analysis High Pass Filter

In this subsection an approach to design analysis HPF is presented for a general third order discrete time system. A third order system is non trivial and would bring out salient features of the design methodology. This is a crucial step as the design of analysis HPF further leads to full filter bank implementation. Let $\mathcal{M} = I$, then the operator \mathcal{W}_j for

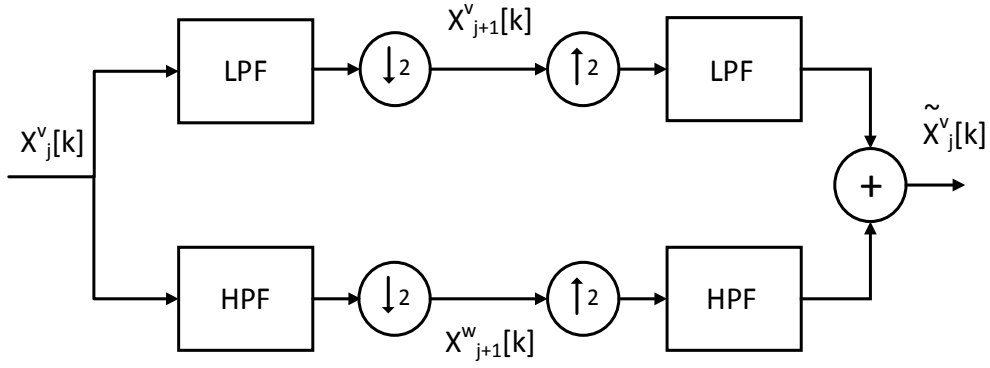


FIGURE 3.1: Block diagram of analysis and synthesis filter bank

the system is given by

$$\mathcal{W}_j = \mathcal{M} \begin{bmatrix} 1 & \alpha_1 & \alpha_1^2 \\ 1 & \alpha_2 & \alpha_2^2 \\ 1 & \alpha_3 & \alpha_3^2 \end{bmatrix}. \quad (3.32)$$

From (3.31) and (3.32)

$$\tilde{W}_j^X = \frac{1}{\Delta} \begin{bmatrix} \alpha_2 \alpha_3 (\alpha_3 - \alpha_2) & (\alpha_2^2 - \alpha_3^2) & (\alpha_3 - \alpha_2) \\ \alpha_1 \alpha_3 (\alpha_1 - \alpha_3) & (\alpha_3^2 - \alpha_1^2) & (\alpha_1 - \alpha_3) \\ \alpha_1 \alpha_2 (\alpha_2 - \alpha_1) & (\alpha_1^2 - \alpha_2^2) & (\alpha_2 - \alpha_1) \end{bmatrix}, \quad (3.33)$$

and Δ is determinant of \mathcal{W}_j . Note that all columns of \tilde{W}_j^X add up to zero except for the first column. Hence, all but the first column qualify to be the high pass analysis filter in a wavelet filter bank. This automatically satisfies the admissibility condition that the Fourier transform of the filter is zero at zero frequency [86]. Values of filter coefficients originating out of the first column are suitably augmented to satisfy the admissibility condition.

Every row of $(\tilde{W}_j^X)^T$ plays the role of half band high-pass analysis filter $g[-k]$ in two-channel perfect reconstruction multirate filter bank *i.e.*

$$g_i[-k] = (\tilde{W}_j^X)_{ik}^T. \quad (3.34)$$

Other half band filters in the filter bank *i.e.* analysis low pass h , synthesis high-pass \tilde{g} and synthesis low pass \tilde{h} filters can be designed by satisfying biorthogonality condition thereby giving the full filter bank structure as shown in Figure 3.1. This is explained in Section 3.2.3 and further derived in Appendix B.2.

3.2.3 Design of Two Channel Biorthogonal Filter bank

The approximation spaces, $\{V_j\}_{j \in \mathbb{Z}}$ and difference spaces, $\{W_j\}_{j \in \mathbb{Z}}$ are spanned by integer translates of scaling and wavelet basis functions, respectively. The basic dilation equation defines synthesis scaling function $\tilde{\phi}$ and synthesis wavelet function $\tilde{\psi}$ through two-scale difference equation

$$\frac{1}{\sqrt{2}}\tilde{\phi}\left(\frac{t}{2}\right) = \sum_{k=-\infty}^{+\infty} \tilde{h}[k]\tilde{\phi}(t-k), \quad (3.35)$$

$$\frac{1}{\sqrt{2}}\tilde{\psi}\left(\frac{t}{2}\right) = \sum_{k=-\infty}^{+\infty} \tilde{g}[k]\tilde{\phi}(t-k). \quad (3.36)$$

Analysis scaling function $\phi(\cdot)$ and analysis wavelet function $\psi(\cdot)$ are related to $h[k]$ and $g[k]$ respectively through similar relations. Projections onto $\{V_j\}_{j \in \mathbb{Z}}$ and $\{W_j\}_{j \in \mathbb{Z}}$ are implemented using the analysis filter bank. Analysis and synthesis filters need to satisfy biorthogonality and perfect reconstruction conditions. The synthesis filter design takes care of alias cancellation thereby resulting in perfect reconstruction. These conditions are summarized in the following.

1. Biorthogonality condition, *i.e.*,

$$\langle \tilde{h}[k], h[k-2l] \rangle = \delta[l],$$

$$\langle \tilde{g}[k], g[k-2l] \rangle = \delta[l],$$

$$\langle \tilde{h}[k], g[k-2l] \rangle = \langle \tilde{g}[k], h[k-2l] \rangle = 0.$$

2. Perfect reconstruction condition

$$g[k] = (-1)^{(1-k)} \tilde{h}[1 - k],$$

$$\tilde{g}[k] = (-1)^{(1-k)} h[1 - k].$$

It may be noted here that perfect reconstruction condition essentially leads to biorthogonality condition. For a decimated wavelet transform, wavelet coefficients or wavelet states in next lower resolution are obtained by downsampling of analysis and synthesis filters' outputs by two. Further, filter banks can be designed to have desired number of vanishing moments with compact support. A wavelet function $\psi(t)$ is said to have K vanishing moment if the associated scaling function can generate polynomials up to degree $K - 1$. This condition is given as

$$\int_{-\infty}^{+\infty} t^m \psi(t) dt = 0, \quad m = 0, 1, \dots, K - 1. \quad (3.37)$$

When designing the filter bank, the vanishing moment constraint is used in addition to the biorthogonality and perfect reconstruction conditions. An analytical example of perfect reconstruction biorthogonal wavelet filter bank (PRBWFB) design is given in Appendix B.2.

3.2.4 Proposed Algorithm

The proposed methodology of multiscale system modeling employs translation invariant but scale adaptive basis functions that completely decorrelate system states in transform domain. Design of this class of wavelet filter bank is based on the nominal model of the system identified in approximation space. Figure 3.2 provides a block diagram of the proposed technique. Steps to obtain a multiscale model are listed below:

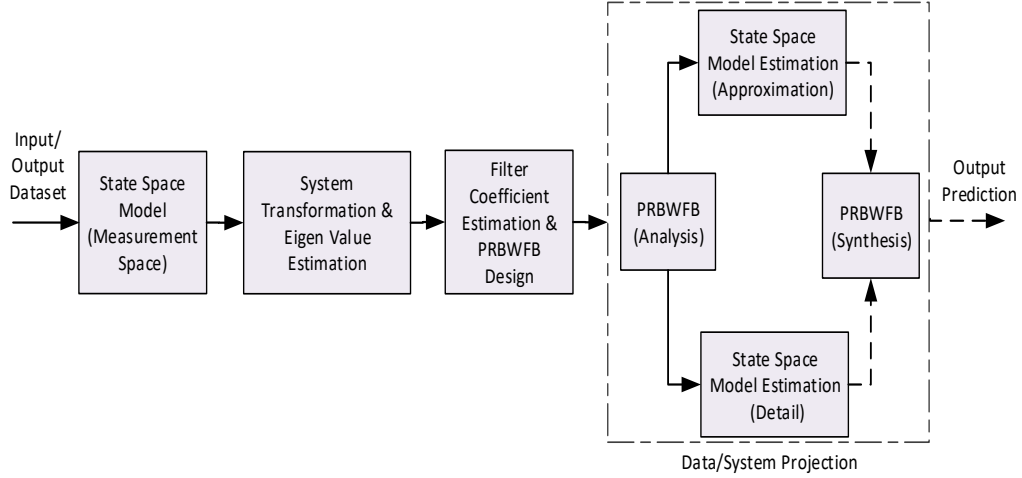


FIGURE 3.2: Block diagram of the proposed projection space modeling technique.

1. Identify a low order LTI model $(\hat{A}_j^v, \hat{B}_j^v, \hat{C}_j^v)$ in approximation space V_j . One can use numerically stable subspace methods to estimate dynamic linear state space model in deterministic/stochastic setup [1, 74, 75].
2. Compute transformation $\overline{A}_j^v = X_j^{-1}[k]A_j^vX_j[k]$.
3. Compute eigenvalues and coefficients of PRBWFB at resolution 2^{-j} .
4. Operate on states of the transformed system $(\overline{A}_j^v, \overline{B}_j^v)$ in V_j to obtain states of (A_{j+1}^v, B_{j+1}^v) in V_{j+1} and that of (A_{j+1}^w, B_{j+1}^w) in W_{j+1} .
5. Estimate $(\hat{A}_{j+1}^w, \hat{B}_{j+1}^w, \hat{C}_{j+1}^w)$. The nominal model may be obtained by (3.15) and (3.18).
6. Repeat steps 1 to 5 till $j + 1 = J$, where 2^{-J} is minimum resolution.

At the end the multiscale model would consist of a set of LTI models in approximation space V_j and in wavelet spaces $W_j, j = 1, 2, \dots, J$.

3.3 Application to Nuclear Reactor

Simulations have been performed for two different cases: 1) using reference dataset and 2) using plant dataset. In Section 3.3.2, an estimation/validation dataset is generated by exciting the point kinetics model with reactivity variation as an input and the corresponding power variation thus obtained as the output of the system. On the other hand, in Section 3.3.2, plant datasets obtained from a 540 MWe Indian PHWR are used for estimation/validation exercise.

3.3.1 Case study using reference dataset

In order to develop wavelet operator for analysis and synthesis and to further model the reactor in projection space, the system given by (C.9)–(C.10) needs to be represented in standard state space form as

$$\dot{x}(t) = Fx(t) + Gu(t), \quad (3.38)$$

where the state vector x , matrix F , and vector G are defined as

$$x = \begin{bmatrix} P & C_1 & C_2 & C_3 & C_4 & C_5 & C_6 \end{bmatrix}^T, \quad (3.39)$$

$$F = \begin{bmatrix} -\sum_{i=1}^6 \beta_i/\Lambda & \lambda_1 & \lambda_2 & \lambda_3 & \lambda_4 & \lambda_5 & \lambda_6 \\ \beta_1/\Lambda & -\lambda_1 & 0 & 0 & 0 & 0 & 0 \\ \beta_2/\Lambda & 0 & -\lambda_2 & 0 & 0 & 0 & 0 \\ \beta_3/\Lambda & 0 & 0 & -\lambda_3 & 0 & 0 & 0 \\ \beta_4/\Lambda & 0 & 0 & 0 & -\lambda_4 & 0 & 0 \\ \beta_5/\Lambda & 0 & 0 & 0 & 0 & -\lambda_5 & 0 \\ \beta_6/\Lambda & 0 & 0 & 0 & 0 & 0 & -\lambda_6 \end{bmatrix}; \quad G = \begin{bmatrix} \frac{P_0}{\Lambda} \\ 0 \\ 0 \\ 0 \\ 0 \\ 0 \\ 0 \end{bmatrix}. \quad (3.40)$$

The delayed neutron parameters for Uranium-235 are given in Appendix C, Table C.1. The steady state value of power i.e. P_0 is set to unity. Substituting the values of various

parameters, the open loop poles of the reactor system described by (3.38) are observed to be located at

$$s = [0, -0.0143, -0.0678, -0.1929, -0.9970, -2.8318, -6.9953]. \quad (3.41)$$

Equations (3.38)-(3.40) however is the continuous time model. The discrete time system representation is given by (3.1) with

$$A = e^{FT_s}, \quad B = \int_0^{T_s} e^{Ft} G dt, \quad (3.42)$$

where T_s is the sampling period for discretization. The z -domain counterpart of the s -domain poles, for a sampling period of 80 msec, are given by

$$z = [0.5714, 0.7973, 0.9233, 0.9847, 0.9946, 0.9989, 1]. \quad (3.43)$$

To find a relation between input, output, and state variables, the system is excited with a known input signal. One of the ways to change input reactivity to the reactor system is by movement of control rod (CR). It may be noted that insertion of CR from its nominal position introduces negative reactivity which decrements reactor power, while withdrawal of CR from its nominal position introduces positive reactivity which increments reactor power. The input reactivity transient is supplied to the point kinetics model of the nuclear reactor to generate variation in the reactor power output. Figure 3.3 shows the change in reactivity test input introduced by CR rod movement and the corresponding reactor power is shown in Figure 3.4.

Wavelet operators \tilde{W}_j^X are designed using (3.31) as described in Subsections 3.2.2 and 3.2.3. Observe that columns of \tilde{W}_j^X play the role of analysis HPF with zero DC gain. These HPFs are used to design synthesis low pass filters (LPF) by employing perfect reconstruction condition. The biorthogonality condition is used to obtain analysis LPF

and synthesis HPF. In general, the HPF coefficients obtained by (3.34) are not symmetric and make cause system of simultaneous equations to be under-determined. To complete the design of PRBWFB, it is required to have one more design equation. While selecting wavelets for function approximation and to have a sparse representation, the choice is made based on the regularity of the basis function that decides number of vanishing moments and support size. The vanishing moment condition is included as an additional design constraint. The PRBWFBs are designed to have length of eight taps and two vanishing moment as given in Table 3.1. Measurement space system states are transformed by these operators to those in the projection space and model parameters are estimated. System dynamics matrix of estimated projection space model is given by

$$A_{j+1}^w,$$

$$A_{j+1}^w = \text{diag} \left[0.6031, 0.7840, 0.9257, 0.9843, 0.9947, 0.9989, 1 \right]. \quad (3.44)$$

Input matrix B_{j+1}^w is given by

$$B_{j+1}^w = \text{diag} \left[60.6203, 0.5653, 3.7426, 3.3408, 6.6988, 1.9073, 0.6616 \right]. \quad (3.45)$$

Different conventional empirical modeling approaches *e.g.* SID, ARX, and OE have also been implemented. The model parameters are estimated from training dataset (Figures 3.3 and 3.4) by minimizing Akaike's Information Criterion. The estimated model parameters are given as follows:

The parameters of estimated OE model from reference dataset are given by

$$\begin{aligned} B(q^{-1}) &= 186.9q^{-1} - 370.9q^{-2} + 184q^{-3}, \\ A(q^{-1}) &= 1 - 1.994q^{-1} + 0.994q^{-2}. \end{aligned} \quad (3.46)$$

The parameters of estimated ARX model from reference dataset are given by

$$\begin{aligned} B(q^{-1}) &= 61.47q^{-1} - 121q^{-2} + 59.58q^{-3}, \\ A(q^{-1}) &= 1 - 2.582q^{-1} + 2.168q^{-2} - 0.586q^{-3}, \end{aligned} \quad (3.47)$$

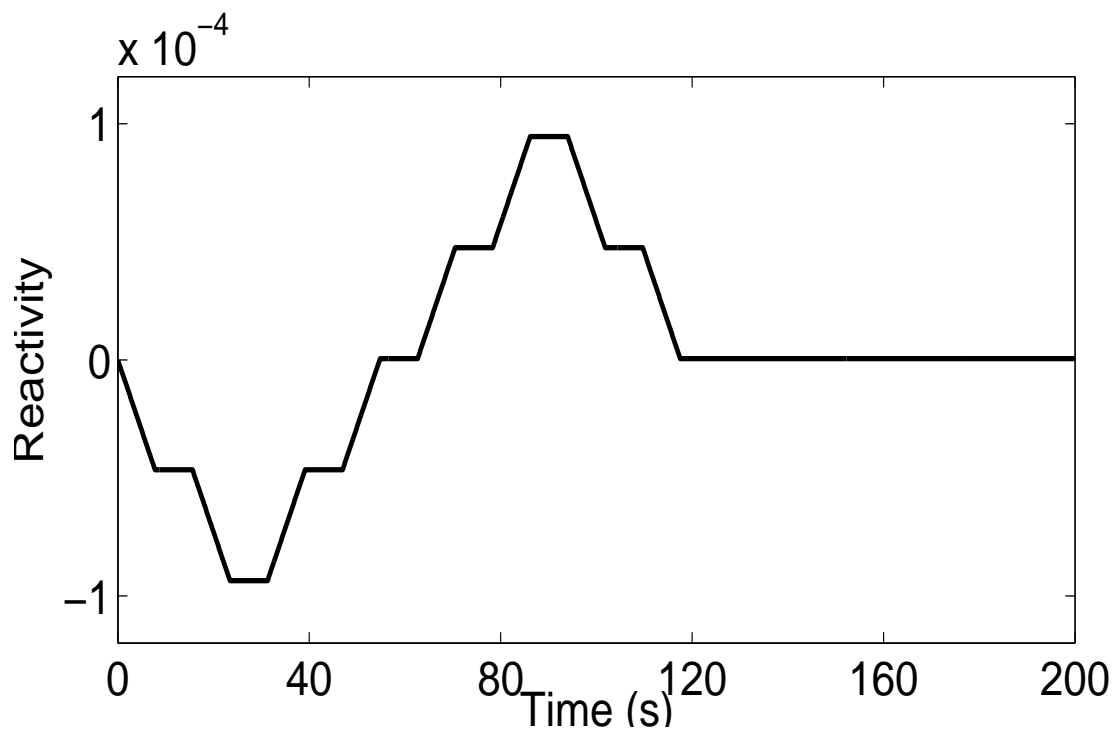


FIGURE 3.3: Variation of reference reactivity estimation input.

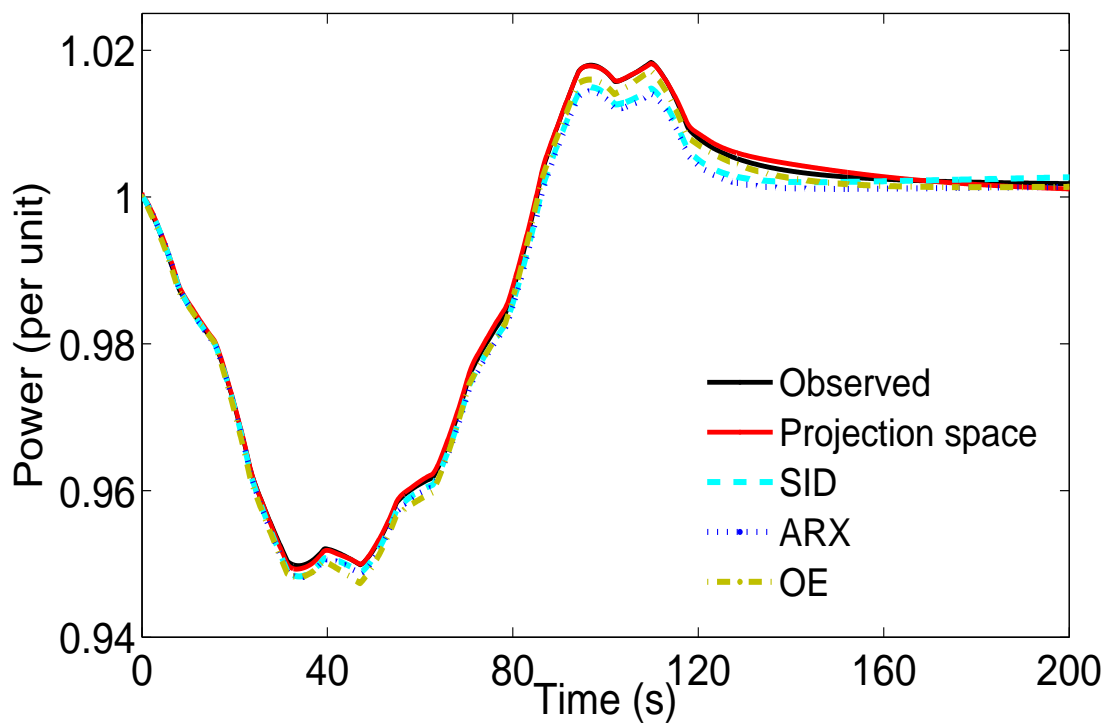


FIGURE 3.4: Outputs of estimated models with observed data for reference input.

TABLE 3.1: Estimated wavelet filter coefficients for different states.

State	Estimated Filters
First	$h[k]=[0, -0.35327, 0.49097, 0.75035, -1.24226, -1.00652, 0.14061, -0.00122]$ $g[k]=[0, 0.56456, -0.78461, 0.25390, -0.03415, 0.00029, 0, 0]$ $\tilde{h}[k]=[0, 0, -0.00029, -0.03415, -0.25390, -0.78461, -0.56456, 0]$ $\tilde{g}[k]=[-0.00122, -0.14061, -1.00652, 1.24226, 0.75035, -0.49097, -0.35327, 0]$
Second	$h[k]=[0, 0.35326, -0.49089, -0.75038, 1.24207, 1.0066, -0.14046, 0.00121]$ $g[k]=[0, -0.56462, 0.78461, -0.25380, 0.03410, -0.00029, 0, 0]$ $\tilde{h}[k]=[0, 0, 0.00029, 0.034106, 0.25380, 0.78461, 0.56462, 0]$ $\tilde{g}[k]=[0.00121, 0.14046, 1.00662, -1.24207, -0.75038, 0.49089, 0.35326, 0]$
Third	$h[k]=[0, -0.35324, 0.49081, 0.75041, -1.24187, -1.00671, 0.14030, -0.00120]$ $g[k]=[0, 0.56468, -0.78460, 0.25369, -0.03405, 0.00029, 0, 0]$ $\tilde{h}[k]=[0, 0, -0.00029, -0.03405, -0.25369, -0.78460, -0.56468, 0]$ $\tilde{g}[k]=[-0.00120, -0.14030, -1.00671, 1.24187, 0.75041, -0.49081, -0.35324, 0]$
Fourth	$h[k]=[0, 0.35322, -0.49073, -0.75044, 1.24167, 1.00681, -0.14014, 0.00119]$ $g[k]=[0, -0.56474, 0.78460, -0.25357, 0.03400, -0.00029, 0, 0]$ $\tilde{h}[k]=[0, 0, 0.00029, 0.03400, 0.25357, 0.78460, 0.56474, 0]$ $\tilde{g}[k]=[0.00119, 0.14014, 1.00681, -1.24167, -0.75044, 0.49073, 0.35322, 0]$
Fifth	$h[k]=[0, -0.35320, 0.49065, 0.75047, -1.24146, -1.00691, 0.13998, -0.00118]$ $g[k]=[0, 0.56480, -0.78459, 0.25345, -0.03395, 0.00028, 0, 0]$ $\tilde{h}[k]=[0, 0, -0.00028, -0.03395, -0.25345, -0.78459, -0.56480, 0]$ $\tilde{g}[k]=[-0.00118, -0.13998, -1.00691, 1.24146, 0.75047, -0.49065, -0.35320, 0]$
Sixth	$h[k]=[0, 0.35318, -0.49056, -0.75051, 1.24124, 1.00702, -0.13980, 0.00117]$ $g[k]=[0, -0.56487, 0.78459, -0.25333, 0.03390, -0.00028, 0, 0]$ $\tilde{h}[k]=[0, 0, 0.00028, 0.03390, 0.25333, 0.78459, 0.56487, 0]$ $\tilde{g}[k]=[0.00117, 0.13980, 1.00702, -1.24124, -0.75051, 0.49056, 0.35318, 0]$
Seventh	$h[k]=[0, -0.35316, 0.49047, 0.75054, -1.24103, -1.00713, 0.13963, -0.00116]$ $g[k]=[0, 0.56494, -0.78458, 0.25321, -0.03384, 0.00028, 0, 0]$ $\tilde{h}[k]=[0, 0, -0.00028, -0.03384, -0.25321, -0.78458, -0.56494, 0]$ $\tilde{g}[k]=[-0.00116, -0.13963, -1.00713, 1.24103, 0.75054, -0.49047, -0.35316, 0]$

and the estimated SID model from reference data is given by

$$\begin{aligned}
 x[k+1] &= \begin{bmatrix} 1 & 0 & 0 \\ -0.001 & 0.891 & -0.120 \\ -0.004 & -0.238 & 0.693 \end{bmatrix} x[k] + \begin{bmatrix} 1.5 \\ 28082 \\ 68668 \end{bmatrix} u[k] + \begin{bmatrix} 0.022 \\ -997 \\ 2860 \end{bmatrix} e[k], \\
 y[k] &= \begin{bmatrix} 53.69 & -0.0007 & 0 \end{bmatrix} x[k] + e[k].
 \end{aligned} \tag{3.48}$$

Figure 3.4 compares the estimates of the reactor power output obtained by various models with the observed data. It can be observed that all of the models are able to estimate reactor power well enough. However, multiscale features might not have been suitably modeled by any of the single scale models. A projection space model is expected to sufficiently capture the multiscale process dynamics due to modeling at appropriate scale.

Moreover, the fact that the underlying process is nonlinear in nature while all of the estimated models are linear adds to the error in the output.

For the purpose of model validation, two validation datasets have been selected whose dynamics are different from that of the estimation dataset. Further, to demonstrate the efficacy of the proposed techniques a quantitative comparison with existing technique has been presented. Validation test inputs shown in Figures 3.5 and 3.6 respectively represent ramp and trapezoidal variations in the reactivity introduced by the movement of CR inside the reactor. They are applied to different estimated models. Outputs of all models are compared with the reference output in Figures 3.7 and 3.8. It is evident that the projection space model shows a better response than that of the other models.

The modeling performance is quantitatively assessed by computing the root mean squared error (RMSE). RMSE between simulation and output observation is calculated by,

$$RMSE = \sqrt{\frac{1}{N} \sum_{k=0}^{N-1} (P[k] - \hat{P}[k])^2} \quad (3.49)$$

where P denotes simulated power and \hat{P} denotes observed power. Table 3.2 shows the value of RMSE in output simulation for different estimated models. The projection space model gives less RMSE in output, for estimation as well as with different validation datasets, than those of the other single scale techniques. The small value of RMSE indicates good modeling performance and enhanced prediction ability of the proposed approach. The estimated model in projection space is able to capture all the system dynamics better due to the fact that it efficiently estimates the multiscale modes evolving at different time-scale. On the other hand, single scale techniques are able to estimate only an approximate model of the multiscale process thereby giving larger RMSE.

3.3.2 Case study using plant dataset

This subsection presents model estimation/validation exercise on transient dataset obtained from 540 MWe Indian PHWR. The plant dataset includes reactor power as output

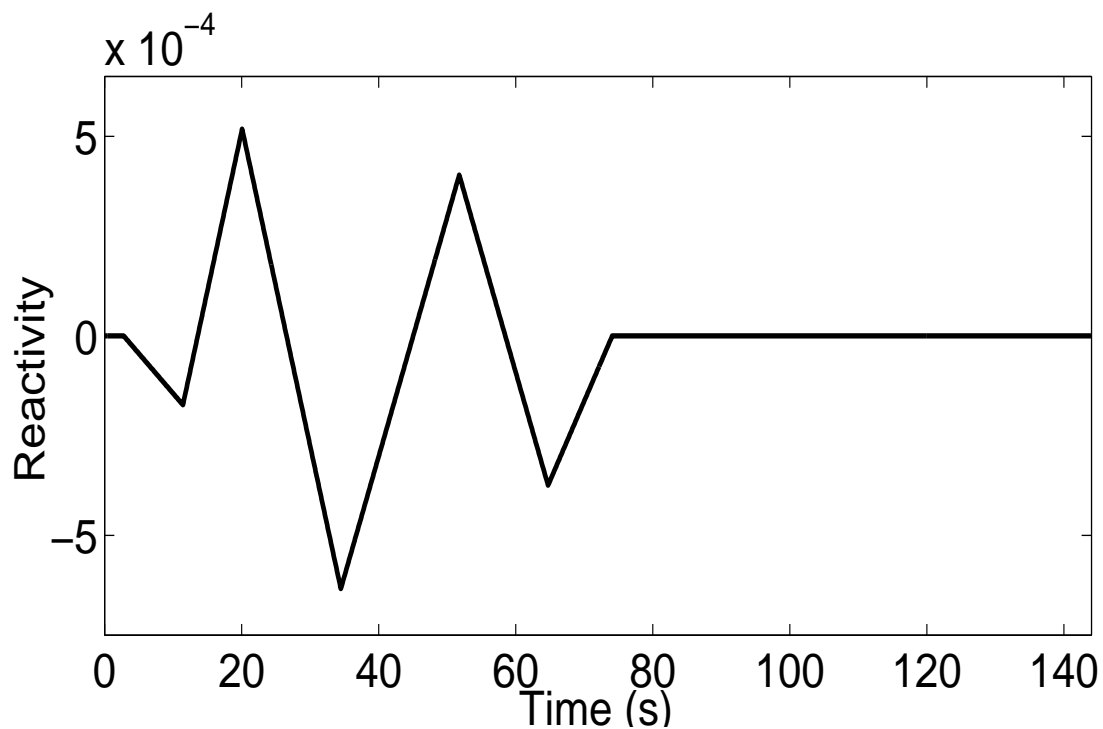


FIGURE 3.5: Variation of reference reactivity validation input (Case A).

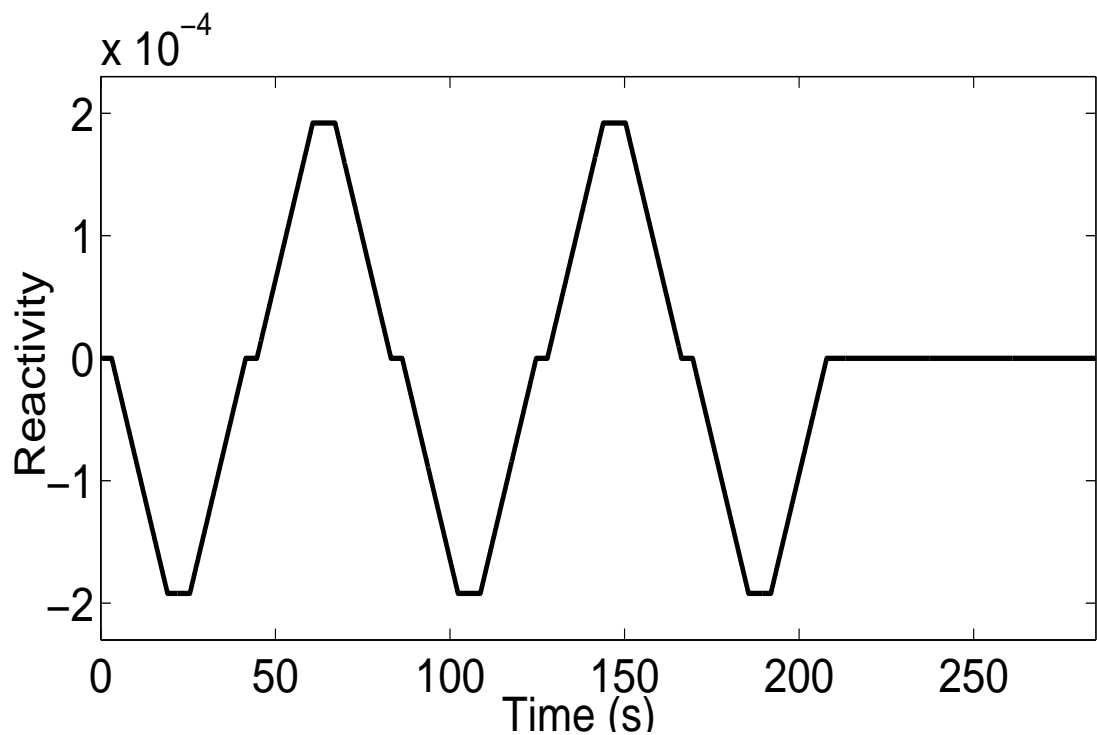


FIGURE 3.6: Variation of reference reactivity validation input (Case B).

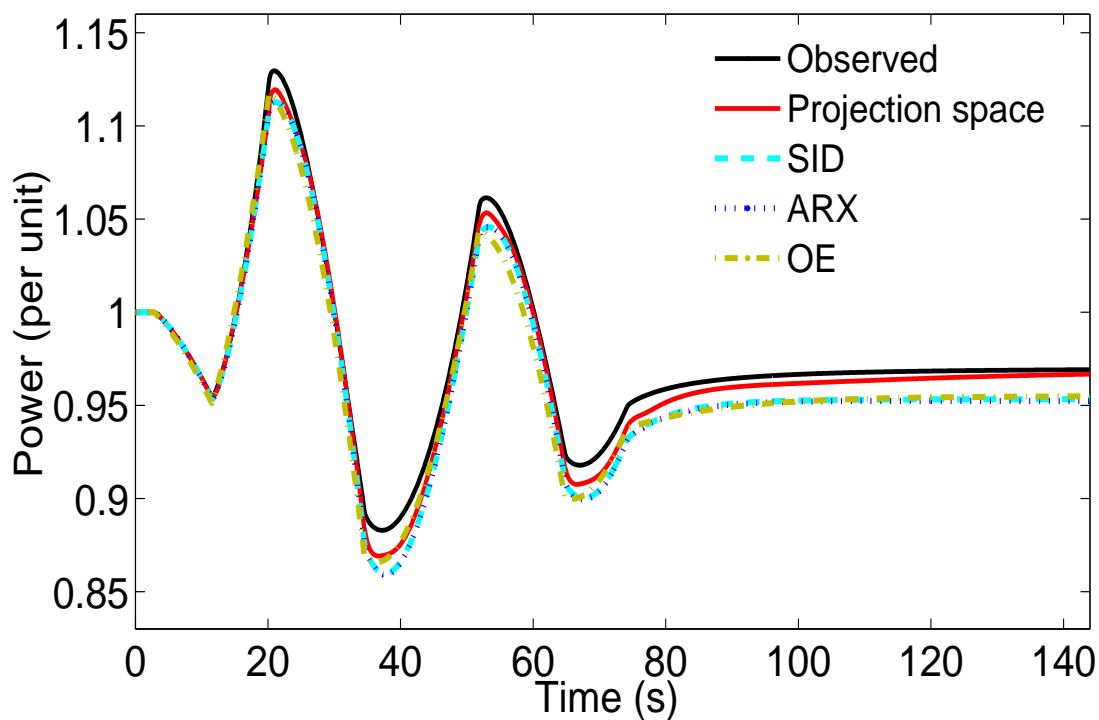


FIGURE 3.7: Outputs of estimated models with observed data for Case A input.

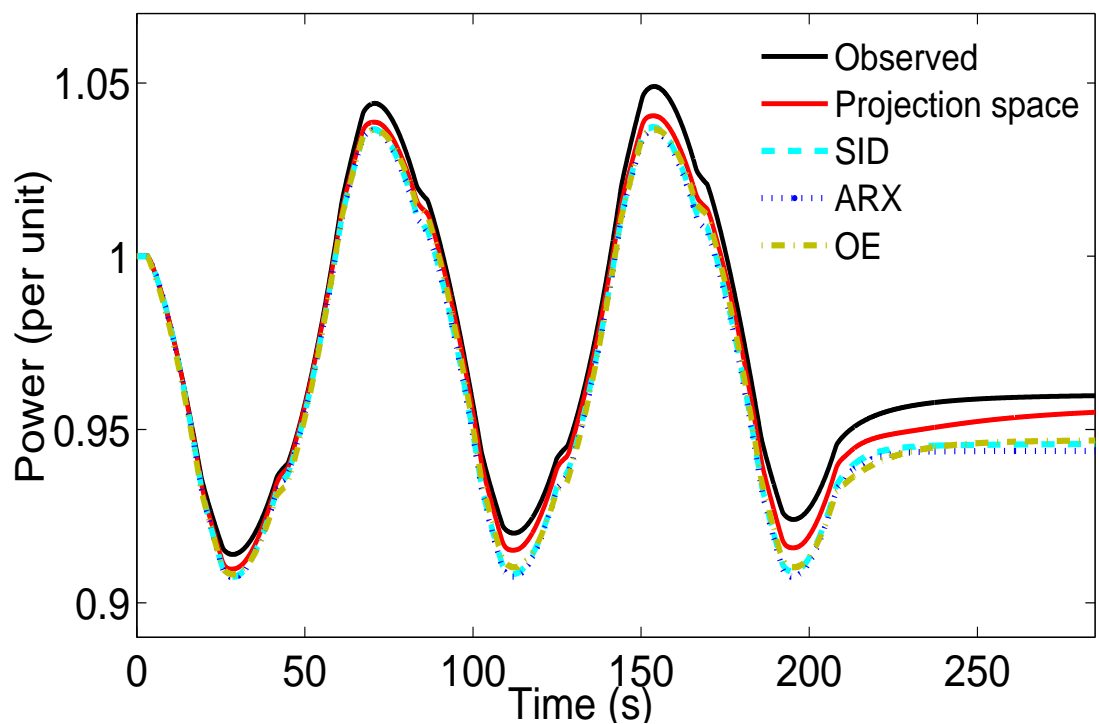


FIGURE 3.8: Outputs of estimated models with observed data for Case B input.

TABLE 3.2: RMSE for simulated reference dataset.

Model \ Dataset	Projection space	SID	ARX	OE
Estimation	4.88×10^{-2}	2.246×10^{-1}	2.818×10^{-1}	1.918×10^{-1}
Validation (Case A)	6.557×10^{-1}	1.0954	1.1358	1.1180
Validation (Case B)	5.292×10^{-1}	1.0247	1.1269	1.0000

and water level in zonal control compartment (ZCC) as input. The inflow variations in ZCC water level cause variation in water level and consequently reactivity variations which result into changes in reactor power. Figures 3.9 and 3.10 respectively show variation in reactivity due to change in water level in ZCC and the corresponding variation in power.

Wavelet operators are designed as described in Subsections 3.2.2 and 3.2.3; this leads to the design of full PRBWFBs. The PRBWFBs are designed to have length of six taps and two vanishing moments as given in Table 3.3. The original measurement space system states are transformed by these operators to those in the projection space and model parameters are estimated. System dynamics matrix of estimated projection space model is given by A_{j+1}^w ,

$$A_{j+1}^w = \text{diag} \left[0.0566, 0.1107, 0.9993 \right]. \quad (3.50)$$

Input matrix B_{j+1}^w is given by

$$B_{j+1}^w = \text{diag} \left[19.035, 2364.8, 94.335, \right]. \quad (3.51)$$

The estimation of reactor power by projection space model is shown in Figure 3.10, which also compares estimates of power obtained by other empirical models. It may be seen that the projection space model suitably predicts the multiscale behavior and gives a better estimate of reactor power than do the other models. In case of ARX approach, the model structure estimates a noise model, however the parameter of noise model is related to process model and thus gives a poor estimate. Besides this, the OE model

TABLE 3.3: Estimated filter coefficients for different states for simulated plant dataset.

State	Estimated Filters
First	$h[k]=[-0.00497, 0.78317, 1.31746, 0.26550, -0.26381, 0]$ $g[k]=[0, 0, 0.00303, -0.47679, 0.47376, 0]$ $\tilde{h}[k]=[0, 0.47376, 0.47679, 0.00303, 0, 0]$ $\tilde{g}[k]=[0, 0.26381, 0.26550, -1.31746, 0.78317, 0.00497]$
Second	$h[k]=[0.00477, -0.52473, -0.88623, -0.17917, 0.17754, 0]$ $g[k]=[0, 0, -0.00645, 0.71031, -0.70385, 0]$ $\tilde{h}[k]=[0, -0.70385, -0.71031, -0.00645, 0, 0]$ $\tilde{g}[k]=[0, -0.17754, -0.17917, 0.88623, -0.52473, -0.00477]$
Third	$h[k]=[-0.02846, 0.49605, 0.89684, 0.19166, -0.18066, 0]$ $g[k]=[0, 0, 0.04172, -0.72704, 0.68532, 0]$ $\tilde{h}[k]=[0, 0.68532, 0.72704, 0.04172, 0, 0]$ $\tilde{g}[k]=[0, 0.18066, 0.19166, -0.89684, 0.49605, 0.02846]$

structure does not evaluate a noise model and approximates the noisy plant output as the output of model. In SID, system parameters estimate Kalman states which leads to a good response. Different estimated models are given as follows. The OE model is given by

$$\begin{aligned}
 B(q^{-1}) &= -3.83q^{-1} + 31.55q^{-2} - 28.27q^{-3}, \\
 A(q^{-1}) &= 1 - 1.042q^{-1} - 0.841q^{-2} + 0.883q^{-3}.
 \end{aligned} \tag{3.52}$$

The ARX model is given by

$$\begin{aligned}
 B(q^{-1}) &= -15.63q^{-1} + 42.93q^{-2} - 25.92q^{-3} - 41.9q^{-4} + 66.34q^{-5} - 25.92q^{-6}, \\
 A(q^{-1}) &= 1 - 2.867q^{-1} + 2.789q^{-2} - 0.975q^{-3} + 0.0541q^{-4},
 \end{aligned} \tag{3.53}$$

and the SID model is given by

$$\begin{aligned}
 x[k+1] &= \begin{bmatrix} 0.999 & -0.003 & 0.004 \\ 0.083 & 0.454 & 0.272 \\ 0.122 & -0.828 & -0.509 \end{bmatrix} x[k] + \begin{bmatrix} 19.035 \\ 2364.8 \\ 94.335 \end{bmatrix} u[k] + \begin{bmatrix} 0.125 \\ 2.266 \\ 0.152 \end{bmatrix} e[k], \\
 y[k] &= \begin{bmatrix} 7.703 & -0.001 & 0.003 \end{bmatrix} x[k] + e[k].
 \end{aligned} \tag{3.54}$$

For the purpose of validation of different estimated models, plant datasets are shown in

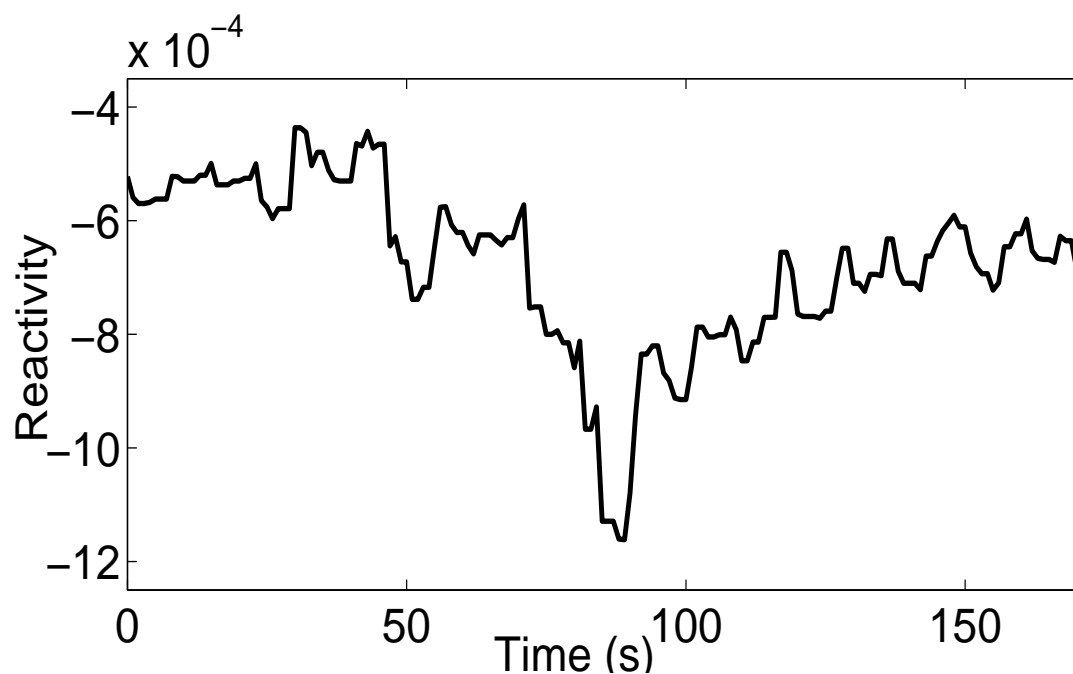


FIGURE 3.9: Variation of plant reactivity estimation input.

TABLE 3.4: RMSE for simulated plant dataset.

Dataset \ Model	Projection space	SID	ARX	OE
Estimation	0.3521	0.3709	0.5985	0.3751
Validation	1.0490	1.1309	1.1805	1.1332

Figures 3.11 and 3.12. These plant datasets are comprised of data on changes in reactivity and corresponding variation in power. Outputs of all estimated models are compared with observed plant output in Figure 3.12. It can be seen that single scale techniques are only able to approximate the multiscale process while the estimated model in projection space efficiently captures system modes evolving at different scale of time, thus giving better prediction result as compared to others. Table 3.4 shows the value of RMSE for different models for the estimation and validation datasets. It may be noted that the projection space approach yields less RMSE than do other single scale techniques thereby outperforming other techniques in estimation as well as in validation in terms of mean squared error in the output.

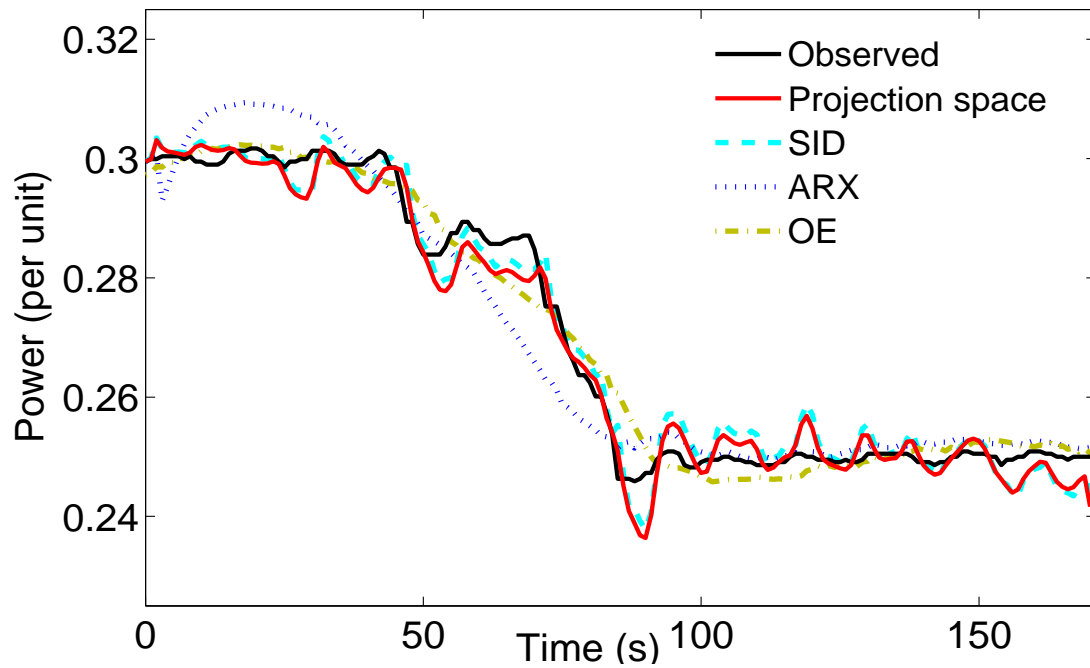


FIGURE 3.10: Outputs of estimated models with observed data for plant input.

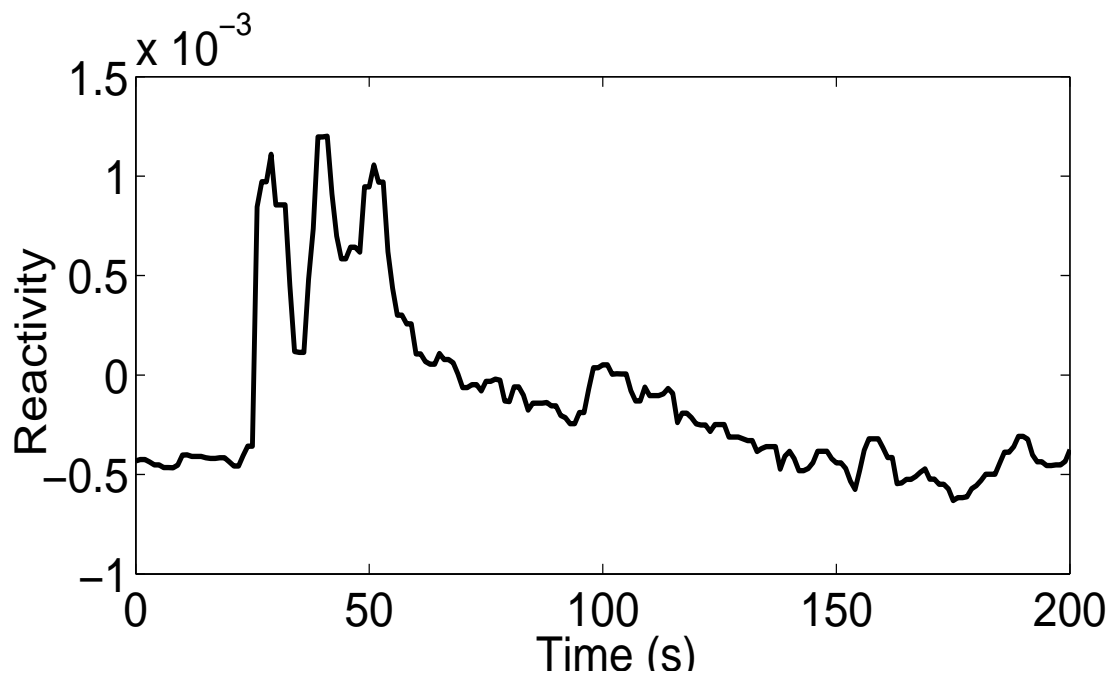


FIGURE 3.11: Variation of plant reactivity validation input.

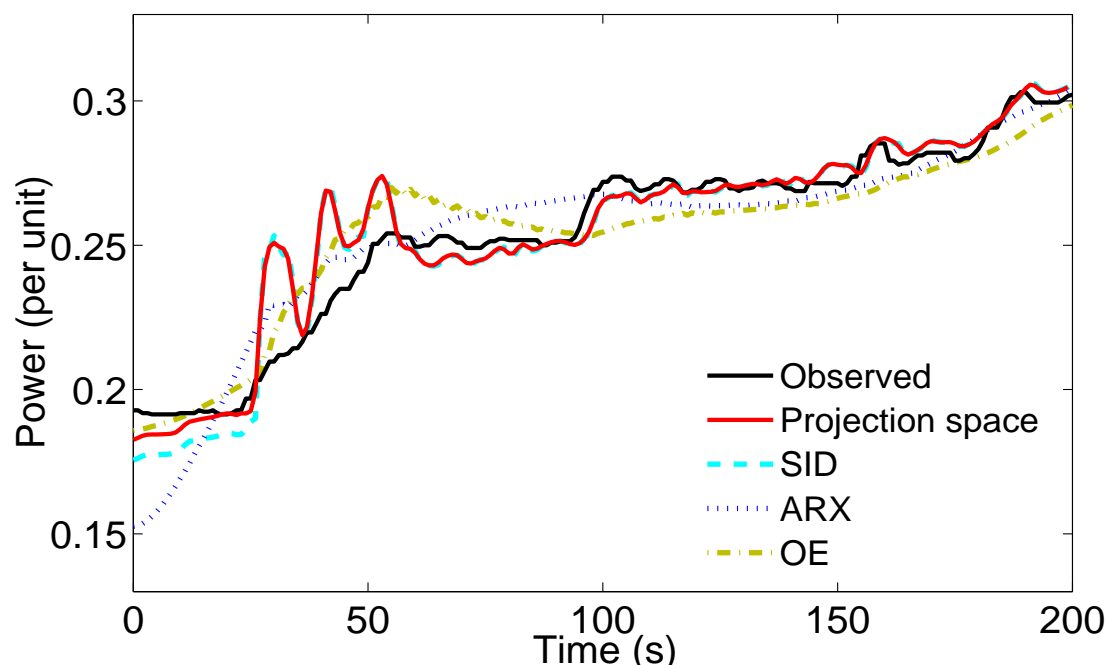


FIGURE 3.12: Outputs of estimated models with observed data for plant input.

3.3.3 Controllability

Controllability of an N^{th} order LTI system can in general be inspected using the following controllability check matrix.

$$Q = [B \ AB \ \dots \ A^{N-1}B] \quad (3.55)$$

A system is said to be controllable if the matrix Q is nonsingular. Controllability of a nuclear reactor system given by (3.40) has already been proved by Liu et al. [178]. It can be proved by establishing the controllability check matrix. For the reactor system, the controllability check matrix suggest that if the following conditions are satisfied then it is controllable [178].

1. $P_0 > 0$
2. $\lambda_1 \neq \lambda_2 \neq \lambda_3 \neq \lambda_4 \neq \lambda_5 \neq \lambda_6 \neq \Lambda$

The above mentioned conditions ensure that the determinant of the controllability check matrix Q is non zero and thus Q is invertible. Condition 1 is met as the reactor is assumed to be operating at a steady state power level. Whereas, Table C.1 shows that condition 2 is satisfied for the reactor system. These two conditions ensure controllability of the point kinetics reactor system considered in this study.

3.4 Summary

This chapter formalizes the design of wavelet operator to transform states of a multivariable system from space of temporal measurements to that of projections in multiresolution. The imposed structure in projection space is justified as wavelets are approximate Eigen functions of convolution operators. It is also shown that given an operator, there exists a definite relationship between the model in the measurement space and that in the projection space. The design methodology is demonstrated by designing multirate filter bank associated with wavelet operators for modeling a multi-timescale nuclear reactor system. It has been validated using reference as well as plant datasets. It is shown that projection space modeling of the reactor system leads to significant improvement in output prediction over single-scale modeling techniques.

Chapter 4

Multiscale System Identification

In this chapter, methodology of multiscale system identification is presented. Specifically, it formulates open-loop and close-loop subspace identification techniques in multiresolution framework. It also discusses on-line implementation of proposed technique for real-time applications. It further discusses various subtle issues such as selection of wavelets and decomposition depth. The efficacy of proposed approach is demonstrated on to the nuclear reactor. Detailed simulation studies are performed to compare proposed technique with other single scale and multiscale approaches.

4.1 Multiscale System Identification

The proposition of multiscale system identification is to estimate a class of empirical models working in multiresolution. Generally, transformation of input-output dataset in multiresolution gives an advantage to look at different modes embedded in the dataset at different time-frequency resolution. Wavelet transform tends to decouple system modes because wavelets are approximate eigenfunction of the convolution operator and the correlation structure of wavelet coefficients decays sharply. As compared to the Fourier-based representation, a suitably selected wavelet basis has compact representation in the time-frequency plane. Moreover, the sparsity in wavelet subspace minimizes

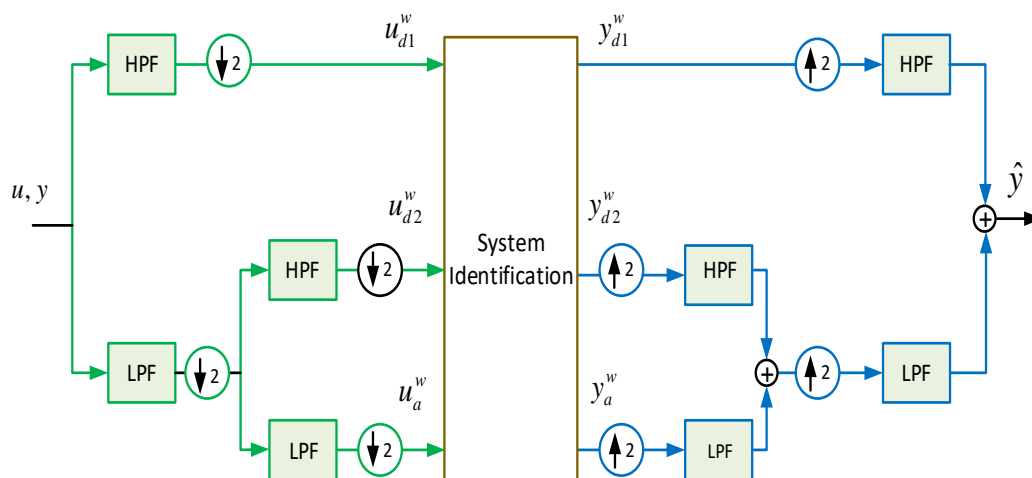


FIGURE 4.1: Block diagram representation of multiscale system identification using dyadic discretization for two levels of decomposition.

size of the parameter vector to estimate and gives reduced order system implicitly. Multiscale system identification using wavelets can be implemented by employing either a dyadic discretization scheme or an integer discretization scheme. Dyadic discretization performs sub-sampling of data. Thus, it gives a compact representation, while integer discretization does not use sub-sampling operation and gives a redundant representation. This makes dyadic discretization suitable for off-line identification. The procedure of multiscale system identification is a two-step process, 1) multiscale data projection or representation, and 2) model identification at different scales. The block diagram representation of the proposed technique is shown in Figure 4.1. The analysis side projects data at different resolutions using suitably selected wavelet. The projection operation is implemented with wavelet filter bank where different filters are operating in different frequency sub-bands. The filtered signal is sub-sampled by two (shown by downward arrow followed by 2) to keep the dimensionality same as that in measurement domain. This operation gives non-redundant wavelet coefficients which are used in estimating models. A number of significant scales are found out for model estimation. The simulation or prediction output of estimated models is combined by projecting the transformed coefficients into measurement space with the help of synthesis low pass filter (LPF) and high pass filter (HPF).

4.1.1 Multiscale Data Representation

Consider a given input (U) and output (Y) time-series where the later is assumed to be contaminated with white Gaussian noise. The DWT operation to transform input and output is given by

$$Y^w = FY; \quad U^w = FU; \quad (4.1)$$

where F is the wavelet transform operator which consists of wavelet filters to transform the given signal into projection space. It is defined as

$$F = \left[\prod_{j=1}^J H_j^T \quad G_J^T \prod_{j=1}^{J-1} H_j^T \quad G_{J-1}^T \prod_{j=1}^{J-2} H_j^T \quad \dots \quad G_1^T \right]^T, \quad (4.2)$$

where H_j and G_j ($2^{J-j} \times 2^J$) matrices are defined by wavelet filter coefficients at j^{th} scale. Scale $j = 1$ and $j = J$ respectively represent initial and final level of decomposition. For the case of Haar wavelet and $J = 2$, F is given by

$$F = \begin{bmatrix} H_2 H_1 \\ G_2 H_1 \\ G_1 \end{bmatrix} = \frac{1}{2} \begin{bmatrix} 1 & 1 & 1 & 1 \\ 1 & 1 & -1 & -1 \\ \sqrt{2} & -\sqrt{2} & 0 & 0 \\ 0 & 0 & \sqrt{2} & -\sqrt{2} \end{bmatrix}. \quad (4.3)$$

The output and input time-series are synthesized using inverse wavelet transform as

$$\hat{Y} = \tilde{F}Y^w; \quad \hat{U} = \tilde{F}U^w; \quad (4.4)$$

where \tilde{F} is the inverse wavelet transform operator. The wavelet and inverse wavelet operator can be orthogonal, or bi-orthogonal, or semi-orthogonal. \hat{Y} and \hat{U} contain processed time-series of output and input respectively. The wavelet transform operation distributes the contribution of noise among all small wavelet coefficients while the contribution from deterministic part will be in small number of high amplitude coefficients. Therefore, no loss of useful information in the processed signal is likely to be caused by an amplitude thresholding of the wavelet coefficients. The nonlinear approximation

of signal via thresholding of the coefficients enables faster convergence [181]. Besides these advantages offered by projection-based formulation, its effectiveness often requires careful selection of wavelet basis, decomposition depth, and significant scales.

4.1.1.1 Selection of Wavelet Basis

Generally, wavelet basis should be selected such that, a) it has good correlation with data thereby ensuring sparse representation in the transformed domain, b) it contains maximum information or minimum entropy at each scale [182], c) it has the desired time-frequency resolution as a short support basis will sacrifice frequency resolution at high levels while a broad support basis will degrade time resolution at lower levels, and d) it has compact representation. For instance, piecewise constant functions (e.g. Haar) are suitable for representing a highly localized event like singularity or sudden change while piecewise polynomial functions (e.g. splines) are preferable for a smoothly varying signal. Further, complex wavelets are preferred for capturing oscillatory behaviour while real ones can be used for the detection of peaks or discontinuities [183].

4.1.1.2 Computation of Decomposition Depth

Decomposition depth or scale (J) is decided to ensure that a minimum number of observations hit the support of each basis function. The maximum theoretical depth however is limited to the integer value of $\log_2(cf_s)$, where f_s is the maximum natural frequency of the sampled signal and c is a number between 10 and 20 [121]. The maximum decomposition depth can also be computed using the Fourier transform. It is selected such that the magnitude of the Fourier transform is above the noise floor-level, i.e.

$$|Y(\pi/2^J)| \geq |Y(\pi/f)|; \quad |U(\pi/2^J)| \geq |U(\pi/f)|. \quad (4.5)$$

4.1.1.3 Selection of Significant Scales

Usually, only some of the scales contribute significantly in determining process behavior and for a parsimonious model representation, the selection of significant scales is a crucial step. There are various ways of finding significant scales, a) it can be decided by computing the energy of wavelet coefficients at each scale, b) level dependent PCA can be calculated to find relevant scales [26], c) prediction capability of estimated models can be analyzed at different scales [125], d) scale-based SVD can be computed to find relevant scales, and e) trace of the estimation error covariance matrix can also be used for proper scale selection [25].

4.1.2 Model Estimation at Different Scales

The notion of system identification can be used to build different multiscale model structures in multiresolution. This section presents multiscale ARX model identification for its representation simplicity. Consider the time invariant ARX model given by

$$y[k] = \sum_{m=1}^p a_m y[k-m] + \sum_{n=1}^q b_n u[k-n] + e[k], \quad (4.6)$$

which can be represented in regression form as

$$y[k] = \zeta^T[k]\theta + e[k], \quad (4.7)$$

where $\zeta[k] = [y[k-1] \ \cdots \ y[k-p] \ u[k-1] \ \cdots \ u[k-q]]^T$ is the regression vector and $\theta = [a_1 \ \cdots \ a_p \ b_1 \ \cdots \ b_q]^T$ is the coefficient vector.

Considering all the N measurements of input and output, we have from (4.7)

$$Y = \Phi\theta + \Xi, \quad (4.8)$$

$$\text{where } Y = \begin{bmatrix} y[1] \\ y[2] \\ \vdots \\ y[N] \end{bmatrix}, \Phi = \begin{bmatrix} \zeta^T[1] \\ \zeta^T[2] \\ \vdots \\ \zeta^T[N] \end{bmatrix}, \text{ and } \Xi = \begin{bmatrix} e[1] \\ e[2] \\ \vdots \\ e[N] \end{bmatrix}.$$

Representation of (4.8) in multiresolution wavelet space is given by

$$y_j[k_j] = \sum_{m=1}^{p_j} a_m^{(j)} y_j[k_j - m] + \sum_{n=1}^{q_j} b_n^{(j)} u_j[k_j - n] + e_j[k_j], \quad j = 1, 2, \dots, J+1, \quad (4.9)$$

where u_j , y_j , and e_j are wavelet coefficients of input, output, and white noise sequence respectively; $a_m^{(j)}$ and $b_n^{(j)}$ are system parameters, $k_j = 2^{-j}k$, where $j = 1, 2, \dots, J$ represents detail at j^{th} scale and $j = J+1$ represents approximation at scale J . In matrix form, (4.9) can be represented as

$$Y_j^w = \zeta_j^w \theta_j + \Xi_j^w, \quad j = 1, 2, \dots, J+1, \quad (4.10)$$

where Y_j^w , ζ_j^w , and Ξ_j^w represent the wavelet coefficients of output time-series, regression vector, and noise vector respectively at j^{th} scale. They are calculated respectively as

$$\begin{aligned} FY &= \begin{bmatrix} (Y_{J+1}^w)^T & (Y_J^w)^T & \dots & (Y_1^w)^T \end{bmatrix}^T, \\ F\Phi &= \begin{bmatrix} (\zeta_{J+1}^w)^T & (\zeta_J^w)^T & \dots & (\zeta_1^w)^T \end{bmatrix}^T, \\ F\Xi &= \begin{bmatrix} (\Xi_{J+1}^w)^T & (\Xi_J^w)^T & \dots & (\Xi_1^w)^T \end{bmatrix}^T. \end{aligned} \quad (4.11)$$

Note that, Ξ_j^w will be a white noise sequence at each scale. Similarly, the coefficient vector is given by $\theta_j = \begin{bmatrix} a_1^{(j)} & \dots & a_{p_j}^{(j)} & b_1^{(j)} & \dots & b_{q_j}^{(j)} \end{bmatrix}^T$.

Therefore, the least-squares solution of (4.10) can be obtained as

$$\hat{\theta}_j = \left((\zeta_j^w)^T \zeta_j^w \right)^{-1} (\zeta_j^w)^T Y_j^w, \quad j = 1, 2, \dots, J+1. \quad (4.12)$$

4.1.3 Model Validation

The task of system identification is incomplete without model validation. The estimated model needs to be validated so that it works not only for the training dataset but also for several sets of test data. Model validation can be carried out by residual analysis which consist of the *whiteness test* and the *independence test* [1]; and by Cross-validation. The first method analyses the innovation sequence/residuals obtained after estimating model from the training dataset. The whiteness test is used to check autocorrelation of the residuals at the output. If the correlation coefficients lie within the confidence interval, then it is concluded that the residuals do not contain any significant information. The test of linear independence calculates the dependency of residuals on past input signal through cross-correlation. The insignificant value of coefficients guarantees that there is nothing lying in the residual to be governed by input to the system. Cross-validation is a rigorous approach where the estimated model is validated using various test data different from the training data. It is rather practical to verify the competence of the model in handling unseen dynamics before employing the model for prediction/forecasting, simulation or control design.

4.2 Multiscale Subspace Identification

Multiscale Subspace Identification (ms-SID) is a time-scale domain based technique for linear state-space model estimation wherein system states are estimated directly from the projection of measurements at different resolution. The approach is concerned about establishing a relationship in projection space with the development of low order state-space models in different frequency bands of the process. A nonlinear system is approximated by a set of linear state-space models estimated at different resolutions. The technique inherits features of robust subspace identification with the added advantage of wavelet basis function enabling multiresolution state-space model development. Moreover, identification of reduced order multiscale state-space models is beneficial

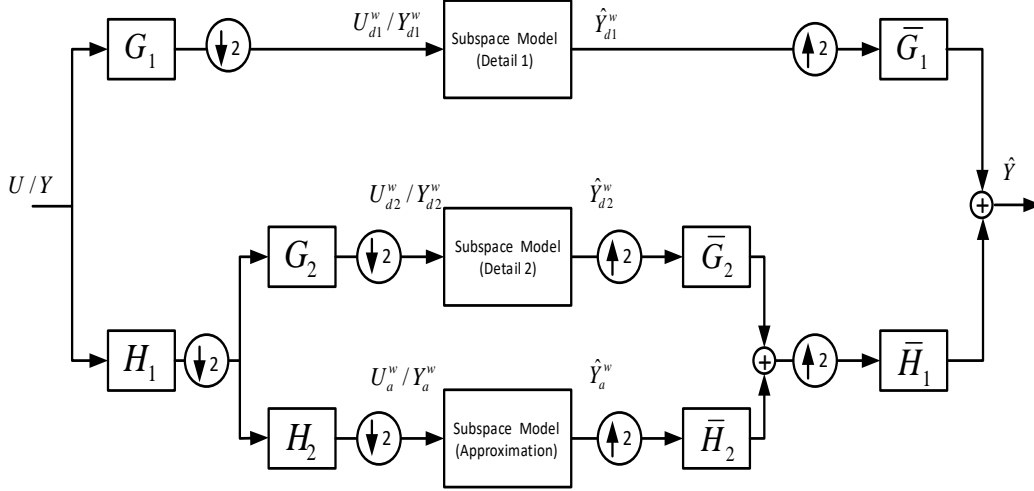


FIGURE 4.2: Block diagram representation of multiscale subspace identification for two levels of decomposition.

for the implementation of control laws in projection space. The proposed technique is shown in Figure 4.2 which depicts a scale-wise implementation for a decomposition depth of two. H_j and G_j respectively denote LPF and HPF at analysis side, whereas \bar{H}_j and \bar{G}_j are LPF and HPF at synthesis side respectively.

4.2.1 Open-Loop Multiscale Subspace Identification

The discrete time state-space model in the projection is given by,

$$x_j[k_j + 1] = A_j x_j[k_j] + B_j u_j[k_j] + K_j e_j[k_j], \quad (4.13)$$

$$y_j[k_j] = C_j x_j[k_j] + D_j u_j[k_j] + e_j[k_j], \quad (4.14)$$

where the state $x_j[k_j] \in \mathbb{R}^{n_j}$, the input $u_j[k_j] \in \mathbb{R}^{m_j}$, the output $y_j[k_j] \in \mathbb{R}^{l_j}$, and innovation sequence $e_j[k_j] \in \mathbb{R}^{l_j}$, with the error covariance matrix $E(e_j[k_j] e_j^T[k_j]) = S_j$. $A_j \in \mathbb{R}^{n_j \times n_j}$, $B_j \in \mathbb{R}^{n_j \times m_j}$, $K_j \in \mathbb{R}^{n_j \times l_j}$, and $C_j \in \mathbb{R}^{l_j \times n_j}$ are system dynamics matrix, input matrix, Kalman gain, and output matrix at j^{th} scale respectively. The innovation sequence at each scale is considered to be uncorrelated white.

The output equation at the j^{th} scale can be written as,

$$Y_{f,j} = \Gamma_{f,j} X_{k,j} + H_{f,j}^d U_{f,j} + H_{f,j}^s E_{f,j}, \quad (4.15)$$

or simply,

$$Y_{f,j} = L_{x,j} Z_{p,j} + H_{f,j}^d U_{f,j} + H_{f,j}^s E_{f,j}, \quad (4.16)$$

where $L_{x,j}$ is related to the states and formed as the product of observability matrix and predictor controllability matrix at j^{th} scale.

In terms of output predictor, (4.16) can also be rewritten as

$$\begin{aligned} \begin{bmatrix} y_j[k_j + 1] \\ y_j[k_j + 2] \\ \vdots \\ y_j[k_j + v] \end{bmatrix} &= \underbrace{\begin{bmatrix} a_{v-1}^{(j)} & \cdots & a_0^{(j)} & b_{v-1}^{(j)} & \cdots & b_0^{(j)} \\ a_v^{(j)} & \cdots & a_1^{(j)} & b_v^{(j)} & \cdots & b_1^{(j)} \\ \vdots & \ddots & \vdots & \vdots & \ddots & \vdots \\ 0 & \cdots & 0 & 0 & \cdots & 0 \end{bmatrix}}_{L_{x,j}} \begin{bmatrix} y_j[k_j - v + 1] \\ \vdots \\ y_j[k_j] \\ u_j[k_j - v] \\ \vdots \\ u_j[k_j - 1] \end{bmatrix} \\ &+ \underbrace{\begin{bmatrix} d_0^{(j)} & 0 & \cdots & 0 \\ d_1^{(j)} & d_0^{(j)} & \cdots & 0 \\ \vdots & \vdots & \ddots & \vdots \\ d_{v-1}^{(j)} & d_{v-2}^{(j)} & \cdots & d_0^{(j)} \end{bmatrix}}_{H_{f,j}^d} \begin{bmatrix} u_j[k_j] \\ u_j[k_j + 1] \\ \vdots \\ u_j[k_j + v - 1] \end{bmatrix} \\ &+ \underbrace{\begin{bmatrix} 1 & 0 & \cdots & 0 \\ s_1^{(j)} & 1 & \cdots & 0 \\ \vdots & \vdots & \ddots & \vdots \\ s_{v-1}^{(j)} & s_{v-2}^{(j)} & \cdots & 1 \end{bmatrix}}_{H_{f,j}^s} \begin{bmatrix} e_j[k_j + 1] \\ e_j[k_j + 2] \\ \vdots \\ e_j[k_j + v] \end{bmatrix}. \end{aligned} \quad (4.17)$$

Observe that the first row of subspace matrix $L_{x,j}$ gives the parameter vector of multiscale high-order ARX model [1], and the last row of $H_{f,j}^d$ and $H_{f,j}^s$ give the impulse response to deterministic and stochastic inputs respectively.

The output equation is expressed as the product of observability and controllability matrix and Toeplitz matrix using the transformed dataset. There are two primary routes for solving this subspace identification problem. The first approach estimates the state

sequence and observability matrix and determines full system matrices in a single step through the least squares. The second technique estimates only the observability matrix. The unifying approach of Overschee et al. [62] employing the second method is explained in the following:

- **Step 1: Estimation of $L_{x,j}$** - The output equation (4.30) is projected onto the orthogonal basis of $U_{j,f}$ such that the contribution from input terms is eliminated leaving the equation with output state and noise terms only, *i.e.*,

$$Y_{f,j}\Pi_{U_{f,j}}^\perp = L_{x,j}Z_{p,j}\Pi_{U_{f,j}}^\perp + H_{f,j}^s E_{f,j}\Pi_{U_{f,j}}^\perp, \quad (4.18)$$

where $\Pi_{U_{f,j}}^\perp = I - U_{f,j}^T(U_{f,j}U_{f,j}^T)^{-1}U_{f,j}$ represents the orthogonal projection of $U_{f,j}$ and I is an identity matrix. The least squares solution of (4.18) gives

$$\begin{aligned} \hat{L}_{x,j} &= Y_{f,j}\Pi_{U_{f,j}}^\perp \left(\Pi_{U_{f,j}}^\perp Z_{p,j}^T \right) \left(Z_{p,j}\Pi_{U_{f,j}}^\perp \Pi_{U_{f,j}}^\perp Z_{p,j}^T \right)^{-1} \\ &= Y_{f,j}\Pi_{U_{f,j}}^\perp Z_{p,j}^T \left(Z_{p,j}\Pi_{U_{f,j}}^\perp Z_{p,j}^T \right)^{-1}. \end{aligned} \quad (4.19)$$

- **Step 2: Performing the SVD** - The SVD of weighted estimated matrix gives, $w_{1,j}\hat{L}_{x,j}w_{2,j} = U_{n,j}\sum_{n,j}V_{n,j}^T$, where $\sum_{n,j}$ contains n largest singular values at the j^{th} scale. The pre and post multiplied weighing matrices are such that, for CVA algorithm [57], $w_{1,j} = \left(Y_{f,j}\Pi_{U_{f,j}}^\perp Y_{f,j}^T \right)^{-1/2}$, $w_{2,j} = \left(Z_{p,j}\Pi_{U_{f,j}}^\perp Z_{p,j}^T \right)^{1/2}$; for MOESP algorithm [184], $w_{1,j} = I$, $w_{2,j} = \left(Z_{p,j}\Pi_{U_{f,j}}^\perp Z_{p,j}^T \right)^{1/2}$; and for N4SID [62], $w_{1,j} = I$ and $w_{2,j} = \left(Z_{p,j}Z_{p,j}^T \right)^{1/2}$. This gives estimated observability matrix, $\hat{\Gamma}_{f,j} = w_{1,j}^{-1}U_{n,j}\sum_{n,j}^{1/2}$.
- **Step 3: Estimation of A_j and C_j** - First estimate of C_j is extracted from the first l rows and all corresponding columns of observability matrix. Then the system dynamics matrix is estimated by pre-multiplying $\hat{\Gamma}_{f-1,j}^{-1}$ to the observability matrix formed by extracting $l+1$ rows to lf rows and all corresponding columns of $\hat{\Gamma}_{f,j}$.

- Step 4: *Estimation of K_j , B_j , D_j and $x_{0,j}$* - For the estimation of K_j , both sides

of (4.30) are projected on to the orthogonal basis formed by $W_j = \begin{bmatrix} Z_{p,j} \\ U_{f,j} \end{bmatrix}$.

Further, as $N/2^j$ becomes large, $\frac{1}{N/2^j} E_{f,j} U_{f,j}^T \rightarrow 0$ and $\frac{1}{N/2^j} E_{f,j} Z_{p,j}^T \rightarrow 0$. Therefore,

$$Y_{f,j} \Pi_{W_j}^\perp = H_{f,j}^s E_{f,j} \Pi_{W_j}^\perp = H_{f,j}^s E_{f,j}. \quad (4.20)$$

The QR decomposition of (4.20) gives the parameters of K_j . Now, to estimate the remaining matrices, the predictor is defined as

$$\begin{aligned} y_j[k_j] = & \left(\hat{C}_j (qI - \hat{A}_{K,j})^{-1} B_{K,j} + D_j \right) u_j[k_j] + \hat{C}_j (qI - \hat{A}_{K,j})^{-1} \hat{K}_j y_j[k_j] \\ & + \hat{C}_j (qI - \hat{A}_{K,j})^{-1} x_{0,j} + e_j[k_j], \end{aligned} \quad (4.21)$$

where $\hat{A}_{K,j} = (\hat{A}_j - \hat{K}_j C_j)$, $B_{K,j} = (B_j - \hat{K}_j D_j)$, $x_{j,0}$ is initial state, and q is a forward shift operator such that $qu[k] = u[k+1]$. Using $e_j[k_j] = R_j \bar{e}_j[k_j]$, where $\bar{e}_j[k_j]$ has an identity covariance matrix, and defining

$$\begin{aligned} \bar{y}_j[k_j] &= R_j^{-1} \left(I - \hat{C}_j (qI - \hat{A}_{K,j})^{-1} \hat{K}_j \right) y_j[k_j], \\ G_j &= R_j^{-1} \hat{C}_j (qI - \hat{A}_{K,j})^{-1}, \\ \bar{D}_j &= R_j^{-1} D_j, \end{aligned} \quad (4.22)$$

we get,

$$\bar{y}_j[k_j] = G_j B_{K,j} u_j[k_j] + \bar{D}_j u_j[k_j] + G_j x_{0,j} + \bar{e}_j[k_j]. \quad (4.23)$$

Then, $B_{K,j}$, D_j , and $x_{0,j}$ matrices are estimated through least squares solution of (4.23), where the parameters are related as, $\hat{D}_j = R_j \bar{D}_j$ and $\hat{B}_j = \hat{B}_{K,j} + \hat{K}_j \hat{D}_j$ [83]. The identified subspace models are of low order due to reduced order state sequence estimation from data and do not require an explicit model order reduction scheme. For consistent identification, the formulation requires that the pair $\{\hat{A}_j, \hat{C}_j\}$ be observable, the projected input must be persistently excited of order $2f$, and f must be higher than the number of states of the model to be identified. Typically, the number of columns

in the Hankel matrix of measurements must be hundred times more than the number of block rows.

4.2.2 Closed-Loop Multiscale Subspace Identification

Considering the LTI system in *predictor form* and writing the output equation (2.16) at j^{th} scale as,

$$y_{fi,j}[k_j+i-1] = \bar{\Gamma}_{fi,j} L_{p,j} z_{p,j}[k_j] + \bar{G}_{fi,j} z_{i-1,j}[k_j] + e_j[k_j+i-1], \quad i = 1, 2, \dots, f \quad (4.24)$$

The extended observability matrix can be estimated as the least squares solution of the following problem

$$\widehat{\bar{\Gamma}_{fi,j} L_{p,j}} = \min_{\bar{\Gamma}_{fi,j} L_{p,j}} \|y_{fi,j} - \bar{\Gamma}_{fi,j} L_{p,j} z_{p,j}\|^2, \quad i = 1, 2, \dots, f. \quad (4.25)$$

An efficient way to compute the least squares solution is using the RQ decomposition.

It is given as

$$\begin{bmatrix} z_{p,j} \\ y_{f1,j} \end{bmatrix} = \underbrace{\begin{bmatrix} R_{11} & 0 \\ R_{21} & R_{22} \end{bmatrix}}_R \underbrace{\begin{bmatrix} Q_1^T \\ Q_2^T \end{bmatrix}}_Q. \quad (4.26)$$

Hence,

$$\widehat{\bar{\Gamma}_{fi,j} L_{p,j}} = \begin{bmatrix} R_{21} & R_{22} \end{bmatrix} \begin{bmatrix} Q_1^T \\ Q_2^T \end{bmatrix} \left(\begin{bmatrix} R_{11} & 0 \end{bmatrix} \begin{bmatrix} Q_1^T \\ Q_2^T \end{bmatrix} \right)^\dagger, \quad (4.27)$$

or, simply

$$\widehat{\bar{\Gamma}_{fi,j} L_{p,j}} = R_{21} R_{11}^\dagger, \quad (4.28)$$

where R_{11}^\dagger denotes the Moore-Penrose pseudo-inverse of R_{11} .

Now, combining the estimate of $\widehat{\Gamma}_{f_i,j}L_{p,j}$ to give

$$\widehat{\Gamma}_f L_p = \begin{bmatrix} \widehat{\Gamma}_{f1} L_p \\ \widehat{\Gamma}_{f2} L_p \\ \vdots \\ \widehat{\Gamma}_{ff} L_p \end{bmatrix} \quad (4.29)$$

The remaining steps to obtain system matrices are similar to Step 2 to Step 4 of the open-loop identification problem.

4.3 On-line Multiscale Subspace Identification

This section extends the notion of ms-SID to design an on-line subspace identification strategy in multiresolution framework. The block diagram representation of the on-line ms-SID is shown in Figure 4.3. The on-line ms-SID is implemented using an integer discretization scheme due to the fact that the integer discretization does not introduces any time delay in the analysis as the case with dyadic discretization scheme. The proposed technique with integer discretization scheme is shown in Figure 4.4 for a decomposition depth of two. The input-output data are measured at finest scale $j = 0$ and assumed to be available up to the current time instant k . A window of $2J$ past observation is formed and decomposed into detail spaces at $j = 1, 2, \dots, J$ and an approximation space at $j = J + 1$. The window is translated by one time step with the availability of new data at time instant $k + 1$, and the wavelet decomposition is performed. The similar procedure is repeated again for new data samples. It may be noted that due to redundancy in representation, only the last (or rightmost) coefficients indexed as $k, k + 1, \dots$ at each scale are stored. The proposed scheme is based on Haar wavelet because of the ability of Haar wavelet to precisely locate features in the time domain. Being compactly supported, Haar wavelet does not introduce delay in the analysis and computes the transformation entirely using data from the past and present only. Further, it avoids undesirable border distortions due to signal extensions. This makes

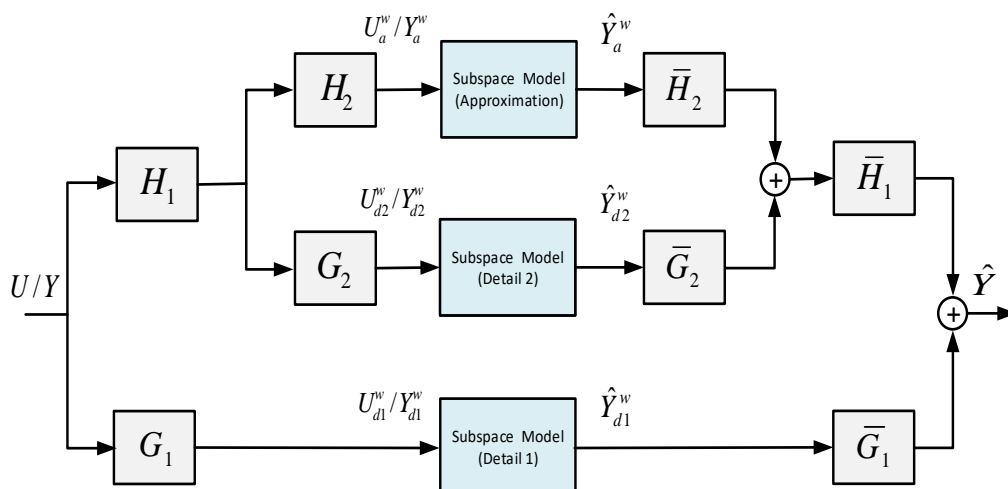


FIGURE 4.3: Block diagram representation of on-line ms-SID for two scale decomposition.

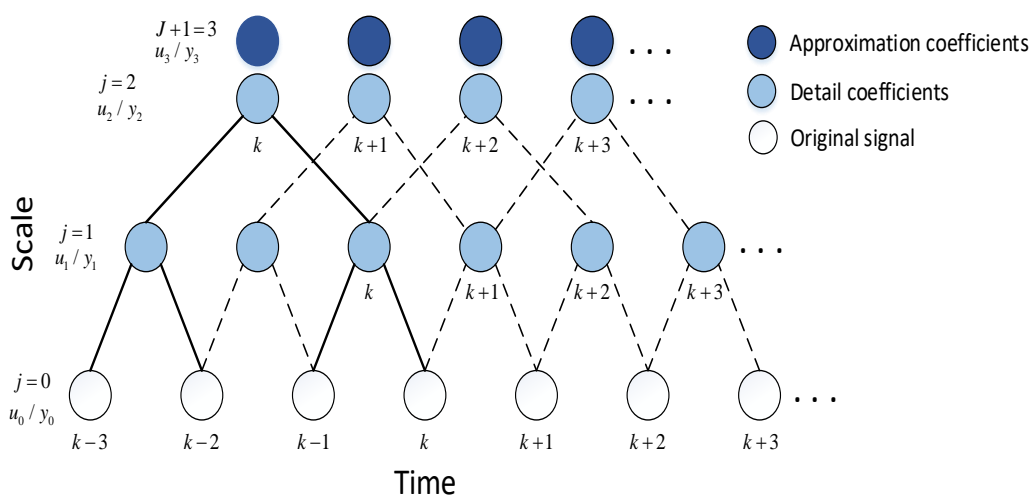


FIGURE 4.4: Implementation of wavelet transform in on-line ms-SID for two scale decomposition.

the on-line ms-SID technique suitable for real time applications like state estimation or control design as wavelet-based modeling approach identifies a system with a set of multi-time-scale minimum memory models.

Now, from (4.16) we know

$$Y_{f,j} = L_{x,j}Z_{p,j} + H_{f,j}^d U_{f,j} + H_{f,j}^s E_{f,j}, \quad (4.30)$$

The estimation of parameters can be written as least squares solution as

$$\begin{bmatrix} L_{x,j} & H_{f,j}^d \end{bmatrix} = Y_{f,j} \begin{bmatrix} Z_{p,j} \\ U_{f,j} \end{bmatrix}^\dagger. \quad (4.31)$$

Assume that a new set of input-output data is available at time instant $k + f + N - 2$.

Then, the updated Hankel matrix, *i.e.* the one appended with new data is defined as

$$U_{f,j}^* = \begin{bmatrix} U_{f,j} & \varphi u_f \end{bmatrix}, \quad Y_{f,j}^* = \begin{bmatrix} Y_{f,j} & \varphi y_f \end{bmatrix}, \quad Z_{p,j}^* = \begin{bmatrix} Z_{p,j} & \varphi z_p \end{bmatrix}, \quad (4.32)$$

where

$$\begin{aligned} \varphi u_f &= \begin{bmatrix} u^T[k + N] & u^T[k + N + 1] & \cdots & u^T[k + f + N - 1] \end{bmatrix}^T, \\ \varphi y_f &= \begin{bmatrix} y^T[k + N] & y^T[k + N + 1] & \cdots & y^T[k + f + N - 1] \end{bmatrix}^T, \\ \text{and } \varphi z_p &= \begin{bmatrix} z^T[k + N - 1] & z^T[k + N - 2] & \cdots & z^T[k + N - p] \end{bmatrix} \end{aligned}$$

are the rightmost columns of updated Hankel matrices. The updated predictor matrices can be estimated using the QR decomposition of newly formed data matrices. However, a full QR decomposition will be a computationally intensive task. Instead of this, we can simply write

$$\begin{bmatrix} Z_{p,j}^* \\ U_{f,j}^* \\ Y_{f,j}^* \end{bmatrix} = \begin{bmatrix} Z_{p,j} & \varphi z_p \\ U_{f,j} & \varphi u_f \\ Y_{f,j} & \varphi y_f \end{bmatrix} = \underbrace{\begin{bmatrix} R_{11} & 0 & 0 & \varphi z_p \\ R_{21} & R_{22} & 0 & \varphi u_f \\ R_{31} & R_{32} & R_{33} & \varphi y_f \end{bmatrix}}_{R^*} \underbrace{\begin{bmatrix} Q_1^T & 0 \\ Q_2^T & 0 \\ Q_3^T & 0 \\ 0 & I_n \end{bmatrix}}_{Q^*}. \quad (4.33)$$

Then, using a series of Givens rotation transformation [67], R^* can be represented in the lower triangular form as

$$R^* Q^* = (R^* G v_1 G v_2 G v_3) (G v_3^T G v_2^T G v_1^T Q^*) = (\bar{R})(\bar{Q}), \quad (4.34)$$

where $G v_i$, $i = 1, 2, 3$ is Givens rotation matrix. \bar{R} is the updated lower triangular matrix whose rightmost column contains all zeros and it can be removed. Thus, the

procedure reduces computation complexity and saves in the computation cost for on-line parameter estimation.

4.4 Application to Nuclear Reactor

For the purpose of black-box identification of a nuclear reactor, reactivity can be seen as an input to the system while reactor power is taken as an output. In the case of PHWR, the reactivity input can be varied by different means like Liquid Zone Control System (LZCS), adjuster rods, control rods, and moderator liquid poison actuation system. However, for this case study, it is considered that reactivity variation is controlled by LZCS only. This is the case for small transients in power. It is assumed that the primary loop is defined by a nonlinear lumped model with pressure and mass flow rate being constant. The heat transfer is by single-phase coolant only, and feedback effects of xenon and fuel depletion are not considered.

4.4.1 Model Estimation

The set of equations (C.9)–(C.14) have been simulated for the reactivity transient shown in Figure 4.5. The input transient is selected such that the resulting power variation does not occur at a rate larger than 0.2% per second. The corresponding neutronic power transient with an additive 60 dB white Gaussian noise simulating measurement error is shown in Figure 4.6. This forms the estimation data from which models are to be identified. The values of various parameters appearing in above set of equations are given in Appendix C, Table C.1.

The Training dataset is projected onto appropriately selected wavelet basis functions to have the multiscale data representation. Note that the input signal is formed of ramps with short periods of discontinuities. On the contrary, the output signal has comparatively smoother variations. This implies that the input would be better modeled by employing a low vanishing moment wavelet basis function while a regular basis is more

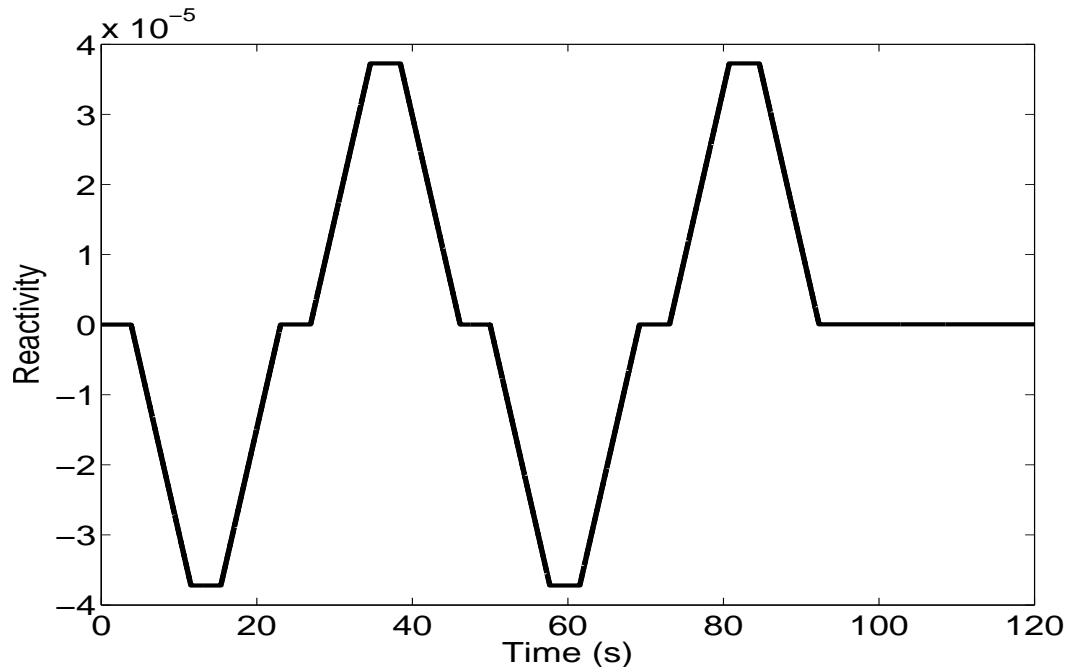


FIGURE 4.5: Assumed reactivity variation (Training input dataset).

appropriate to represent the output. Although, different basis functions can be used for input and output, for simplicity a common basis function, namely *Bior3.3* [12], has been chosen for this simulation. *Bior3.3* has three vanishing moments and is considered to be suitable to efficiently represent the input-output dataset. A frequency domain technique is used to check the estimation of maximum decomposition depth [185]. Figure 4.18 shows the Fourier transform of power signal. The magnitude of the Fourier Transform is seen to be approaching the noise floor level approximately after $\pi/62$ rad/sample. Hence, the decomposition depth is decided such that $\pi/2^J \geq \pi/62$. Thus, the maximum scale for decomposition is $J = 5$.

The notion of significant scale is demonstrated here with the help of scatter plot which is a useful exploratory data analysis technique [125]. It evaluates the output prediction capability of various scales through correlation analysis. The plots are drawn between one-step-ahead-prediction and observed value at each scale and are shown in Figure 4.19. A closer look at Figure 4.19 reveals that scale $j = 1$ does not carry significant predictive capability as compared to scales $j = 2$ to 5 and hence the scale $j = 1$

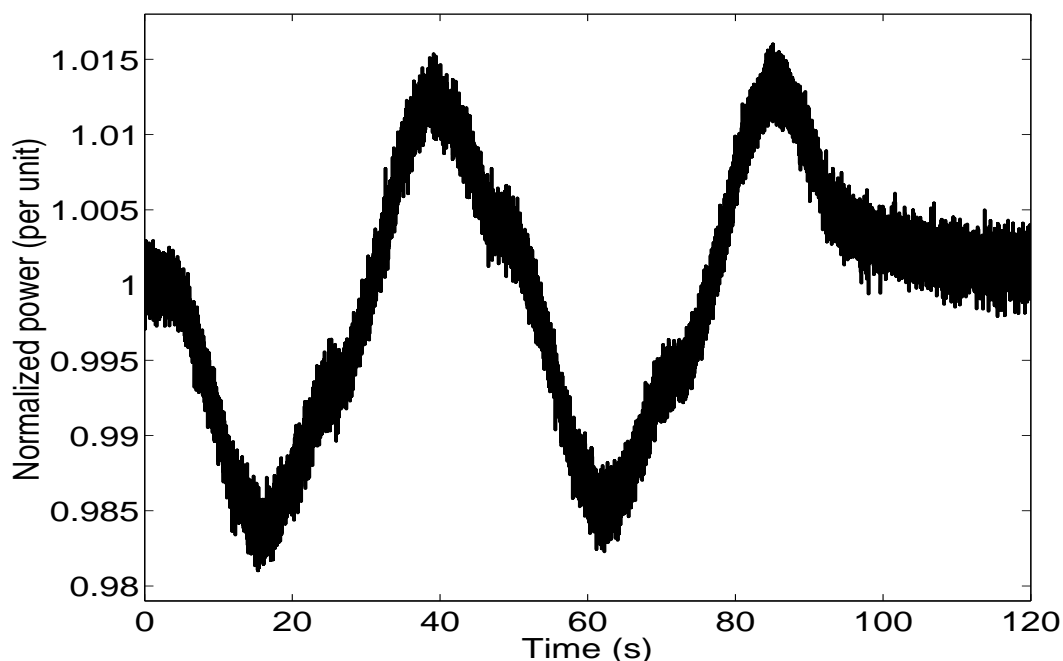


FIGURE 4.6: Reactor power variation for Figure 4.5 (Training output dataset).

need not be considered for the modeling task. At scale $J + 1 = 6$ approximation coefficients carry the trend in the data. Now, modeling exercise reduces to identifying models in detail space indexed by $j = 2$ to 5 and in approximation space indexed by $J + 1 = 6$. Although the total number of models is more compared to single-scale approach, each of these models is of lower order. Reduction of model order is expected since a complex process is broken down into sub-processes evolving at their respective time-scales.

4.4.2 Model Validation

For the purpose of model validation, two different measures have been adopted. First, it is confirmed through correlation analysis that the residuals of output are white and uncorrelated with the past input, indicating that the estimated models are sufficiently able to capture the process behaviour. The residual analysis plots for significant scales ($j = 2$ to 5 and $J + 1 = 6$) indicating 99% confidence interval are shown in Figures 4.9 and 4.10 respectively. The cross-correlation of the residuals with the input shows that residuals are independent from past input.

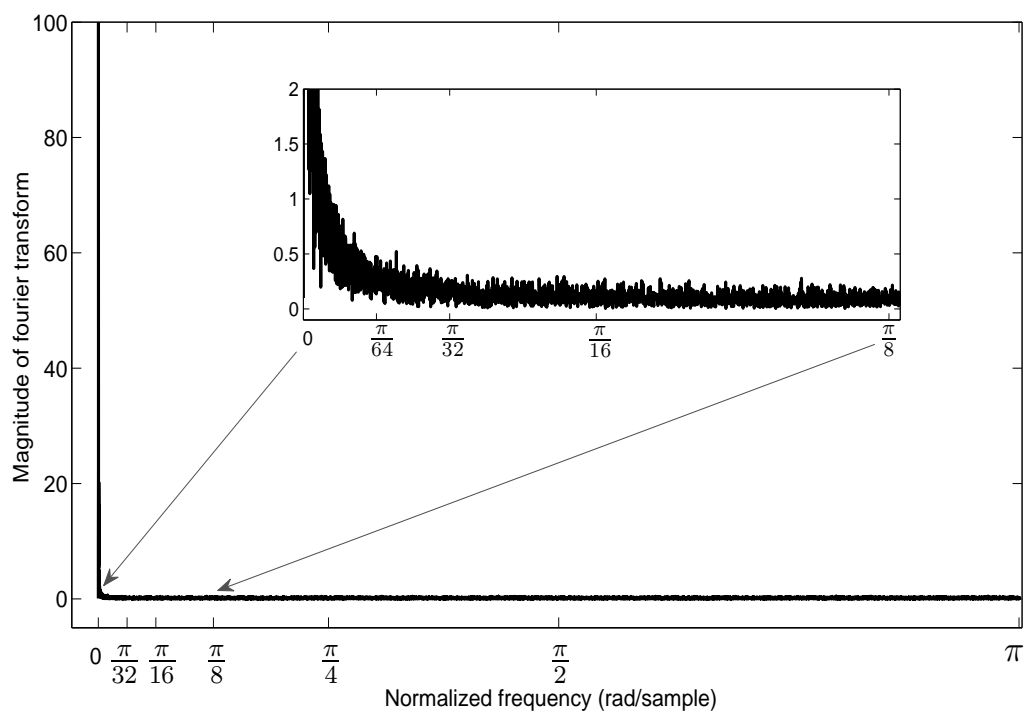


FIGURE 4.7: The discrete-time Fourier transform of the reactor power signal shown in Figure 4.6.

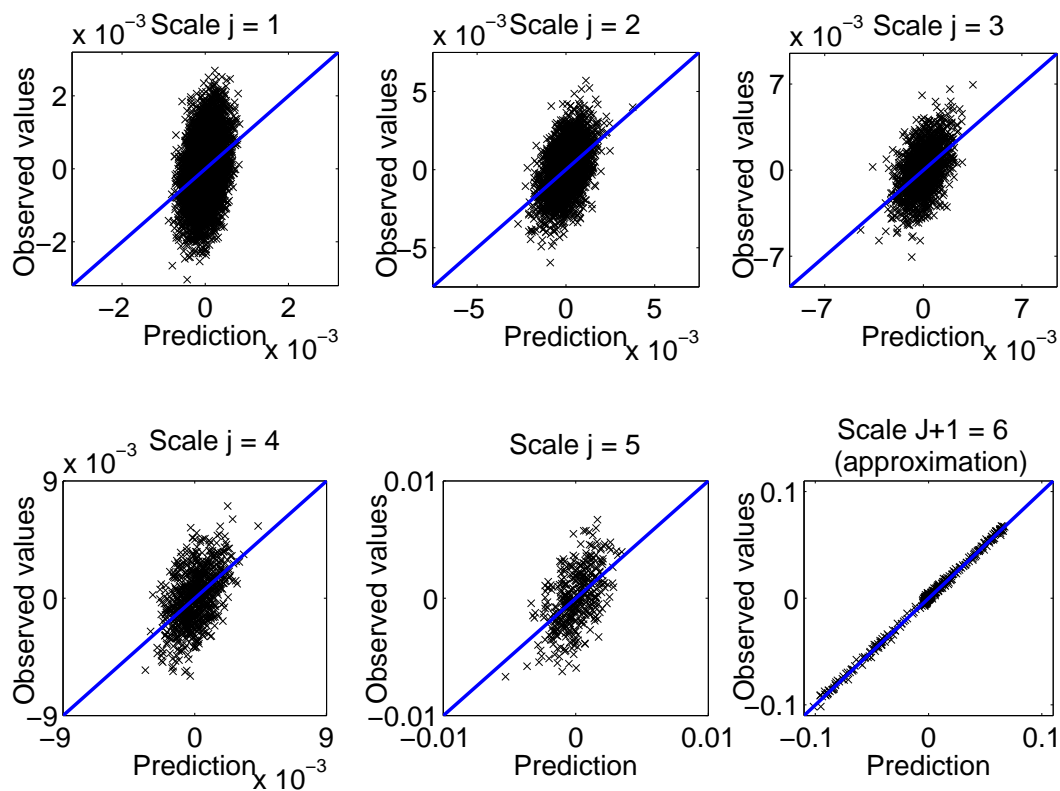


FIGURE 4.8: Scatter plots between one-step-ahead-prediction and observed values at different scales.

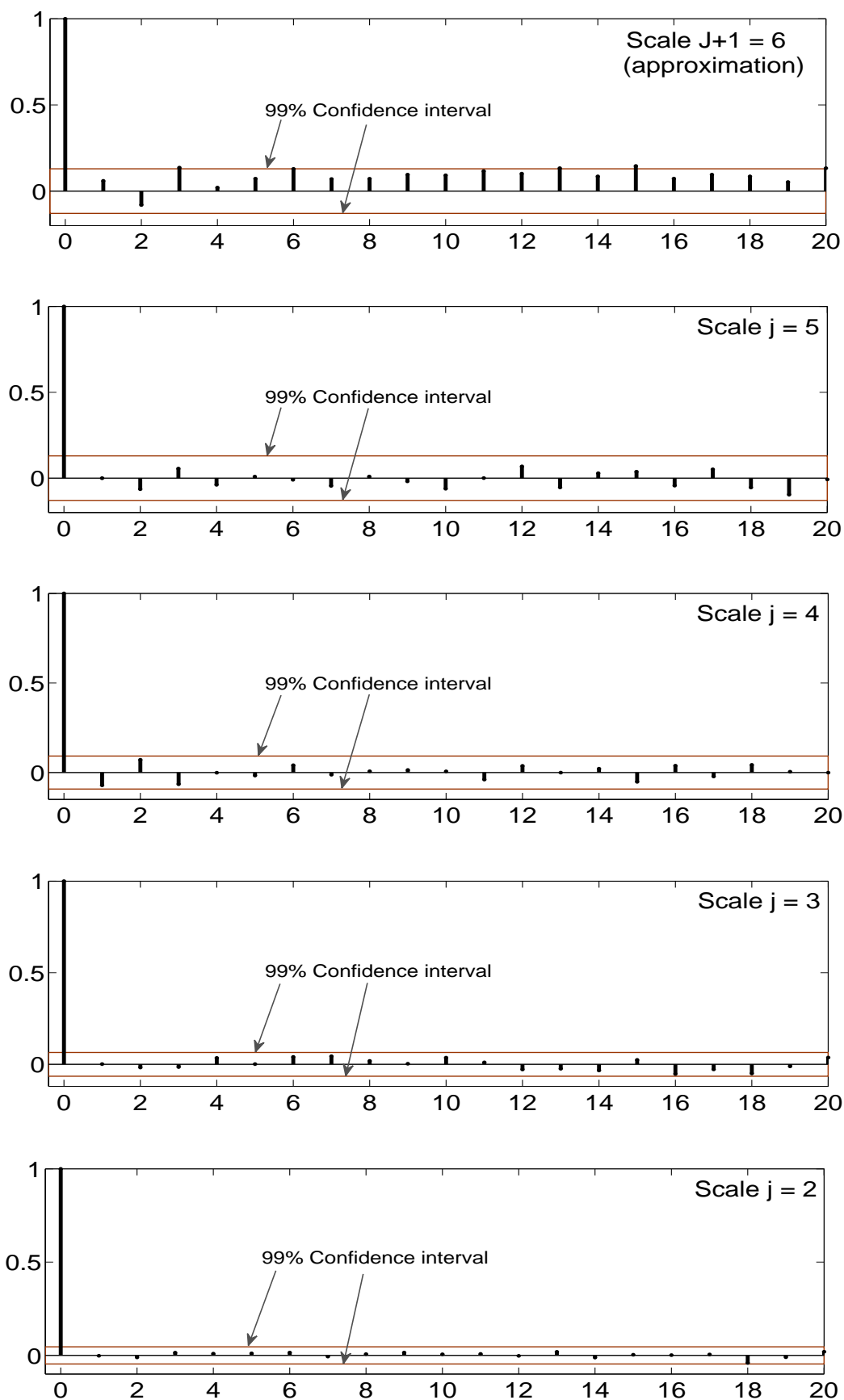


FIGURE 4.9: Autocorrelation function of the residuals for output power at significant scales for different lags.

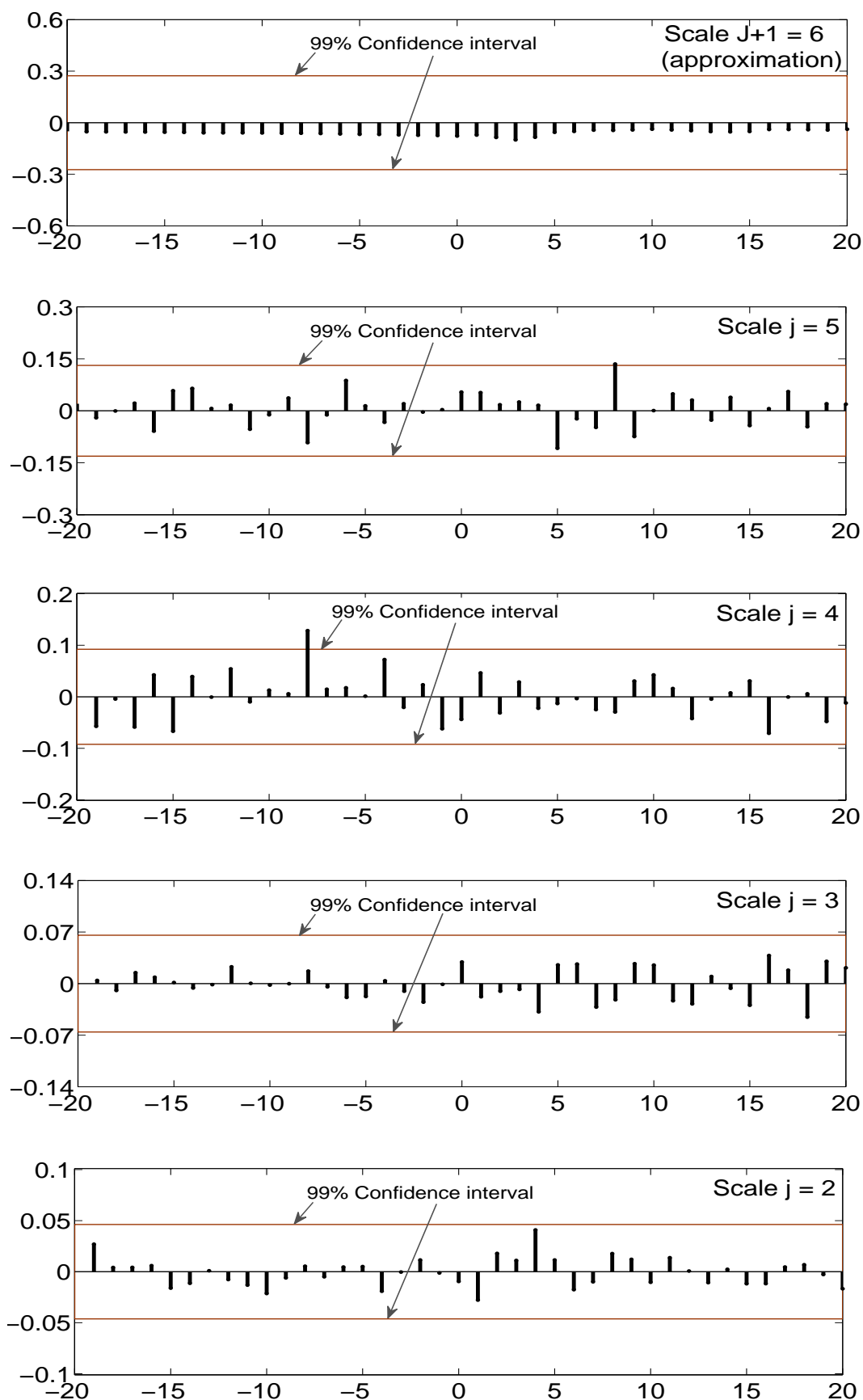


FIGURE 4.10: Cross-correlation function of the residuals with the input reactivity at significant scales for different lags.

The second measure of validation is cross-validation with different datasets. Two validation datasets, different from the estimation dataset have been selected. Further, to demonstrate the efficacy of the proposed techniques a comprehensive comparison with conventional empirical modeling approaches such as ARX, SID, BJ, and ms-ARX have been made. While applying ARX, SID, BJ, and ms-ARX techniques, the model parameters are estimated from the same dataset used for training (Figure 4.5 and 4.6) by minimizing Akaike's Information Criterion [1]. Validation test inputs shown in Figures 4.11 and 4.12 are applied to different models. Outputs of all estimated models are compared with reference output generated by directly solving (C.9)–(C.14) and shown in Figure 4.13 and 4.14. It is evident that the response of ms-SID model shows best match with the reference. The estimated traditional subspace model and ARX model fail to follow process behaviour adequately in the noisy environment. The BJ model captures noise dynamics better than that done by ARX possibly because of better noise modeling of BJ. However, multiscale features are not suitably modeled by any of the single scale models. Both ms-SID and ms-ARX are able to sufficiently capture the multiscale process dynamics due to modeling at appropriate scales.

Figure 4.15 shows the logarithm (log) of singular values of the covariance matrix constructed from the estimation dataset. For single-scale approach, the singular values reduced by an order of two for six states. It indicates that a sixth order state-space model is suitable in measurement space. On the other hand, in case of multiscale approach, the sharp reduction in the log of singular values indicates that a second order model in approximation space is sufficient. Further, a first order model in detail space i.e. at scales $j = 2$ to 5 would be sufficient. Therefore, the overall model order of the multiscale method would be approximately equal or less than that of the single-scale approach.

To statistically validate the implementation of various models, Monte Carlo simulation (100 runs) has been performed at different noise power levels in the estimation dataset. For each run at a particular noise level, all the models, discussed in the preceding section have been estimated from the training data. Then the estimated models are used for

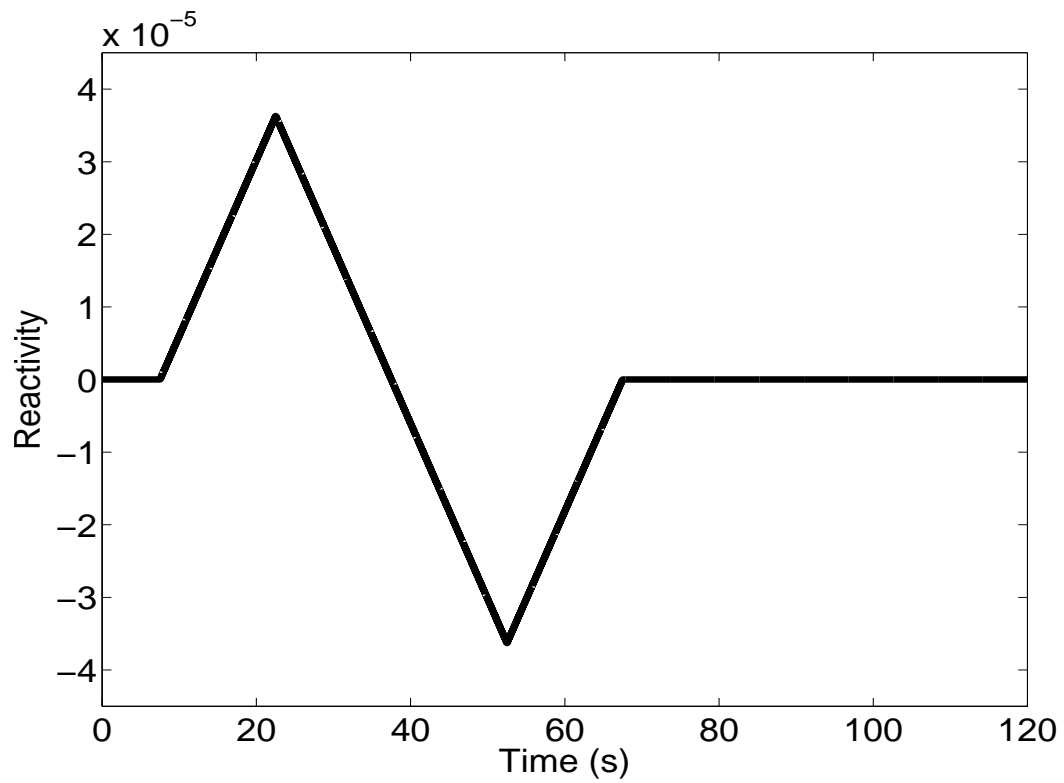


FIGURE 4.11: Triangular variation in reactivity (Validation dataset input).

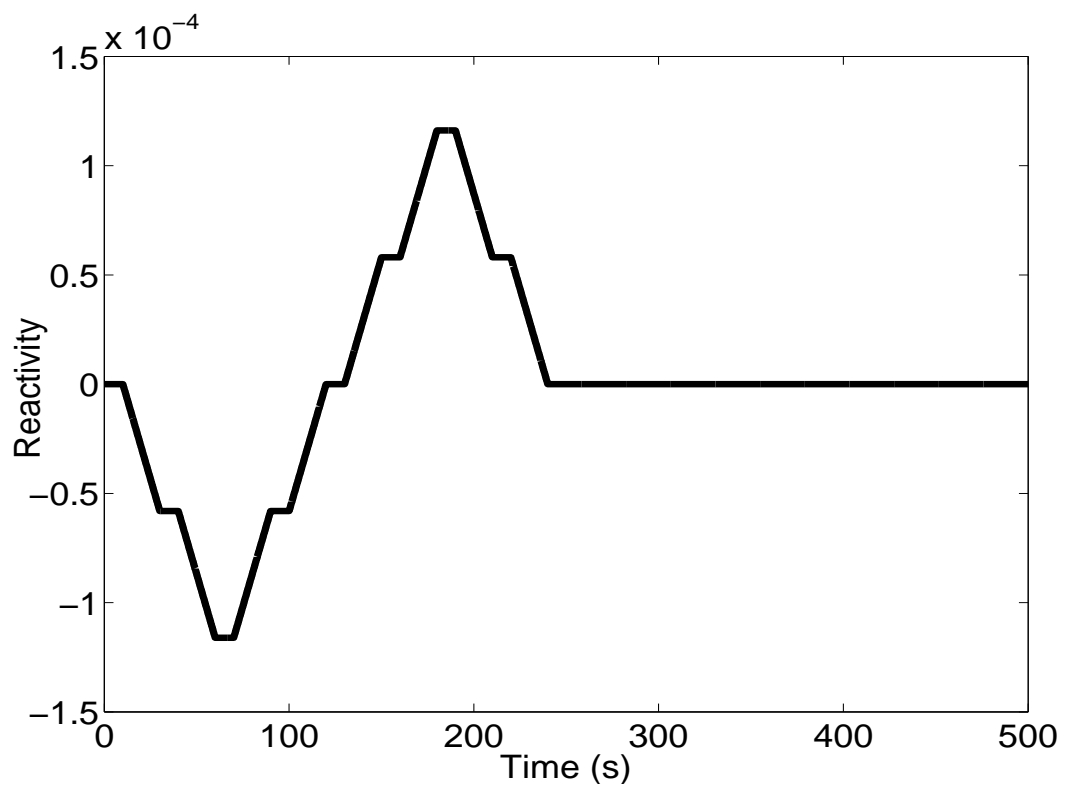


FIGURE 4.12: Step variation in reactivity (Validation dataset input).

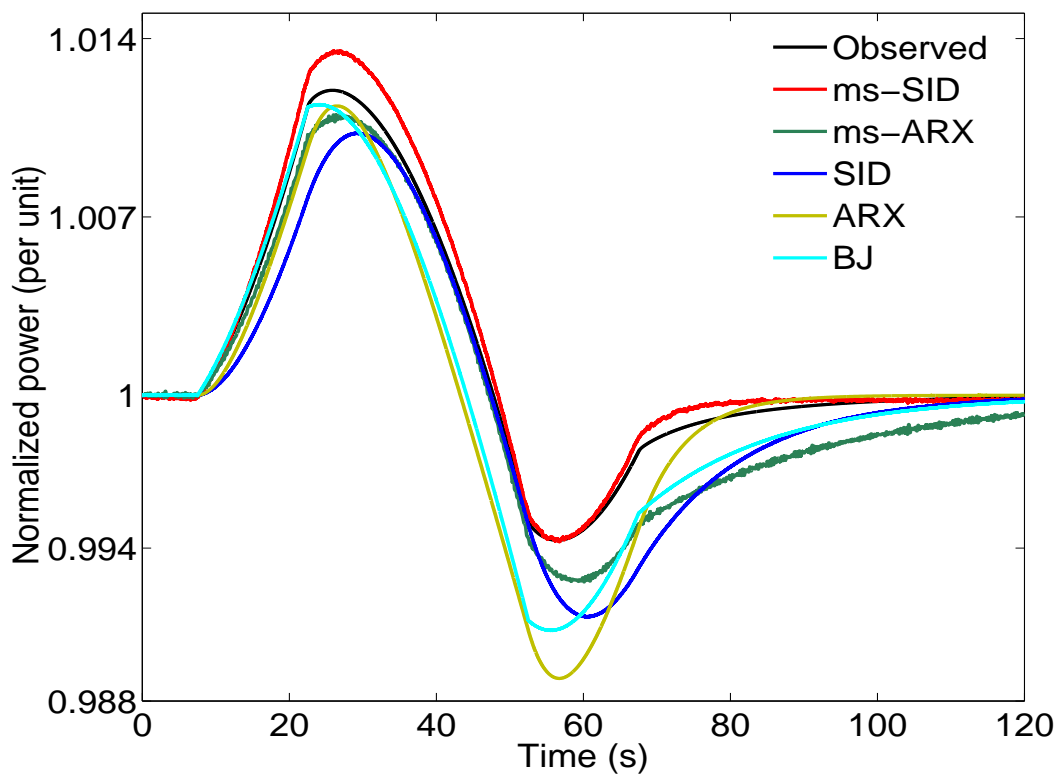


FIGURE 4.13: Outputs of estimated ms-SID, ms-ARX, classical subspace (SID), ARX, and BJ models with observed data for input shown in Figure 4.11 (simulation).

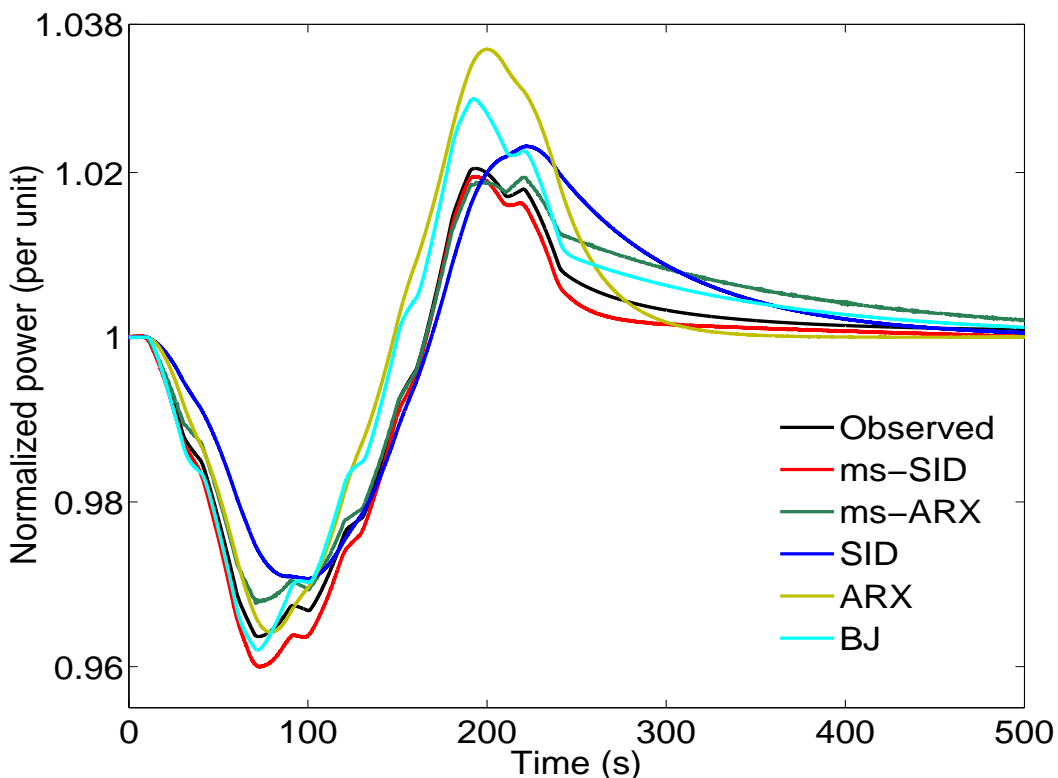


FIGURE 4.14: Outputs of estimated ms-SID, ms-ARX, classical subspace (SID), ARX, and BJ models with observed data for input shown in Figure 4.12 (simulation).

output prediction from validation inputs (Figures 4.11 and 4.12). Several Monte Carlo runs are equivalent to performing multiple experiments to model stochastic nature of noise. Root mean squared error (RMSE) between output observation (noise-free output) and simulation/prediction is defined as

$$RMSE = \sqrt{\frac{1}{N} \sum_{k=0}^{N-1} (P[k] - \hat{P}[k])^2} \quad (4.35)$$

has been evaluated and the values so obtained are given in Table 4.4, in one-step-ahead-prediction/simulation cases for different models at distinct values of the signal to noise ratios (SNR). The small value of RMSE indicates better prediction/simulation capability of a particular model. In practice, simulation denotes infinite-step ahead prediction and it is a critical measure for verifying model performances. It is observed that the multiscale approaches have better prediction capabilities as compared to their single-scale counterparts. The ms-SID performs better even compared to the ms-ARX model. Moreover, it is found that even a lower order ms-SID model gives better output prediction than a higher order ms-ARX model.

The performance of multiscale approaches are dependent on the decomposition depth. Therefore an appropriate scale selection is necessary. Tables 4.2 and 4.3 compare the RMSE of ms-SID model simulations, for various decomposition depths, obtained from different validation datasets. Monte Carlo simulation of 100 runs is performed at different SNR. It is worth noting that the optimum decomposition depth increases with the decrease in SNR as the extraction of signal features requires additional filtering. Besides, at a particular noise power level, the prediction accuracy enhances at coarser scales. However, after a certain level, the RMSE increases due to over smoothing of low-level features. Therefore, the selection of optimum depth and significant scale is crucial.

TABLE 4.1: RMSE in output prediction by various approaches for different validation datasets (Monte Carlo simulation)

SNR (dB)	Model	Triangular Input		Sum of Step Input	
		Prediction	Simulation	Prediction	Simulation
10	ARX	3.5×10^{-3}	4.0×10^{-3}	1.02×10^{-2}	1.07×10^{-2}
	SID	3.6×10^{-3}	4.4×10^{-3}	1.12×10^{-2}	1.19×10^{-2}
	BJ	3.8×10^{-3}	4.3×10^{-3}	1.21×10^{-2}	1.26×10^{-2}
	ms-ARX	3.1×10^{-3}	3.4×10^{-3}	4.50×10^{-3}	1.04×10^{-2}
	ms-SID	2.9×10^{-3}	3.3×10^{-3}	3.60×10^{-3}	9.50×10^{-3}
20	ARX	3.2×10^{-3}	3.6×10^{-3}	9.7×10^{-3}	1.03×10^{-2}
	SID	3.0×10^{-3}	3.6×10^{-3}	1.01×10^{-2}	1.07×10^{-2}
	BJ	2.3×10^{-3}	3.2×10^{-3}	9.3×10^{-3}	1.05×10^{-2}
	ms-ARX	1.8×10^{-3}	2.9×10^{-3}	3.8×10^{-3}	1.01×10^{-2}
	ms-SID	1.6×10^{-3}	2.8×10^{-3}	2.7×10^{-3}	8.40×10^{-3}
40	ARX	1.9×10^{-3}	3.5×10^{-3}	5.8×10^{-3}	1.02×10^{-2}
	SID	4.1×10^{-4}	2.8×10^{-3}	1.3×10^{-3}	9.8×10^{-3}
	BJ	5.8×10^{-4}	2.6×10^{-3}	1.7×10^{-3}	6.5×10^{-3}
	ms-ARX	5.2×10^{-4}	2.5×10^{-3}	1.4×10^{-3}	6.1×10^{-3}
	ms-SID	2.6×10^{-4}	2.2×10^{-3}	7.3×10^{-4}	4.3×10^{-3}
60	ARX	7.1×10^{-5}	3.3×10^{-3}	2.4×10^{-4}	9.3×10^{-3}
	SID	5.2×10^{-5}	2.4×10^{-3}	1.9×10^{-4}	5.5×10^{-3}
	BJ	1.4×10^{-4}	1.9×10^{-3}	4.2×10^{-4}	4.0×10^{-3}
	ms-ARX	4.9×10^{-5}	2.0×10^{-3}	1.7×10^{-4}	4.0×10^{-3}
	ms-SID	4.6×10^{-5}	1.8×10^{-3}	1.3×10^{-4}	3.7×10^{-3}
80	ARX	2.5×10^{-5}	2.3×10^{-3}	9.4×10^{-5}	5.6×10^{-3}
	SID	2.4×10^{-5}	2.1×10^{-3}	1.0×10^{-4}	5.0×10^{-3}
	BJ	3.1×10^{-5}	2.2×10^{-3}	1.2×10^{-4}	5.4×10^{-3}
	ms-ARX	1.4×10^{-5}	1.8×10^{-3}	7.1×10^{-5}	3.9×10^{-3}
	ms-SID	1.4×10^{-5}	1.7×10^{-3}	6.2×10^{-5}	3.5×10^{-3}
100	ARX	6.1×10^{-6}	2.0×10^{-3}	8.7×10^{-6}	5.0×10^{-3}
	SID	6.5×10^{-6}	1.9×10^{-3}	9.2×10^{-6}	5.2×10^{-3}
	BJ	1.3×10^{-5}	2.2×10^{-3}	2.1×10^{-5}	5.5×10^{-3}
	ms-ARX	5.0×10^{-6}	1.6×10^{-3}	8.0×10^{-6}	3.7×10^{-3}
	ms-SID	5.0×10^{-6}	1.6×10^{-3}	8.0×10^{-6}	3.4×10^{-3}

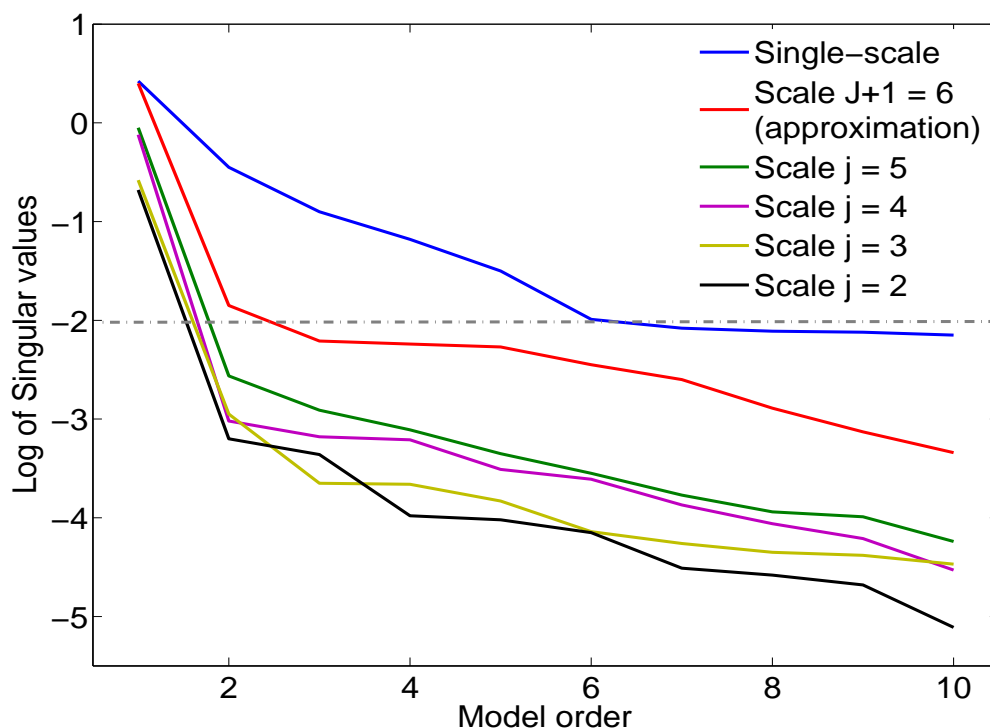


FIGURE 4.15: Singular values of the covariance matrix constructed from estimation data.

TABLE 4.2: RMSE of ms-SID model simulations at various decomposition depths for triangular input validation dataset (Monte Carlo simulation)

SNR \ J	10	20	40	60	80	100
1	8.7×10^{-3}	7.5×10^{-3}	3.0×10^{-3}	1.9×10^{-3}	1.9×10^{-3}	1.7×10^{-3}
2	5.9×10^{-3}	4.1×10^{-3}	2.8×10^{-3}	1.9×10^{-3}	1.8×10^{-3}	1.7×10^{-3}
3	5.4×10^{-3}	3.4×10^{-3}	2.5×10^{-3}	1.9×10^{-3}	1.7×10^{-3}	1.5×10^{-3}
4	5.1×10^{-3}	3.5×10^{-3}	2.3×10^{-3}	1.8×10^{-3}	1.8×10^{-3}	1.5×10^{-3}
5	4.8×10^{-3}	3.3×10^{-3}	2.1×10^{-3}	1.7×10^{-3}	1.7×10^{-3}	1.6×10^{-3}
6	4.1×10^{-3}	3.8×10^{-3}	2.4×10^{-3}	1.8×10^{-3}	1.9×10^{-3}	1.7×10^{-3}
7	6.4×10^{-3}	3.9×10^{-3}	2.6×10^{-3}	1.9×10^{-3}	1.9×10^{-3}	1.6×10^{-3}
8	7.9×10^{-3}	5.7×10^{-3}	3.1×10^{-3}	2.1×10^{-3}	2.0×10^{-3}	1.7×10^{-3}

4.5 On-line Identification of Nuclear Reactor

This section presents simulation studies on a point kinetics nuclear reactor system for on-line identification. Figs. 4.16 and 4.17 show the reactivity variation and the corresponding reactor power output added with 30 dB white Gaussian noise. This forms the estimation dataset for parameter identification. The Fourier transform of estimation dataset is used to find the decomposition depth. Fig. 4.18 shows the Fourier transform

TABLE 4.3: RMSE of ms-SID model simulations at various decomposition depths for sum of step input validation dataset (Monte Carlo simulation)

SNR \ J	10	20	40	60	80	100
1	2.01×10^{-2}	1.65×10^{-2}	1.0×10^{-2}	4.2×10^{-3}	4.0×10^{-3}	3.9×10^{-3}
2	1.81×10^{-2}	1.40×10^{-2}	9.6×10^{-3}	4.2×10^{-3}	3.9×10^{-3}	3.7×10^{-3}
3	1.55×10^{-2}	1.36×10^{-2}	7.8×10^{-3}	4.1×10^{-3}	3.7×10^{-3}	3.6×10^{-3}
4	1.42×10^{-2}	1.24×10^{-2}	6.1×10^{-3}	4.0×10^{-3}	3.7×10^{-3}	3.6×10^{-3}
5	1.31×10^{-2}	1.11×10^{-2}	4.5×10^{-3}	3.9×10^{-3}	3.9×10^{-3}	3.8×10^{-3}
6	1.26×10^{-2}	1.13×10^{-2}	4.7×10^{-3}	3.9×10^{-3}	4.0×10^{-3}	4.0×10^{-3}
7	1.39×10^{-2}	1.25×10^{-2}	4.7×10^{-3}	4.1×10^{-3}	4.2×10^{-3}	4.0×10^{-3}
8	1.48×10^{-2}	1.29×10^{-2}	5.1×10^{-3}	4.4×10^{-3}	4.2×10^{-3}	4.3×10^{-3}

of input and output signal. It can be seen that the magnitude of the Fourier transform approaches the noise floor level approximately after $\pi/124$ rad/sample. Therefore, the maximum scale for decomposition is selected such that $\pi/2^J \geq \pi/124$, i.e. $J = 6$. The estimation data is then represented in multiresolution using Haar wavelet up to $J = 6$. A scatter plot between one-step-ahead prediction and observed value is plotted to find significant scales. It is evident from Fig. 4.19 that scales $j = 1$ to 3 do not contain any significant information as compared to that of scales $j = 4$ to 6 and thus the former can be ignored for model estimation. Thus, models are estimated at scale $j = 4, 5, 6$ and $J + 1 = 7$ by minimizing Akaike's Information Criterion. The estimated models are first validated by residual analysis. It is found that the residuals do not contain any significant information.

Subsequently the estimated model is validated using cross-validation with different dataset. The results of the proposed on-line Multiscale Subspace Identification (MSID) are compared with conventional single-scale SID approach and the Multi Scale ARX (MSARX) approach proposed by [23]. Two distinct validation inputs, used for case studies I and II are shown in Figs. 4.20 and 4.22 respectively. Output estimation of different models mentioned above for the respective inputs are shown in Figs. 4.21 and 4.23. The prediction accuracy is validated by computing the RMSE between the observed value and simulation/one-step-ahead prediction. Table 4.4 compares the RMSE of various estimated models for different validation datasets. Small value of RMSE suggests better prediction capability of a particular model. It is evident that multiscale

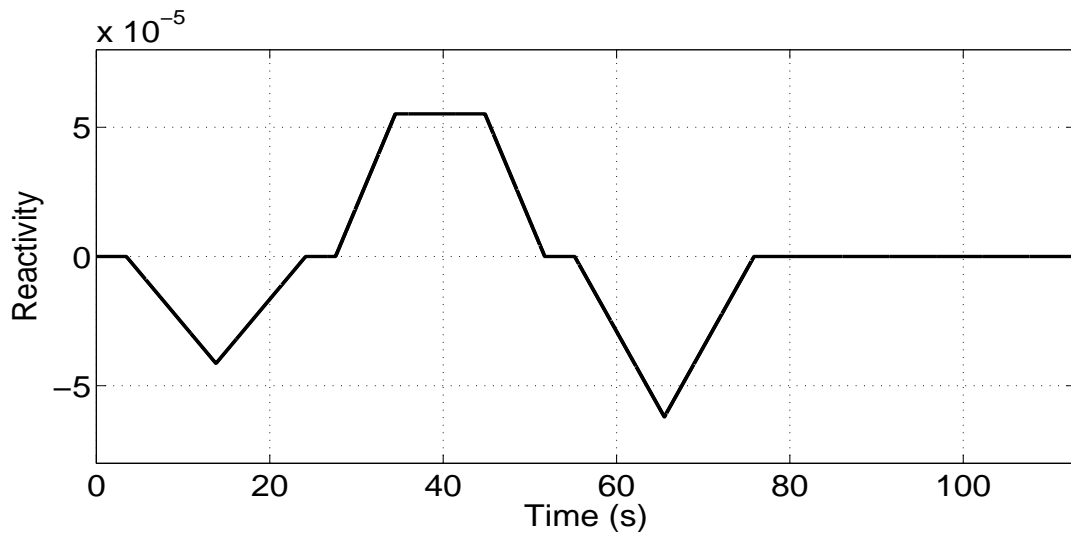


FIGURE 4.16: Variation of reactivity.

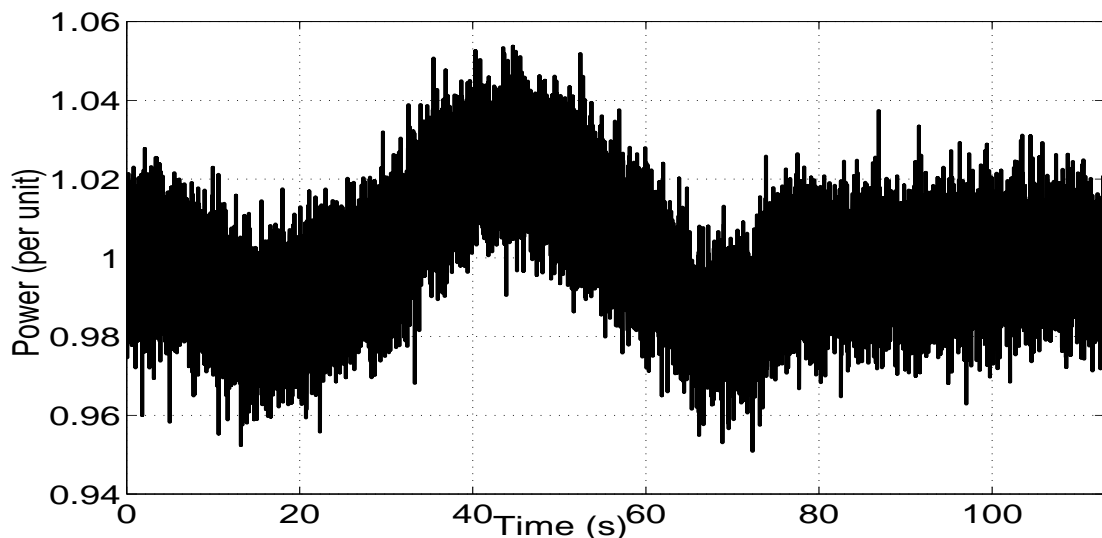


FIGURE 4.17: Reactor power added with white Gaussian noise.

model captures better dynamic response as compared to that of the single-scale model. MSID gives better output prediction than MSARX approach of [23].

4.6 Summary

In this chapter, a novel approach of multiscale subspace identification for modeling of a point kinetic nuclear reactor coupled with thermal hydraulics has been presented. The identified ms-SID model estimates system modes more precisely than the traditional

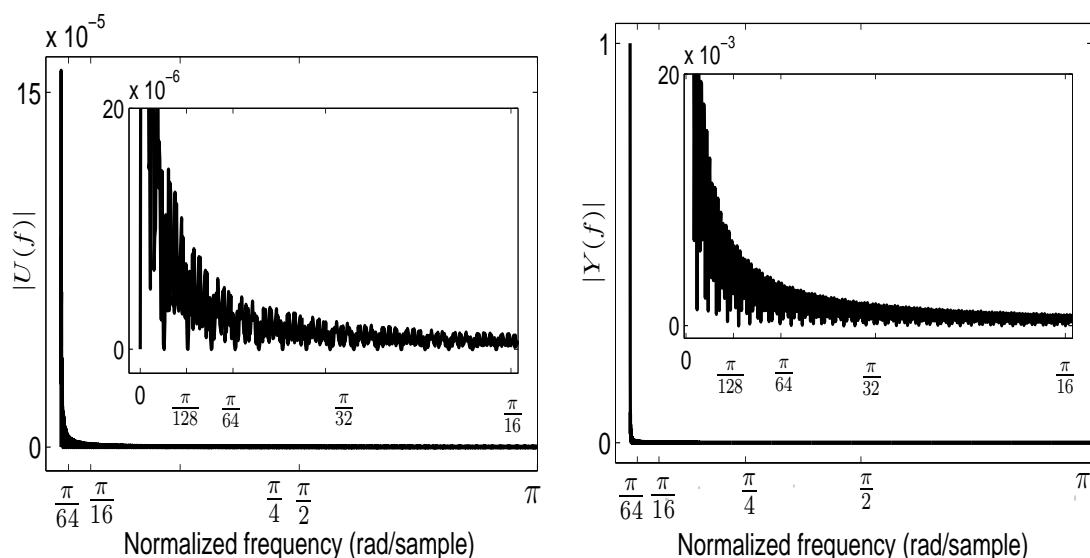


FIGURE 4.18: Fourier transform of the input-output signal.

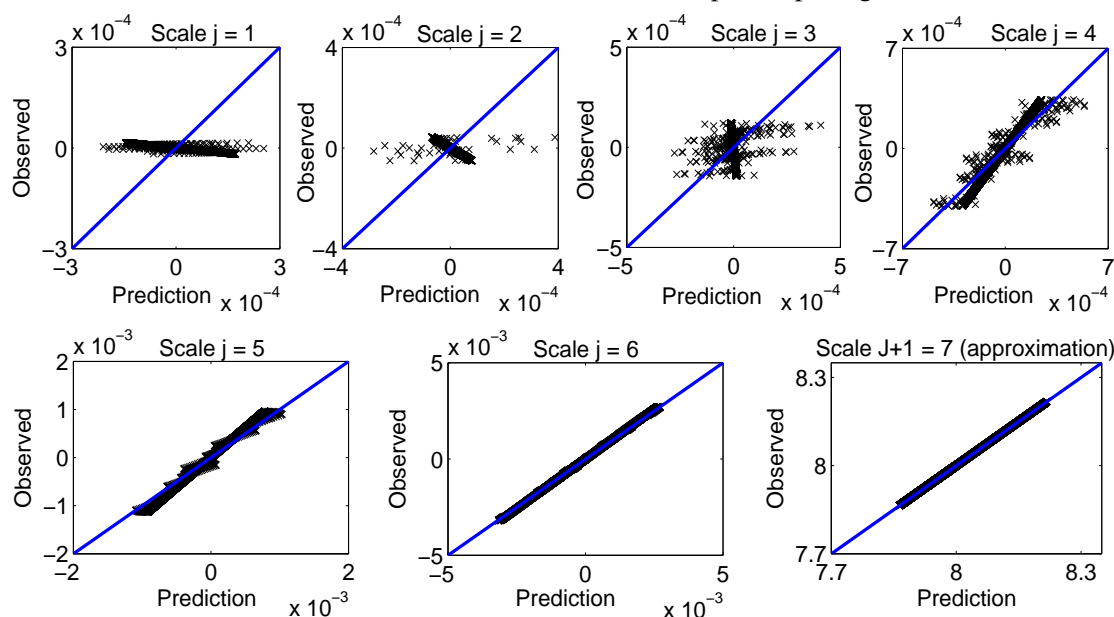


FIGURE 4.19: Scatter plots between one-step-ahead prediction and observed output.

approaches do, and a good neutronic power prediction has been achieved even from training dataset with low SNR. An important contribution of the proposed work is to develop a framework for state-space modeling at significant scales leading to a parsimonious model description with less computational burden. In most of the modeling exercises, it reduces dimensionality with improved output prediction capability. The identified reactor model is validated in prediction as well as in simulation environment. The root mean squared error is compared with various single scale (ARX, SID, BJ)

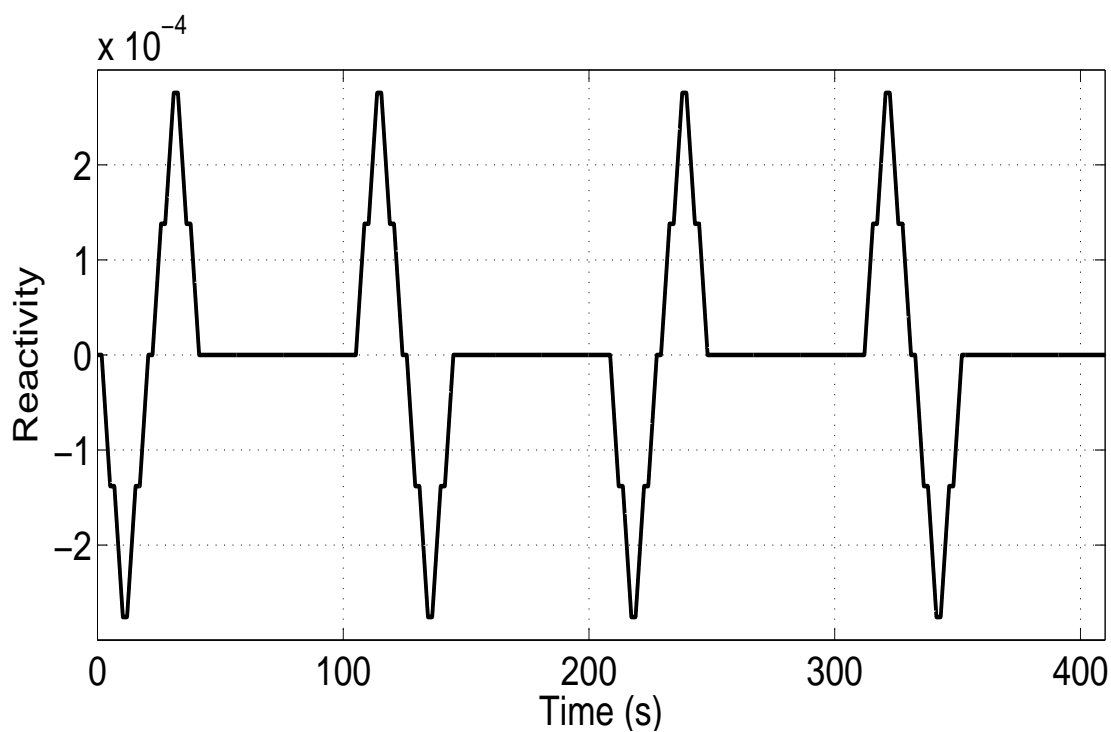


FIGURE 4.20: Variation of reactivity (Case I).

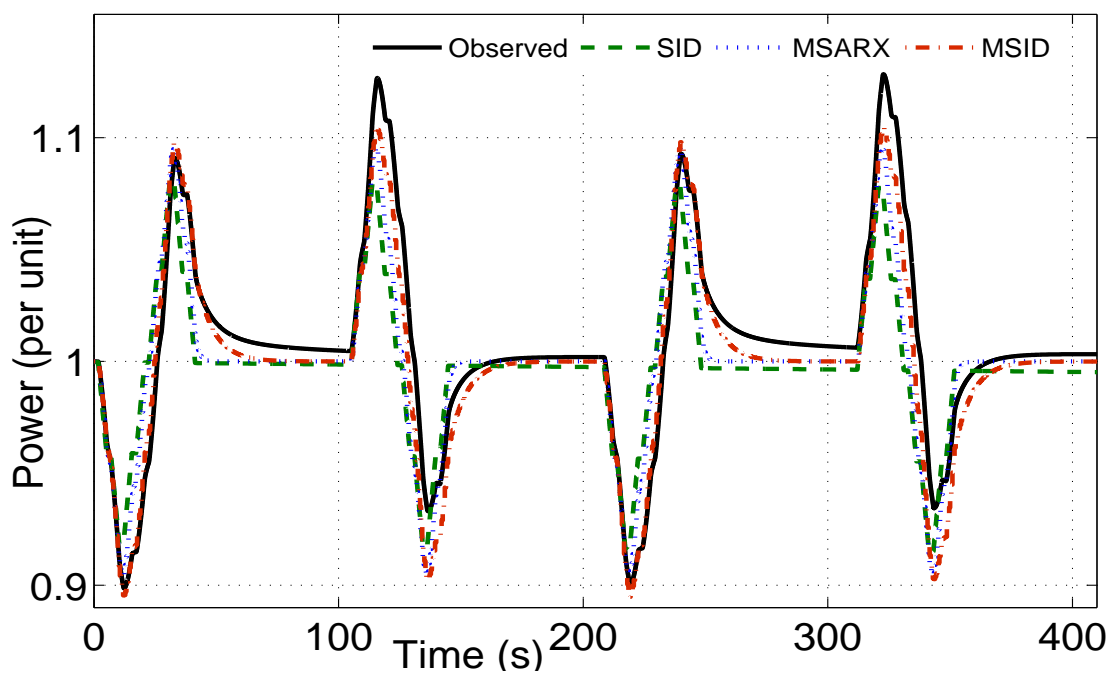


FIGURE 4.21: Comparison of simulation outputs of SID, MSARX, and MSID approaches (Case I).

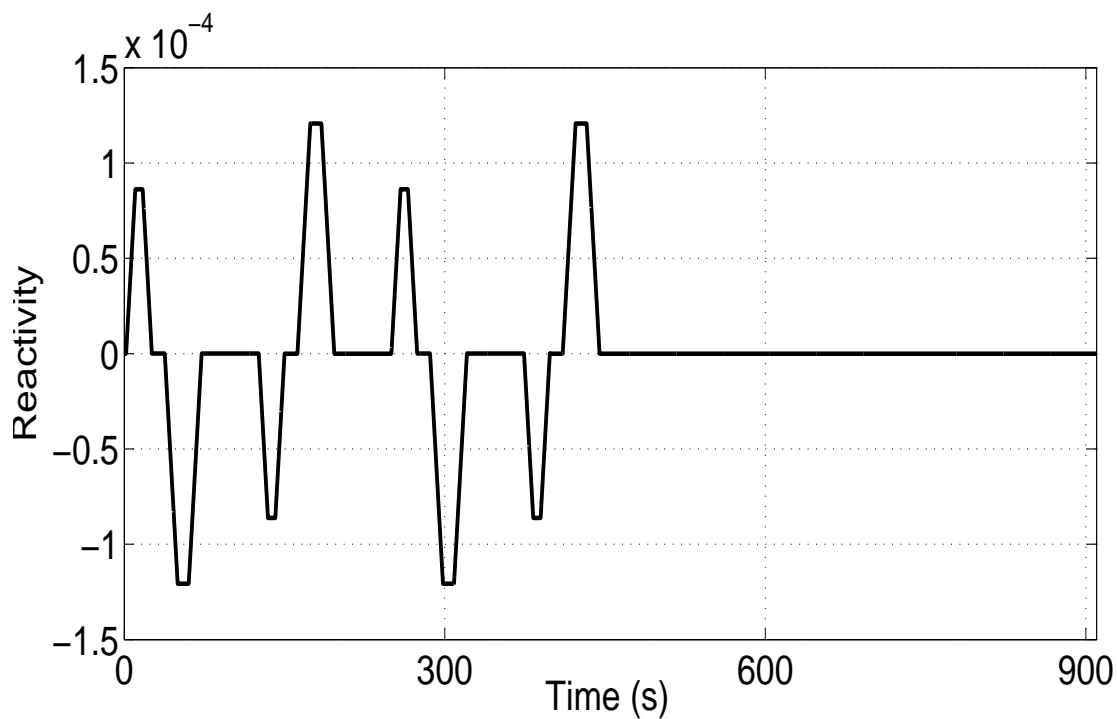


FIGURE 4.22: Variation of reactivity (Case II).

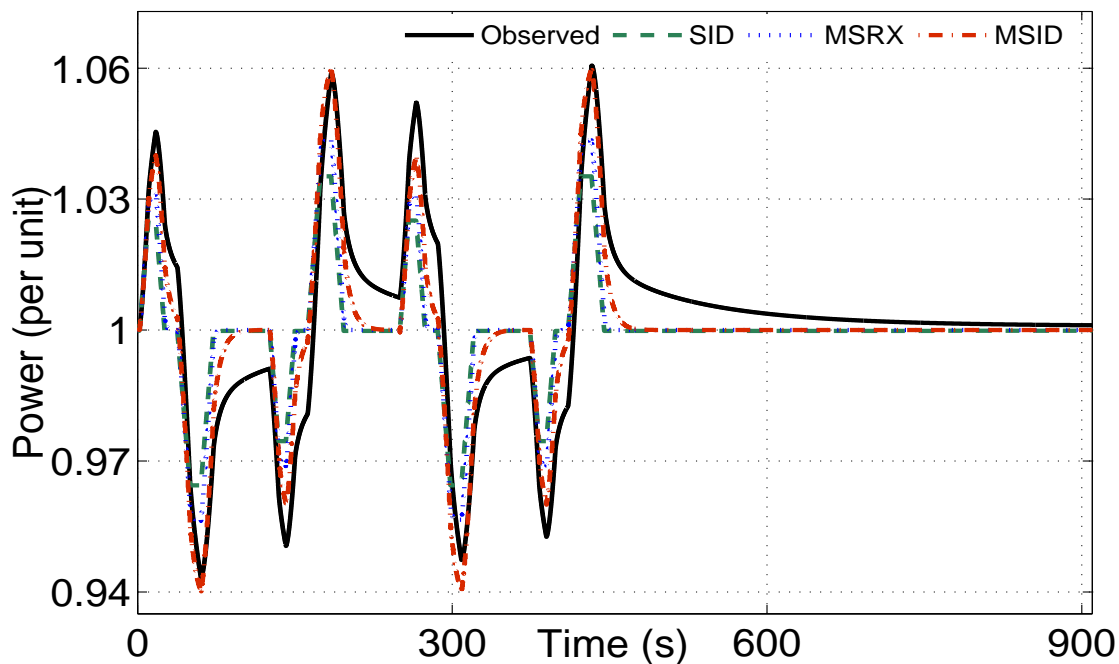


FIGURE 4.23: Comparison of simulation outputs of SID, MSARX, and MSID approaches (Case II).

TABLE 4.4: Comparison of the root mean squared error (10 Monte Carlo runs)

Model	Case I		Case II	
	Prediction	Simulation	Prediction	Simulation
SID	5.83×10^{-4}	0.0271	1.701×10^{-4}	0.0137
MSARX	4.98×10^{-4}	0.0213	1.213×10^{-4}	0.0119
MSID	3.23×10^{-4}	0.0127	1.197×10^{-4}	0.0085

and multiscale (ms-ARX) approaches, for multiple validation datasets, suggesting better modeling performance with enhanced prediction capability by the proposed method of ms-SID at different noise levels.

Chapter 5

Wavelet Pre-processed Subspace Predictive Control

This chapter presents methodology of data-driven predictive control technique based on subspace methods. It formulates an open-loop and a close-loop subspace predictive control integrated with wavelet-preprocessing. It also discusses incorporation of different design features. The control performance is analyzed through a parameter sensitivity approach. The developed technique is then applied to the nuclear reactor, discussed in Appendix C.

The goal of this work is to integrate wavelet pre-processing and data-driven control design approaches. The proposed approach does not require the system model for predictive control design. Moreover, the controller is directly estimated from pre-processed input-output data and implemented. In addition, no assumptions have been made about a priori knowledge of model order or structure. To take care of time-variations in the process, the predictor parameters are estimated recursively with the availability of new data. Further, the chapter discusses incorporation of feed-forward control, integrating action, and constraints in the control design. The efficacy of the proposed algorithm is validated for demand load set-point variations as well as for load rejection transients. The controller is effectively able to cope up with ramp and step variations in the demand

power. In order to analyze the control performances, detailed parameter sensitivity analysis has been performed.

5.1 Wavelet Pre-processing

Wavelets are the time-frequency atoms with excellent multiresolution approximation and signal localization property. These characteristics make them particularly suitable for analyzing short-lived high-frequency features and long-lived low-frequency features occurring simultaneously in a signal very effectively. Thresholding in wavelet domain followed by signal synthesis is a well established signal denoising technique that enables nonlinear approximation of a function. It preserves the relevant signal components while efficiently removing the contribution due to noise. It is proved to be near optimum in the minimax sense and gives better convergence rate as compared to other linear methods of approximation over a wide class of function spaces [90]. The signal to be denoised is either hard thresholded whereby the wavelet coefficients below a certain threshold are made equal to zero or soft thresholded wherein the wavelet coefficients are reduced by the given threshold. There are different wavelet-based thresholding approaches for denoising a signal corrupted with noise viz. *minimax*, *VisuShrink* (universal threshold) [90], and *SureShrink* (level-dependent threshold) [91]. The process of denoising starts with projecting the signal on suitable wavelet basis. The projection operation decorrelates wavelet coefficients of signal from that of the noise. The threshold is usually applied to the detail coefficients. The denoised signal in measurement domain is reconstructed by employing inverse wavelet transform to get denoised or wavelet filtered signal. The amplitude thresholding of the wavelet coefficients is justified as there is no significant loss of useful information in the denoised signal. However, the effectiveness of algorithm requires careful selection of wavelet basis and decomposition depth.

5.2 Open-Loop Subspace Predictive Control

5.2.1 Design of Linear Predictor

A linear predictor estimates future outputs from past input-output data and future input data. Assume that the input and output time-series data are collected from $k \in \{1, 2, \dots, N\}$ and are pre-processed using wavelet filtering. Further, let us set up the block Hankel matrices using pre-processed data as

$$Y_P = \begin{bmatrix} y[1] & y[2] & \cdots & y[N-2f+1] \\ y[2] & y[3] & \cdots & y[N-2f+2] \\ \vdots & \vdots & \ddots & \vdots \\ y[f] & y[f+1] & \cdots & y[N-f] \end{bmatrix}; Y_F = \begin{bmatrix} y[f+1] & u[f+2] & \cdots & y[N-f+1] \\ y[f+2] & u[f+3] & \cdots & y[N-f+2] \\ \vdots & \vdots & \ddots & \vdots \\ y[2f] & u[2f+1] & \cdots & f[N] \end{bmatrix}, \quad (5.1)$$

where f is the order of predictor matrix. $U_P \in \mathbb{R}^{fm \times (N-2f+1)}$ and $U_F \in \mathbb{R}^{fm \times (N-2f+1)}$ respectively are *past* and *future* pre-processed input data Hankel matrices. The order of the past Hankel matrix must be equal to or greater than the order of the system. The number of columns in the above defined Hankel matrices should be sufficiently large compared to the number of rows, to reduce noise sensitivity. For simplicity, here the number of block rows in *past* and *future* data matrices are taken to be equal. Define $U_P \in \mathbb{R}^{fl \times (N-2f+1)}$ and $E_P \in \mathbb{R}^{fl \times (N-2f+1)}$ as *past* input and *past* innovations matrices respectively. Similarly, define $U_F \in \mathbb{R}^{fl \times (N-2f+1)}$ and $E_F \in \mathbb{R}^{fl \times (N-2f+1)}$ as the *future* input and *future* innovations matrices respectively. Further, let

$$X_P = \begin{bmatrix} x[1] & x[2] & \cdots & x[N-2f+1] \end{bmatrix}, \quad (5.2)$$

and $X_F = \begin{bmatrix} x[f+1] & x[f+2] & \cdots & x[N-f+1] \end{bmatrix}.$

Then

$$\begin{aligned}
 Y_P &= \Gamma_f X_P + H_f^d U_P + H_f^s E_P, \\
 Y_F &= \Gamma_f X_F + H_f^d U_F + H_f^s E_F, \\
 \text{and } X_F &= A^f X_P + \Delta_f^d U_P + \Delta_f^s E_P,
 \end{aligned} \tag{5.3}$$

where $\Delta_f^d \in \mathbb{R}^{n \times fm}$ and $\Delta_f^s \in \mathbb{R}^{n \times fl}$ respectively are deterministic and stochastic reverse extended controllability matrices given as

$$\Delta_f^d = \begin{bmatrix} A^{f-1}B & A^{f-2}B & \dots & B \end{bmatrix}; \quad \Delta_f^s = \begin{bmatrix} A^{f-1}K & A^{f-2}K & \dots & K \end{bmatrix}. \tag{5.4}$$

Note that, (5.4) is similar to (2.6). Now, for a sufficiently large dataset, the output predictor can be written as

$$\hat{Y}_F = L_w W_P + L_u U_F, \tag{5.5}$$

where $W_P = \begin{bmatrix} Y_P^T & U_P^T \end{bmatrix}^T \in \mathbb{R}^{f(m+l) \times (N-2f+1)}$, $L_w \in \mathbb{R}^{fl \times f(m+l)}$ and $L_u \in \mathbb{R}^{fl \times fm}$ are predictor matrices and are estimated through least-squares. The future output prediction are found out by orthogonally projecting the row space of future output onto the row space spanned by past input-output and future input [28]. It is given by

$$\hat{Y}_F = Y_F / \begin{bmatrix} W_P \\ U_F \end{bmatrix} = Y_F \begin{bmatrix} W_P \\ U_F \end{bmatrix}^\dagger \begin{bmatrix} W_P \\ U_F \end{bmatrix}. \tag{5.6}$$

Note that,

$$\begin{bmatrix} L_w & L_u \end{bmatrix} = Y_F \begin{bmatrix} W_P \\ U_F \end{bmatrix}^\dagger, \tag{5.7}$$

where X/Y represents the projection of row space of X on the row space of Y . Predictor coefficients are estimated by efficiently solving (5.7) through numerically stable SVD and QR decomposition techniques.

It is to note that the system parameters $\{A, B, C, D, K\}$ can be determined by estimating state sequence or observability matrix. However, the methodology of SPC does not require their explicit estimation as further explained in the next section.

5.2.2 Unconstrained OLSPC

The predictive control problem is formulated as follows. Given a future set-point signal

$$\mathbf{r}_f = \begin{bmatrix} r^T[t+1] & r^T[t+2] & \cdots & r^T[t+N_p] \end{bmatrix}^T \text{ and a prediction of outputs}$$

$$\hat{\mathbf{y}}_f = \begin{bmatrix} \hat{y}^T[t+1] & \hat{y}^T[t+2] & \cdots & \hat{y}^T[t+N_p] \end{bmatrix}^T, \text{ find an input sequence}$$

$$\mathbf{u}_f = \begin{bmatrix} u^T[t+1] & u^T[t+2] & \cdots & u^T[t+N_c] \end{bmatrix}^T \text{ such that the following cost function is minimized:}$$

$$(\hat{\mathbf{y}}_f - \mathbf{r}_f)^T Q_f (\hat{\mathbf{y}}_f - \mathbf{r}_f) + \Delta \mathbf{u}_f^T R_f \Delta \mathbf{u}_f, \quad (5.8)$$

where N_p and $N_c (\leq N_p)$ are prediction and control horizons respectively. $Q_f = I_{N_p} \otimes Q$ denotes the weighing diagonal matrix penalizing the error between set-point and output, where \otimes represents the Kronecker product, I_{N_p} is an $N_p \times N_p$ identity matrix, and Q is a positive semi-definite matrix of dimension $l \times l$. Similarly, $R_f = I_{N_c} \otimes R$ denotes the weighing diagonal matrix penalizing the rate of change of input, where R is a positive definite matrix of dimension $m \times m$.

$\Delta \mathbf{u}_f = \begin{bmatrix} \Delta u^T[t+1] & \Delta u^T[t+2] & \cdots & \Delta u^T[t+N_c] \end{bmatrix}^T$ denotes the incremental input sequence where the difference operator is $\Delta = 1 - z^{-1}$, z^{-1} is backward shift operator. In the receding horizon control philosophy, the control strategy is calculated by solving an optimization problem and only the first of the N_c control inputs is implemented as the current control input [151]. The same strategy is repeated for next data samples.

To include the subspace-based predictor into MPC formulation, the order of the future Hankel data matrix is taken equal to the prediction horizon, input is assumed to be

constant outside the control horizon, and only the leftmost column of \hat{Y}_f is considered to predict the output [28]. Therefore, the predictor equation (5.5) is rewritten as

$$\hat{\mathbf{y}}_f = L_w \mathbf{w}_p + L_u \mathbf{u}_f, \quad (5.9)$$

where $\mathbf{w}_p = \begin{bmatrix} y^T[t-M+1] & \cdots & y^T[t] & u^T[t-M+1] & \cdots & u^T[t] \end{bmatrix}^T$. In terms of rate of change of input, $\hat{\mathbf{y}}_f$ given by (5.9), can also be expressed as

$$\hat{\mathbf{y}}_f = \bar{I}_l y[t] + O_l L_w \Delta \mathbf{w}_p + O_l L_u \Delta \mathbf{u}_f, \quad (5.10)$$

where $\Delta \mathbf{w}_p = \begin{bmatrix} \Delta y^T[t-M+1] & \cdots & \Delta y^T[t] & \Delta u^T[t-M+1] & \cdots & \Delta u^T[t] \end{bmatrix}^T$,

$$\bar{I}_l = \begin{bmatrix} I_l \\ I_l \\ \vdots \\ I_l \end{bmatrix} \in R^{N_p l \times l}, O_l = \begin{bmatrix} I_l & 0 & \cdots & 0 \\ I_l & I_l & \cdots & 0 \\ \vdots & \vdots & \ddots & \vdots \\ I_l & I_l & \cdots & I_l \end{bmatrix} \in R^{N_p l \times N_p l}, \text{ and } I_l \text{ is an } l \times l \text{ identity}$$

matrix. Define, $\bar{\mathbf{y}}[t] = \bar{I}_l y[t]$, $\bar{L}_w = O_l L_w$, and $\bar{L}_u = O_l L_u$. Then, (5.10) can be simply written as

$$\hat{\mathbf{y}}_f = \bar{\mathbf{y}}[t] + \bar{L}_w \Delta \mathbf{w}_p + \bar{L}_u \Delta \mathbf{u}_f. \quad (5.11)$$

Thus, the change in input that minimizes the cost function is obtained as

$$\Delta \mathbf{u}_f = - \left((\bar{L}_u)^T Q_f \bar{L}_u + R_f \right)^{-1} (\bar{L}_u)^T Q_f (\bar{\mathbf{y}}[t] - \mathbf{r}_f + \bar{L}_w \Delta \mathbf{w}_p), \quad (5.12)$$

or simply,

$$\Delta \mathbf{u}_f = -K_u (\bar{\mathbf{y}}[t] - \mathbf{r}_f) - K_w \Delta \mathbf{w}_p \quad (5.13)$$

where gain matrices are defined as

$$\begin{aligned} K_u &= \left((\bar{L}_u)^T Q_f \bar{L}_u + R_f \right)^{-1} (\bar{L}_u)^T Q_f, \\ K_w &= \left((\bar{L}_u)^T Q_f \bar{L}_u + R_f \right)^{-1} (\bar{L}_u)^T Q_f \bar{L}_w. \end{aligned} \quad (5.14)$$

Now, the control signal is updated using only the first of the N_c control moves as the current control input

$$u(t+1) = \Delta \mathbf{u}_f(1) + u(t). \quad (5.15)$$

5.2.3 Constrained OLSPC

SPC formulation is able to deal with hard or soft constraints such as

$$\begin{aligned} U_{\min} \leq \mathbf{u}_f \leq U_{\max}; \quad \Delta U_{\min} \leq \Delta \mathbf{u}_f \leq \Delta U_{\max}; \\ Y_{\min} \leq \mathbf{y}_f \leq Y_{\max}; \quad \Delta Y_{\min} \leq \Delta \mathbf{y}_f \leq \Delta Y_{\max}. \end{aligned} \quad (5.16)$$

where

$$\begin{aligned} U_{\min} &= \begin{bmatrix} u_{\min}^T & \cdots & u_{\min}^T \end{bmatrix}^T; \quad \Delta U_{\min} = \begin{bmatrix} \Delta u_{\min}^T & \cdots & \Delta u_{\min}^T \end{bmatrix}^T, \\ Y_{\min} &= \begin{bmatrix} y_{\min}^T & \cdots & y_{\min}^T \end{bmatrix}^T; \quad \Delta Y_{\min} = \begin{bmatrix} \Delta y_{\min}^T & \cdots & \Delta y_{\min}^T \end{bmatrix}^T, \end{aligned} \quad (5.17)$$

and the same notation also holds for parameters with subscript max. For the inclusion of constraints in the optimization problem, the cost function is modified as

$$\min_{\Delta \mathbf{u}_f} \left((\hat{\mathbf{y}}_f - \mathbf{r}_f)^T Q_f (\hat{\mathbf{y}}_f - \mathbf{r}_f) + \Delta \mathbf{u}_f^T R_f \Delta \mathbf{u}_f \right) \quad (5.18)$$

such that $A_{cons} \Delta \mathbf{u}_f \leq \mathbf{b}_{cons}$,

where matrices A_{cons} and \mathbf{b}_{cons} are given as

$$\begin{aligned} A_{cons} &= \begin{bmatrix} I_{N_{cm}}^T & -I_{N_{cm}}^T & O_m^T & -O_m^T & L_u^T & -L_u^T & \bar{L}_u^T & -\bar{L}_u^T \end{bmatrix}^T, \\ \mathbf{b}_{cons} &= \begin{bmatrix} \Delta U_{\max}^T & -\Delta U_{\min}^T & (U_{\max} - \bar{\mathbf{u}}[t])^T & (-U_{\min} + \bar{\mathbf{u}}[t])^T \\ (\Delta Y_{\max} - L_w \Delta \mathbf{w}_p)^T & (-\Delta Y_{\min} + L_w \Delta \mathbf{w}_p)^T \\ (Y_{\max} - \bar{\mathbf{y}}[t] - \bar{L}_w \Delta \mathbf{w}_p)^T & (-Y_{\min} + \bar{\mathbf{y}}[t] + \bar{L}_w \Delta \mathbf{w}_p)^T \end{bmatrix}^T. \end{aligned} \quad (5.19)$$

This quadratic constrained optimization problem is solved through Quadratic Programming approach [156].

5.2.4 Inclusion of New Data

Suppose a new set of input-output data is available at time instant $N + 1$. It is assumed that the new input is persistently exciting to avoid any ill-conditioning of the predictor matrices. Therefore, the updated Hankel matrix, *i.e.* the one appended with new data is given by

$$\begin{aligned} U_P^{N+1} &= \begin{bmatrix} U_P & \varphi u_P \end{bmatrix}; & U_F^{N+1} &= \begin{bmatrix} U_F & \varphi u_F \end{bmatrix}; \\ Y_P^{N+1} &= \begin{bmatrix} Y_P & \varphi y_P \end{bmatrix}; & Y_F^{N+1} &= \begin{bmatrix} Y_F & \varphi y_F \end{bmatrix}, \end{aligned} \quad (5.20)$$

where $\varphi u_P = \begin{bmatrix} u[N - 2f + 2] \\ u[N - 2f + 3] \\ \vdots \\ u[N - f + 1] \end{bmatrix}$ and $\varphi u_F = \begin{bmatrix} u[N - f + 2] \\ u[N - f + 3] \\ \vdots \\ u[N + 1] \end{bmatrix}$ respectively represent the rightmost columns of updated *past* and *future* Hankel matrices in (5.1). Similarly, we can write for φy_P and φy_F . Therefore, the updated predictor parameters are given by

$$\begin{bmatrix} L_w^* & L_u^* \end{bmatrix} = Y_F^{N+1} \begin{bmatrix} W_P^{N+1} \\ U_F^{N+1} \end{bmatrix}^\dagger, \quad (5.21)$$

where $W_P^{N+1} = \begin{bmatrix} W_P & \varphi w_P \end{bmatrix}$ and $\varphi w_P = \begin{bmatrix} \varphi y_P \\ \varphi u_P \end{bmatrix}$. This procedure recursively estimates the predictor parameters with the arrival of new data. However, it will be computationally intensive as it requires to solve the QR decomposition at each instant. Moreover, as the data length increases, there should be proper weighting to the new data. In [31, 67], authors presented efficient recursive updating procedure to minimize the computational cost and the same has been deployed by us too.

5.2.5 Incorporating Feed-forward Control

This section presents the inclusion of feed-forward with feedback law as discussed in Kadali *et al.* [29]. Under the consideration that some process disturbances which can not be manipulated but measured, the state-space representation of the system becomes

$$\begin{aligned} x[k+1] &= Ax[k] + \bar{B}\bar{u}[k] + Ke[k] \\ y[k] &= Cx[k] + \bar{D}\bar{u}[k] + e[k] \end{aligned} \quad (5.22)$$

where $\bar{B} = \begin{bmatrix} B & B_v \end{bmatrix}$, $\bar{D} = \begin{bmatrix} D & D_v \end{bmatrix}$, $\bar{u}[k] = \begin{bmatrix} u^T[k] & v^T[k] \end{bmatrix}^T$, and $v[k]$ is the measured disturbance. Therefore, the predictor is given by

$$\hat{Y}_F = L_w^v W_P^v + L_u^v U_F + L_v V_F, \quad (5.23)$$

where $W_P^v = \begin{bmatrix} Y_P^T & U_P^T & V_P^T \end{bmatrix}^T$, V_p and V_f are *past* and *future* Hankel matrices formed from measured disturbances. L_w^v , L_u^v , and L_v are predictor parameters. Note that, the value of measured disturbances in (5.23) are available up to current time instant.

Thus, the predictor is given by

$$\hat{\mathbf{y}}_f = \bar{I}_l y[t] + O_l L_w^v \Delta \mathbf{w}_p^v + O_l L_u^v \Delta \mathbf{u}_f \quad (5.24)$$

or

$$\hat{\mathbf{y}}_f = \bar{\mathbf{y}}[t] + \bar{L}_w^v \Delta \mathbf{w}_p^v + \bar{L}_u^v \Delta \mathbf{u}_f, \quad (5.25)$$

where $\Delta \mathbf{w}_p^v = \begin{bmatrix} \Delta \mathbf{w}_p^T & \Delta v^T[t-M+1] & \cdots & \Delta v^T[t] \end{bmatrix}^T$, $\bar{\mathbf{y}}[t] = \bar{I}_l y[t]$, $\bar{L}_w^v = O_l L_w^v$, and $\bar{L}_u^v = O_l L_u^v$. Solving the cost function with the above defined predictor gives control law

$$\Delta \mathbf{u}_f = - \left((\bar{L}_u^v)^T Q_f \bar{L}_u^v + R_f \right)^{-1} (\bar{L}_u^v)^T Q_f (\bar{\mathbf{y}}[t] - \mathbf{r}_f + \bar{L}_w^v \Delta \mathbf{w}_p^v). \quad (5.26)$$

5.2.6 Incorporating Integrating Control

To handle integrating type of non-stationary disturbances in the measurement data and to have a guaranteed integral action, a set of measures has been proposed in [29],[31]. The basic idea is similar to that of the GPC design that the measurement noise entering to the system is represented by an integrated white Gaussian noise sequence [1]. Therefore, the system can be represented as

$$\begin{aligned}x[k+1] &= Ax[k] + Bu[k] + K\tilde{e}[k], \\y[k] &= Cx[k] + Du[k] + \tilde{e}[k],\end{aligned}\tag{5.27}$$

or

$$\begin{aligned}\Delta x[k+1] &= A\Delta x[k] + B\Delta u[k] + Ke[k], \\ \Delta y[k] &= C\Delta x[k] + D\Delta u[k] + e[k],\end{aligned}\tag{5.28}$$

where $\tilde{e}[k] = \frac{e[k]}{\Delta}$ is the integrated white noise and $e[k]$ is white noise. The predictor will be similar to (5.11) except that the predictor parameters are estimated from differenced dataset. However, by differencing the estimation dataset, the noise could get amplified drastically especially in case of low signal to noise ratio (SNR). Therefore, it is necessary to pre-process the data before employing in control design.

5.3 Closed-Loop Subspace Predictive Control

5.3.1 Design of Linear Predictor

The system representation in *predictor* form is given as

$$x[k+1] = A_K x[k] + \bar{B}_K z[k],\tag{5.29}$$

$$y[k] = Cx[k] + Du[k] + e[k].\tag{5.30}$$

Now, we know that,

$$Y_f = \Gamma_f L_p Z_p + \Gamma_f A_K^p X_{k-p} + H_f^d U_f + H_f^s E_f, \quad (5.31)$$

Equation (5.31) is composed of f block rows in each term and thus after simplifying we can write for first row

$$Y_{f1} = CA_K^p X_{k-p} + \Psi_0 W_p + DU_1 + E_{f1}, \quad (5.32)$$

where $\Psi_0 = \begin{bmatrix} CA_K^{p-1} \bar{B}_K & CA_K^{p-2} \bar{B}_K & \cdots & C \bar{B}_K \end{bmatrix}$ and

$$W_p = \begin{bmatrix} z[k-p] & z[k-p+1] & \cdots & z[k-p+N-1] \\ z[k-p+1] & z[k-p+2] & \cdots & z[k-p+N] \\ \vdots & \vdots & \ddots & \vdots \\ z[k-1] & z[k] & \cdots & z[k+N-2] \end{bmatrix}.$$

For large of p , $A_K^p \simeq 0$. Taking $D = 0$ and $\bar{B} = \begin{bmatrix} B & K \end{bmatrix}$ thus, (5.32) can be approximated as

$$Y_{f1} = \Psi_0 W_p + E_{f1} \quad (5.33)$$

Let t and f denote current time instant and future time horizon, then using (5.31), subspace predictor can be written as,

$$\begin{bmatrix} \hat{y}[t+1] \\ \hat{y}[t+2] \\ \vdots \\ \hat{y}[t+f-1] \end{bmatrix} = \underbrace{\begin{bmatrix} 0 & CA_K^{p-1} \bar{B} & CA_K^{p-2} \bar{B} & \cdots & \cdots & CA_K \bar{B} \\ 0 & 0 & CA_K^{p-1} \bar{B} & \cdots & \cdots & \vdots \\ \vdots & \vdots & \ddots & \ddots & \ddots & \vdots \\ 0 & 0 & \cdots & CA_K^{p-1} \bar{B} & \cdots & CA_K^{f-1} \bar{B} \end{bmatrix}}_{\Psi} \underbrace{\begin{bmatrix} w[t-p] \\ w[t-p+1] \\ \vdots \\ w[t-1] \end{bmatrix}}_w + \begin{bmatrix} C \bar{B} & 0 & \cdots & 0 \\ CA_K \bar{B} & C \bar{B} & \cdots & 0 \\ \vdots & \vdots & \ddots & \vdots \\ CA_K^{f-2} \bar{B} & CA_K^{f-3} \bar{B} & \cdots & C \bar{B} \end{bmatrix} \begin{bmatrix} w[t] \\ w[t+1] \\ \vdots \\ w[t+f-2] \end{bmatrix} + \begin{bmatrix} CA_K^p x[t-p+1] \\ CA_K^p x[t-p+2] \\ \vdots \\ CA_K^p x[t-p+f-1] \end{bmatrix}$$

or, approximately by ignoring the higher order terms of $CA_K^{p+\tau}\bar{B}$, $\forall 0 \leq \tau < f$.

$$\begin{bmatrix} \hat{y}[t+1] \\ \hat{y}[t+2] \\ \vdots \\ \hat{y}[t+f-1] \end{bmatrix} \approx \begin{bmatrix} \Psi_1 \\ \Psi_2 \\ \vdots \\ \Psi_{f-1} \end{bmatrix} W + \begin{bmatrix} C\bar{B} & 0 & \cdots & 0 \\ CA_K\bar{B} & C\bar{B} & \cdots & 0 \\ \vdots & \vdots & \ddots & \vdots \\ CA_K^{f-2}\bar{B} & CA_K^{f-3}\bar{B} & \cdots & C\bar{B} \end{bmatrix} \begin{bmatrix} w[t] \\ w[t+1] \\ \vdots \\ w[t+f-2] \end{bmatrix} + \begin{bmatrix} CA_K^{p+1} \\ CA_K^{p+2} \\ \vdots \\ CA_K^{p+f-1} \end{bmatrix} x[t-p] \quad (5.34)$$

For sufficiently large value of p such that $\|A_K^p\| \ll 1$, output predictor is given by

$$\begin{bmatrix} \hat{y}[t+1] \\ \hat{y}[t+2] \\ \vdots \\ \hat{y}[t+f-1] \end{bmatrix} = \underbrace{\begin{bmatrix} \Gamma_1 \\ \Gamma_2 \\ \vdots \\ \Gamma_{f-1} \end{bmatrix}}_{\Gamma} W + \underbrace{\begin{bmatrix} \Lambda_1 & 0 & \cdots & 0 \\ \Lambda_2 & \Lambda_1 & \cdots & 0 \\ \vdots & \ddots & \ddots & \vdots \\ \Lambda_{f-1} & \Lambda_{f-2} & \cdots & \Lambda_1 \end{bmatrix}}_{\Lambda} \begin{bmatrix} u[t] \\ u[t+1] \\ \vdots \\ u[t+f-2] \end{bmatrix} \quad (5.35)$$

where Γ and Λ are predictor matrices and their elements are related as

$$\begin{aligned} \Gamma_i &= \Psi_i + \sum_{\tau=0}^{i-1} CA_K^{i-\tau-1} K \Gamma_{\tau} \\ \Lambda_i &= CA_K^{i-1} B + \sum_{\tau=0}^{i-1} CA_K^{i-\tau-1} K \Lambda_{\tau} \end{aligned} \quad (5.36)$$

with $\Gamma_0 = \Psi_0$ and $\Lambda_1 = CB$.

In the derivation of (5.36), the persistency of excitation in the input data guarantees consistency in the estimates. To accurately predict the system outputs using subspace predictor it is required that the available input-output data contains sufficient information on the system. To assure persistency of excitation in the data a measure has been suggested in [165]. In addition, the recursive formulation of CLSPC is able to deal with unanticipated situations and ill-conditioning if the input data is persistently excited.

5.3.2 Unconstrained CLSPC

The predictive control problem is formulated as follows. Given a future set-point signal

$$\mathbf{r}_f = \begin{bmatrix} r^T[t+1] & r^T[t+2] & \cdots & r^T[t+N_p] \end{bmatrix}^T \text{ and a prediction of outputs}$$

$$\hat{\mathbf{y}}_f = \begin{bmatrix} \hat{y}^T[t+1] & \hat{y}^T[t+2] & \cdots & \hat{y}^T[t+N_p] \end{bmatrix}^T, \text{ find an input sequence}$$

$$\mathbf{u}_f = \begin{bmatrix} u^T[t+1] & u^T[t+2] & \cdots & u^T[t+N_c] \end{bmatrix}^T \text{ such that the following cost function is minimized:}$$

$$(\hat{\mathbf{y}}_f - \mathbf{r}_f)^T Q_f (\hat{\mathbf{y}}_f - \mathbf{r}_f) + \Delta \mathbf{u}_f^T R_f \Delta \mathbf{u}_f, \quad (5.37)$$

Therefore, the predictor equation (5.35) can be rewritten as

$$\hat{\mathbf{y}}_f = \Gamma W + \Lambda \bar{\mathbf{I}} \mathbf{u}_f \quad (5.38)$$

$$\text{where } \bar{\mathbf{I}} = \begin{bmatrix} I_m & 0 & \cdots & 0 & 0 & \cdots & 0 \\ 0 & I_m & \ddots & \vdots & \vdots & \ddots & \vdots \\ \vdots & \ddots & \ddots & 0 & 0 & \cdots & 0 \\ 0 & \cdots & 0 & I_m & I_m & \cdots & I_m \end{bmatrix}^T.$$

In terms of rate of change of input, $\hat{\mathbf{y}}_f$ given by (5.38), can also be expressed as

$$\hat{\mathbf{y}}_f = \tilde{I} y[t] + O_l \Gamma \Delta W + O_l \Lambda \bar{\mathbf{I}} \Delta \mathbf{u}_f, \quad (5.39)$$

$$\text{where } \tilde{I} = \begin{bmatrix} I_l \\ I_l \\ \vdots \\ I_l \end{bmatrix}, O_l = \begin{bmatrix} I_l & 0 & \cdots & 0 \\ I_l & I_l & \cdots & 0 \\ \vdots & \vdots & \ddots & \vdots \\ I_l & I_l & \cdots & I_l \end{bmatrix}, \Delta W = \begin{bmatrix} \Delta w[t-p] \\ \Delta w[t-p+1] \\ \vdots \\ \Delta w[t-1] \end{bmatrix}, \Delta w[k] = \begin{bmatrix} \Delta u[k] \\ \Delta y[k] \end{bmatrix}, \text{ and } I_l \text{ is an } l \times l \text{ identity matrix.}$$

Define, $\bar{y}[t] = \tilde{I}_l y[t]$, $\tilde{\Gamma} = O_l \Gamma$, and $\tilde{\Lambda} = O_l \Lambda I$. Then, (5.39) can be simply written as

$$\hat{y}_f = \bar{y}[t] + \tilde{\Gamma} \Delta W + \tilde{\Lambda} \Delta u_f \quad (5.40)$$

Thus, the change in input that minimizes cost function is obtained as

$$\Delta u_f = -\left(\tilde{\Lambda}^T Q_f \tilde{\Lambda} + R_f\right)^{-1} \tilde{\Lambda}^T Q_f \left(\bar{y}[t] - r_f + \tilde{\Gamma} \Delta W\right), \quad (5.41)$$

or simply,

$$\Delta u_f = -K_u (\bar{y}[t] - r_f) - K_w \Delta w_p \quad (5.42)$$

where gain matrices are defined as

$$\begin{aligned} K_u &= \left(\tilde{\Lambda}^T Q_f \tilde{\Lambda} + R_f\right)^{-1} \tilde{\Lambda}^T Q_f, \\ K_w &= \left(\tilde{\Lambda}^T Q_f \tilde{\Lambda} + R_f\right)^{-1} \tilde{\Lambda}^T Q_f \tilde{\Gamma}. \end{aligned} \quad (5.43)$$

Now, the control signal is updated using only the first control input

$$u(t+1) = \Delta u_f(1) + u(t). \quad (5.44)$$

The formulation of CLSPC is easily able to deal with hard or soft constraints. In addition, other design features can also be included in the design. The formulation of these features in the CLSPC is similar to that in the OLSPC approach.

5.4 Parameter Sensitivity Analysis

In the formulation of SPC, various design parameters like N_P , N_C , Q , and R decide the necessary control action as well as the stability. Their selection is also crucial for desired control performance. The proof of closed-loop stability of this type of control algorithm is not available [30]. Usually, long prediction and control horizons ensure stability of the SPC as the algorithm converges to classical MPC when N_P goes to infinity [28].

However, a large value of control horizon increases the computational cost as well as control efforts. Therefore, a good tuning of different controller parameters is necessary for stable closed-loop response. Usually, the control performance or effort is evaluated on the basis of three factors namely, mean squared error (MSE) between output and desired set-point, total variation (TV) of input, and the l_2 -norm ($\|U\|_2$) of input. These measures analyze the effect of control action on output as well as on input and are given by

$$MSE = \frac{1}{N} \sum_{k=1}^N (y[k] - r[k])^2, \quad (5.45)$$

$$TV = \sum_{k=1}^N |(u[k+1] - u[k])|, \quad (5.46)$$

$$\|U\|_2 = \left(\sum_{k=1}^N (u[k])^2 \right)^{1/2}. \quad (5.47)$$

A detailed analysis on the performance of control efforts with respect to changes in parameters is given in Section 5.4.

5.5 Application to Nuclear Reactor

The techniques presented in the preceding sections have been applied to nuclear reactor described by the point kinetics model with six groups of delayed neutrons and lumped thermal hydraulics model as discussed in Chapter C. For the purpose of control design directly from measurement data, reactivity and power can be regarded as input to and output from the reactor system respectively. In the study, it is assumed that the primary loop is defined by a nonlinear lumped model with pressure and mass flow rate held constant. The heat produced in the core is conveyed by single-phase coolant only, and xenon and fuel depletion effects are not considered. Further, the total reactivity is contributed by regulating rod movement (ρ_{RR}) and due to temperature feedback. Only $\alpha_F = \alpha_1^F$ and $\alpha_C = \alpha_1^C$ be the non-zero temperature coefficient of reactivity are considered; The parameters have been taken from [150] and are listed in Table 5.1.

The complete dynamic model is rewritten below for immediate reference:

$$\frac{dP}{dt} = \frac{\rho_T - \sum_{i=1}^6 \beta_i}{\Lambda} P + \frac{\sum_{i=1}^6 \beta_i C_i}{\Lambda}, \quad (5.48)$$

$$\frac{dC_i}{dt} = \lambda_i (P - C_i), \quad i = 1, 2, \dots, 6, \quad (5.49)$$

$$\frac{dT_F}{dt} = H_F P - \gamma_f (T_F - T_C), \quad (5.50)$$

$$\frac{dT_C}{dt} = -H_C (T_{out} - T_{in}) + \gamma_c (T_F - T_C), \quad (5.51)$$

$$\frac{dT_{in}}{dt} = \frac{1}{\tau_{cold}} (T_{cold} - T_{in}), \quad (5.52)$$

$$\frac{dT_{hot}}{dt} = \frac{1}{\tau_{hot}} (T_{out} - T_{hot}), \quad (5.53)$$

$$\frac{dT_{sg}}{dt} = -\frac{1}{\tau_{sg}} (T_{sg} - T_{hot}) - D_1 L_T, \quad (5.54)$$

$$T_{cold} = D_2 T_{sg} - D_3 T_{hot}, \quad (5.55)$$

$$\rho_T = \rho_{RR} + \alpha_F T_F + \alpha_C T_C. \quad (5.56)$$

5.5.1 Implementation of Proposed Methodology

The block diagram of the proposed technique for application to nuclear reactor is shown in Figure 5.1. The nuclear reactor described by the set of equations (5.48)–(5.56), is excited by supplying reactivity variation caused by regulating rod (RR) movement. Estimation dataset is constructed where reactivity and neutronic power (with additive random noise) act as input and output respectively. This dataset is fed to the wavelet pre-processing block for multiscale data analysis. The data are projected up to J levels of decomposition using appropriately selected wavelet. The threshold is then computed and applied to the wavelet coefficients. The denoised estimation dataset is reconstructed from thresholded coefficients using inverse wavelet transform. The pre-processed estimation data are now used for estimating predictor coefficients and subsequently for solving the optimization problem. The control input trajectory is designed using only the first of the N_c optimal inputs and subsequently given to the process for tracking set-point. The same steps are repeated for subsequent data samples.

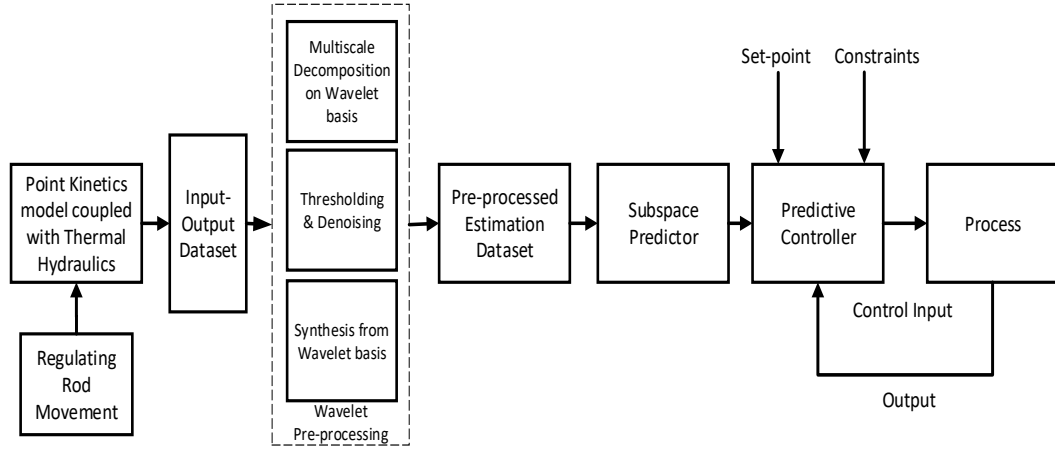


FIGURE 5.1: Block diagram representation of the proposed scheme with application to nuclear reactor.

TABLE 5.1: Neutronic and thermal-hydraulic parameters

Group, i	1	2	3	4	5	6
$\lambda_i (s^{-1})$	0.0125	0.0308	0.1152	0.3109	1.240	3.3287
β_i	0.000216	0.001416	0.001349	0.00218	0.00095	0.000322
$H_F ({}^{\circ}C s^{-1})$	$H_C (s^{-1})$	$\gamma_F (s^{-1})$	$\gamma_C (s^{-1})$	$\alpha_F ({}^{\circ}C^{-1})$	$\alpha_C ({}^{\circ}C^{-1})$	$\Lambda (s)$
102.7	0.2401	0.1792	0.0124	-2×10^{-5}	-5×10^{-5}	5×10^{-4}
$\tau_{cold} (s)$	$\tau_{hot} (s)$	$\tau_{sg} (s)$	$D_1 ({}^{\circ}C s^{-1})$	D_2	D_3	
7.0	5.0	11.3	3.746	0.7005	-0.2995	

In this study, initially the reactor is assumed to be operating at 90% of full power (FP). The single-input and single-output estimation dataset comprises of input reactivity as shown in Figure 5.2 and the corresponding output power mixed with an additive 50 dB white Gaussian noise as shown in Figure 5.3. The maximum depth of decomposition (J) is computed using Fourier Transform [185]. Figure 5.4 shows the discrete-time Fourier Transform of the reactor power signal. The magnitude of the Fourier Transform is seen to be approaching the noise floor level for $\pi/250$ rad/sample and higher values of normalized frequencies. The depth of decomposition is decided such that $\pi/2^J \geq \pi/250$, i.e. $J = 7$. Now, the reactor power signal is projected to seven levels of decomposition using different wavelets with varying vanishing moments and support. The signal is then reconstructed after performing thresholding operation on to the wavelet coefficients.

The performance of denoising technique is evaluated by computing signal to noise ratio and mean squared error of the denoised signal. The denoised signal to noise ratio (DNSNR) is defined as

$$DNSNR = 10\log_{10} \left(\frac{\sum_{k=1}^N (\bar{y}[k])^2}{\sum_{k=1}^N (y[k] - \bar{y}[k])^2} \right), \quad (5.57)$$

and the denoised mean squared error (DNMSE) is defined as

$$DNMSE = \frac{1}{N} \sum_{k=1}^N (y[k] - \bar{y}[k])^2. \quad (5.58)$$

where \bar{y} and y denote original noiseless power signal and denoised power signal respectively. The value of SNR and MSE before denosing are 49.2887 dB and 3.6152×10^{-5} respectively. Table 5.2 compares the performances of different hard and soft denoising techniques, for some of the popular families of wavelets, viz. *Haar*, *Daubechies*, *Coiflet* and *Symlet* [86]. It is observed from Table 5.2 that *Daubechies-4*, *Symlet-7*, and *Coiflet-2* from their respective wavelet families give highest DNSNR and lowest DNMSE. However, overall performance evaluation and denoised response indicate that *Daubechies-4* wavelet is better suited to represent the estimation dataset over other wavelets. It is further found that *VisuShrink* offers the best denoising performance compared to *MiniMax* and *SureShrink* thresholding techniques for reactor power signal. It may also be noted that the soft thresholding-based algorithms have better DNSNR and DNMSE over the hard thresholding-based schemes. Further, to demonstrate the dependence on decomposition depth, the performances of *Daubechies-4* wavelet at different depth of decompositions is tabulated in Table 5.3. The performance has enhanced with the increase in decomposition depth up to level seven and after that it starts decreasing mainly due to over smoothing of reactor dynamics at higher level. Thus, for the case studied here, it is observed that the best results in terms of DNSNR and DNMSE correspond to the level seven of the *Daubechies-4* wavelet decomposition and to a *VisuShrink*-based soft threshold technique.

Now, to validate the efficacy of wavelet pre-processing, the 40 largest singular values of

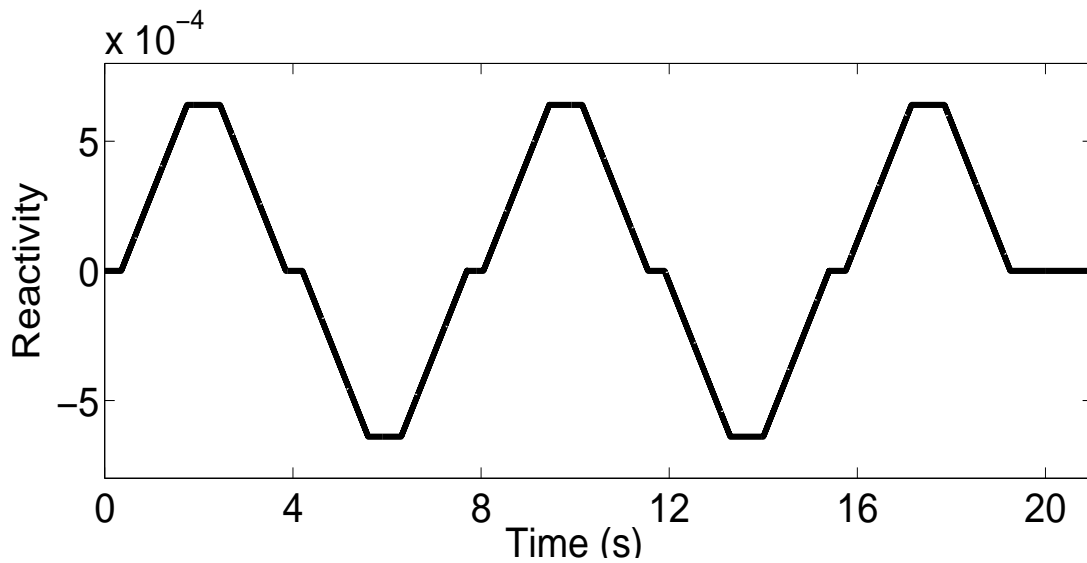


FIGURE 5.2: Assumed reactivity variation (estimation input data).

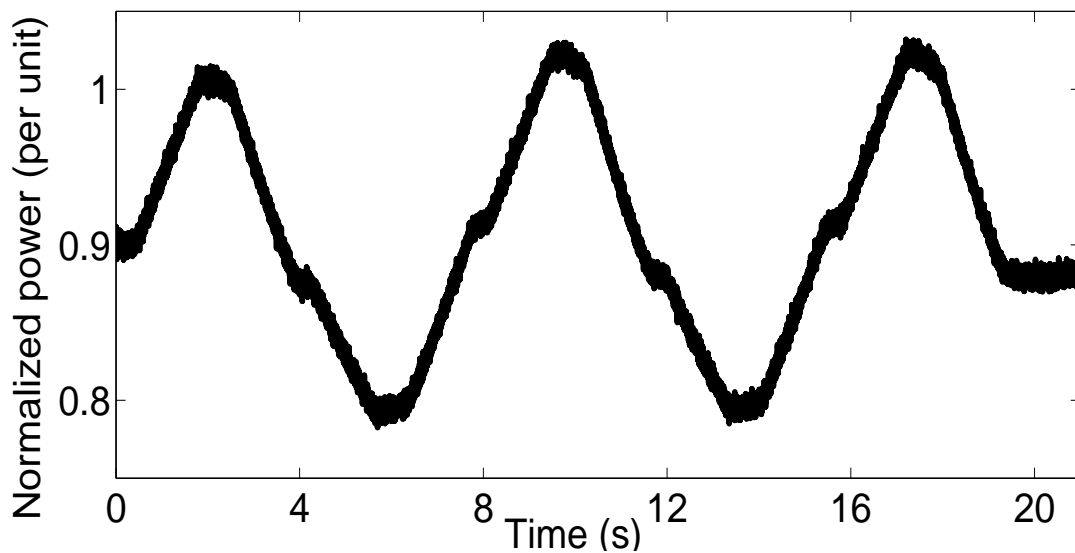


FIGURE 5.3: Reactor power variation corresponding to reactivity variation shown in Figure 5.2 (estimation output data).

the covariance matrix constructed from the unprocessed measured noisy data and that from pre-processed measurement data are shown in Figure 5.5. In the case of unprocessed data, only the first singular value of signal is identifiable. Remaining singular values of signal are not well-separable from that of the noise. On the other hand, it is apparent that wavelet pre-processing efficiently separates out the singular values of signal from that of the noise and enables very effective noise filtering in multiresolution as shown in Figure 5.5.

TABLE 5.2: Comparison of performances of denoised signal for Haar, Daubechies, Symlet and Coiflet wavelet families at $J = 7$

Wavelet	DNSNR (dB)						DNMSE					
	Soft Threshold			Hard Threshold			Soft Threshold			Hard Threshold		
	MiniMax	VisuShrink	SureShrink	MiniMax	VisuShrink	SureShrink	MiniMax	VisuShrink	SureShrink	MiniMax	VisuShrink	SureShrink
<i>Haar</i>	58.6794	57.0981	63.0562	59.4172	59.7311	59.2753	1.1358×10^{-6}	1.6346×10^{-6}	4.1460×10^{-7}	9.5834×10^{-7}	8.9152×10^{-7}	9.9019×10^{-7}
<i>Daubechies-2</i>	69.6024	69.6967	69.2247	64.6779	69.6067	63.4508	9.1833×10^{-8}	8.9862×10^{-8}	1.0017×10^{-7}	2.2670×10^{-7}	8.9862×10^{-8}	3.7858×10^{-7}
<i>Daubechies-3</i>	70.4464	70.5691	69.6119	64.6509	70.5691	63.7326	7.5614×10^{-8}	7.3508×10^{-8}	8.5387×10^{-8}	2.8717×10^{-7}	7.3508×10^{-8}	2.8183×10^{-7}
<i>Daubechies-4</i>	70.7255	70.8988	69.9185	65.4364	70.9191	64.8083	7.0908×10^{-8}	6.8134×10^{-8}	7.2632×10^{-8}	2.0628×10^{-7}	6.8134×10^{-8}	2.5259×10^{-7}
<i>Daubechies-5</i>	70.7228	70.8429	69.8315	65.3712	70.8429	62.9030	7.0952×10^{-8}	6.9016×10^{-8}	8.7115×10^{-8}	2.3966×10^{-7}	6.9016×10^{-8}	4.2948×10^{-7}
<i>Daubechies-6</i>	70.3996	70.5450	69.5190	64.8264	70.1549	62.6409	7.6433×10^{-8}	7.3917×10^{-8}	9.3614×10^{-8}	2.7580×10^{-7}	8.0864×10^{-8}	4.5619×10^{-7}
<i>Daubechies-7</i>	70.4930	70.6724	69.2361	64.5233	70.2800	63.6119	7.4807×10^{-8}	7.1780×10^{-8}	7.9366×10^{-8}	2.9574×10^{-7}	7.8567×10^{-8}	3.6480×10^{-7}
<i>Daubechies-8</i>	70.6246	70.8191	68.7154	63.9055	70.8918	59.4466	7.0940×10^{-8}	6.9816×10^{-8}	1.1264×10^{-7}	3.4095×10^{-7}	6.7816×10^{-8}	9.5188×10^{-7}
<i>Daubechies-9</i>	70.5841	70.8180	69.8544	64.5312	70.8180	61.8476	7.3254×10^{-8}	6.9412×10^{-8}	8.4685×10^{-8}	2.9520×10^{-7}	6.9412×10^{-8}	5.4762×10^{-7}
<i>Daubechies-10</i>	70.3967	70.5850	68.9919	64.3806	70.5850	59.8825	7.6484×10^{-8}	7.3238×10^{-8}	1.0596×10^{-7}	3.0562×10^{-7}	7.3238×10^{-8}	8.6098×10^{-7}
<i>Symlet-4</i>	70.6171	70.7858	70.4646	64.4204	70.7858	64.3296	7.2699×10^{-8}	6.9930×10^{-8}	7.5298×10^{-8}	3.0283×10^{-7}	6.9930×10^{-8}	3.0923×10^{-7}
<i>Symlet-5</i>	70.3898	70.6592	69.1087	64.5593	70.1869	60.8852	7.6605×10^{-8}	7.1999×10^{-8}	1.0289×10^{-7}	2.9330×10^{-7}	8.0269×10^{-8}	6.8347×10^{-7}
<i>Symlet-6</i>	70.6444	70.8131	70.0156	64.7835	70.8131	62.1610	7.2243×10^{-8}	6.9491×10^{-8}	8.3500×10^{-8}	2.7854×10^{-7}	6.9491×10^{-8}	5.0950×10^{-7}
<i>Symlet-7</i>	70.7342	70.9045	70.1727	65.1671	71.0503	64.6718	7.1758×10^{-8}	6.7798×10^{-8}	7.3447×10^{-8}	2.8884×10^{-7}	6.5798×10^{-8}	2.2701×10^{-7}
<i>Symlet-8</i>	70.6377	70.8283	69.2990	64.1155	70.8283	60.7766	7.2356×10^{-8}	6.9249×10^{-8}	9.8478×10^{-8}	3.2485×10^{-7}	6.9249×10^{-8}	7.0078×10^{-7}
<i>Symlet-9</i>	70.4532	70.6739	69.3817	64.7223	70.6739	61.2596	7.5496×10^{-8}	7.1755×10^{-8}	9.6621×10^{-8}	2.8249×10^{-7}	7.1755×10^{-8}	6.2702×10^{-7}
<i>Symlet-10</i>	70.6766	70.8042	70.2930	64.6897	70.8042	63.6042	7.1710×10^{-8}	6.9633×10^{-8}	7.8332×10^{-8}	2.8462×10^{-7}	6.9633×10^{-8}	3.6544×10^{-7}
<i>Coiflet-1</i>	69.6849	69.8827	68.9685	64.0409	69.4746	61.2835	9.0106×10^{-8}	8.6093×10^{-8}	1.0626×10^{-7}	3.3048×10^{-7}	9.4576×10^{-8}	6.2357×10^{-7}
<i>Coiflet-2</i>	70.5690	70.7880	69.6754	64.5391	70.3705	61.6287	7.3509×10^{-8}	6.9895×10^{-8}	9.0302×10^{-8}	2.9466×10^{-7}	7.6948×10^{-8}	5.7563×10^{-7}
<i>Coiflet-3</i>	70.4659	70.7124	70.0573	64.4555	70.2276	63.5800	7.5275×10^{-8}	7.1122×10^{-8}	8.2701×10^{-8}	3.0039×10^{-7}	7.9521×10^{-8}	3.6749×10^{-7}
<i>Coiflet-4</i>	70.5376	70.7604	68.7291	63.7813	70.2604	59.7926	7.4043×10^{-8}	7.0341×10^{-8}	1.1228×10^{-7}	3.5084×10^{-7}	7.0341×10^{-8}	8.7899×10^{-7}
<i>Coiflet-5</i>	70.5305	70.7784	69.9869	64.0221	70.3202	62.0840	7.4165×10^{-8}	6.9967×10^{-8}	8.4053×10^{-8}	3.3192×10^{-7}	7.9844×10^{-8}	5.1861×10^{-7}

TABLE 5.3: Comparison of performances of denoised signal with respect to depth of decomposition for Daubechies-4 wavelet.

Scale	DNSNR (dB)						DNMSE					
	Soft Threshold			Hard Threshold			Soft Threshold			Hard Threshold		
	MinMax	VisuShrink	SureShrink	MinMax	VisuShrink	SureShrink	MinMax	VisuShrink	SureShrink	MinMax	VisuShrink	SureShrink
1	52.2338	52.2344	52.2344	52.1497	52.2344	52.2344	5.0103 × 10 ⁻⁶	5.0095 × 10 ⁻⁶	5.0095 × 10 ⁻⁶	5.1082 × 10 ⁻⁶	5.0095 × 10 ⁻⁶	5.0095 × 10 ⁻⁶
2	55.1941	55.1959	55.1956	54.9655	55.1959	55.1616	2.5341 × 10 ⁻⁶	2.5330 × 10 ⁻⁶	2.5333 × 10 ⁻⁶	2.6711 × 10 ⁻⁶	2.5330 × 10 ⁻⁶	2.5532 × 10 ⁻⁶
3	58.3185	58.3256	58.2653	57.6961	58.3256	57.2229	1.2342 × 10 ⁻⁶	1.2322 × 10 ⁻⁶	1.2494 × 10 ⁻⁶	1.4243 × 10 ⁻⁶	1.2322 × 10 ⁻⁶	1.5883 × 10 ⁻⁶
4	61.5305	61.5492	61.4081	60.1528	61.5492	59.2627	5.8910 × 10 ⁻⁷	5.8657 × 10 ⁻⁷	6.0594 × 10 ⁻⁷	8.0903 × 10 ⁻⁷	5.8657 × 10 ⁻⁷	9.9304 × 10 ⁻⁷
5	64.7028	64.7434	64.4036	62.1169	64.7434	60.4638	2.8376 × 10 ⁻⁷	2.8112 × 10 ⁻⁷	3.0400 × 10 ⁻⁷	5.1469 × 10 ⁻⁷	2.8112 × 10 ⁻⁷	7.5312 × 10 ⁻⁷
6	68.2397	68.3367	67.5767	63.6567	68.3367	61.3978	1.2568 × 10 ⁻⁷	1.2290 × 10 ⁻⁷	1.4641 × 10 ⁻⁷	3.6105 × 10 ⁻⁷	1.2290 × 10 ⁻⁷	6.0738 × 10 ⁻⁷
7	70.7255	70.8988	69.9515	65.4364	70.9191	64.8083	7.0908 × 10 ⁻⁸	7.8134 × 10 ⁻⁸	8.4632 × 10 ⁻⁸	2.0628 × 10 ⁻⁷	6.8134 × 10 ⁻⁸	2.5259 × 10 ⁻⁷
8	70.3510	70.2703	69.9501	64.2757	70.2884	61.8620	7.7294 × 10 ⁻⁸	6.8743 × 10 ⁻⁸	8.4740 × 10 ⁻⁸	3.1309 × 10 ⁻⁷	7.8415 × 10 ⁻⁸	5.4580 × 10 ⁻⁷
9	66.8130	65.0088	69.9483	64.0248	68.8465	61.8628	1.7455 × 10 ⁻⁷	2.6446 × 10 ⁻⁷	8.4804 × 10 ⁻⁸	3.3171 × 10 ⁻⁷	1.0929 × 10 ⁻⁷	5.4571 × 10 ⁻⁷
10	64.9020	62.6155	69.9383	63.9955	68.7608	61.8628	2.7104 × 10 ⁻⁷	4.5887 × 10 ⁻⁷	8.4999 × 10 ⁻⁸	3.3396 × 10 ⁻⁷	1.1147 × 10 ⁻⁷	5.4571 × 10 ⁻⁷

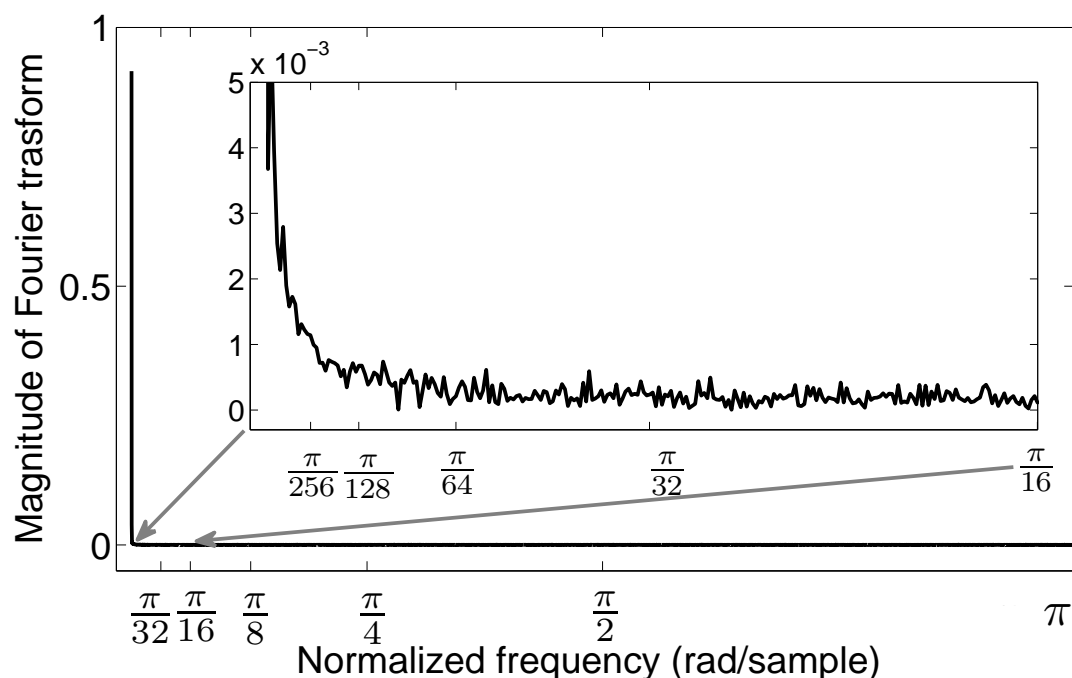


FIGURE 5.4: The discrete-time Fourier transform of the reactor power signal shown in Figure 5.3.

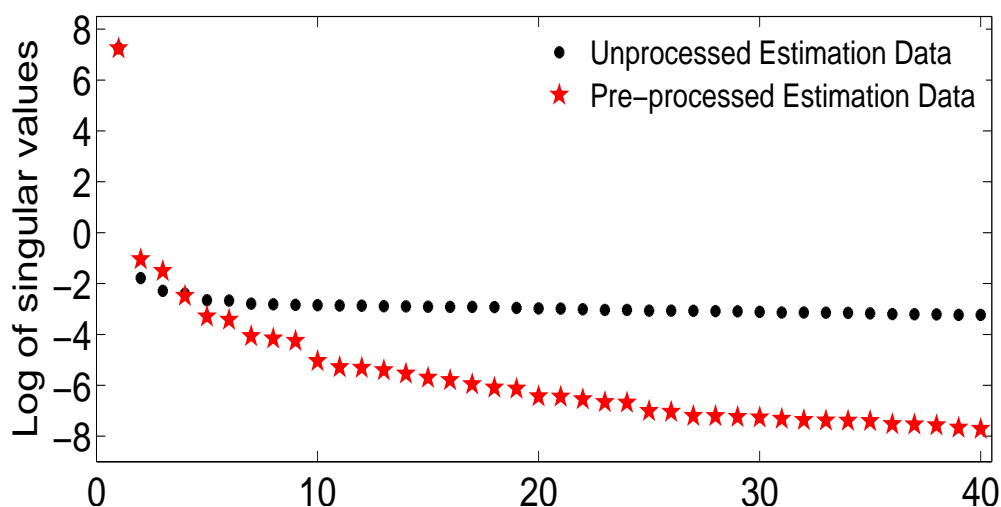


FIGURE 5.5: First 40 singular values of extended Hankel matrices for measured and pre-processed data.

5.5.2 Case Studies

Now, some case studies in which the values of control parameters for simulations are set to, $N_P = 5$, $N_C = 5$, and $M = 100$ are presented. Also, as there is only one input and one output, Q and R are scalars. These are assumed as $Q = 1 \times 10^{-2}$, and $R = 4 \times 10^3$. A detailed discussion on the selection of control parameters is given in Section 5.4.

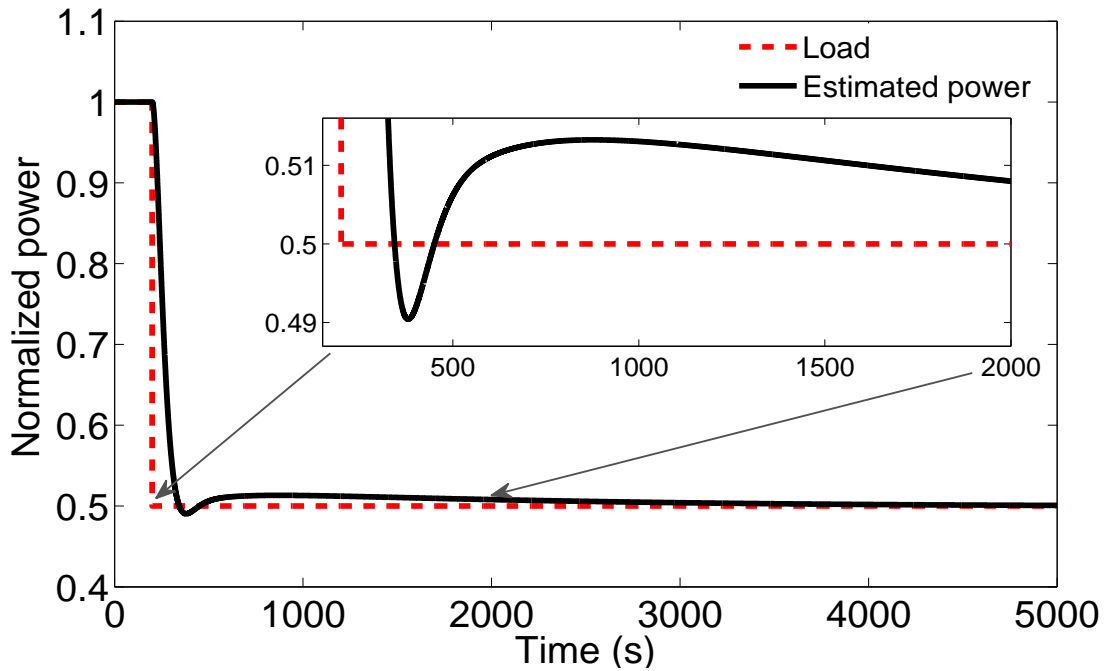


FIGURE 5.6: Reactor power variation for 50% load rejection transient.

5.5.2.1 Load Rejection to 50% FP

Initially, the reactor is assumed to be in steady state operation at 100% full power (FP). At $t = 200$ s, a 50% step decrease in load is applied. The purpose of such a large step transient is mainly to verify the wide-range tracking performance of the estimated controller. It is observed that the controller is able to track the sharp decrease in the load smoothly as shown in Figure 5.6 with undershoot of 1.92% only.

5.5.2.2 Load Rejection to 25% FP

In this case, the reference power value is brought down from 100% to 25% FP, to simulate an emergency operation of 75% step decrease in load. The reactor is assumed to be in steady state operation at 100% FP. At $t = 200$ s, a sudden reduction of load is assumed to take place. The performance of proposed controller in such a situation is shown in Figure 5.7. The controller is able to track the large step variation in the demand power with undershoot of 2.45% only.

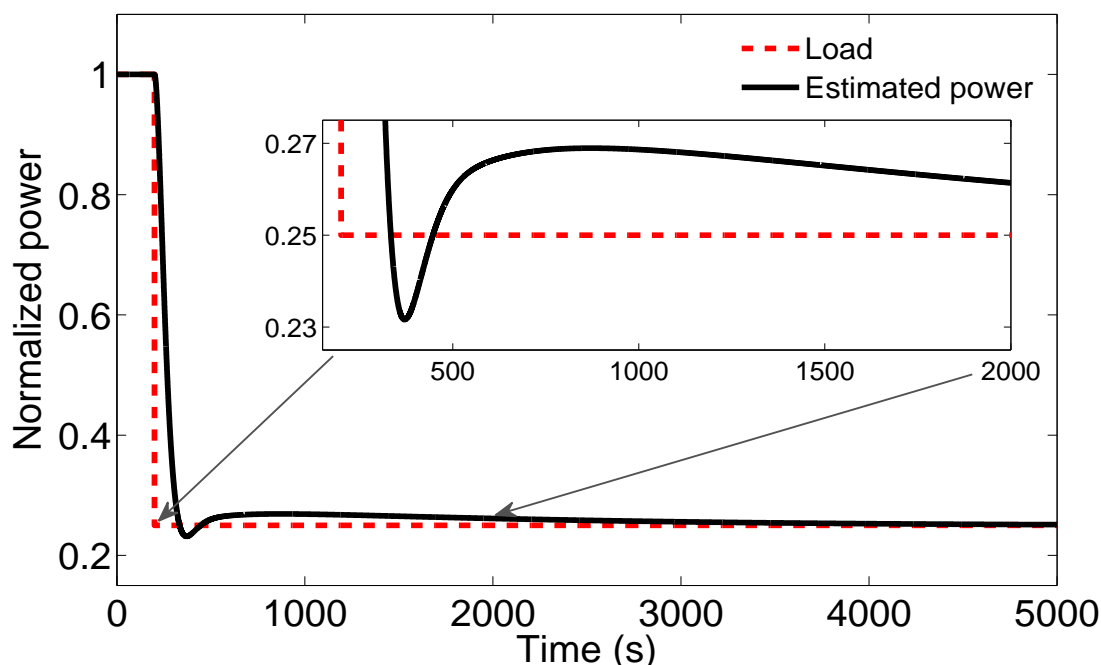


FIGURE 5.7: Reactor power variation for 75% load rejection transient.

5.5.2.3 Load-Following Transient

Here, a load-following transient similar to that given in [150] is considered to study typical power variations at 5%/min ramp and 10% step. Initially for 200 s, the desired power is maintained at 50% FP; then it is changed from 50% to 90% FP in 480 s; held at 90% FP for 300 s; then it is reduced from 90% to 75% FP in 180 s; held at 75% FP for 300 s; then a 10% step increase is applied at 1460ths; held at 85% FP for 500 s; then a 10% step decrease is applied at 1960ths and held at 75% FP for 540 s. The performance of the proposed controller for tracking the set-point is shown in Figure 5.8(a) by solid line. It is observed that the controller output is able to track the variation smoothly as envisaged. The control signal and rate of change of controlled signal variations are also shown in Figures 5.8(b) and 5.8(c) respectively.

In case of a nuclear reactor, variation in turbine load acts as measured disturbance. The knowledge of measured disturbance can be taken into account to design a feed-forward control along with the feedback control. The inclusion of feed-forward control law compensates for measured disturbances thereby improving the performance as depicted

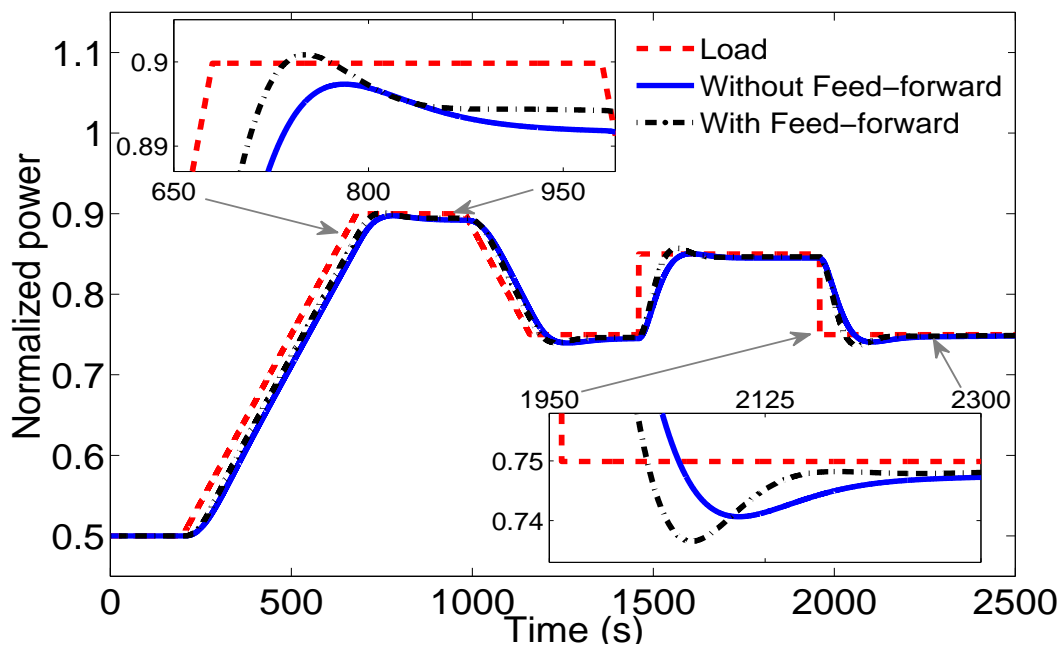
by dash-dot lines in Figure 5.8. The controller with feed-forward action converges rapidly to the demand set-point without much increase in the control efforts.

5.5.2.4 Effects of Integrating Control Action

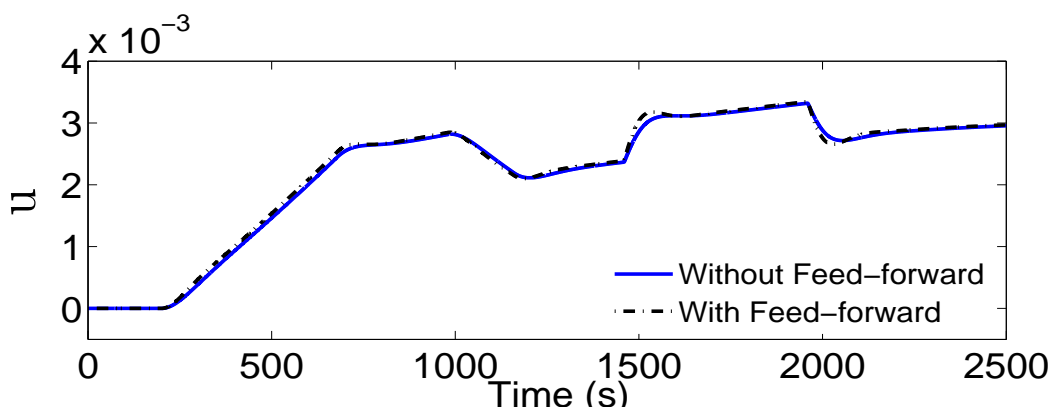
The output power in estimation dataset (Figure 5.3) is added with an integrating white Gaussian noise. To handle integrating type of non-stationarity in the controller design, the predictor parameters are obtained by first differencing the estimation noisy dataset. The differentiation of data ensures integrating control action. Figures 5.9(a), 5.9(b), and 5.9(c) compare the performance with and without differencing the estimation dataset for the load-following transient shown in Figure 5.8(a). The presence of integrator removes the nonzero offset error in tracking the set-point and improves the control performance significantly.

5.5.2.5 Handling Time variations and Constraints

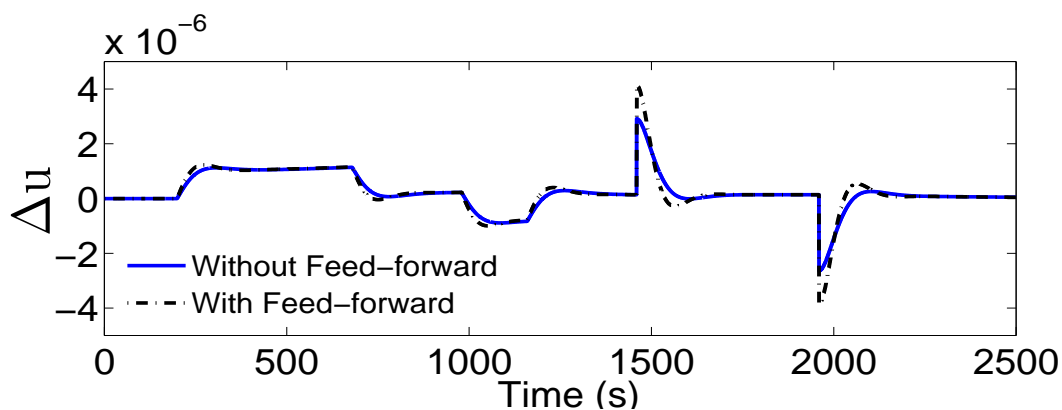
To handle any possible time variation in reactor parameters, the predictor is recursively estimated. In this case, it is considered that at $t = 800$ s the process parameters changed to new respective values as, $\alpha_f = -2.25 \times 10^{-5} \text{ } ^\circ\text{C}^{-1}$, $\alpha_c = -4.75 \times 10^{-5} \text{ } ^\circ\text{C}^{-1}$, $H_f = 103.7 \text{ } ^\circ\text{C s}^{-1}$, $H_c = 0.2347 \text{ } \text{s}^{-1}$, $\gamma_f = 0.1825 \text{ } \text{s}^{-1}$, and $\gamma_c = 0.0126 \text{ } \text{s}^{-1}$. In addition, constraints on input and output are also considered. The constraints on input determine the insertion/withdrawal limit and the rate of movement of RR. The constraint on output decides the maximum power output. For this case study, the following constraints are applied, $0.495 \leq P \leq 0.905$, $-4 \times 10^{-3} \leq \rho_{RR} \leq 4 \times 10^{-3}$, and $-1 \times 10^{-4} \leq \frac{\Delta \rho_{RR}}{t_s} \leq 1 \times 10^{-4}$ where t_s is the sampling period. Figures 5.10(a), 5.10(b), and 5.10(c) compare the performance for recursive and non-recursive SPC. Both the techniques result in control actions that preserve the constraints. However, the recursively updated controller shows better set-point tracking with less overshoot. In addition, the recursive SPC spends less control efforts as compared to that of the non-recursive algorithm.



(a) Variation of reactor power with set-point.

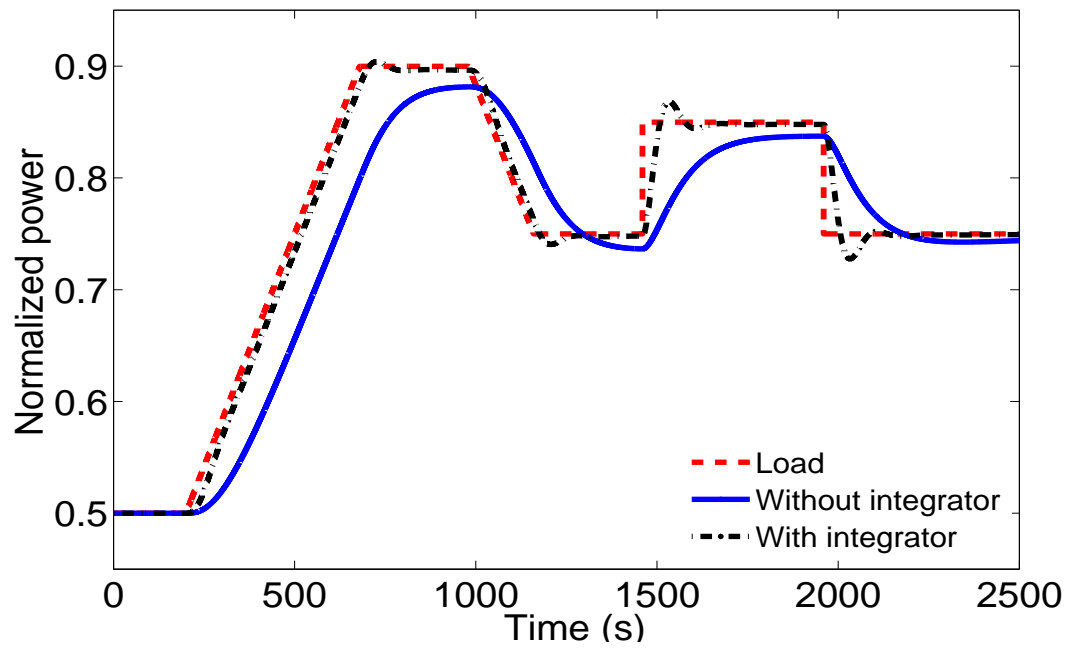


(b) Variation of control input.

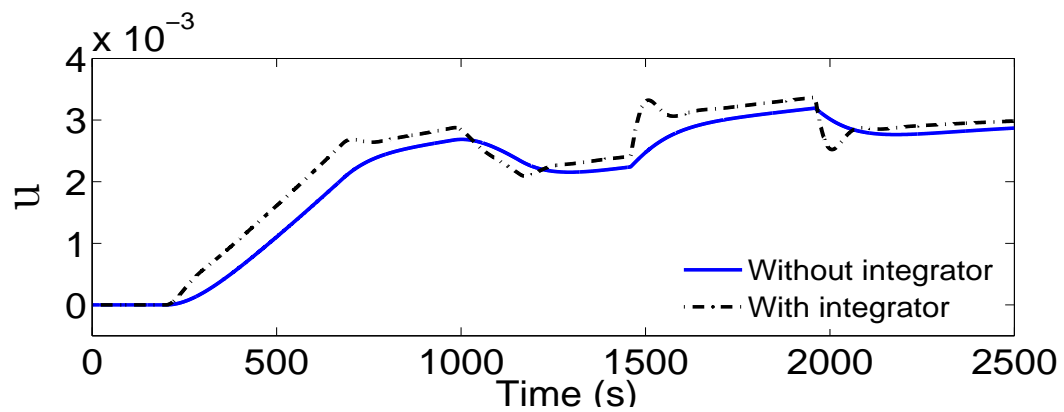


(c) Variation of rate of change of control input.

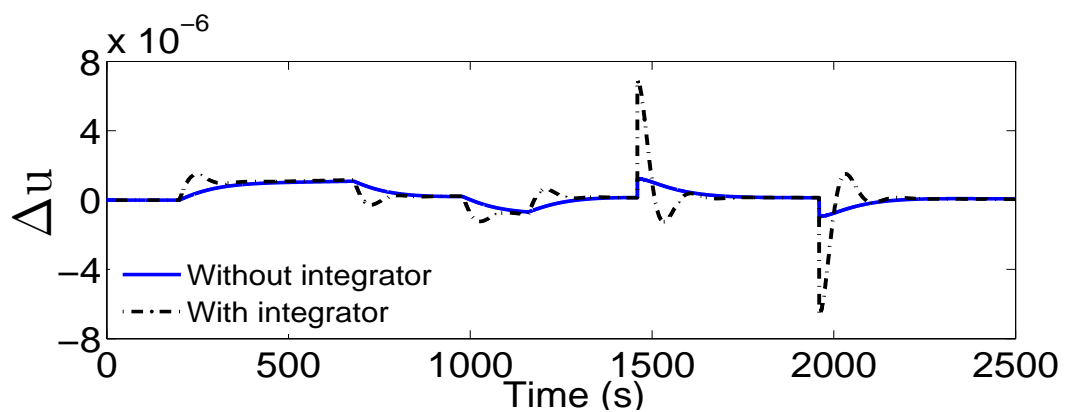
FIGURE 5.8: Comparison of the performance between SPC with feed-forward control and SPC without feed-forward control, (a) reactor power, (b) control input, and (c) rate of change of control input.



(a) Variation of reactor power with set-point.

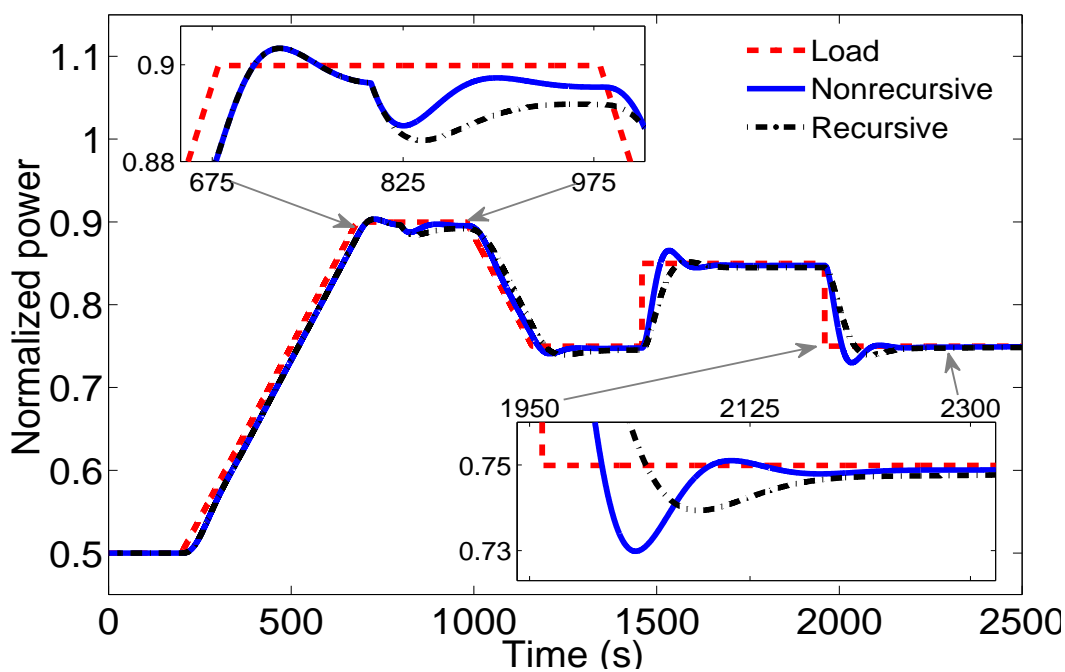


(b) Variation of control input.

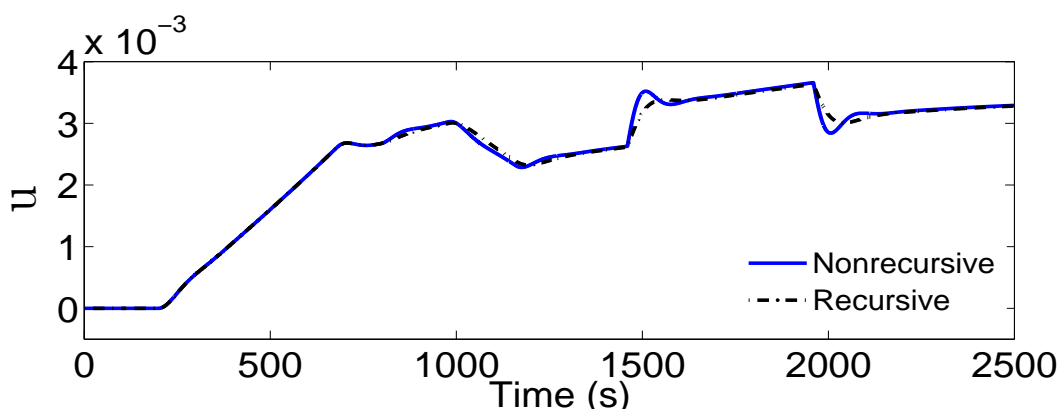


(c) Variation of rate of change of control input.

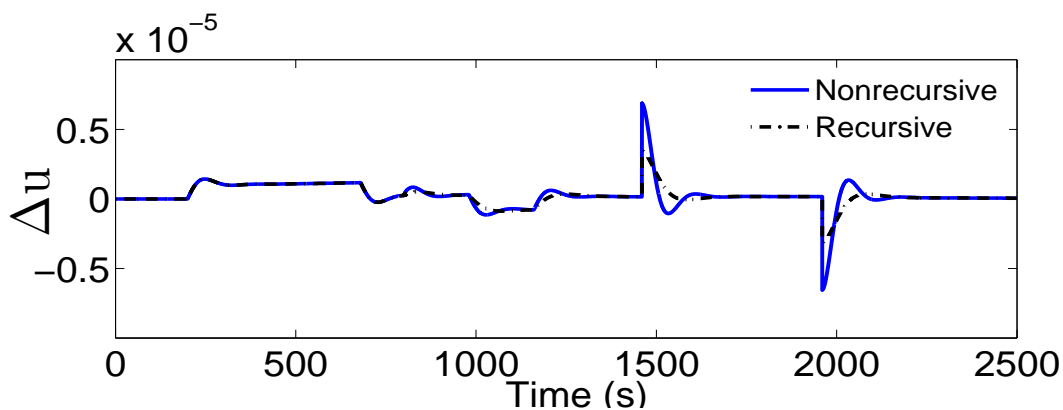
FIGURE 5.9: Comparison of the performance between SPC with integrator and SPC without integrator, (a) reactor power, (b) control input, and (c) rate of change of control input.



(a) Variation of reactor power with set-point.



(b) Variation of control input.



(c) Variation of rate of change of control input.

FIGURE 5.10: Comparison of the performance between recursive and non-recursive SPC, (a) reactor power, (b) control input, and (c) rate of change of control input.

TABLE 5.4: Comparison of performances of classical SPC with wavelet pre-processed SPC.

Transient	Technique	MSE	TV	$\ U\ _2$
Load rejection to 50% FP	Classical SPC	1.9826×10^{-3}	1.9521×10^{-2}	1.2346
	Wavelet SPC	1.7571×10^{-3}	6.3414×10^{-3}	0.8077
Load rejection to 25% FP	Classical SPC	4.3918×10^{-3}	1.4768×10^{-2}	1.2312
	Wavelet SPC	2.1461×10^{-3}	9.5512×10^{-3}	1.2122
Load-following Transient	Classical SPC	9.1579×10^{-4}	5.7720×10^{-3}	0.2762
	Wavelet SPC	4.4928×10^{-4}	5.3618×10^{-3}	0.2720

The wavelet-based data pre-processing efficiently removes noise contribution from reactor dynamics by amplitude thresholding of wavelet coefficients and thus improves the control performance. Table 5.4 compares the performance of classical SPC with that of the wavelet pre-processed SPC for different transients. SPC derived after data pre-processing takes lower control efforts. The improvement in performance becomes more significant when the SNR is low while the classical method is unable to perform satisfactorily. For large values of SNR both the techniques perform equally well, though.

5.6 Parameter Sensitivity Analysis

This section analyzes the performance of SPC with respect to variation in N_P , N_C , Q , and R for the set-point shown in Figure 5.8(a). To present statistically valid argument Monte Carlo simulations of 25 runs are performed.

5.6.1 Variation in Horizons

Figures 5.11(a), 5.11(b), and 5.11(c) respectively show variation of MSE, TV, and $\|U\|_2$ for variation of N_P in the range $3 \leq N_P \leq 40$ and $N_C \leq N_P$. The values of other parameters are set to $M = 100$, $Q = 2 \times 10^{-2}$, and $R = 5 \times 10^3$. As the value of prediction horizon is increased for a fixed value of control horizon, the controller gives better set-point tracking. Due to linear predictor, large value of N_P may induce large

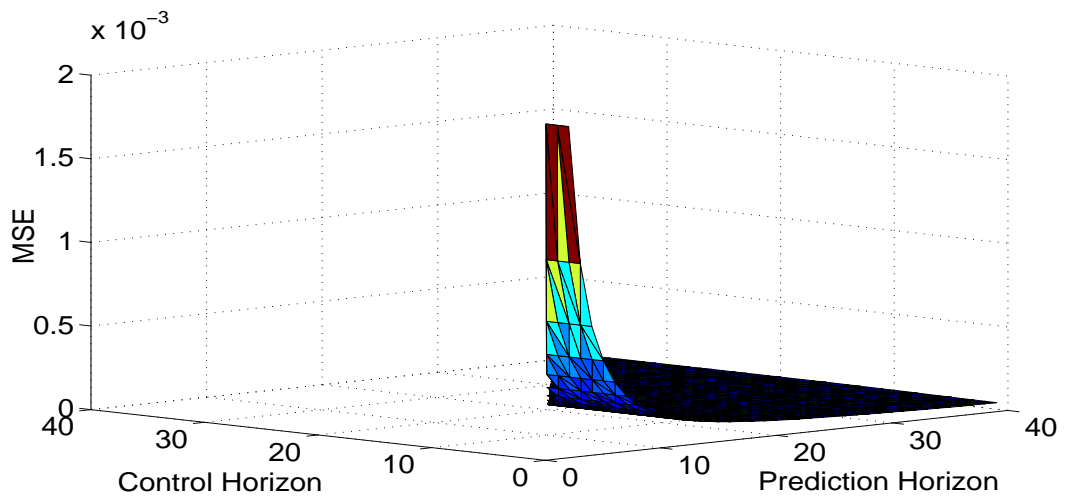
prediction error. It can be noted that increasing the prediction horizon beyond 20 did not yield any significant improvement on the performance. However, increasing the control horizon for a fixed value of prediction horizon, the controller acts to take aggressive control action. The value of N_C greater than one makes controller more robust against unmeasured disturbances and can be taken around one fourth of prediction horizon [186]. Therefore, N_P and N_C can be taken as 20 and 5 respectively. However, to avoid aggressive control action we have taken the values of $N_P = 5$ in Section 5.5.

5.6.2 Variation in Weights on Output

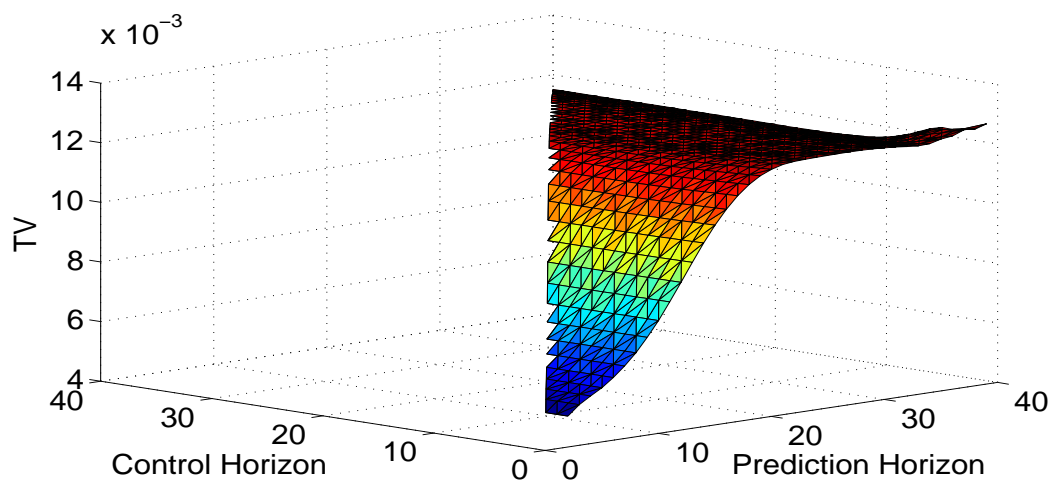
Figure 5.12 shows variation of MSE, TV, and $\|U\|_2$ for different values of Q ranging from 1×10^{-3} to 10. The values of other parameters are as follows, $N_P = 5$, $N_C = 5$, $M = 100$, and $R = 5 \times 10^3$. Increasing the value of Q penalizes more output variation and thus decreasing the MSE. The value of MSE decreases at a faster rate up to $Q = 2 \times 10^{-1}$ and after that it decreases very slowly. The control efforts are increased thereby increasing TV and $\|U\|_2$. Moreover, if the weight is increased beyond 4×10^{-2} then due to aggressive control action high frequency variation comes at the step change in set-point. Therefore, the value of Q is selected as 1×10^{-2} .

5.6.3 Variation in Weights on Rate of Change of Input

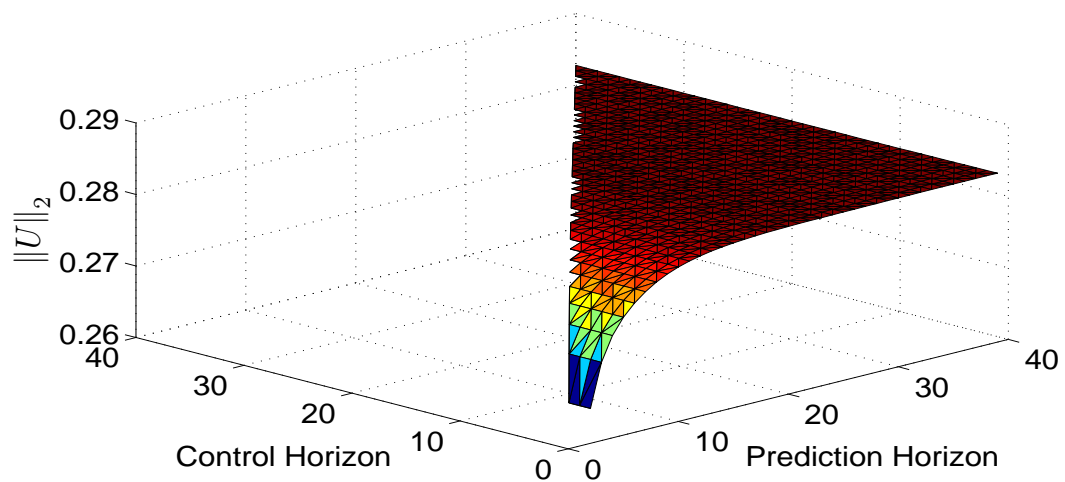
Figure 5.13 shows variation of MSE, TV, and $\|U\|_2$ for values of R varying from 1×10^2 to 1×10^5 . The values of other parameters are as follows, $N_P = 5$, $N_C = 5$, $M = 100$, and $Q = 1 \times 10^{-2}$. As we increase the value of R , it penalizes the rate of change of input variation more, thus controller takes cautious action and thereby decreasing TV and $\|U\|_2$. The value of TV decreases very sharply up to $R = 2 \times 10^3$ and after that it decreases at a slower rate. Moreover, MSE keeps on increasing due to less weight on minimization of error. Therefore, to avoid large overshoot during set-point tracking as well as large error from set-point, the value of R is selected as 4×10^3 .



(a) Variation of MSE in output.



(b) Variation of TV of input.

(c) Variation of l -2 norm of input.FIGURE 5.11: Variation of (a) MSE in output, (b) TV of input, and (c) l -2 norm of input for different prediction and control horizons.

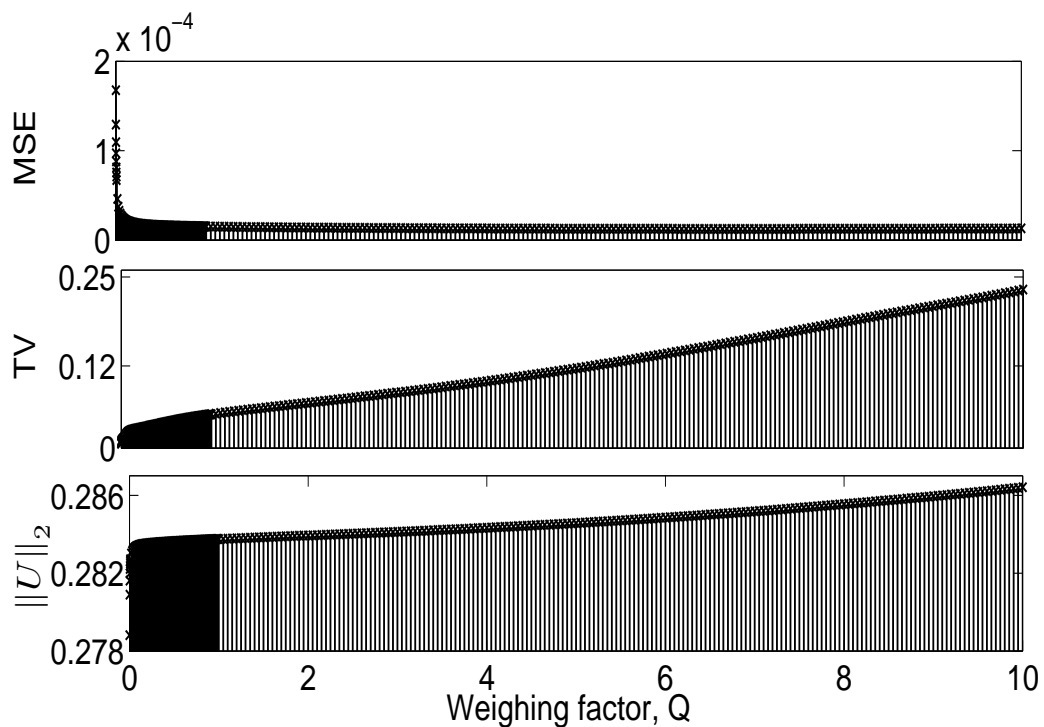


FIGURE 5.12: Variation of MSE in output, TV of input, and l_2 norm of input for different value of Q .

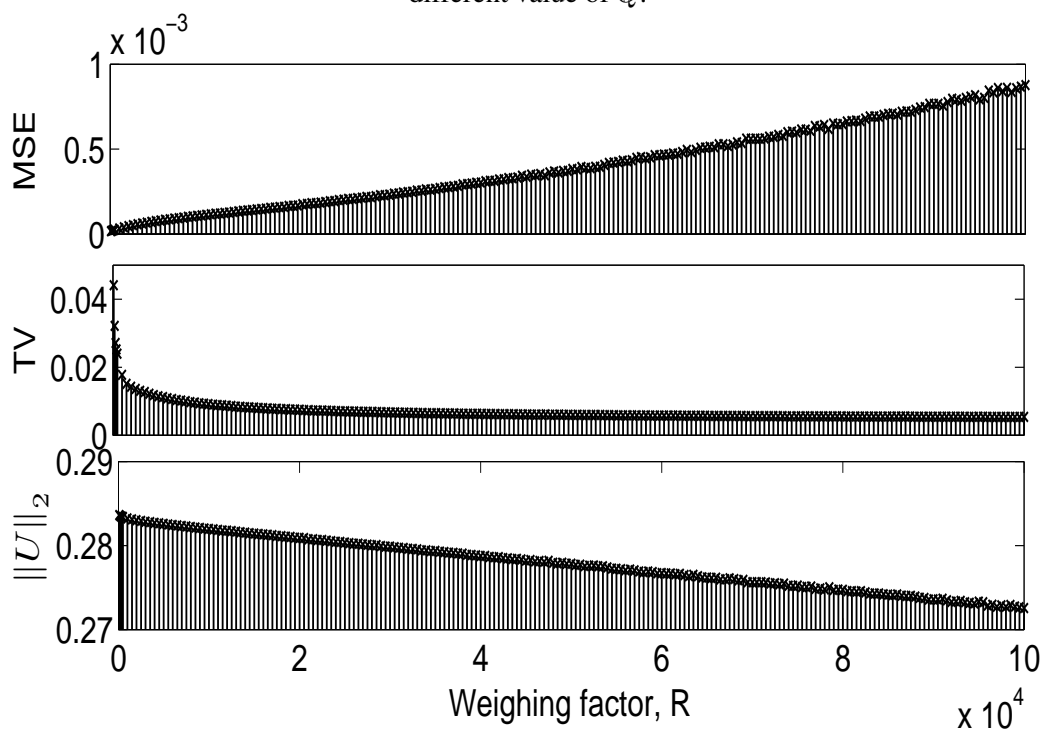


FIGURE 5.13: Variation of MSE in output, TV of input, and l_2 norm of input for different value of R .

5.7 Controller performance for different SNR

Monte Carlo (MC) simulations are carried out to demonstrate the advantage of wavelet preprocessed SPC (W-SPC) over classical SPC. MC simulation is a standard numerical experimentation technique. Here, the purpose of MC simulation is to validate the enhancement in controller performance empirically. For several MC simulation runs, at a fixed noise power level, the estimation dataset varies for each run due to change in noise sequence as the latter is a stochastic phenomenon. This mechanism is equivalent to performing several experiments. Furthermore, simulations are performed at various noise levels to show the robustness of the proposed scheme in estimating the predictor coefficients in noisy environment. Here, the effect of noise is considered only on the output power. The noisy dataset is used for estimating the predictor matrices. The load-following operation shown in Figure 5.8(a) is taken as the desired set point.

5.7.1 Simulation with White Gaussian Noise

A white Gaussian noise sequence is superimposed on reactor power output in the estimation dataset. MC simulations of 50 runs are carried out at each noise level. In addition to this, simulations are performed for SNR varying from 15 dB to 80 dB. The value of parameters are taken as: $N_P = 5$, $N_C = 5$. Figures 5.14, 5.15 and 5.16 show output and input performance of classical SPC [28, 187] and W-SPC. It is to be noted that the data filtering method proposed in [187] becomes equivalent to SPC for white Gaussian noise sequence. For large values of SNR both the algorithms perform equally well but for low SNR, the W-SPC can reduce SSE significantly with both lower control effort as well as lesser TV. On further increase in the SNR, the W-SPC is observed to reduce the SSE but at the cost of increasing control effort and TV. This result is mainly due to smoothing of the dataset by wavelet filter. However, the performance of SPC remains invariable.

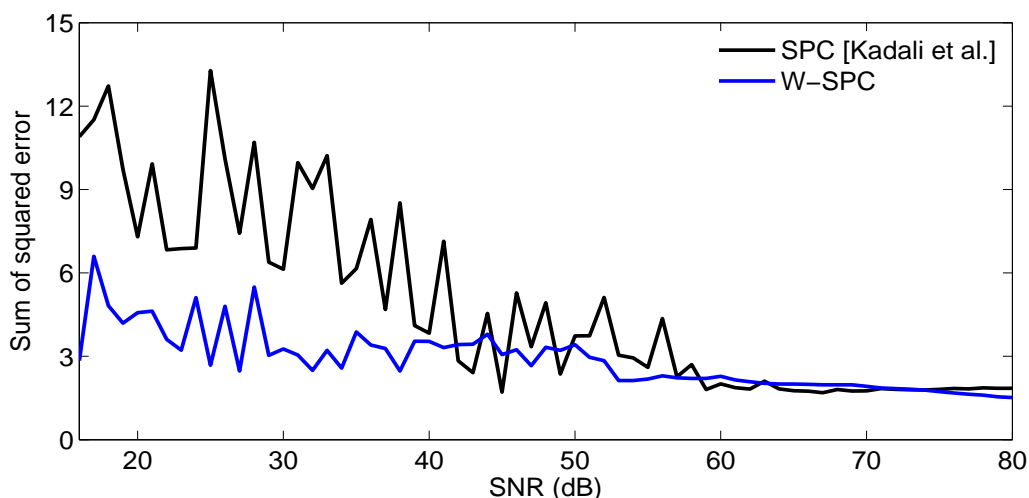


FIGURE 5.14: Sum of squared error between output and desired set point at different SNR for white Gaussian noise sequence.

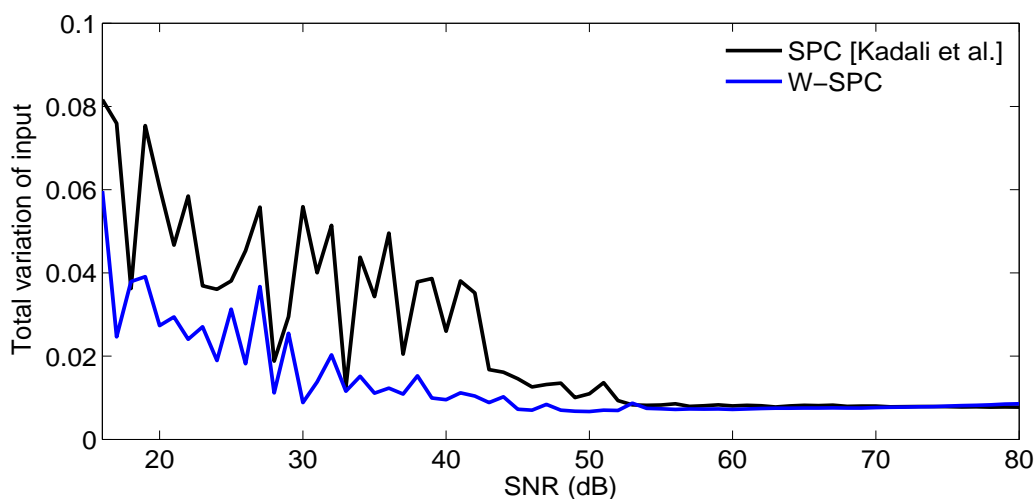


FIGURE 5.15: TV of input at different SNR for white Gaussian noise sequence.

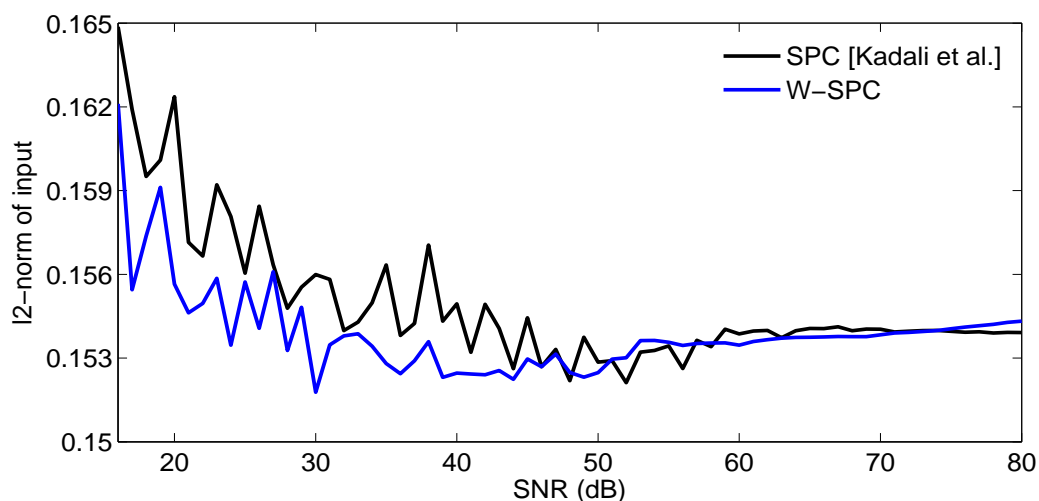


FIGURE 5.16: l_2 -norm of input at different SNR for white Gaussian noise sequence.

5.7.2 Simulation with Integrating White Gaussian Noise

An integrating white Gaussian noise sequence is added with the reactor power to generate an estimation dataset. MC simulations of 50 runs are carried out for SNR varying from 20 dB to 80 dB. The values of N_P and N_C are taken as in the case of simulation with white Gaussian noise. An integrating action is brought into the controller by the differencing the estimation dataset before calculating the predictor coefficients. It will be helpful in removing offset for non-zero set points. It is to be noted that the data filtering measure proposed in [187] is equivalent to differenced data based SPC for integrated white Gaussian noise. However, by differencing the estimation dataset during low SNR, the noise got amplified, and it is advisable to process it before using in parameter estimation. For a non-white noise, thresholds are rescaled by a level-dependent estimation of the level noise. Figures 5.17, 5.18, and 5.19 compare the performance of SPC, W-SPC, differenced data based SPC and differenced data based W-SPC. It can be seen clearly that the error in output is much less in the case of differenced data but with more control effort. Moreover, wavelet filtering is able to reject noise significantly with comparatively better control performance.

5.8 Summary

In this chapter, methodology of subspace based predictive control with wavelet-preprocessing is presented. The strategy that can incorporate constraints and optimize control performance has been investigated for the core power control in load-following mode of nuclear reactor. It is directly designed from the pre-processed dataset and does not require reactor model explicitly. The inclusion of wavelet filtering in the formulation improves the SNR and enhances prediction accuracy of the estimated controller. The data-driven scheme is easily adapted to the time variation in the process. Detailed simulation studies verify the performance of proposed control algorithm with necessary tuning of control

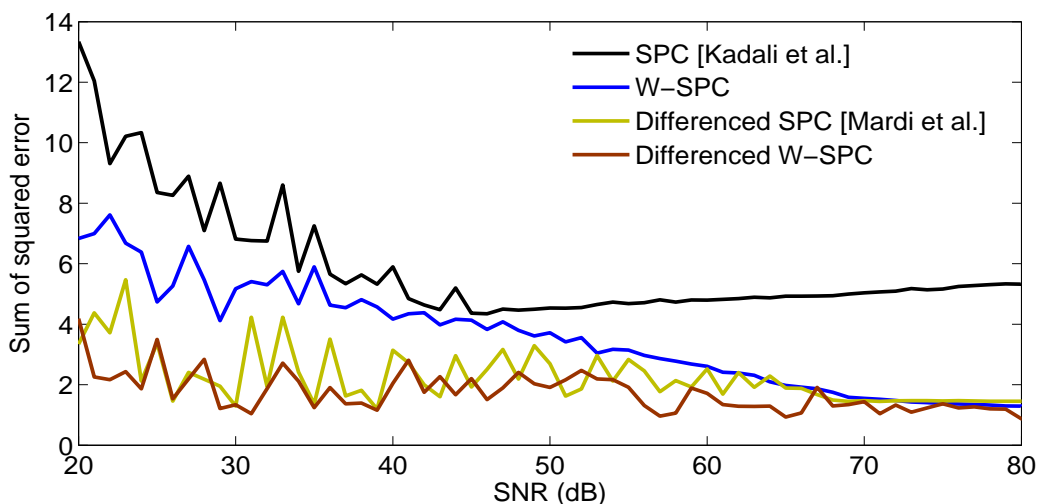


FIGURE 5.17: Sum of squared error between output and desired set point at different SNR for integrating white Gaussian noise sequence.

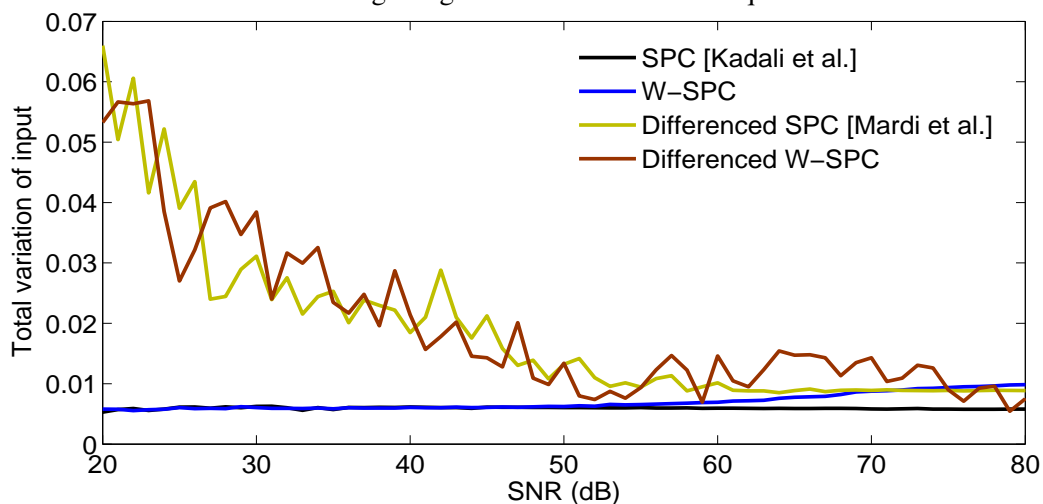


FIGURE 5.18: TV of input at different SNR for integrating white Gaussian noise sequence.

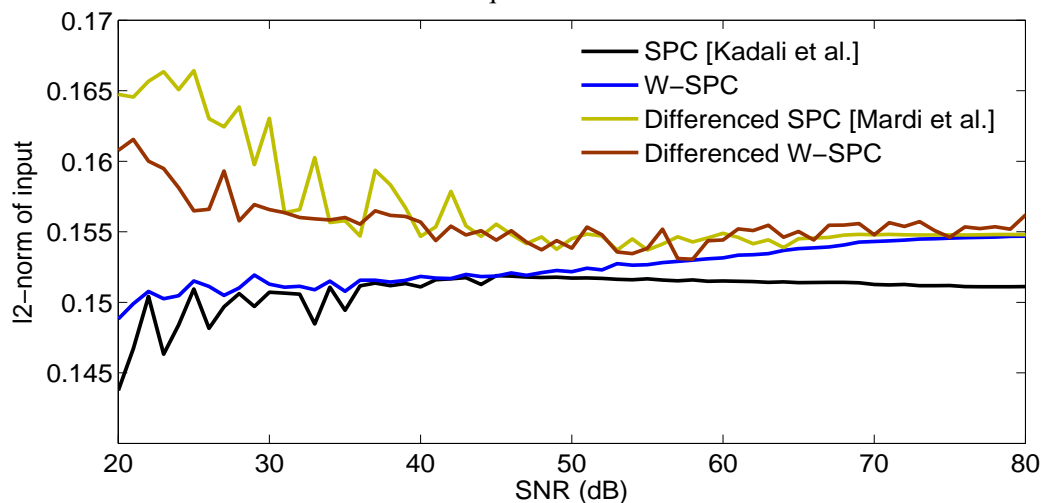


FIGURE 5.19: l_2 -norm of input at different SNR for integrating white Gaussian noise sequence.

parameters. The controller suitably accommodates measured disturbances and gives wide range offset-free tracking for ramp as well as step variations in the load.

Chapter 6

Conclusions and Future Work

In this chapter, conclusions are drawn and the major contribution of the thesis are pointed out. It also suggests directions for the future work.

6.1 Conclusions

A nuclear reactor is a complex nonlinear multiscale system in which different dynamic modes interact simultaneously at different timescales. These modes are located in separate clusters governing slow as well as fast timescale behavior. It has been found that modeling of such systems using single scale approaches would approximate its prediction capabilities. The single scale approach may sometimes leads to ill-conditioning. Moreover, various multiscale features residing in a process may not be clearly visible in measurement domain. Therefore, it is imperative to have transformation of data and visualization in a multiresolution framework around a proper set of scales. Wavelet basis functions adopted for data visualization, have been preferred over other bases due to their excellent multiresolution approximation ability, as evident from several applications brought out in this work. The notion of multiscale subspace identification proposed in thesis to estimate low order state-space model directly from the wavelet projections helps to develop a framework for state-space modeling at significant scales

leading to a parsimonious model description with less computational burden. It is evident from the application of the proposed approach to point kinetics model of nuclear reactor that the identified multiscale subspace model estimates system modes more precisely than the traditional approaches do, and a good neutronic power prediction has been achieved even from training dataset with low SNR. The identified reactor model is validated in prediction as well as in simulation environment. The proposed algorithm suggests better modeling performance with enhanced prediction capability over other single scale and multiscale approaches in terms of root mean square error at different noise levels. It has also been found that in most of the modeling exercises the proposed approach reduces dimensionality.

The design of wavelet operators proposed in the thesis is suitable for multiscale modeling. It imposes a diagonal structure on the system in wavelet subspace. In fact, the imposed structure in projection space is justified as wavelets are approximate Eigen functions of convolution operators. The methodology suggests application of different wavelet filters for analyzing different states of the system. The proposed novel approach has been applied successfully to a point kinetics nuclear reactor. It designs perfect reconstruction biorthogonal wavelet filter banks associated with wavelet operators from the given estimation dataset instead of selecting them a priori. From the application to nuclear reactor, it has been found that the projection space modeling leads to a significant improvement in output prediction over single-scale modeling techniques.

The thesis further advocates integration of wavelet preprocessing and data-driven control techniques. To be specific, it proposes wavelet preprocessed subspace predictive control technique. The proposed approach does not require the complex reactor model for predictive control design. The controller is directly estimated from the preprocessed input-output data and implemented for the control of core power. The predictor parameters are estimated recursively to handle time-variation occurring in the system. The controller also incorporates feed-forward control, integrating action, and constraints in the control design. Moreover, the controller parameters are tuned after a detailed parameter sensitivity analysis to obtain desired control performance. The proposed controller

is applied to control demand load set-point variations as well as for load rejection transients. The controller is effectively able to cope up with the ramp and step variations in the demand power. From the detailed simulation analysis it has been validated that the proposed approach gives better control performance as compared to other approaches at different SNRs.

6.2 Future Work

The work carried out in this thesis provides some directions for future scope in identification and data-driven control. In particular, the following topics can be considered:

- Wavelet operators can be used to implement decoupled control law in multiresolution.
- The idea of designing wavelet operators from measurements can be extended to designing of semi-orthogonal wavelet operators.
- The notion of multiscale subspace identification can be employed in designing model-based controller or in state estimation in the multiresolution framework.
- Subspace identification using multiwavelet basis function can be further studied.
- Subspace predictive control approach can be formulated to design predictive control in multi resolution.
- Subspace predictive control technique can be extended to design nonlinear predictive control law.

Appendix A

A.1 General Family of Model Structures

The general model structure is given by

$$A(q)y[k] = \frac{B(q)}{F(q)}u[k] + \frac{C(q)}{D(q)}e[k] \quad (\text{A.1})$$

$$y[k] = \frac{B(q)}{A(q)F(q)}u[k] + \frac{C(q)}{A(q)D(q)}e[k] \quad (\text{A.2})$$

or simply, we can write

$$y[k] = G(q)u[k] + H(q)e[k] \quad (\text{A.3})$$

where $G(q) = \frac{B(q)}{A(q)F(q)}$ and $H(q) = \frac{C(q)}{A(q)D(q)}$. The one step ahead prediction is given by

$$\hat{y}[k|\theta] = H^{-1}(q)G(q)u[k] + (1 - H^{-1}(q))e[k] \quad (\text{A.4})$$

or,

$$\hat{y}[k|\theta] = \frac{B(q)D(q)}{C(q)F(q)}u[k] + \left(1 - \frac{A(q)D(q)}{C(q)}\right)e[k] \quad (\text{A.5})$$

In the form of recursion, we can write

$$C(q)F(q)\hat{y}[k|\theta] = B(q)D(q)u[k] + (C(q)F(q) - F(q)A(q)D(q))e[k]. \quad (\text{A.6})$$

Define, the prediction error as

$$\varepsilon[k, \theta] = y[k] - \hat{y}[k | \theta] \quad (\text{A.7})$$

$$\varepsilon[k, \theta] = \frac{D(q)}{C(q)} \left(A(q)y[k] - \frac{B(q)}{F(q)}u[k] \right) \quad (\text{A.8})$$

and

$$w[k, \theta] = \frac{B(q)}{F(q)}u[k] \quad (\text{A.9})$$

$$\text{and } v[k, \theta] = A(q)y[k] - w[k, \theta]. \quad (\text{A.10})$$

Then

$$\varepsilon[k, \theta] = \frac{D(q)}{C(q)}v[k, \theta]. \quad (\text{A.11})$$

Now, define the polynomials

$$B(q^{-1}) = b_1q^{-1} + b_2q^{-2} + \dots + b_{n_b}q^{-n_b}, \quad (\text{A.12})$$

$$A(q^{-1}) = 1 + a_1q^{-1} + a_2q^{-2} + \dots + a_{n_a}q^{-n_a}, \quad (\text{A.13})$$

$$C(q^{-1}) = 1 + c_1q^{-1} + c_2q^{-2} + \dots + c_{n_c}q^{-n_c}, \quad (\text{A.14})$$

$$D(q^{-1}) = 1 + d_1q^{-1} + d_2q^{-2} + \dots + d_{n_d}q^{-n_d}. \quad (\text{A.15})$$

$$\text{and } F(q^{-1}) = 1 + f_1q^{-1} + f_2q^{-2} + \dots + f_{n_f}q^{-n_f}. \quad (\text{A.16})$$

Thus, (A.9), (A.10), and (A.11) can be written as

$$\begin{aligned} w[k, \theta] &= b_1u[k-1] + \dots + b_{n_b}u[k-n_b] - f_1w[k-1, \theta] - \dots - f_{n_f}w[k-n_f, \theta] \\ v[k, \theta] &= y[k] + a_1y[k-1] + \dots + a_{n_a}y[k-n_a] - w[k, \theta] \\ \varepsilon[k, \theta] &= v[k, \theta] + d_1v[k-1, \theta] + \dots + d_{n_d}v[k-n_d, \theta] - c_1\varepsilon[k-1, \theta] - \dots - \varepsilon[k-n_c, \theta] \end{aligned} \quad (\text{A.17})$$

Now, defining the parameter vector as

$$\theta = \begin{bmatrix} a_1 & \dots & a_{n_a} & b_1 & \dots & b_{n_b} & f_1 & \dots & f_{n_f} \\ & & & c_1 & \dots & c_{n_c} & d_1 & \dots & d_{n_d} \end{bmatrix} \quad (\text{A.18})$$

and regression vector as

$$\varphi[k, \theta] = \begin{bmatrix} -y[k-1] & \cdots & -y[k-n_a] & -u[k-1] & \cdots & -u[k-n_b] \\ -w[k-1, \theta] & \cdots & -w[k-n_f, \theta] & -\varepsilon[k-1, \theta] & \cdots & -\varepsilon[k-n_c, \theta] \\ & & & -v[k-1, \theta] & \cdots & -v[k-n_d, \theta] \end{bmatrix}^T \quad (\text{A.19})$$

Hence, the predictor is given by

$$\hat{y}[k|\theta] = \varphi^T[k, \theta] \theta \quad (\text{A.20})$$

Thus, the parameters can be find out using least squares method.

It can be noted that different common structures can be obtained by selecting polynomials from (A.1) as follows: If A and B are selected then the structure is called as ARX model. If A , B , and C are selected then it is known as ARMAX model. If B and F are selected then it is known as OE model. If B , F , C and D are selected then it is called as BJ model structure.

Appendix B

B.1 Vandermonde structure of \mathcal{W}_j

General structure of the linear transformation \mathcal{W}_j satisfying $A_{j+1}^w \mathcal{W}_j = \mathcal{W}_j \tilde{A}$ is computed as follows. Let

$$\mathcal{W}_j = \begin{bmatrix} v_{11} & v_{12} & \cdots & v_{1N} \\ v_{21} & v_{22} & \cdots & v_{2N} \\ \vdots & \vdots & \ddots & \vdots \\ v_{N1} & v_{N2} & \cdots & v_{NN} \end{bmatrix}. \quad (\text{B.1})$$

Then,

$$\begin{bmatrix} \alpha_1 & 0 & \cdots & 0 \\ 0 & \alpha_2 & \cdots & 0 \\ \vdots & \vdots & \ddots & \vdots \\ 0 & 0 & \cdots & \alpha_N \end{bmatrix} \begin{bmatrix} v_{11} & v_{12} & \cdots & v_{1N} \\ v_{21} & v_{22} & \cdots & v_{2N} \\ \vdots & \vdots & \ddots & \vdots \\ v_{N1} & v_{N2} & \cdots & v_{NN} \end{bmatrix} = \begin{bmatrix} v_{11} & v_{12} & \cdots & v_{1N} \\ v_{21} & v_{22} & \cdots & v_{2N} \\ \vdots & \vdots & \ddots & \vdots \\ v_{N1} & v_{N2} & \cdots & v_{NN} \end{bmatrix} \begin{bmatrix} 0 & 0 & \cdots & -a_N \\ 1 & 0 & \cdots & -a_{N-1} \\ 0 & 1 & \cdots & -a_{N-2} \\ \vdots & \vdots & \ddots & \vdots \\ 0 & 0 & \cdots & -a_1 \end{bmatrix} \quad (\text{B.2})$$

implies

$$\begin{aligned} \alpha_i v_{i1} &= v_{i2}, \\ \alpha_i v_{i2} &= v_{i3}, \\ &\vdots \\ \alpha_i v_{i(N-1)} &= v_{iN}, \\ \alpha_i v_{iN} &= -a_N v_{i1} - a_{N-1} v_{i2} \cdots -a_1 v_{iN}, \forall i=1, 2, \dots, N. \end{aligned} \quad (\text{B.3})$$

Since $\alpha_i, i=1, 2, \dots, N$ are the eigenvalues of \overline{A}_j^v , one can write

$$\begin{aligned}
 v_{iN} &= \alpha_i v_{1(N-1)} = \alpha_i^2 v_{i(N-2)} = \dots = \alpha_i^{(N-1)} v_{i1}, \\
 v_{i(N-1)} &= \alpha_i v_{1(N-2)} = \alpha_i^2 v_{i(N-3)} = \dots = \alpha_i^{(N-2)} v_{i1}, \\
 &\vdots \\
 v_{i2} &= \alpha_i v_{i1}, \\
 \forall i &= 1, 2, \dots, N.
 \end{aligned} \tag{B.4}$$

One can assume $v_{i1} = m_i, \forall i=1, 2, \dots, N$ to get the *Vandermonde* structure of \mathcal{W}_j as given in (3.30).

B.2 An analytical example of PRBWFB design

Consider that the analysis HPF coefficients g are known to us as

$$g = \begin{bmatrix} g_1 & g_2 & g_3 & g_4 \end{bmatrix}. \tag{B.5}$$

Using perfect reconstruction condition, synthesis LPF \tilde{h} are given by

$$\tilde{h} = \begin{bmatrix} -g_4 & g_3 & -g_2 & g_1 \end{bmatrix}. \tag{B.6}$$

Let the analysis LPF h , to be computed, is given by

$$h = \begin{bmatrix} h_1 & h_2 & h_3 & h_4 \end{bmatrix}. \tag{B.7}$$

Applying the biorthogonality condition between h and g

$$\begin{aligned}
 -h_1 g_4 + h_2 g_3 - h_3 g_2 + h_4 g_1 &= 1, \\
 -h_1 g_2 + h_2 g_1 &= 0, \\
 -h_3 g_4 + h_4 g_3 &= 0.
 \end{aligned} \tag{B.8}$$

To design the filter bank with one vanishing moment constrain, the vanishing moment condition is given by

$$-h_1 + h_2 - h_3 + h_4 = 0. \quad (\text{B.9})$$

The system of equations (B.8) and (B.9) give coefficients of analysis LPF h , and further synthesis HPF \tilde{g} is designed.

$$\tilde{g} = \begin{bmatrix} h_4 & -h_3 & h_2 & -h_1 \end{bmatrix}. \quad (\text{B.10})$$

Similarly, the design can be extended for desired number of vanishing moments after increasing length of filter by appending zeros to it.

Appendix C

C.1 Nuclear Reactor Dynamics

In a nuclear reactor neutrons are used to induce fission reactions in heavy nuclei. These reactions split the heavier nuclei into lighter nuclei and produce fission products accompanied by the release of energy plus several additional neutrons. The fission neutrons can then be utilized to induce further fission reactions which thereby give rise to a chain of fission events. Thus, the main role of a nuclear fission reactor is to carry out controlled nuclear fission chain reactions and maintains it [37]. If the rate of neutron production in a fission reaction is balanced by neutron loss via absorption and leakage then the reactor operates at a fixed power level. Any change from this balance condition will result in variation of the neutron population in time. This may occur due to change in core multiplication. This variation in time behavior of the neutron population due to change in core multiplication is determined by nuclear reactor kinetics. The core multiplication depends on various other factors which are directly or indirectly dependent on the neutron concentration. The analysis of time-dependence of all such related processes involved in deducing the multiplication as a function of the power level of the reactor is known as nuclear reactor dynamics.

Modeling of reactor cores is a primary work for the design of power control or for load-following control of cores in a NPP. A nuclear reactor is described as a complex nonlinear multiscale system in which different dynamic modes interact simultaneously

at different time scales [24]. These modes are located in separate clusters governing slow as well as fast time-scale behavior. A cluster of modes lying near the origin on the s -plane governs slow dynamics of the process while the second cluster lying away from the origin is responsible for fast dynamics. A control oriented nuclear reactor model should be suitably able to describe short term transients *i.e.* with time scale of milliseconds and long term transients *i.e.* having time scale of minutes. For instance, the effects of control rod movement are categorized as short term transient while, the transient length during a load change operation belongs to long time transients. The transient behavior of a reactor can be suitably explained by the point kinetics model which assumes that the spatial flux shape does not change with time. It describes the behavior of neutron density with the influence of delayed neutrons. It is derived from the one-speed diffusion model under the assumption that the spatial dependence of the flux can be described by only the fundamental mode.

The study of reactor dynamical behavior should also consider the thermal analysis in addition to the neutronic analysis. The variation of temperature in a core affects core multiplication and thereby influences the reactivity. This variation is usually characterized by variation in temperature coefficient of reactivity due to fuel, coolant, moderator, *etc.*

During the course of operation of a nuclear reactor various fission fragments and their decay products gather. These fission products may have a significant influence on the reactivity and is governed by the condition of operation of the reactor as well as on the nature of fission product. Xenon-135 and Samarium-149 are two important fission products and they affect the multiplication factor mainly by decreasing the thermal utilization as their thermal neutron absorption cross-sections are very large. These fission products also affect the reactor core control. Provision must be made to provide for the reactivity deficit caused due to accumulation of fission products and to compensate for time varying xenon load characterized by xenon-iodine dynamics. Besides, in case of large reactors where xenon variation might influence the flux distribution as well as it might cause xenon-induced spatial oscillations. In case of PHWR, the reactor regulating

system controls the total reactor power and zonal powers. The total reactor power control is essential during short term operational transients whereas the zonal power control is for regulating the relatively slower xenon-induced oscillations. The accuracy of controller synthesis or dynamic analysis or simulation study is largely dependent on the correctness of employed model. Hence, it is important to study the behavior of neutron density to various situations, especially change in the effective multiplication factor, in the temperature, and as a result of the accumulation of fission-product poisons.

In this study, the reactor is modeled using point kinetics model with six groups of delayed neutron precursors. Internal reactivity feedbacks due to variation in temperatures of fuel and coolant are considered as they decide the dynamical behavior of the system. Further, feedbacks from xenon and iodine dynamics are also considered.

C.2 Point Kinetics Reactor Core Model

The point kinetics model is given by,

$$\frac{dP}{dt} = \left(\frac{\rho_T - \beta}{\Lambda} \right) P + \sum_{i=1}^6 \lambda_i C_i, \quad (\text{C.1})$$

$$\frac{dC_i}{dt} = \frac{\beta_i}{\Lambda} P - \lambda_i C_i, \quad i = 1, 2, \dots, 6 \quad (\text{C.2})$$

where Λ is prompt neutron life time, P denotes the neutron density and reactor power is proportional to it, ρ_T is total reactivity. λ_i , β_i , and C_i are decay constant, fraction of delayed neutrons, and delayed neutron precursors' concentration of i^{th} group respectively and $\beta = \sum_{i=1}^6 \beta_i$. At the steady state of reactor operation, the value of delayed neutron precursors' concentration C_{i0} and power P_0 are related as $C_{i0} = \frac{\beta_i}{\Lambda \lambda_i} P_0$. Equation (C.1) describes the rate of change of reactor power and (C.2) describes the rate of change of concentration of the delayed neutron precursors. The term $\sum_{i=1}^6 \lambda_i C_i$ gives the total rate of formation of delayed neutrons while, the rate of prompt neutron production is governed by the rest of the terms in it.

If the rate of neutron production is equal to neutron lost then the reactor is said to be critical. Any fractional departure of a system from criticality is represented using reactivity and it is given by

$$\rho = \frac{k - 1}{k} \quad (\text{C.3})$$

where k denotes the effective multiplication factor and is given as the ratio of rate of neutron production to the rate of neutron removal through absorption and leakage. The value of k is used to define the criticality states of a reactor. In the absence of an extraneous source, $k = 1$ means the reactor is critical, $k < 1$ means it is subcritical, and $k > 1$ means it is supercritical. For the point kinetics model, it is related to the one-group nonleakage probability (P_{n1}) and infinite multiplication factor (k_∞) by $k = k_\infty P_{n1}$. The infinite multiplication factor can be evaluated from the neutronic properties of material and it assumes that there is no loss of neutrons through leakage. The one-group nonleakage probability is a measure of probability that neutrons will not leak out of the finite system but will remain until absorbed. It is dependent on the reactor material as well as on the geometry. The prompt neutron lifetime is defined using mean lifetime (Λ_∞) and nonleakage probability of thermal neutrons and is given by $\Lambda = \Lambda_\infty P_{n1}$.

The aforementioned system of equations can be normalized by their respective full power values. Normalizing (C.1) with respect to its steady state full power value P_0

$$\frac{d}{dt} \left(\frac{P}{P_0} \right) = \left(\frac{\rho_T - \beta}{\Lambda} \right) \left(\frac{P}{P_0} \right) + \left(\frac{1}{P_0} \right) \sum_{i=1}^6 \lambda_i C_i \quad (\text{C.4})$$

The steady state value of delayed neutron precursor concentration can be computed by equating (C.2) to zero, is given by

$$C_{i0} = \frac{\beta}{\Lambda \lambda_i} P_0 \quad (\text{C.5})$$

Thus, we can write

$$\frac{d}{dt} \left(\frac{P}{P_0} \right) = \left(\frac{\rho_T - \beta}{\Lambda} \right) \left(\frac{P}{P_0} \right) + \sum_{i=1}^6 \left(\frac{\beta_i}{\Lambda} \right) \left(\frac{C_i}{C_{i0}} \right) \quad (\text{C.6})$$

Similarly, normalizing (C.2) with respect to its steady state value C_{i0}

$$\frac{d}{dt} \left(\frac{C_i}{C_{i0}} \right) = \left(\frac{\beta_i}{\Lambda} \right) \left(\frac{P}{C_{i0}} \right) - \lambda_i \left(\frac{C_i}{C_{i0}} \right) \quad (\text{C.7})$$

Substituting the value of C_{i0} , we get

$$\frac{d}{dt} \left(\frac{C_i}{C_{i0}} \right) = \lambda_i \left(\frac{P}{P_0} \right) - \lambda_i \left(\frac{C_i}{C_{i0}} \right) \quad (\text{C.8})$$

Therefore, the normalized core neutronics model is written as,

$$\frac{dP_r}{dt} = \left(\frac{\rho_T - \beta}{\Lambda} \right) P_r + \left(\frac{\sum_{i=1}^6 \beta_i C_{ir}}{\Lambda} \right), \quad (\text{C.9})$$

$$\frac{dC_{ir}}{dt} = \lambda_i (P_r - C_{ir}), \quad i = 1, 2, \dots, 6, \quad (\text{C.10})$$

where the subscript r denotes normalized parameter and $C_{ir0} = P_{r0}$.

A simple case of the point kinetics reactor model can be obtained by considering one group of delayed neutrons. The delayed neutron fraction and decay constant of the one effective delayed neutron are given by

$$\beta = \sum_{i=1}^6 \beta_i, \quad (\text{C.11})$$

and

$$\lambda = \frac{\beta}{\sum_{i=1}^6 \frac{\beta_i}{\lambda_i}}. \quad (\text{C.12})$$

C.3 Core Thermal-Hydraulics Model

In order to compute the effects of temperature over reactivity, a lumped model for core thermal hydraulics can be derived from Newton's law of cooling on fuel and coolant.

The temperature of the fuel and coolant satisfy the energy balance equations and describe the variations in reactor thermal power. It is stated as follows [2],[150]

$$\frac{dT_F}{dt} = H_F P - \gamma_F (T_F - T_C), \quad (\text{C.13})$$

$$\frac{dT_C}{dt} = H_C (T_F - T_C) - \gamma_C (T_{out} - T_{in}), \quad (\text{C.14})$$

where T_F is fuel temperature; T_C is coolant temperature; T_{out} is core outlet temperature; T_{in} is core inlet temperature; T_C , T_{in} , and T_{out} are assumed to be related as $T_C = (T_{out} + T_{in}) / 2$. H_F and H_C respectively characterize the rate of rise of fuel and coolant temperatures. γ_F is inverse mean time for heat transfer from fuel to coolant; γ_C is inverse mean time for heat transfer from core outlet to inlet. These parameters are given by

$$H_F = \frac{F_\phi}{M_F C_F}; \quad \gamma_F = \frac{U_{FC} A_F}{M_F C_F}; \quad (\text{C.15})$$

$$H_C = \frac{U_{FC} A_F}{M_C C_C}; \quad \gamma_C = \frac{m_p}{M_C}; \quad (\text{C.16})$$

where $M_F C_F$ and $M_C C_C$ are heat capacity of the fuel and coolant respectively; F_ϕ is reactor heat power per 1% of neutron flux; U_{FC} is heat transfer coefficient between the fuel and the coolant; m_p is mass flow rate of coolant; and A_F is area of a fuel rod. The values of various neutronic and thermal hydraulic parameters appearing in the above equations (C.1)–(C.16) are given in Table C.1 [38].

The inlet and outlet temperatures are further related as follows:

$$\frac{dT_{in}}{dt} = \frac{1}{\tau_{cold}} (T_{cold} - T_{in}), \quad (\text{C.17})$$

$$\frac{dT_{hot}}{dt} = \frac{1}{\tau_{hot}} (T_{out} - T_{hot}), \quad (\text{C.18})$$

$$\frac{dT_{sg}}{dt} = -\frac{1}{\tau_{sg}} (T_{sg} - T_{hot}) - D_1 L_T, \quad (\text{C.19})$$

$$T_{cold} = D_2 T_{sg} - D_3 T_{hot}, \quad (\text{C.20})$$

TABLE C.1: Neutronic and Thermal-Hydraulic Parameters

Group, i	1	2	3	4	5	6
$\lambda_i (s^{-1})$	0.012	0.031	0.115	0.301	0.905	2.760
$\beta_i (\times 10^{-3})$	0.1611	1.0020	0.8458	1.8330	0.9682	0.2088
$H_F (^\circ C s^{-1})$ 39.90	$H_C (s^{-1})$ 0.1596	$\gamma_F (s^{-1})$ 0.1250	$\gamma_C (s^{-1})$ 1.158	$\Lambda (s)$ 8.696×10^{-4}	$T_{F0} (^\circ C)$ 601.2	$T_{C0} (^\circ C)$ 282
$\alpha_0^F (^\circ C^{-1})$ 3.3559×10^{-3}	$\alpha_1^F (^\circ C^{-1})$ -1.473×10^{-5}	$\alpha_2^F (^\circ C^{-1})$ 1.0×10^{-8}	$\alpha_0^C (^\circ C^{-1})$ -1.180×10^{-3}		$\alpha_1^C (^\circ C^{-1})$ -0.0147×10^{-3}	

where T_{hot} and T_{cold} are hot and cold leg temperatures respectively; T_{sg} is steam generator temperature; τ_{hot} , τ_{cold} , and τ_{sg} are time constants for hot leg, cold leg, and steam generator respectively; D_1 , D_2 , and D_3 are constants; and L_T is turbine load which acts as a measured disturbance.

C.4 Xenon-Iodine Model

During the course of operation of a nuclear reactor various fission products accumulate. These products affect the multiplication factor and act as reactor poisons. Among these, xenon-135 is of particular interest due to its large thermal neutron absorption cross section. Formation of xenon and removal by its own radioactive decay occurs over several tens of hours, which is of the order of the local variation cycle in power reactors.

The xenon is formed directly as fission product however, a major portion results from the subsequent radioactive decay of iodine whose half life period is 6.2 h. The thermal neutron absorption cross section of xenon is extremely large and it undergoes radioactive decay at a relatively slower rate than iodine does. This plays a significant role in the overall neutron balance and it directly affects system reactivity both in steady state and as well as during transients. It also introduces xenon-induced oscillation in loosely coupled reactors having physical dimensions several times larger than the neutron migration length.

The rate of change of iodine-135 is given by

$$\frac{dI}{dt} = -\lambda_I I - \sigma_I \phi I + \gamma_I \Sigma_f \phi \quad (\text{C.21})$$

where I denotes the concentration of iodine; λ_I is decay constant of iodine; γ_I is fission yield of iodine; σ_I is thermal neutron absorption cross section and is quite small; Σ_f and Σ_a represent macroscopic thermal neutron absorption and fission cross sections respectively; and ϕ is thermal neutron flux; The first two term on the right of equation give the rate of removal of iodine-135 by radioactive decay and neutron capture respectively whereas, the third term represents its rate of formation by fission.

The equilibrium concentration of iodine is given by

$$I_0 = \frac{\gamma_I \Sigma_f \phi}{\lambda_I + \sigma_I \phi} \approx \frac{\gamma_I \Sigma_f \phi}{\lambda_I} \quad (\text{C.22})$$

The rate of change of xenon-135 is given by

$$\frac{dX}{dt} = -\lambda_X X - \sigma_X \phi X + \lambda_I I + \gamma_X \Sigma_f \phi \quad (\text{C.23})$$

where X denotes the concentration of xenon; λ_X is decay constant of xenon; γ_X is fission yield of xenon; and σ_X denotes microscopic thermal neutron absorption cross section of xenon. The first two terms on the right of equation (C.23) give the rate of removal of xenon-135 by radioactive decay and neutron capture respectively. The third and fourth terms represent its rate of formation by decay of iodine-135 and by fission respectively.

The equilibrium concentration of xenon is given by

$$X_0 = \frac{\lambda_I I_0 + \gamma_X \Sigma_f \phi}{\lambda_X + \sigma_X \phi} \approx \frac{(\gamma_I + \gamma_X) \Sigma_f \phi}{\lambda_X + \sigma_X \phi}. \quad (\text{C.24})$$

C.5 Reactivity Model

In nuclear reactors, the reactivity can be varied by different means like movement of control rods or burnable poison. Generally, the fine adjustment of reactivity for power regulation and control of reactor is done by the control rods. The reactivity is also affected by different internal feedbacks. The variation in the temperature of the system affects the effective multiplication factor in an operating reactor. The reactivity variation is characterized by variation in temperature coefficient of reactivity due to fuel and coolant. Such variation may be due to nonuniformity of structure affecting the flow of coolant or due to change in power demand. Transient changes in the effective multiplication factor in an operating reactor also occur due to xenon. These reactivity effects can be represented as follows:

$$\rho_T = \rho_U + \rho_F + \rho_C + \rho_X, \quad (\text{C.25})$$

$$\rho_F = \alpha_0^F + \alpha_1^F (T_F - T_{F0}) + \alpha_2^F (T_F - T_{F0})^2, \quad (\text{C.26})$$

$$\rho_C = \alpha_0^C + \alpha_1^C (T_C - T_{C0}), \quad (\text{C.27})$$

where ρ_T is total reactivity; ρ_U is reactivity contributed by all reactivity devices; ρ_F and ρ_C are reactivity feedbacks due to variation in fuel and coolant temperatures respectively; ρ_X is reactivity feedback due to xenon and is given by

$$\rho_X = -\frac{\sigma_X X}{\Sigma_a} \quad (\text{C.28})$$

The reactivity equivalent ρ_{X0} of the equilibrium xenon poisoning effect is consequently

$$\rho_{X0} \approx \frac{\sigma_X X_0}{\Sigma_a} = -\frac{\sigma_X (\gamma_I + \gamma_X) \sum_f \phi}{\Sigma_a (\lambda_I + \sigma_X \phi)}. \quad (\text{C.29})$$

In (C.26)–(C.27), T_{F0} and T_{C0} are steady state fuel and coolant temperatures at full power operating condition. α_i^F , $i = 0, 1, 2$ and α_i^C , $i = 0, 1$ respectively denote fuel and coolant temperature coefficients of reactivity. The effective multiplication factor

will change with temperature depending on the temperature coefficient of reactivity. If the temperature coefficient of reactivity is positive, then an any increase in operating power level, it would increase the reactivity thereby increasing the neutron density and rate of heat generation. This would cause a positive reactivity feedback. On the other hand, if the temperature coefficient of reactivity is negative, then an any increase in the power level of operation, it would decrease the reactivity thereby decreasing the rate of heat generation and thus introduce a negative reactivity feedback. Generally, the fuel and coolant temperature coefficients of reactivity are different in magnitude and the time scales in which they occur, due to their dependency on different characteristics. The time constant for fuel is short and often referred as prompt coefficient whereas the time constant for coolant is long and described as delayed coefficient.

In the case of PHWR, the reactivity input ρ_U can be varied by different means like liquid zone control system (LZCS), adjuster rods, control rods, and moderator liquid poison actuation system. Under normal operating conditions, the reactivity variation ρ_U is only due to LZCS *i.e.*, $\rho_U = \rho_Z$, as movement of other reactivity devices is not required. The variation of reactivity ρ_Z due to inflow variations in zonal control compartments can be represented using a second order polynomial as given by

$$\rho_Z = a_0 + a_1h + a_2h^2 \quad (C.30)$$

where h denotes the average water level (% full height) in ZCC and a_i , $i = 0, 1, 2$ is constant.

Bibliography

- [1] L. Ljung, *System identification: Theory for the user*, 2nd ed. Prentice Hall, Upper Saddle River, NJ, 1999.
- [2] G. T. Park and G. H. Miley, "Application of adaptive control to a nuclear power plant," *Nuclear Science and Engineering*, vol. 94, pp. 145–156, 1986.
- [3] R. K. Munje, B. M. Patre, and A. P. Tiwari, *Investigation of Spatial Control Strategies - Application to Advanced Heavy Water Reactor*. Springer, 2017.
- [4] A. Gabor, C. Fazekas, G. Szederkenyi, and K. M. Hangos, "Modeling and identification of a nuclear reactor with temperature effects and xenon poisoning," *European Journal of Control*, vol. 17, no. 1, pp. 104–115, 2011.
- [5] P. Van Overschee and B. De Moor, *Subspace identification for linear systems*. Kluwer Academic Publishers, 1996.
- [6] P. V. Kokotovic, R. E. O'Malley, and P. Sannuti, "Singular perturbations and order reduction in control theory: An overview," *Automatica*, vol. 12, pp. 123–132, 1976.
- [7] R. G. Phillips, "Reduced order modeling and control of two-time-scale discrete systems," *International Journal of Control*, vol. 31, pp. 765–780, 1980.
- [8] D. S. Naidu, "Singular perturbations and time scales in control theory and applications," *Dynamics of Continuous Discrete and Impulsive Systems Series B: Applications and Algorithms*, vol. 9, pp. 233–278, 2002.
- [9] S. R. Shimjith, A. P. Tiwari, and B. Bandyopadhyay, "A three-timescale approach for design of linear state regulator for spatial control of advanced heavy water reactor," *IEEE Transactions on Nuclear Science*, vol. 58, no. 3, pp. 1264–1276, 2011.
- [10] A. K. Tangirala, S. Mukhopadhyay, and A. P. Tiwari, "Wavelets applications in modeling and control," *Advances in Chemical Engineering*, vol. 43, pp. 107–204, 2013.
- [11] T. Abuhamdia and S. Taheri, "Wavelets as a tool for systems analysis and control," *Journal of Vibration and Control*, vol. 23, no. 9, pp. 1377–1416, 2017.
- [12] G. Strang and T. Nguyen, *Wavelets and Filter Banks*. Wellesley-Cambridge Press, 1996.

- [13] J. F. Carrier and G. Stephanopoulos, "Wavelet-based modulation in control-relevant process identification," *AIChE Journal*, vol. 44, no. 2, pp. 341–360, 1998.
- [14] K. C. Chou, A. S. Willsky, and A. Benveniste, "Multiscale recursive estimation, data fusion, and regularization," *IEEE Transactions on Automatic Control*, vol. 39, no. 3, pp. 464–478, 1994.
- [15] D. Coca and S. A. Billings, "Non-linear system identification using wavelet multiresolution models," *International Journal of Control*, vol. 74, no. 18, pp. 1718–1736, 2001.
- [16] X. W. Chang and L. Qu, "Wavelet estimation of partially linear models," *Computational statistics and data analysis*, vol. 47, no. 1, pp. 31–38, 2004.
- [17] Y. Li, H. L. Wei, and S. A. Billings, "Identification of time-varying systems using multi-wavelet basis functions," *IEEE Transactions on Control Systems Technology*, vol. 19, no. 3, pp. 656–663, 2011.
- [18] F. He, H. L. Wei, and S. A. Billings, "Identification and frequency domain analysis of non-stationary and nonlinear systems using time-varying NARMAX models," *International Journal of Systems Science*, vol. 46, no. 11, pp. 2087–2100, 2015.
- [19] S. Mukhopadhyay, D. Mukherjee, and A. P. Tiwari, "Model structures with wavelet basis functions," in *Proc. of the IEEE International Conference on Control Applications (CCA)*, 2013, pp. 418–423.
- [20] M. N. Nounou and H. N. Nounou, "Multiscale fuzzy system identification," *Journal of Process Control*, vol. 15, pp. 763–770, 2005.
- [21] M. N. Nounou, "Multiscale finite impulse response modeling," *Engineering Applications of Artificial Intelligence*, vol. 19, no. 3, pp. 289–304, 2006.
- [22] H. M. Paiva and R. K. H. Galvao, "Wavelet-packet identification of dynamic systems in frequency subbands," *Signal Processing*, vol. 86, pp. 2001–2008, 2006.
- [23] M. N. Nounou and H. N. Nounou, "Improving the prediction and parsimony of ARX models using multiscale estimation," *Applied Soft Computing*, vol. 7, pp. 711–721, 2007.
- [24] S. Mukhopadhyay and A. P. Tiwari, "Consistent output estimate with wavelets: An alternative solution of least squares minimization problem for identification of the LZC system of a large PHWR," *Annals of Nuclear Energy*, vol. 37, pp. 974–984, 2010.
- [25] X. Shan and J. B. Burl, "Continuous wavelet based linear time-varying system identification," *Signal Processing*, vol. 91, pp. 1476–1488, 2011.
- [26] B. R. Bakshi, "Multiscale PCA with application to multivariate statistical process monitoring," *AIChE Journal*, vol. 44, no. 7, pp. 1596–1610, 1998.
- [27] E. G. Gilbert, "Controllability and observability in multivariable control systems," *Journal of SIAM Control*, vol. 1, no. 2, pp. 128–151, 1963.

-
- [28] W. Favoreel and B. De Moor, "SPC: Subspace predictive control," in *Proc. of the IFAC World Congress, Beijing*, 1998, pp. 235–240.
- [29] R. Kadali, B. Huang, and A. Rossiter, "A data driven subspace approach to predictive controller design," *Control Engineering Practice*, vol. 11, no. 3, pp. 261–278, 2003.
- [30] X. Wang, B. Huang, and T. Chen, "Data-driven predictive control for solid oxide fuel cells," *Journal of Process Control*, vol. 17, pp. 103–114, 2007.
- [31] N. A. Mardi and L. Wang, "Subspace-based model predictive control of time-varying systems," in *Proc. 48th Conf. Decision and Control, China*, Dec 2009, pp. 4005–4010.
- [32] X. Wu, J. Shen, Y. Li, and K. Y. Lee, "Data-driven modeling and predictive control for boilerturbine unit using fuzzy clustering and subspace methods," *ISA Transactions*, vol. 53, pp. 699–708, 2014.
- [33] T. Soderstrom and P. Stoica, *System Identification*. Prentice Hall, London, 1989.
- [34] A. K. Tangirala, *Principles of system identification: Theory and practice*. CRC Press, 2014.
- [35] M. Gevers, "A personal view of the development of system identification: A 30-year journey through an exciting field," *IEEE Control Systems Magazine*, vol. 26, no. 6, pp. 93–105, 2006.
- [36] T. Soderstrom and P. Stoica, *Instrumental variable methods in system identification*. Springer-Verlag, Berlin, 1983.
- [37] J. J. Duderstadt and L. J. Hamilton, *Nuclear Reactor Analysis*. New York: Wiley, 1976.
- [38] C. S. Subudhi, T. U. Bhatt, and A. P. Tiwari, "A mathematical model for total power control loop of large PHWRs," *IEEE Transactions on Nuclear Science*, vol. 63, no. 3, pp. 1901–1911, June 2016.
- [39] A. P. Tiwari, B. Bandyopadhyay, and G. Govindarajan, "Spatial control of large pressurized heavy water reactor," *IEEE Transactions on Nuclear Science*, vol. 43, no. 4, pp. 2440–2453, 1996.
- [40] H. Javidnia, J. Jiang, and M. Borairi, "Modeling and simulation of a CANDU reactor for control system design and analysis," *Nuclear Technology*, vol. 165, no. 2, pp. 174–189, 2009.
- [41] A. J. Gaikwad, R. Kumar, S. F. Vhora, G. Chakraborty, and V. V. Raj, "Transient analysis following tripping of a primary circulating pump for 500-MWe PHWR power plant," *IEEE Transactions on Nuclear Science*, vol. 50, no. 2, pp. 288–293, 2003.
- [42] M. E. Pomerantz, C. R. Calabreseb, and C. Grant, "Nuclear reactor power and flux distribution fitting from a diffusion theory model and experimental data," *Annals of Nuclear Energy*, vol. 29, no. 9, pp. 1073–1083, 2002.

- [43] D. Lathouwers, A. Agug, T. H. J. J. Van Der Hagen, H. Van Dam, C. C. Pain, C. R. E. de Oliveira, and A. J. H. Goddard, "Dynamics modeling and stability analysis of a fluidized bed nuclear reactor," *Annals of Nuclear Energy*, vol. 43, no. 1–4, pp. 437–443, 2003.
- [44] W. C. Venter and E. C. Lamprecht, "Pebble bed micro model system identification," *Annals of Nuclear Energy*, vol. 46, pp. 1–10, 2012.
- [45] S. Das, S. Das, and A. Gupta, "Fractional order modeling of a PHWR under step-back condition and control of its global power with a robust *PID* controller," *IEEE Transactions on Nuclear Science*, vol. 58, no. 5, pp. 2431–2441, 2011.
- [46] C. Fazekas, G. Szederkenyi, and K. M. Hangos, "A simple dynamic model of the primary circuit in VVER plants for controller design purposes," *Nuclear Engineering and Design*, vol. 237, pp. 1071–1087, 2007.
- [47] J. J. Sohn and P. H. Seong, "A steam generator model identification and robust h_{∞} controller design with v-gap metric for a feedwater control system," *Annals of Nuclear Energy*, vol. 37, pp. 180–195, 2010.
- [48] W. Polifke, "Black-box system identification for reduced order model construction," *Annals of Nuclear Energy*, vol. 67, pp. 109–128, 2014.
- [49] H. G. Kim, S. H. Chang, and B. H. Lee, "Pressurized water reactor core parameter prediction using an artificial neural network," *Nuclear Science and Engineering*, vol. 113, no. 1, pp. 70–76, 1993.
- [50] F. Cadini, E. Zio, and N. Pedroni, "Simulating the dynamics of the neutron flux in a nuclear reactor by locally recurrent neural network," *Annals of Nuclear Energy*, vol. 34, no. 6, pp. 483–495, 2007.
- [51] E. Zio, M. Broggi, and N. Pedroni, "Nuclear reactor dynamics on-line estimation by locally recurrent neural network," *Progress in Nuclear Energy*, vol. 51, no. 3, pp. 573–581, 2009.
- [52] M. Boroushaki, M. B. Ghofrani, C. Lucas, and M. J. Yazdanpanah, "Identification and control of a nuclear reactor core (VVER) using recurrent neural networks and fuzzy systems," *IEEE Transactions on Nuclear Science*, vol. 50, no. 1, pp. 159–174, Feb 2003.
- [53] H. Khalafi and M. S. Terman, "Development of a neural simulator for research reactor dynamics," *Progress in Nuclear Energy*, vol. 51, no. 1, pp. 135–140, 2009.
- [54] M. Marseguerra, E. Zio, and P. Avogadri, "Model identification by neuro-fuzzy techniques: Predicting the water level in a steam generator of a PWR," *Progress in Nuclear Energy*, vol. 44, no. 3, pp. 237–252, 2004.
- [55] B. L. Ho and R. E. Kalman, "Effective construction of linear state-variable models from input/output functions," *Regelungstechnik*, vol. 12, pp. 545–548, 1965.
- [56] H. Zeiger and A. McEwen, "Approximate linear realizations of given dimension via Ho's algorithm," *IEEE Transactions on Automatic Control*, vol. 19, no. 2, pp. 153–153, Apr 1974.

-
- [57] W. E. Larimore, "Canonical variate analysis in identification, filtering, and adaptive control," in *Proc. of the 29th IEEE Conference on Decision and Control*, Dec 1990, pp. 596–604 vol.2.
- [58] M. Verhaegen and P. Dewilde, "Subspace identification part i: The output-error state space model identification class of algorithms," *International Journal of Control*, vol. 56, no. 5, pp. 1187–1210, 1992.
- [59] —, "Subspace model identification part 2: Analysis of the elementary output error state-space model identification algorithm," *International Journal of Control*, vol. 56, no. 5, pp. 1211–1241, 1992.
- [60] P. Van Overschee and B. De Moor, "N4SID: Subspace algorithms for the identification of combined deterministic-stochastic systems," *Automatica*, vol. 30, no. 1, pp. 75–93, 1994.
- [61] M. Viberg, "Subspace-based methods for the identification of linear time-invariant systems," *Automatica*, vol. 31, no. 12, pp. 1835–1851, Dec 1995.
- [62] P. Van Overschee and B. De Moor, "A unifying theorem for three subspace system identification algorithms," *Automatica*, vol. 31, no. 12, pp. 1853–1864, 1995.
- [63] B. Haverkamp, *Subspace method identification, theory and practice*. PhD thesis, TU Delft, The Netherlands, 2000.
- [64] P. Trnks, *Subspace identification methods*. PhD thesis, Czech Technical University, 2007.
- [65] B. Wahlberg, M. Jansson, T. Matsko, and M. A. Molander, *Experiences from subspace system identification – Comments from process industry users and researchers*. Springer, Berlin, Heidelberg, 2007, vol. 364.
- [66] K. Kameyama and A. Ohsumi, "Subspace-based prediction of linear time-varying stochastic systems," *Automatica*, vol. 43, no. 12, pp. 2009–2021, 2007.
- [67] M. Lovera, T. Gustafsson, and M. Verhaegen, "Recursive subspace identification and non-linear wiener state-space models," *Automatica*, vol. 36, no. 11, pp. 1639–1650, 2000.
- [68] G. Mercere, L. Bako, and S. Lecoecuche, "Propagator-based methods for recursive subspace model identification," *Signal Processing*, vol. 88, no. 3, pp. 468–491, 2008.
- [69] H. Oku and H. Kimura, "Recursive 4SID algorithms using gradient type subspace tracking," *Automatica*, vol. 38, no. 6, pp. 1035–1043, June 2002.
- [70] P. Van Overschee and B. De Moor, "Continuous-time frequency domain subspace system identification," *Signal Processing*, vol. 52, no. 2, pp. 179–194, 1996.
- [71] R. Pintelon, "Frequency-domain subspace system identification using non-parametric noise models," *Automatica*, vol. 38, no. 8, pp. 1295–1311, 2002.
- [72] S. Bittani, E. Gatti, G. Ripamonti, and S. M. Savaresi, "High-accuracy fit of the poles of spectroscopy amplifiers designed for mixed analog-digital filtering," *IEEE Transactions on Nuclear Science*, vol. 44, no. 2, pp. 125–133, April 1997.
-

- [73] S. Bittanti, E. Gatti, G. Ripamonti, and S. M. Savaresi, "Poles identification of an analog filter for nuclear spectroscopy via subspace-based techniques," *IEEE Transactions on Control Systems Technology*, vol. 8, no. 1, pp. 127–137, 2000.
- [74] C. Shiguo, Z. Ruanyu, W. Peng, and L. Taihua, "Enhance accuracy in pole identification of system by wavelet transform de-noising," *IEEE Transactions on Nuclear Science*, vol. 51, no. 1, pp. 250–255, Feb 2004.
- [75] F. Previdi, S. M. Savaresi, P. Guazzoni, and L. Zetta, "Detection and clustering of light charged particles via system-identification techniques," *International Journal of Adaptive Control and Signal Processing*, vol. 21, pp. 375–390, 2007.
- [76] M. Verhaegen, "Application of a subspace model identification technique to identify LTI systems operating in closed-loop," *Automatica*, vol. 29, no. 4, pp. 1027–1040, Jul 1993.
- [77] C. T. Chou and M. Verhaegen, "Subspace algorithms for the identification of multivariable dynamic errors-in-variables models," *Automatica*, vol. 33, no. 10, pp. 1857–1869, 1997.
- [78] P. Van Overschee and B. De Moor, "Closed loop subspace systems identification," in *Proc. 36th IEEE conference on decision & control, San Diego, CA, 1997*, pp. 1848–1853.
- [79] L. Ljung and T. McKelvey, "Subspace identification from closed loop data," *Signal Processing*, vol. 52, no. 2, pp. 209–216, 1996.
- [80] S. J. Qin and L. Ljung, "Closed-loop subspace identification with innovation estimation," in *IFAC Proceedings Volumes*, vol. 36, no. 16, Sep 2003, pp. 861–866.
- [81] M. Jansson, "Subspace identification and ARX modeling," in *IFAC Proceedings Volumes*, vol. 36, no. 16, Sep 2003, pp. 1585–1590.
- [82] A. Chiuso and G. Picci, "Consistency analysis of some closed-loop subspace identification methods," *Automatica*, vol. 41, no. 3, pp. 377–391, Mar 2005.
- [83] S. J. Qin, "An overview of subspace identification," *Computers & Chemical Engineering*, vol. 30, no. 10, pp. 1502–1513, 2006.
- [84] G. van der Veen, J.-W. van Wingerden, M. Bergamasco, M. Lovera, and M. Verhaegen, "Closed-loop subspace identification methods: an overview," *IET Control Theory and Applications*, vol. 7, no. 10, pp. 1339–1358, 2013.
- [85] A. Haar, "Zur theorie der orthogonalen funktionensysteme," *Mathematische Annalen*, vol. 69, no. 3, pp. 331–371, 1910.
- [86] S. G. Mallat, *A wavelet tour of signal processing: the sparse way*, 3rd ed. Academic Press, 2009.
- [87] M. Vetterli and J. Kovacevic, *Wavelets and subband coding*. Prentice Hall, Englewood Cliffs, NJ, 1993.

-
- [88] Y. Meyer, *Wavelets and Operators*, ser. Cambridge Studies in Advanced Mathematics. Cambridge University Press, 1993, vol. 1.
- [89] I. Daubechies, *Ten Lectures on Wavelets*. Society for Industrial and Applied Mathematics, 1992.
- [90] D. L. Donoho and I. M. Johnstone, “Ideal spatial adaptation via wavelet shrinkage,” *Biometrika*, vol. 81, pp. 425–4550, 1994.
- [91] ———, “Adapting to unknown smoothness via wavelet shrinkage,” *Journal of the American Statistical Association*, vol. 90, no. 432, pp. 1200–1224, Dec 1995.
- [92] M. Unser, “Sampling-50 years after shannon,” in *Proc. of the IEEE*, vol. 88, no. 4, 2000, pp. 569–587.
- [93] K. C. Chou, A. S. Willsky, and R. Nikoukhah, “Multiscale systems, Kalman filters, and Riccati equations,” *IEEE Transactions on Automatic Control*, vol. 39, no. 3, pp. 479–492, 1994.
- [94] L. Hong, G. Cheng, and C. K. Chui, “A filter-bank-based kalman filtering technique for wavelet estimation and decomposition of random signals,” *IEEE Transactions on Circuits and Systems II: Analog and Digital Signal Processing*, vol. 45, no. 2, pp. 237–241, 1998.
- [95] G. Stephanopoulos, O. Karsligil, and M. Dyer, “Multiscale theory for linear dynamic processes: Part 1 foundations,” *Computers & Chemical Engineering*, vol. 32, no. 4–5, pp. 857–884, April 2008.
- [96] ———, “Multiscale theory for linear dynamic processes: Part 2 multiscale model predictive control (MS-MPC),” *Computers & Chemical Engineering*, vol. 32, no. 4–5, pp. 885–912, April 2008.
- [97] A. Krishnan and K. A. Hoo, “A multiscale model predictive control strategy,” *Industrial Engineering Chemical Research*, vol. 38, no. 5, pp. 1973–1986, 1999.
- [98] L. Zhang, Q. Pan, B. Paul, and H. C. Zhang, “The discrete Kalman filtering of a class of dynamic multiscale systems,” *IEEE Transactions on Circuits and Systems II: Analog and Digital Signal Processing*, vol. 49, no. 10, pp. 668–676, Oct 2002.
- [99] L. Zhang, X. Wu, Q. Pan, and H. C. Zhang, “Multiresolution modeling and estimation of multisensor data,” *IEEE Transactions on Signal Processing*, vol. 52, no. 11, pp. 3170–3182, Nov 2004.
- [100] H. M. Nounou and M. N. Nounou, “Multiscale fuzzy kalman filtering,” *Engineering Applications of Artificial Intelligence*, vol. 19, no. 5, pp. 439–450, 2006.
- [101] L. Zhao and Y. Jia, “Robust transcale state estimation for multiresolution discrete-time systems based on wavelet transform,” *IET Signal Processing*, vol. 7, no. 3, pp. 228–238, May 2013.
- [102] M. Misra, H. Yue, S. J. Qin, and C. Ling, “Multivariate process monitoring and fault diagnosis by multi-scale PCA,” *Computers & Chemical Engineering*, vol. 26, no. 9, pp. 1281–1293, 2002.
-

- [103] M. N. Nounou, B. R. Bakshi, P. K. Goel, and X. Shen, "Improving principal component analysis using bayesian estimation," in *Proc. of the American Control Conference, Arlington, VA, 2001*, pp. 3666–3671.
- [104] B. R. Bakshi, M. N. Nounou, P. K. Goel, and X. Shen, "Process modeling by bayesian latent variable regression," *AIChE Journal*, vol. 48, no. 8, pp. 1775–1793, 2002.
- [105] R. Ganesan, T. K. Das, and V. Venkataraman, "Wavelet-based multiscale statistical process monitoring: A literature review," *IIE Transactions*, vol. 36, no. 9, pp. 787–806, 2004.
- [106] B. R. Bakshi and G. Stephanopoulos, "A multiresolution hierarchical neural network with localized learning," *AIChE Journal*, vol. 39, no. 1, pp. 57–81, 1993.
- [107] Q. Zhang and A. Benveniste, "Wavelet networks," *IEEE Transactions on Neural Networks*, vol. 3, no. 6, pp. 889–898, 1992.
- [108] M. Thuillard, "A review of wavelet networks, wavenets, fuzzy wavenets and their applications," in *Proc. of the ESIT*, 2000.
- [109] P. Aadaleesan, N. Miglan, R. Sharma, and P. Saha, "Nonlinear system identification using wiener type laguerre-wavelet network model," *Chemical Engineering Science*, vol. 63, pp. 3932–3941, 2008.
- [110] Z. Lu, J. Sun, and K. Butts, "Linear programming support vector regression with wavelet kernel: a new approach to nonlinear dynamical systems identification," *Mathematics Computer Simulation*, vol. 79, pp. 2051–2063, 2009.
- [111] J. Sjoberg, Q. H. Zhang, L. Ljung, A. Benveniste, B. Delyon, R. Y. Glorennec, H. Hjalmarsen, and A. Juditsky, "Nonlinear black-box modeling in system identification: a unified overview," *Automatica*, vol. 31, no. 12, pp. 1691–1724, 1995.
- [112] A. Juditsky, H. Hjalmarsen, A. Benveniste, B. Delyon, L. Ljung, J. Sjoberg, and Q. Zhang, "Nonlinear black-box models in system identification: Mathematical foundations," *Automatica*, vol. 31, no. 12, pp. 1725–1750, 1995.
- [113] M. Basseville, A. Benveniste, K. C. Chou, S. A. Golden, R. Nikoukhah, and A. S. Willsky, "Modeling and estimation of multiresolution stochastic processes," *IEEE Transactions on Information Theory*, vol. 38, no. 2, pp. 766–784, Mar 1992.
- [114] M. K. Tsatsanis and G. B. Giannakis, "Time-varying system identification and model validation using wavelets," *IEEE Transactions on Signal Processing*, vol. 41, no. 12, pp. 3512–3523, Dec 1993.
- [115] M. I. Doroslovacki and H. Fan, "Wavelet-based linear system modeling and adaptive filtering," *IEEE Transactions on Signal Processing*, vol. 44, no. 5, pp. 1156–1167, 1996.
- [116] B. R. Bakshi, "FIR model identification: Parsimony through kernel compression with wavelets," *AIChE Journal*, vol. 44, no. 1, pp. 141–150, 1998.

-
- [117] H. Zhao and J. Bentsman, "Biorthogonal wavelet based identification of fast linear time-varying systems – part I: System representations," *Journal of Dynamic Systems, Measurement, and Control*, vol. 123, no. 4, pp. 585–592, 2001.
- [118] R. Ghanem and F. Romeo, "A wavelet-based approach for the identification of linear time-varying dynamical systems," *Journal of Sound and Vibration*, vol. 234, no. 4, pp. 555–576, 2000.
- [119] Y. Dorfan, A. Feuer, and B. Porat, "Modeling and identification of LPTV systems by wavelets," *Signal Processing*, vol. 84, pp. 1285–1297, 2004.
- [120] J. Satoa, P. Morettina, P. Arantes, and E. J. Amaro, "Wavelet based time-varying vector autoregressive modelling," *Computational Statistical Data Analysis*, vol. 51, pp. 5847–5866, 2008.
- [121] S. A. Billings and H. L. Wei, "The wavelet-NARMAX representation: A hybrid model structure combining polynomial models with multiresolution wavelet decompositions," *International Journal of Systems Science*, vol. 36, no. 3, pp. 137–152, 2005.
- [122] H. L. Wei and S. A. Billings, "Identification of time-varying systems using multiresolution wavelet models," *International Journal of Systems Science*, vol. 33, no. 15, pp. 1217–1228, 2002.
- [123] Z. Vana and H. A. Preisig, "System identification in frequency domain using wavelets: conceptual remarks," *Systems & Control Letters*, vol. 61, pp. 1041–1051, 2012.
- [124] S. Palavajjhala, R. L. Motard, and B. Joseph, "Process identification using discrete wavelet transforms: Design of prefilters," *AIChE Journal*, vol. 42, no. 3, pp. 777–790, 1996.
- [125] M. S. Reis, "A multiscale empirical modeling framework for system identification," *Journal of Process Control*, vol. 19, no. 9, pp. 1546–1557, 2009.
- [126] S. L. Chen, J. Liang, and K. C. Ho, "Parametric identification of nonlinear systems by Haar wavelets: Theory and experimental validation," *Journal of Vibration and Acoustics*, vol. 134, no. 3, pp. 31 005–31 012, 2012.
- [127] X. Xu, Z. Y. Shi, and Q. You, "Identification of time-varying systems using a wavelet-based state-space method," *Mechanical Systems and Signal Processing*, vol. 26, pp. 91–103, 2012.
- [128] Y. Shimazu, "A feasibility study on wavelet transform for reactivity coefficient estimation," *Journal of Nuclear Science and Technology*, vol. 37, no. 12, pp. 1009–1014, 2000.
- [129] G. Heo, S. S. Choi, and S. H. Chang, "Thermal power estimation by fouling phenomena compensation using wavelet and principal component analysis," *Nuclear Engineering and Design*, vol. 199, pp. 31–40, 2000.
- [130] G. Y. Park, J. Park, and P. Y. Seong, "Application of wavelets noise-reduction technique to water-level controller," *Nuclear Technology*, vol. 145, pp. 177–188, 2004.
-

- [131] B. Majumder, S. Das, I. Pan, S. Das, and A. Gupta, “Denoising SPND signal by discrete wavelet analysis for efficient power feedback in regulating system of PHWRs under noisy environment,” in *Proc. of the 2nd National Conference on Emerging Trends and Applications in Computer Science*, 2011.
- [132] K. Hadad, M. Pourahmadi, and H. Majidi-Maraghi, “Fault diagnosis and classification based on wavelet transform and neural network,” *Progress in Nuclear Energy*, vol. 53, no. 1, pp. 41 – 47, 2011.
- [133] C. Montalvo and A. Garca-Berrocal, “Improving the in situ measurement of RTD response times through discrete wavelet transform in npp,” *Annals of Nuclear Energy*, vol. 80, pp. 114 – 122, 2015.
- [134] Y. Cao, M. Liu, J. Yang, Y. Cao, and W. Fu, “A method for extracting weak impact signal in NPP based on adaptive morlet wavelet transform and kurtosis,” *Progress in Nuclear Energy*, vol. 105, pp. 211 – 220, 2018.
- [135] G. Espinosa-Paredes, A. Nunez-Carrera, A. Prieto-Guerrero, and M. Cecenas, “Wavelet approach for analysis of neutronic power using data of ringhals stability benchmark,” *Nuclear Engineering And Design*, vol. 237, pp. 1009–1015, 2007.
- [136] A. Prieto-Guerrero and G. Espinosa-Paredes, “Decay ratio estimation of BWR signals based on wavelet ridges,” *Nuclear Science and Engineering*, vol. 160, no. 3, pp. 302–317, 2008.
- [137] M. Antonopoulos-Domis and T. Tambouratzis, “System identification during a transient via wavelet multiresolution analysis followed by spectral techniques,” *Annals of Nuclear Energy*, vol. 25, no. 6, pp. 465–480, 1998.
- [138] T. Tambouratzis and M. Antonopoulos-Domis, “Parameter estimation during a transient application to BWR stability,” *Annals of Nuclear Energy*, vol. 31, no. 18, pp. 2077–2092, 2004.
- [139] A. Patra and S. Saha Ray, “Numerical simulation based on Haar wavelet operational method to solve neutron point kinetics equation involving sinusoidal and pulse reactivity,” *Annals of Nuclear Energy*, vol. 73, pp. 408–412, 2014.
- [140] C. R. Cutler and B. L. Ramaker, “Dynamic matrix control?? a computer control algorithm,” in *Joint Automatic Control Conference*, 1980.
- [141] J. Richalet, A. Rault, J. L. Testud, and J. Papon, “Model predictive heuristic control: Applications to industrial processes,” *Automatica*, vol. 14, pp. 413–428, 1978.
- [142] D. W. Clarke, C. Mohtadi, and P. S. Tuffs, “Generalized predictive control–Part I the basic algorithm,” *Automatica*, vol. 23, no. 2, pp. 137–148, 1987.
- [143] ———, “Generalized predictive control–Part II extensions and interpretations,” *Automatica*, vol. 23, no. 2, pp. 149–160, 1987.
- [144] K. R. Muske and J. B. Rawlings, “Model predictive control with linear models,” *AIChE Journal*, vol. 39, no. 2, pp. 262–287, 1993.

-
- [145] M. V. Kothare, B. Mettler, M. Morari, P. Bendotti, and C. M. Falinower, "Level control in the steam generator of a nuclear power plant," *IEEE Transaction on Control System Technology*, vol. 8, no. 1, pp. 55–69, Jan 2000.
- [146] M. G. Na, "A model predictive controller for the water level of nuclear steam generators," *Journal of Korean Nuclear Society*, vol. 33, no. 1, pp. 102–110, Feb 2003.
- [147] K. Hu and J. Yuan, "Multi-model predictive control method for nuclear steam generator water level," *Energy Conversion and Management*, vol. 49, pp. 1167–1174, 2008.
- [148] H. Eliasi, H. Davilu, and M. B. Menhaj, "Adaptive fuzzy model based predictive control of nuclear steam generators," *Nuclear Engineering and Design*, vol. 237, no. 6, pp. 668–676, 2007.
- [149] K. Kavaklioglu, "Support vector regression model based predictive control of water level of U-tube steam generators," *Nuclear Engineering and Design*, vol. 278, pp. 651–660, 2014.
- [150] M. G. Na, S. H. Shin, and W. C. Kim, "A model predictive controller for nuclear reactor power," *Journal of Korean Nuclear Society*, vol. 35, no. 5, pp. 399–411, Oct 2003.
- [151] M. G. Na, D. W. Jung, S. H. Shin, J. W. Jang, K. B. Lee, and Y. J. Lee, "A model predictive controller for load-following operation of PWR reactors," *IEEE Transactions on Nuclear Science*, vol. 52, no. 4, pp. 1009–1020, Aug 2005.
- [152] T. Yun, H. Su-Xia, L. Chong, and Z. Fu-Yu, "An improved implicit multiple model predictive control used for movable nuclear power plant," *Nuclear Engineering and Design*, vol. 240, pp. 3582–3585, 2010.
- [153] H. Eliasi, M. B. Menhaj, and H. Davilu, "Robust nonlinear model predictive control for nuclear power plants in load following operations with bounded xenon oscillations," *Nuclear Engineering and Design*, vol. 241, pp. 533–543, 2011.
- [154] ———, "Robust nonlinear model predictive control for a PWR nuclear power plant," *Progress in Nuclear Energy*, vol. 54, pp. 177–185, 2012.
- [155] A. Etchepareborda and J. Lolich, "Research reactor power controller design using an output feedback nonlinear receding horizon control method," *Nuclear Engineering and Design*, vol. 237, pp. 268–276, 2007.
- [156] G. Wang, J. Wu, B. Zeng, Z. Xu, W. Wu, and X. Ma, "State-space model predictive control method for core power control in pressurized water reactor nuclear power stations," *Nuclear Engineering Technology*, vol. 49, no. 1, pp. 134–140, 2017.
- [157] Y. Xia, W. Xie, B. Liu, and X. Wang, "Data-driven predictive control for networked control systems," *Information Science*, vol. 235, pp. 45–54, 2013.
- [158] X. Wu, J. Shen, Y. Li, and K. Y. Lee, "Data-driven modeling and predictive control for boiler-turbine unit," *IEEE Transactions on Energy Conversion*, vol. 28, no. 3, pp. 470–481, Sep 2013.
-

- [159] W. Favoreel, B. De Moor, P. Van Overschee, and M. Gevers, "Model-free subspace-based LQG-design," in *Proc. of the American Control Conference*, vol. 5, 1999, pp. 3372–3376.
- [160] B. R. Woodley, J. P. How, and R. L. Kosut, "Subspace based direct adaptive h_∞ control," *International Journal of Adaptive Control and Signal Processing*, vol. 15, pp. 535–561, 2001.
- [161] W. Favoreel, B. De Moor, M. Gevers, and P. Van Overschee, "Closed-loop model-free subspace-based LQG design," in *Proc. of the Mediterranean Conference on Control and Automation, Haifa, Israel, June 1999*.
- [162] J. Dong and M. Verhaegen, "On the equivalence of closed-loop subspace predictive control with LQG," in *Proc. of 47th IEEE Conference on Decision and Control, Cancun, 2008*, pp. 4085–4090.
- [163] J. Dong, M. Verhaegen, and E. Holweg, "Closed-loop subspace predictive control for fault tolerant MPC design," in *Proc. 17th IFAC World Congress, Korea, July 2008*, pp. 3216–3221.
- [164] R. Hallouzi and M. Verhaegen, "Fault-tolerant subspace predictive control applied to a Boeing 747 model," *Journal of Guidance Control and Dynamics*, vol. 31, no. 4, pp. 873–883, 2008.
- [165] —, "Persistency of excitation in subspace predictive control," *IFAC Proceedings Volumes*, vol. 41, no. 2, pp. 11 439 – 11 444, 2008.
- [166] J. Dong, B. Kulcsar, J. W. van Wingerden, and M. Verhaegen, "Closed-loop subspace predictive control for linear parameter varying systems (i) - the nominal case," in *Proc. of the European Control Conference (ECC)*, Aug 2009, pp. 2009–2014.
- [167] B. Kulcsar, J. Dong, and M. Verhaegen, "Closed-loop subspace predictive control for linear parameter varying systems (ii) - a supervisory and robust approach," in *Proc. of the European Control Conference (ECC)*, Aug 2009, pp. 2021–2026.
- [168] B. Kulcsar, J. W. van Wingerden, J. Dong, and M. Verhaegen, "Closed-loop subspace predictive control for hammerstein systems," in *Proc. of 48th IEEE Conference on Decision and Control (CDC) held jointly with 28th Chinese Control Conference, 2009*, pp. 2604–2609.
- [169] S. T. Navalkar, E. van Solingen, and J. W. van Wingerden, "Wind tunnel testing of subspace predictive repetitive control for variable pitch wind turbines," *IEEE Transactions on Control Systems Technology*, vol. 23, no. 6, pp. 2101–2116, 2015.
- [170] C.-C. Ku, K. Y. Lee, and R. M. Edwards, "Improved nuclear reactor temperature control using diagonal recurrent neural networks," *IEEE Transactions on Nuclear Science*, vol. 39, no. 6, pp. 2298–2308, Dec 1992.
- [171] M. N. Khajavi, M. B. Menhaj, and A. A. Suratgar, "A neural network controller for load following operation of nuclear reactors," *Annals of Nuclear Energy*, vol. 35, pp. 2051–2058, 2008.

-
- [172] H. Arab-Alibeik and S. Setayeshi, "Adaptive control of a PWR core power using neural networks," *Annals of Nuclear Energy*, vol. 32, pp. 588–605, 2005.
- [173] M. N. Khajavi, M. B. Menhaj, and A. A. Suratgar, "Fuzzy adaptive robust optimal controller to increase load following capability of nuclear reactors," in *Proc. of the 4th IEEE Int. Power Control Conference, Australia*, Dec 2000, pp. 4–7.
- [174] S. S. Khorramabadi, M. Boroushaki, and C. Lucas, "Emotional learning based intelligent controller for a PWR nuclear reactor core during load following operation," *Annals of Nuclear Energy*, vol. 35, pp. 2051–2058, 2008.
- [175] M. G. Na, I. J. Hwang, and Y. J. Lee, "Design of a fuzzy model predictive power controller for pressurized water reactors," *IEEE Transactions on Nuclear Science*, vol. 53, no. 3, pp. 1504–1514, June 2006.
- [176] S. W. Lee, J. H. Kim, M. G. Na, D. S. Kim, K. J. Yu, and H. G. Kim, "Design of a load following controller for APR+ nuclear plants," *Nuclear Engineering Technology*, vol. 44, pp. 369–378, 2012.
- [177] M. G. Na and B. R. Upadhyaya, "Model predictive control of an SP-100 space reactor using support vector regression and genetic optimization," *IEEE Transactions on Nuclear Science*, vol. 53, no. 4, pp. 2318–2327, Aug 2006.
- [178] D. Liu, X. Luan, T. Yu, W. Zhao, and L. Liu, "The controllability of the point reactor neutron kinetics equations," in *Proc. of the 22nd International Conference on Nuclear Engineering ICONE22*, July 2014, pp. 1–6.
- [179] X. Liu, D. Jiang, and K. Y. Lee, "Decentralized fuzzy MPC on spatial power control of a large PHWR," *IEEE Transactions on Nuclear Science*, vol. 63, no. 4, pp. 2343–2351, Aug 2016.
- [180] B. Friedland, *Control Systems Design: An introduction to state-space Methods*. McGraw-Hill Higher Education, 1985.
- [181] D. L. Donoho, "De-noising by soft-thresholding," *IEEE Transactions on Information Theory*, vol. 41, pp. 613–627, May 1995.
- [182] R. R. Coifmann and M. V. Wickerhauser, "Entropy-based algorithms for best-basis selection," *IEEE Transactions on Information Theory*, vol. 38, pp. 713–719, Mar 1992.
- [183] C. Torrence and G. P. Compo, "A practical guide to wavelet analysis," *Bulletin of the American Meteorological Society*, vol. 79, no. 1, pp. 61–78, Jan 1998.
- [184] M. Verhaegen, "Identification of the deterministic part of MIMO state space models given in innovations form from input-output data," *Automatica*, vol. 30, no. 1, pp. 61–74, 1994.
- [185] A. E. Cetin and M. Tofghi, "Projection-based wavelet denoising [lecture notes]," *IEEE Signal Processing Magazine*, vol. 32, no. 5, pp. 120–124, 2015.
- [186] J. L. Garriga and M. Soroush, "Model predictive control tuning methods: A review," *Industrial & Engineering Chemistry Research*, vol. 49, pp. 3505–3515, 2010.
-

- [187] N. A. Mardi and L. Wang, "Subspace-based model predictive control with data prefiltering," in *Proc. UKACC Int. Conf. Control, Manchester, UK*, 2008.